

Sept 1966

SATURN HISTORY DOCUMENT
University Of Alabama Research Institute
History Of Science & Technology Group
Date _____ Doc. No. _____

A Reproduced Copy

OF

III. 5

X67-17704

NO LONGER RETENTION
RETURN TO NASA

Available from NASA to NASA
offices, NASA Centers, and
NASA contractors only.

Reproduced for NASA

by the

NASA Scientific and Technical Information Facility

FACILITY FORM 802

X67-17704

(ACCESSION NUMBER)

(THRU)

234

(PAGES)

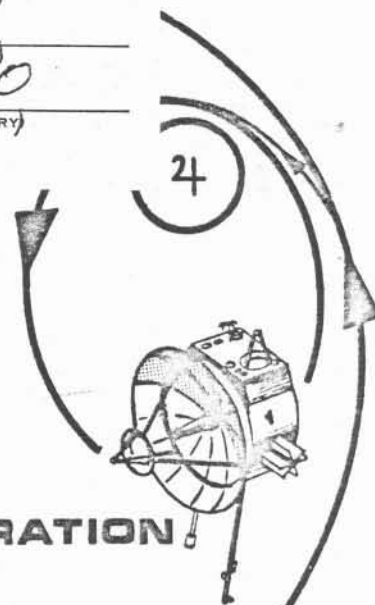
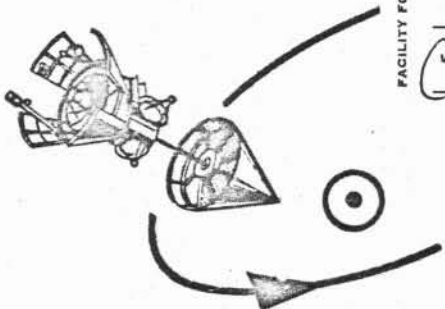
(CODE)

CR 84968

(NASA CR OR TMX OR AD NUMBER)

30

(CATEGORY)



**APPLICATION OF THE
SATURN V LAUNCH VEHICLE
TO UNMANNED SCIENTIFIC EXPLORATION
OF THE SOLAR SYSTEM**

- JUPITER ORBITER / SOLAR PROBE MISSION STUDY
- ADVANCED MISSION INVESTIGATIONS



Prepared for:

**NATIONAL AERONAUTICS AND SPACE ADMINISTRATION
GEORGE C. MARSHALL SPACE FLIGHT CENTER
Aero-Astrodynamic Laboratory**

PREPARED UNDER CONTRACT NAS8-20082

NORTHROP SPACE LABORATORIES

6025 TECHNOLOGY DRIVE, HUNTSVILLE, ALABAMA 35805
TELEPHONE 837-0580

P. O. BOX 1484

NASA and NASA Contractors Only

Eq-42149

APPLICATION OF
THE SATURN V LAUNCH VEHICLE
TO UNMANNED SCIENTIFIC EXPLORATION
OF THE SOLAR SYSTEM

- Jupiter Orbiter/Solar Probe Mission Study
- Advanced Mission Investigations

By:

P. R. Odom, Project Engineer
A. S. Hill
B. G. Brown
M. C. Thadani
C. M. MacKenzie

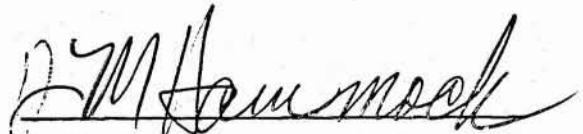
Prepared for:

NATIONAL AERONAUTICS AND SPACE ADMINISTRATION
GEORGE C. MARSHALL SPACE FLIGHT CENTER
AERO-ASTRODYNAMICS LABORATORY

Under Contract No. NAS8-20082



Dr. S. S. Hu
Director
Research & Analysis Section



D. M. Hammock
Director
Systems Section

NORTHROP SPACE LABORATORIES
HUNTSVILLE DEPARTMENT
HUNTSVILLE, ALABAMA

NASA and NASA Contractors Only

FOREWORD

This report presents the results of a twelve-week mission and systems analysis of a combined Jupiter orbiter/solar probe mission utilizing the Saturn V launch vehicle. Missions are considered during the 1970-1980 time period with the close solar probe orbit (typically 0.1-AU perihelion) based on Jupiter gravity-assist. This work was performed under Schedule Order No. 17, Appendix F-1, of Contract NAS8-20082. The NASA Technical Coordinator for the study was Mr. H. F. Thoma of the Advanced Studies Office, Aero-Astrodynamic Laboratory, MSFC.

The authors acknowledge the technical contributions of the following members of the Northrop staff: L. C. Allen, III, W. L. Bronner, J. V. Butler, W. J. Couchois, C. O. DeLong, C. L. Densmore, J. E. Ligocki, W. C. Lucas, D. L. Shady, and R. Silber.

Note: The adjective "Jovian" as used in this report refers to the planet Jupiter and not to any of the other outer-solar-system planets.

TABLE OF CONTENTS

<u>Section</u>	<u>Title</u>	<u>Page</u>
	LIST OF FIGURES.....	iv
	LIST OF TABLES.....	xi
	GENERAL SUMMARY.....	xiii
I	INTRODUCTION.....	1-1
II	JUPITER ORBITER/SOLAR PROBE MISSION.....	2-1
	2.1 MISSION ANALYSIS.....	2-1
	2.1.1 Mission Ground Rules.....	2-1
	2.1.2 Mission Concept.....	2-1
	2.1.3 Heliocentric Trajectory Analysis.....	2-7
	2.1.4 Earth Launch Window Analysis.....	2-59
	2.1.5 Capture Orbit Analysis.....	2-61
	2.1.6 Mission Performance.....	2-67
	2.2 SYSTEMS ANALYSIS.....	2-84
	2.2.1 Mission and Trajectory Selection.....	2-84
	2.2.2 Sterilization.....	2-94
	2.2.3 Communication Subsystem.....	2-97
	2.2.4 Spacecraft Thermal Control.....	2-116
	2.2.5 Power Supply System.....	2-132
	2.2.6 Propulsion and Attitude Control Subsystems.....	2-148
	2.2.7 Guidance and Navigation.....	2-169
	2.2.8 Reliability Analysis.....	2-171
	2.3 SPACECRAFT CONCEPTUAL DESIGNS.....	2-197
	2.3.1 Propulsion.....	2-199
	2.3.2 Power Supply.....	2-199
	2.3.3 Communications.....	2-199
	2.3.4 Thermal Control.....	2-200
	2.3.5 Guidance Control.....	2-200
	2.3.6 Inboard Profiles.....	2-200
III	ADVANCED MISSIONS.....	3-1
	3.1 JOVIAN MOON EXPLORATION.....	3-1
	3.1.1 Description of the Jovian Satellite System.....	3-2
	3.1.2 Jupiter Orbiter - Moons Communication Distance.....	3-4
	3.1.3 Sphere-of-Influence Concept for the Jovian Moon.....	3-7
	3.2 OUTER SOLAR SYSTEM EXPLORATION VIA THE JUPITER SWINGBY MODE.....	3-12
	3.2.1 Saturn and Uranus Missions.....	3-13
	3.2.2 Asteroid Belt Mission.....	3-13
	3.3 SPACECRAFT FAMILY.....	3-19
IV	REFERENCES.....	4-1

LIST OF FIGURES

<u>Figure No.</u>	<u>Title</u>	<u>Page</u>
	ADVANCED MISSION SPACECRAFT CONCEPTS BASED ON COMMON UTILIZATION OF JUPITER ORBITER	xxii
2-1	SPACE VEHICLE CONFIGURATION	2-3
2-2	JUPITER ORBITER/SOLAR PROBE CONCEPT	2-4
2-3	JUPITER ORBITER/SOLAR PROBE PROFILE	2-5
2-4	HYPERBOLIC EXCESS SPEEDS FOR FAST EARTH-JUPITER TRANSFERS DURING 1970-1980	2-9
2-5	DEPARTURE AND ARRIVAL HYPERBOLIC-EXCESS SPEEDS FOR 1972 EARTH-JUPITER TRANSFERS	2-10
2-6	DEPARTURE AND ARRIVAL HYPERBOLIC-EXCESS SPEEDS FOR 1975 EARTH-JUPITER TRANSFERS	2-11
2-7	DEPARTURE AND ARRIVAL HYPERBOLIC-EXCESS SPEEDS FOR 1978 EARTH-JUPITER TRANSFERS	2-12
2-8	EARTH-JUPITER TRAJECTORIES 1975: PLANETARY CONSTELLATIONS AT JUPITER ARRIVAL FOR FAST TRANSFERS	2-13
2-9	VELOCITY VECTOR DIAGRAMS FOR DIRECT AND RETROGRADE PLANETARY SWINGBYS	2-15
2-10	JUPITER SWINGBY TRAJECTORY MODEL	2-18
2-11	JUPITER SWINGBY GEOMETRY	2-20
2-12	MISS DISTANCE AT JUPITER AS A FUNCTION OF SWINGBY DISTANCE	2-21
2-13	HYPERBOLIC-EXCESS VELOCITY VECTOR BEND ANGLE AT JUPITER AS A FUNCTION OF SWINGBY DISTANCE	2-22
2-14	1975 SOLAR PROBE TRAJECTORY VIA JUPITER SWINGBY: PERIHELION DISTANCE	2-24
2-15	1975 SOLAR PROBE TRAJECTORY VIA JUPITER SWINGBY: TRANSFER TIME FROM EARTH DEPARTURE TO SOLAR FLYBY	2-25
2-16	1975 SOLAR PROBE TRAJECTORY VIA JUPITER SWINGBY: TRAJECTORY PLANE INCLINATION	2-26
2-17	EFFECT OF INCLINATION OF JUPITER ENCOUNTER HYPERBOLA ON PERIHELION OF SOLAR PROBE ORBIT	2-27
2-18	EFFECT OF INCLINATION OF JUPITER ENCOUNTER HYPERBOLA ON INCLINATION OF SOLAR PROBE ORBIT	2-28

LIST OF FIGURES (Continued)

<u>Figure No.</u>	<u>Title</u>	<u>Page</u>
2-19	SOLAR PROBE TRAJECTORY VIA JUPITER SWINGBY: PERIHELION DISTANCE	2-30
2-20	1975 SOLAR PROBE TRAJECTORY VIA JUPITER SWINGBY: PERIHELION DISTANCE	2-31
2-21	1975 SOLAR PROBE TRAJECTORY VIA JUPITER SWINGBY: PERIHELION DISTANCE	2-32
2-22	1975 SOLAR PROBE TRAJECTORY VIA JUPITER SWINGBY: TRANSFER TIME FROM EARTH DEPARTURE TO SOLAR FLYBY	2-33
2-23	1975 SOLAR PROBE TRAJECTORY VIA JUPITER SWINGBY: TRANSFER TIME FROM EARTH DEPARTURE TO SOLAR FLYBY	2-34
2-24	1975 SOLAR PROBE TRAJECTORY VIA JUPITER SWINGBY: TRAJECTORY PLANE INCLINATION	2-35
2-25	1975 SOLAR PROBE TRAJECTORY VIA JUPITER SWINGBY: TRAJECTORY PLANE INCLINATION	2-36
2-26	1972 SOLAR PROBE TRAJECTORY VIA JUPITER SWINGBY: PERIHELION DISTANCE	2-38
2-27	1972 SOLAR PROBE TRAJECTORY VIA JUPITER SWINGBY: PERIHELION DISTANCE	2-39
2-28	1972 SOLAR PROBE TRAJECTORY VIA JUPITER SWINGBY: PERIHELION DISTANCE	2-40
2-29	1972 SOLAR PROBE TRAJECTORY VIA JUPITER SWINGBY: TRANSFER TIME FROM EARTH DEPARTURE TO SOLAR FLYBY	2-41
2-30	1972 SOLAR PROBE TRAJECTORY VIA JUPITER SWINGBY: TRAJECTORY PLANE INCLINATION	2-42
2-31	1978 SOLAR PROBE TRAJECTORY VIA JUPITER SWINGBY: PERIHELION DISTANCE	2-43
2-32	1978 SOLAR PROBE TRAJECTORY VIA JUPITER SWINGBY: TRANSFER TIME FROM EARTH DEPARTURE TO SOLAR FLYBY	2-44
2-33	1978 SOLAR PROBE TRAJECTORY VIA JUPITER SWINGBY: TRAJECTORY PLANE INCLINATION	2-45
2-34	1978 SOLAR PROBE TRAJECTORY VIA JUPITER SWINGBY: PERIHELION DISTANCE	2-46
2-35	1978 SOLAR PROBE TRAJECTORY VIA JUPITER SWINGBY: TRANSFER TIME FROM EARTH DEPARTURE TO SOLAR FLYBY	2-47

LIST OF FIGURES (Continued)

<u>Figure No.</u>	<u>Title</u>	<u>Page</u>
2-36	1978 SOLAR PROBE TRAJECTORY VIA JUPITER SWINGBY: TRAJEC- TORY PLANE INCLINATION	2-48
2-37	1978 SOLAR PROBE TRAJECTORY VIA JUPITER SWINGBY: PERI- HELION DISTANCE	2-49
2-38	1978 SOLAR PROBE TRAJECTORY VIA JUPITER SWINGBY: TRANSFER TIME FROM EARTH DEPARTURE TO SOLAR FLYBY	2-50
2-39	1978 SOLAR PROBE TRAJECTORY VIA JUPITER SWINGBY: TRAJEC- TORY PLANE INCLINATION	2-51
2-40	SOLAR PROBE TRAJECTORY VIA JUPITER SWINGBY: PERIHELION AND EARTH-JUPITER TRANSFER TIME FOR CONSTANT GROSS MASS	2-53
2-41	SOLAR PROBE ORBIT: REQUIRED ANGULAR POSITION OF EARTH FOR COMMUNICATION AT SOLAR FLYBY	2-55
2-42	SOLAR PROBE ORBIT: REQUIRED ANGULAR POSITION OF EARTH FOR COMMUNICATION AT SOLAR FLYBY	2-56
2-43	1975 SOLAR PROBE TRAJECTORY VIA JUPITER SWINGBY: EARTH POSITION AT SOLAR FLYBY	2-57
2-44	JUPITER ORBITER/SOLAR PROBE MISSION: APPROACH MANEUVER V AT JUPITER	2-60
2-45	DECLINATION OF OUTGOING GEOCENTRIC ASYMPTOTE FOR FAST EARTH-JUPITER TRANSFERS DURING 1970-1980	2-62
2-46	1975 EARTH-JUPITER TRAJECTORIES: RIGHT ASCENSION AND DECLINATION OF OUTGOING GEOCENTRIC ASYMPTOTE FOR 500-DAY TRANSFERS	2-63
2-47	EARTH-JUPITER TRAJECTORIES 1975: DAILY SURFACE LAUNCH WINDOW FOR 500-DAY TRANSFERS	2-64
2-48	EARTH-JUPITER TRAJECTORIES 1978: DAILY SURFACE LAUNCH WINDOWS FOR 540-DAY TRANSFERS	2-65
2-49	OPTIMUM JOVIAN CAPTURE ORBIT PERIJOVE FOR MINIMUM BRAKING VELOCITY INCREMENT	2-66
2-50	MINIMUM VELOCITY INCREMENT FOR JOVIAN CAPTURE BRAKING	2-68
2-51	VELOCITY INCREMENT REQUIRED FOR JOVIAN CAPTURE BRAKING	2-69
2-52	VELOCITY INCREMENT REQUIRED FOR JOVIAN CAPTURE BRAKING	2-70
2-53	PERIOD OF JOVIAN CAPTURE ORBIT AS A FUNCTION OF APSIDAL RATIO	2-71

LIST OF FIGURES (Continued)

<u>Figure No.</u>	<u>Title</u>	<u>Page</u>
2-54	THREE-STAGE SATURN V PERFORMANCE CAPABILITY FOR HIGH-ENERGY MISSIONS	2-72
2-55	SATURN V PERFORMANCE FOR 1972 JUPITER ORBITER/SOLAR PROBE MISSION	2-74
2-56	1972 JUPITER ORBITER/SOLAR PROBE MISSION PERFORMANCE	2-76
2-57	1972 JUPITER ORBITER/SOLAR PROBE MISSION PERFORMANCE: EFFECT OF VARIATION OF SOLAR PROBE MASS	2-77
2-58	SATURN V PERFORMANCE FOR 1975 JUPITER ORBITER/SOLAR PROBE MISSION	2-78
2-59	1975 JUPITER ORBITER/SOLAR PROBE MISSION PERFORMANCE	2-79
2-60	SATURN V PERFORMANCE FOR 1978 JUPITER ORBITER/SOLAR PROBE MISSION	2-80
2-61	1978 JUPITER ORBITER/SOLAR PROBE MISSION PERFORMANCE	2-81
2-62	SPACECRAFT MASS VS EARTH DEPARTURE DATE	2-86
2-63	COMPARISON OF CAPTURE ORBIT APSIDAL RATIOS VS PERIJOVE DISTANCE	2-87
2-64	DECLINATION OF OUTGOING GEOCENTRIC ASYMPTOTE FOR JUPITER PROBE VS EARTH DEPARTURE DATE	2-88
2-65	JUPITER PROBE TRIP TIME REDUCTION - HELIOCENTRIC TRANSFER TIME VS EARTH DEPARTURE DATE	2-89
2-66	JUPITER MOON FLYBY SHOWING CLOSEST APPROACH VS PERIJOVE ARGUMENT	2-93
2-67	STERILIZATION TIME-TEMPERATURE CYCLES	2-96
2-68	PARABOLIC ANTENNA CHARACTERISTICS	2-102
2-69	TRANSMITTER POWER REQUIREMENTS VS TRANSMITTER GAIN	2-103
2-70	DISTANCE FROM EARTH VS SIGNAL LOSSES	2-105
2-71	SKY NOISE TEMPERATURE VS TRANSMISSION FREQUENCY	2-106
2-72	BACKGROUND NOISE LEVELS VS SIGNAL LOSSES	2-108
2-73	DATA RATE VS DSIF RECEIVER GAIN	2-110
2-74	TYPICAL COMMUNICATIONS GEOMETRY FOR JUPITER ORBITER VS DAYS FROM EARTH DEPARTURE	2-114

LIST OF FIGURES (Continued)

<u>Figure No.</u>	<u>Title</u>	<u>Page</u>
2-75	COMMUNICATION SYSTEM BLOCK DIAGRAM FOR JUPITER ORBITER/ SOLAR PROBE	2-115
2-76	TEMPERATURE VS DISTANCE FROM SUN FOR AN INSULATED FLAT PLATE FACING SUN	2-118
2-77	SPACECRAFT HEAT ENERGY BALANCE	2-120
2-78	VARIATION OF T_s/T_n WITH NUMBER OF THERMAL SHIELDS	2-121
2-79	HEAT TRANSFER BETWEEN TWO FLAT PLATES FOR VARIOUS α/ϵ RATIOS	2-122
2-80	TEMPERATURE OF LAST PLATE IN FLAT PLATE SHADOW SHIELD VS DISTANCE FROM THE SUN FOR VARIOUS MATERIALS	2-123
2-81	CONICAL SHADOW SHIELD TEMPERATURE VS LENGTH TO DIAMETER RATIOS FOR VARYING SOLAR DISTANCES	2-124
2-82	SHADOW SHIELD GEOMETRY	2-126
2-83	SECONDARY SHIELD TEMPERATURE VS SEPARATION DISTANCE IN METERS	2-127
2-84	HEAT TRANSFER FOR SECONDARY SHIELD WITH SUPERINSULATION FOR VARIOUS α/ϵ RATIOS	2-128
2-85	EFFECT OF SPACECRAFT-SUN MISALIGNMENT ANGLE UPON SHIELD TEMPERATURES FOR VARYING DISTANCES FROM THE SUN	2-129
2-86	MATERIAL TEMPERATURE LIMITATIONS AS A FUNCTION OF VARIOUS SHAPES AND PROXIMITY TO THE SUN	2-130
2-87	DISTANCE FROM SUN VS SOLAR INTENSITY FILTERING AND RESULTANT EFFECT UPON SOLAR CELL OPERATION	2-133
2-88	RTG THERMOELECTRIC SYSTEMS	2-134
2-89	JUPITER TYPICAL MISSION POWER PROFILES	2-138
2-90	RELIABILITY OF ALTERNATE POWER SUPPLY SYSTEMS USING Pu-238 FUEL	2-140
2-91	POWER SYSTEM SUCCESS PROBABILITY VS PROBABILITY OF PUMP SUCCESS	2-141
2-92	RTG FIN TEMPERATURE VS FIN HEAT CAPACITY	2-145
2-93	COMBINED ISOTOPIIC POWER AND PROPULSION UNITS FOR THERMIONIC AND FLUID POWER CYCLES	2-146
2-94	PERFORMANCE OF ISOTOPIIC PROPULSION SYSTEMS WITH BURN TIME	2-150
2-95	PROPELLANT PERFORMANCE VS MISSION STORAGE TIME	2-151

LIST OF FIGURES (Continued)

<u>Figure No.</u>	<u>Title</u>	<u>Page</u>
2-96	VARIATION OF SPECIFIC INSULATION MASS WITH HEAT FLUX FOR VARYING INSULATION SURFACE TEMPERATURES	2-152
2-97	HEATING REQUIRED TO MAINTAIN STORABLE LIQUID PROPELLANTS AT ROOM TEMPERATURE	2-153
2-98	TOTAL SYSTEM MASS COMPARISONS FOR MONOPROPELLANT AND BI-PROPELLANT SYSTEMS	2-155
2-99	JUPITER CAPTURE PROPULSION ENGINE SYSTEM	2-156
2-100	STABILIZATION CHARACTERISTICS FOR JUPITER/SOLAR PROBES	2-159
2-101	ATTITUDE CONTROL THRUST REQUIREMENTS VS THRUSTER MOMENT ARM	2-161
2-102	SOLAR RADIATION PRESSURE VS DISTANCE FROM SUN	2-163
2-103	SOLAR WIND PRESSURE VS DISTANCE FROM SUN	2-165
2-104	SOLAR RADIATION CONTROL FORCES VS DISTANCE FROM SUN	2-166
2-105	MASS VARIATION OF REACTION GAS ATTITUDE-CONTROL SYSTEMS VS TOTAL IMPULSE	2-168
2-106	PROBABILITY OF PROGRAM SUCCESS AS A FUNCTION OF MULTIPLE SPACECRAFT LAUNCHES	2-172
2-107	BOOSTER SUCCESS HISTORY VS LAUNCH DATES (UNMANNED SPACECRAFT)	2-178
2-108	LAUNCH SUCCESS EXPECTATION (UNMANNED SPACECRAFT)	2-179
2-109	COMPONENT LIFETIME IMPROVEMENT	2-181
2-110	MEAN-TIME-TO-FAILURE VS COMPONENT FAILURE RATES	2-182
2-111	PROBABILITY OF ELECTRONIC COMPONENT SUCCESS VS MISSION DURATION	2-183
2-112	EXPECTED ELECTRONIC COMPONENT SUCCESS OF DEEP-SPACE PROBES VS TIME	2-184
2-113	EFFECT OF REDUNDANCY UPON ELECTRONIC COMPONENT FAILURE	2-186
2-114	EFFECT OF MULTIPLE COMPONENT FAILURE ACCEPTANCE UPON MISSION SUCCESS FOR 600- AND 1200-DAY MISSIONS	2-188
2-115	COMETARY AND ASTEROIDAL METEOROID MASS DISTRIBUTION VS SOLAR DISTANCE	2-190
2-116	MINIMUM PARTICLE RELATIVE VELOCITY, DIAMETER, AND DENSITY TO CAUSE PUNCTURE LEADING TO SPACECRAFT FAILURE	2-191

LIST OF FIGURES (Concluded)

<u>Figure No.</u>	<u>Title</u>	<u>Page</u>
2-117	COMETARY AND ASTEROIDAL METEOROID RELATIVE VELOCITIES VS NUMBER OF IMPACTS AND PENETRATIONS IN ALUMINUM PLATES	2-192
2-118	STRUCTURAL MASS VS PROBABILITY OF METEOROID PUNCTURE FOR VARIOUS STRUCTURAL CONCEPTS	2-194
2-119	MISSION DURATION VS SPACECRAFT AREA AND PROBABILITY OF NO PUNCTURES FOR A SELF-SEALING STRUCTURE CONCEPT	2-195
2-120	SUBSYSTEM PROBABLE SUCCESS HISTORY	2-196
2-121	LAUNCH CONFIGURATION JUPITER ORBITER WITH CLOSE SOLAR PROBE	2-198
2-122	INBOARD PROFILE, JUPITER ORBITING SPACECRAFT	2-202
2-123	INBOARD PROFILE CLOSE SOLAR PROBE	2-203
3-1	COMMUNICATION DISTANCE BETWEEN THE JOVIAN SATELLITE I AND THE ORBITING SPACECRAFT VS ELAPSED TIME AFTER PERIJOVE ESTABLISHMENT	3-5
3-2	RADAR DETECTION (JUPITER MOONS)	3-6
3-3	LAPLACE SPHERE OF INFLUENCE DOMAIN OF VALIDITY	3-7
3-4	LIBRATION POINT GEOMETRY	3-8
3-5	GEOMETRY OF THE OUT-OF-PLANE ENCOUNTER	3-10
3-6	SATURN V PERFORMANCE CAPABILITY FOR SATURN AND URANUS CAPTURE MISSION (JUPITER SWINGBY MODE)	3-14
3-7	ADVANCED CAPTURE DESIGN (SATURN OR URANUS)	3-15
3-8	SATURN AND URANUS CAPTURE	3-16
3-9	DEEP SPACE COMMUNICATIONS	3-17
3-10	ASTEROID-SPACECRAFT COMMUNICATION DISTANCE	3-18
3-11	VESTA DISTANCE OF CLOSEST APPROACH	3-20
3-12	ASTEROID BELT CIRCULARIZATION	3-21
3-13	JUPITER ORBITER/ASTEROID PROBE	3-22
3-14	CONCEPTUAL FAMILY DESIGNS	3-23
3-15	ADVANCED MISSION SUCCESS	3-25

LIST OF TABLES

<u>Table No.</u>	<u>Title</u>	<u>Page</u>
2-1	SENSITIVITY OF SOLAR PROBE ORBIT CHARACTERISTICS TO ERRORS IN JUPITER SWINGBY DISTANCE	2-58
2-2	1975 SATURN V JUPITER ORBITER/SOLAR PROBE TYPICAL MISSION SUMMARY	2-82
2-3	1975 SATURN V JUPITER ORBITER/SOLAR PROBE TYPICAL MISSION SUMMARY	2-83
2-4	EXPERIMENT REQUIREMENTS JUPITER ORBITER/SOLAR PROBES	2-91
2-5	COMMAND AND CONTROL GROUND-TO-SPACECRAFT LINK	2-99
2-6	EFFECTIVE NOISE TEMPERATURE	2-107
2-7	TELEMETRY SYSTEM PERFORMANCE JUPITER ORBITER	2-111
2-8	TELEMETRY SYSTEM PERFORMANCE CLOSE SOLAR PROBE	2-112
2-9	COMMUNICATION SYSTEM CHARACTERISTICS FOR JUPITER ORBITER/SOLAR PROBE	2-117
2-10	SOLAR DISTANCE LIMITATIONS	2-131
2-11	THERMOELECTRIC POWER SYSTEMS	2-136
2-12	MISSION POWER REQUIREMENTS	2-137
2-13	RELIABILITY AND MASS FOR ALTERNATE POWER SYSTEMS COMPARISON	2-142
2-14	ISOTOPE AVAILABILITY	2-147
2-15	MAGNITUDE OF DISTURBING FORCES	2-158
2-16	ATTITUDE CONTROL REQUIREMENTS-JUPITER ORBITER/SOLAR PROBE	2-162
2-17	REACTION GAS SYSTEMS FOR ATTITUDE CONTROL	2-167
2-18	REACTION GAS SYSTEM MASS	2-170
2-19	PROBABILITY OF JUPITER ORBITER SUCCESS FOR 600-DAY MISSION	2-175
2-20	PROBABILITY OF CLOSE SOLAR PROBE SUCCESS FOR 1200-DAY MISSION	2-176
2-21	NUMBER OF SPACECRAFT REQUIRED TO ACHIEVE DESIRED SUCCESS PROBABILITY FOR JUPITER ORBITER/SOLAR PROBE	2-177
2-22	SEQUENCING DUPLICATE SYSTEMS TO ACHIEVE DESIRED MISSION SUCCESS	2-187

LIST OF TABLES (Concluded)

<u>Table No.</u>	<u>Title</u>	<u>Page</u>
2-23	SUBSYSTEM SUCCESS PROBABILITIES	2-197
2-24	MASS SUMMARY	2-201
3-1	SELECTED PHYSICAL AND ORBITAL PARAMETERS OF THE JOVIAN SATELLITE SYSTEM	3-3
3-2	COMPARISON OF SPHERE OF INFLUENCE CONCEPTS	3-11
3-3	EXTENSIVE EXPLORATION PROGRAM	3-26
3-4	NUMBER OF SPACECRAFT	3-27

GENERAL SUMMARY

A preliminary mission and systems analysis of a combined Jupiter orbiter/solar probe (close solar flyby at typically 0.1 AU) payload utilizing the Saturn V launch vehicle was conducted with a twofold purpose:

1. To determine the technical feasibility of such an application of the Saturn V based on Jupiter gravity-assist to establish the solar probe orbit, and
2. To define the principal characteristics of the combined mission in terms of flight profile, trajectories, launch windows, capture orbit parameters, mission performance, scientific experiments, systems requirements, and conceptual spacecraft designs.

The conceptual spacecraft designs were based on maximum utilization of existing hardware. In parallel to this study, several investigations were conducted in related advanced mission areas including: Jovian moon exploration, outer planet missions via Jupiter swingbys, and exploration of the asteroids in conjunction with Jupiter missions.

The results of the study indicate that the Jupiter orbiter/solar probe mission is a potentially attractive application of the Saturn V launch vehicle to unmanned scientific exploration of the solar system. The entire study, including the advanced mission investigations, is summarized in the following paragraphs.

MISSION ANALYSIS

A mission analysis was performed to define the Jupiter orbiter/solar probe mission concept in terms of the overall space vehicle concept, flight profile, and sequence of events. The flight mechanical and performance characteristics of the mission were established within the constraints imposed by communications requirements, launch and parking orbit operations, launch vehicle performance capability, scientific experiment requirements, and spacecraft design characteristics.

The space vehicle is composed of the three-stage Saturn V and the combined Jupiter orbiter/solar probe spacecraft mounted above the Instrument Unit and shrouded by a standard 260-inch nose fairing during boost through the atmosphere. Launch is from the Atlantic Missile Range (AMR) with launch azimuths typically between 70° and 110° . A second burn of the S-IVB third stage injects the spacecraft out of a low Earth parking orbit into a fast (typically 500 to 550 days) Earth-Jupiter transfer. Upon arrival at Jupiter's sphere of influence, the solar probe is separated from the orbiter and continues on a swingby trajectory about the planet. The post-encounter heliocentric trajectory, produced by the swingby, takes the solar probe on a close flyby of the Sun (typically at 0.1 AU). The orbiter is maneuvered for a close approach to Jupiter to establish a capture orbit by single-impulse, propulsive braking. A typical capture orbit has a perijove (r_p) of 1.1 Jovian radii and an apsidal ratio (r_a/r_p) of about 40. Experiments data are transmitted to Earth from the orbiter in capture orbit, and from both the orbiter and solar probe during all phases of heliocentric flight, especially from the probe during solar flyby.

An important characteristic of the combined Jupiter orbiter/solar probe mission is that a relatively fast Earth-Jupiter transfer is required to achieve a post-encounter solar probe orbit with a perihelion close to the Sun. The perihelion distance of interest is of the order of 0.1 AU. The study showed that the required Earth-Jupiter transfer times generally range between 500 and 600 days. For a given transfer time, the combined effects of Earth departure and Jupiter arrival energies are such that the best mission performance opportunities occur during the 1972-1976 time period. However, the effect of higher arrival energies early and late in the decade leads to a tradeoff between mission performance and the solar probe orbit characteristics that are strongly dependent upon the Earth-Jupiter transfer time. The overall result, from a total mission standpoint, is that adequate Saturn V performance capability exists for reasonable launch periods during all opportunities across the 1970-1980 decade. Launch opportunities are available approximately every 13 months.

A Jupiter gravity-assisted solar probe orbit that passes close to the Sun at perihelion requires that the Jupiter swingby be retrograde with respect to the planet. Two factors determine the characteristics of the solar probe orbit: (1) The Jupiter arrival conditions in the Earth-Jupiter transfer trajectory, and (2) The aim point at the Jovian sphere of influence. The arrival conditions are a function of launch date and Earth-Jupiter transfer time. The aiming point is defined by the inclination of the Jupiter encounter hyperbola and the swingby distance. An analysis was performed to interrelate the solar probe orbit characteristics with the above parameters. For three representative launch opportunities, 1972, 1975, and 1978, the perihelion distance, total trip time from launch to solar flyby, and orbit inclination with respect to the ecliptic plane were determined for launch periods up to 50 days. Typical results for 1975 with 500-day Earth-Jupiter transfers and a 20-day launch period were as follows: For a 0.1-AU perihelion distance, the trip time from launch to perihelion was 1090-1155 days; the orbit inclination was about 21° ; and the required Jupiter swingby distance varied from 6.7 to 9.9 Jovian radii across the launch period.

An analysis of the communication distance and geometry associated with the Earth-Jupiter trajectory showed that the orbiter must be designed for a maximum communication distance of about 6 AU. An Earth-spacecraft line-of-sight occultation by the Sun at Jupiter arrival is not a problem for the Jupiter orbiter/solar probe mission. An analysis was performed to determine if the solar probe during solar flyby at perihelion would be able to communicate with the Earth. For typical solar probe orbit geometry and probe antenna characteristics, it was determined that favorable heliocentric Earth positions would exist for communications during a representative 1975 mission. It should be noted, however, that the spacecraft may store data during the solar flyby for later transmission to Earth.

A study of the planetary guidance requirements, from a mission analysis standpoint, indicated that achieving a solar probe orbit via the Jupiter swingby mode should not present any real problems in utilization of existing guidance techniques. The solar probe orbit is designed on the basis that no midcourse corrections will be made in the post-encounter heliocentric trajectory. Therefore,

the accuracy of the solar probe orbit is determined by the accuracy of the Jupiter swingby trajectory. For constant Earth-Jupiter transfers, the solar probe orbit perihelion distance, trip time, and inclination are relatively insensitive to errors in Jupiter swingby distance. An allowable error appears to be on the order of ± 0.5 Jovian radii ($\pm 35,000$ km) for a typical 0.1-AU mission. By proper variation of Earth-Jupiter transfer time over the launch period, the error in perihelion distance relative to swingby distance error can be made very small. A swingby distance error of 3 or 4 planet radii could be allowed with little effect on the perihelion. The associated variances in trip time and orbit inclination would be much larger; however, these parameters should not be as important to the mission objectives as the perihelion distance at solar flyby. A total midcourse velocity correction budget of 150 m/sec was estimated for the mission. An analysis of the Jupiter approach maneuver performed by the orbiter spacecraft after separation of the solar probe, indicated a typical ΔV requirement of about 200 m/sec.

A digital computer program was used to analyze the Earth surface launch window characteristics for the Jupiter orbiter/solar probe mission. For fast Earth-Jupiter transfers and typical launch periods, the declination of the out-going geocentric asymptote over the 1970-1980 decade varies between approximately $\pm 30^\circ$. Therefore, the daily surface launch windows from AMR present no difficulties. For a $70-110^\circ$ range in launch azimuth, two daily windows of 5-hours duration each are available for typical 1975 missions. The 1978 opportunity is representative of the worst launch window conditions during the decade. However, for $70-110^\circ$ launch azimuths, two daily windows of 2.6- to about 5-hours duration are available across the launch period.

An analysis of the characteristics of Jovian capture orbits was made based on single-impulse, propulsive braking at the periapsis of the approach hyperbola. For a given capture apsidal ratio ($n = r_a/r_p$), there exists an "optimum" perijove radius that minimizes the required braking ΔV_B as a function of arrival energy. However, for the ranges of arrival energies and apsidal ratios under consideration, the ΔV_B penalties for fixed perijove distances near the planet are small. A typical capture orbit chosen for the Jupiter orbiter mission has an apsidal ratio of 40 and a perijove radius of 1.1 planet radii. The ΔV_B for a representative arrival speed of 0.4 EMOS* is about 2 km/sec. For the apsidal ratios (20 to 40) of interest, the capture orbit period ranges from 4 to about 20 days for perijove radii from 1.1 to 1.5 planet radii.

Parametric mission performance data were generated for the three representative launch opportunities - 1972, 1975, and 1978. Mission mass histories were developed based on a solar probe mass (1400-lb) specified by the systems analysis and given capture orbits defined by perijove radius and apsidal ratios. Net injected mass at Earth departure and gross capture mass at Jupiter are presented as functions of departure date across launch periods during each of the three representative years. Data are given for Earth-Jupiter transfer times from 500 to 600 days. These data must be correlated with the parametric solar probe orbit data to arrive at missions that satisfy performance, trajectory, and systems requirements and constraints. Mission performance/solar probe orbit tradeoffs are illustrated for the 1978 opportunity for a 0.1-AU solar flyby.

* Earth Mean Orbital Speed (29.78 km/sec)

On the basis of the parametric mission analysis data the characteristics of representative Jupiter orbiter/solar probe missions may be determined. A typical 0.1-AU solar flyby mission during the 1975 launch opportunity is summarized as follows:

1975 SATURN V JUPITER ORBITER/SOLAR PROBE TYPICAL MISSION SUMMARY

LAUNCH PERIOD:

20 Days, 17 June - 7 July 1975
(Julian 244-2580.5 - 244-2600.5)

DAILY WINDOWS:

Two Daily 5-Hr Windows with 70-110°
Launch Azimuths from AMR

EARTH-JUPITER TRANSFER: 500 Days

Net Injected Wt: 12,000 - 14,000 Lb
(Across Launch Period)

JUPITER ENCOUNTER:

Capture Orbit: $n = 40$, $r_p = 1.1$ Jovian Radii
Gross Capture Wt: 4400 Lb
Solar Probe Swingby Distance: 6.7-9.9 Jovian Radii
Solar Probe Wt: 1400 Lb

JUPITER-SUN TRANSFER: 590-655 Days

Perihelion Distance: 0.1 AU
Inclination to Ecliptic: 21 Deg
Total Time from Earth Departure to Perihelion:
1090-1155 Days

SYSTEMS ANALYSIS

Based on a detailed experiment survey completed by Northrop and documented in reference 3, tables of instruments, power requirements, and masses were developed for the Jupiter orbiter and close solar probe experiments. These are summarized on the following page:

JUPITER ORBITER/SOLAR PROBE EXPERIMENTS

Phenomenon to be Investigated	Total Power		Total Mass	
	Jupiter Orbiter	Solar Probe	Jupiter Orbiter	Solar Probe
Solar Plasma	17.0 watts	26.0 watts	15.5 kg	11.8 kg
Magnetic Fields	13.3	13.3	4.4	4.4
Trapped Radiation	0.8	0.8	2.0	2.0
Solar Neutrons	---	2.0	---	6.8
Cosmic Radiation	2.0	2.0	6.8	6.8
Electromagnetic Fields	5.0	5.0	8.6	8.6
Particulate Matter	40.0	5.0	13.6	4.6
Jupiter Ionsphere	14.0	---	14.1	---
Jupiter Atmosphere	233.0	---	97.0	---
Jupiter Moon Surface	469.0	---	234.5	---
TOTALS	794.1 watts	54.1 watts	396.5 kg	45.0 kg

The usefulness of the instruments to observe the surface of Jupiter moons is dependent upon the approach distance to those bodies. For Jupiter capture orbits of low perijove and high eccentricity, an analysis was conducted to determine the minimum line-of-sight distance to the four largest moons. Depending on the capture orbit parameters, approaches ranging from 3 to 5 Jupiter radii are easily achieved. However, to use radar surface imaging devices capture orbits must be selected which permit Jupiter moon approaches of less than about 0.05 Jovian radius.

NASA's stated policy of planetary quarantine was applied to the Jupiter orbiter/solar probe mission. Spacecraft impact on bodies in the solar system is not planned. However, the possibility of spacecraft system malfunctions leading to collision with Jupiter or one of its moons must be considered.

Since heat sterilization is very effective, the concept of heating the Jupiter orbiter and solar probe enroute to Jupiter was briefly studied. Based on JPL data for the Voyager landing capsule sterilization, a time-temperature sterilization cycle was determined. If this extrapolation is valid, the spacecraft on this mission must be heated to 330°K for complete sterility at Jupiter encounter. This does not appear possible. High reliability must be maintained in the program to preclude malfunction and loss of Earth-based control of the trajectory, and thereby avoid contaminating the solar system bodies associated with the mission.

The Saturn V exhibits a relatively large variance in launch capability for the mission during a finite launch period. This can be used in a number of ways including: (1) a fixed gross launch payload, sized for the launch period, could be launched using the excess Saturn V capability to reduce the trip time, (2) a fixed trip time could be selected and the vehicle gross launch mass modified daily by varying the Jupiter capture orbit braking propellant loading, or (3) a fixed

September 1966

capture orbit perijove could be selected for scientific reasons and the gross launch mass of the spacecraft modified daily by varying the capture orbit braking propellant loading. These modes were compared for Jupiter capture orbit parameters and Saturn V launch guidance requirements.

The capture orbits, vary, but not significantly, for these modes. The fixed gross launch mass concept, utilizing a constant propellant loading, offers ease in orbiter spacecraft design, testing, and launch operation and can achieve capture orbits of high eccentricity and low perijove. This mode appears to be the best choice from a systems viewpoint. The launch guidance requirements during a particular launch window are not affected by selecting one or the other mode. The declination of the outgoing geocentric asymptote is almost identical for either the fixed-gross-mass trajectory or the constant-trip-time trajectory.

A study was undertaken to estimate the reliability expected for the Jupiter orbiter and solar probe during the next decade. On the basis of extrapolations of current and completed program histories and accounting for redundancies, the probabilities of successful launch, electronics and other spacecraft subsystems successes, and probabilities of avoiding collision with asteroids were developed. Total spacecraft reliability was determined and the number of launches required to achieve given program success levels were computed. These data are summarized below. It is concluded that for a program initiated early in the next decade, about 3 spacecraft must be launched to achieve a mission success greater than .90.

SPACECRAFT RELIABILITY IN 1970-1980 TIME PERIOD

Year	Probability of Success of Jupiter Probe	Probability of Success of Solar Probe	Probability of Success per Launch	Mission Success Goal	Number of Spacecraft in Program
1968	.840	.771	.648	.90	3
1970	.876	.870	.718	.90	2
1972	.899	.853	.768	.90	2
1974	.966	.865	.836	.90	2
1976	.969	.873	.846	.90	2

On the assumption of operation at S-band frequencies utilizing the 64-meter antenna at Goldstone, the theoretical tradeoffs were developed for spacecraft power, antenna size, and data transmission rates. Parametric data were computed for the range of antenna sizes and power levels postulated for the Jupiter orbiter and solar probe conceptual designs. An important factor influencing this analysis was the space propagation losses that were computed for different antenna sizes and communication distances. An omnidirectional system was included for use as a reference. Superimposed on these losses is the system degradation due to background noise. The various sources of noise in the galaxy, the solar system, and on the Earth were analyzed and the received signal degradation estimated. It was concluded that for the Jupiter orbiter, 20 to 30 db signal loss due to background noise must be accounted for. Communication with the solar probe in the direct vicinity of the Sun will be difficult. However, with high-power transmission at the relatively short communication distance, and by storing data for re-transmission

at more favorable times, a high probability of data return can be expected of the solar probe. System parameters were defined for application to the spacecraft conceptual design. Using 40 watts r.f. power, 4.5-meter and 2-meter diameter antennas were used for the Jupiter orbiter/solar probe, respectively, to maintain positive net operating signal noise margins.

Because of the long mission lifetimes for both the Jupiter orbiter and the solar probe spacecraft, passive thermal control is desirable. In the deep-space regions of the solar system, it will be necessary to heat many systems aboard the spacecraft to maintain their operating temperatures. A spacecraft energy balance was made assuming superinsulation around critical areas and the availability of electrical power for make-up resistance-type heaters. Under normal modes of operation considerable excess power is available from the radioisotope power supply (RTG) units to thermally control both spacecraft. In the event one of the multiple RTG units fails, the Jupiter orbiter spacecraft will still be capable of maintaining thermal control with a reasonable amount of insulation. Under emergency conditions for the solar probe, the available power is marginal and about 8-cm of superinsulation will be necessary to maintain the required internal temperatures.

At close distances to the Sun, it will be necessary to shield the solar probe. A shadow shield was developed consisting of a conical primary shield and a secondary flat shield separated by a low-conductive structure. The second flat shield forms the base of the spacecraft which is confined within the shadow of the primary shield. The shield and spacecraft temperatures depend on many parameters including the length-to-diameter ratio of the cone, size of the shadow shield, separation distance between primary and secondary shields, material characteristics, and distance from the Sun. Typical configurations and surface temperatures appropriate for conceptual design were analyzed. It was concluded that using titanium primary shields, solar approaches down to about 0.1 AU are possible with passive shadow shield thermal control. To determine the degree of accuracy required for orientation of the shadow shield, a thermal analysis was made of a typical spacecraft for a variety of time-dependent misalignments. For short-duration excursions out of the shadow cone, spacecraft transient temperatures will be tolerable if the misalignment angles do not exceed 5°. Based on the attitude control studies, this appears to be easily achieved.

The long durations of the Jupiter capture and solar probe missions imply that radioisotope power supplies are required. Of the units which are currently under study, only two types closely match the power requirements of the spacecraft: (1) Po-210-fueled units which have too short a lifetime and (2) the Pu-238-fueled units. Passively and actively cooled RTG concepts are being considered by the AEC. To select the power supply units, power profiles were developed for the Jupiter orbiter and solar probe spacecraft to show the variance in power requirements for different phases of the mission. For the Jupiter orbiter, the use of three 250-watt passively cooled Pu-238 units will provide enough power for all phases of the mission. Should one unit fail, the remaining two RTG units will permit completion of the mission if some of the higher power experiments are shut off. The solar probe requires two of the passively cooled Pu-238 units and will also be able to complete its mission with one RTG unit out. The use of multiple passively cooled radioisotope units offers the advantages of redundancy, high reliability, capability of mission completion on partial power, and small total mass systems.

September 1966

A number of propulsive functions exist for the Jupiter orbiter and solar probe spacecraft. Besides the conventional requirement for attitude control, there are midcourse corrections and a planetary braking maneuver to be performed. The capture orbit braking propulsion system must remain dormant during the long transfer time to Jupiter. A study was performed to compare various liquid propellant combinations. Cryogenic systems cannot be economically stored for the required mission duration with present technology. The "storables", however, exhibit little degradation in performance if it is assumed they are not permitted to freeze. Use of excess RTG power to heat the propellant tanks was considered. Assuming that superinsulation is used around the tanks, it was concluded that a very nominal power drain is required to make up the heat lost by radiation from the spacecraft. To conform to a study groundrule of using existing systems as much as possible, the Apollo LEM ascent-stage engine and associated hardware was used in the conceptual design of the Jupiter orbiter. N_2O_4/N_2H_4 - UDMH storable propellants are used with this engine and this system will be used for both Jupiter capture and midcourse corrections.

The total attitude control impulse requirements were estimated for the spacecraft. Typical moments of inertia were used; therefore, the results may change if detailed mass and balance analyses are conducted for a specific spacecraft. On the basis of these typical values, mass tradeoffs of cold gas and monopropellant attitude control systems were performed. For the larger spacecraft (the Jupiter orbiter), a monopropellant system offers significant mass savings. For the solar probe, the distinction is less severe, and to minimize the propellant tank requirements, a monopropellant system was also chosen for use on the conceptual design. The propulsion systems selected for attitude control and midcourse correction were summarized for each spacecraft. The Jupiter orbiter can logically use both low-thrust and high-thrust attitude control systems due to the extreme differences in torque requirements during heliocentric coast and for propulsive maneuvers such as capture orbit braking. During this latter maneuver, thrust misalignment torques of the high-thrust capture propulsion system must be reacted with high accuracy.

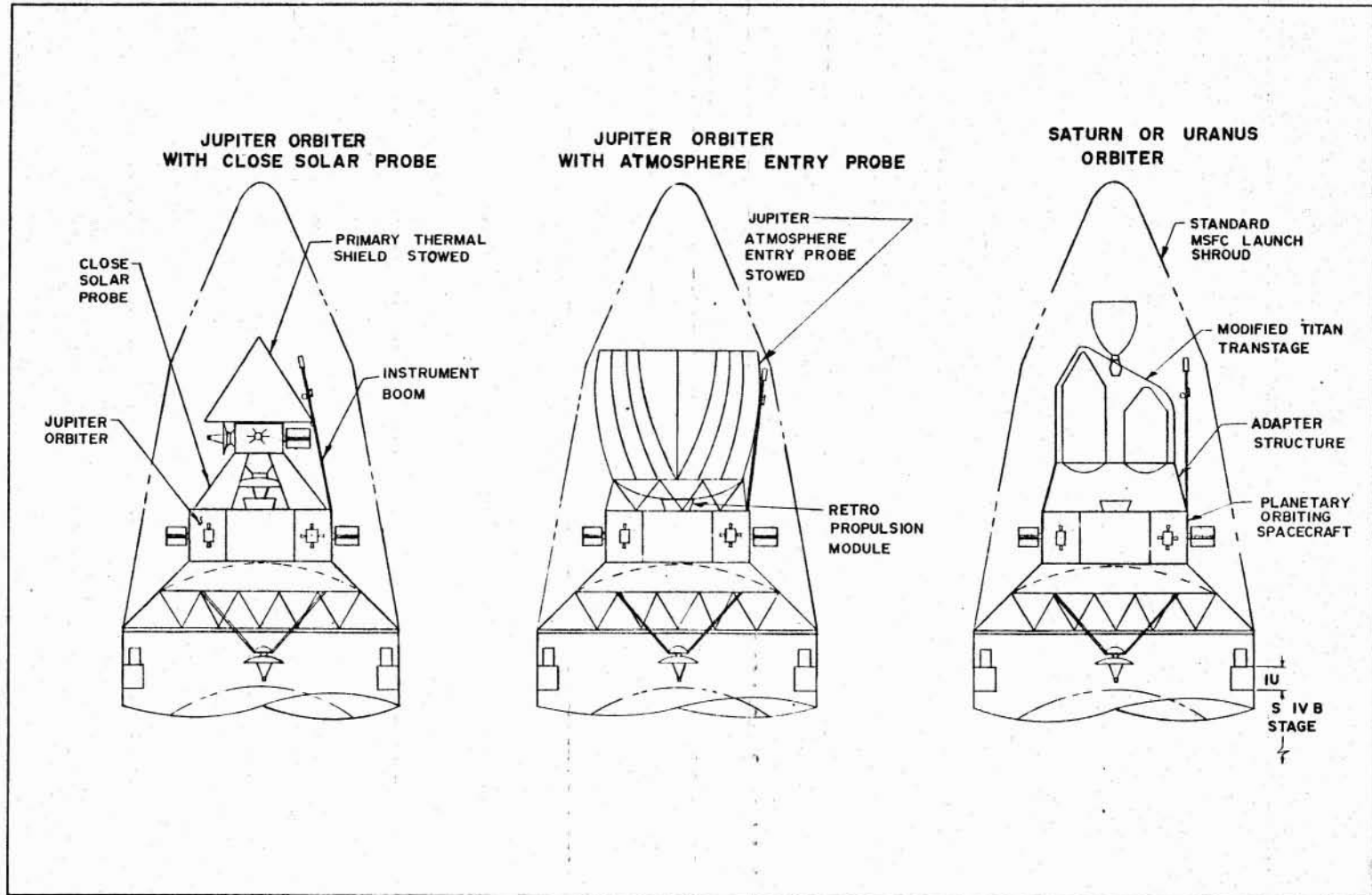
ADVANCED MISSIONS

The advanced mission portion of the study includes consideration of Saturn and Uranus capture missions via Jupiter gravity-assist, exploration of the Jovian satellite system (specifically the inner moons) during a Jupiter mission, and inspection of regions of the asteroid belt. To accomplish these missions a family of spacecraft is defined which uses a Jupiter orbiter as a basic module. The advanced mission configurations, and the data on which they are based, must be considered preliminary at this time as many important aspects of their development must be studied in detail. One such aspect is the effect of a finite launch period requirement.

Notwithstanding the cursory analysis of some aspects of the mission under consideration, several significant conclusions can be reached. They include:

1. Meaningful inspection of the Jovian moons during a Jupiter capture mission will require close passes to the moons. The present technique of the mission analyst in dealing with such trajectories, that of the patched conic approach, is inadequate for the Jovian satellite system.
2. Communication with acceptable data transmission bit rates is feasible for S-band systems of the Jupiter orbiter spacecraft design anywhere in the solar system out to and including the orbit of Uranus.
3. Inspection of some regions of the asteroid belt is an acceptable secondary mission via a Jupiter swingby mode, but due to the inclination and diameters of most of the asteroids an inspection enroute to Jupiter will not be possible.
4. A family of spacecraft utilizing the Jupiter orbiter as a basic module can be designed to provide an extensive exploration program including the Jupiter capture mission and advanced missions such as a combined Jupiter orbiter/atmospheric probe, Jupiter orbiter/solar probe, Saturn or Uranus capture, and asteroid belt missions. The latter three missions utilize a Jupiter gravity-assist mode. The figure on the next page illustrates three such design concepts for the Jupiter orbiter/solar probe, Jupiter orbiter/atmospheric entry probe, and the Saturn or Uranus capture mission.
5. Due to the long lifetime required in some advanced mission concepts, extrapolation of present subsystems reliability indicates that a reasonable mission success goal would require multiple Saturn V launches.

FIG. 1



ADVANCED MISSION SPACECRAFT CONCEPTS BASED ON COMMON UTILIZATION OF JUPITER ORBITER

SECTION I

INTRODUCTION

This document presents the results of a continuing study of the potential utilization of the Saturn V launch vehicle for unmanned scientific exploration of the solar system. The initial phase of this effort was reported in reference 1 which presented an analysis of straightforward Jupiter capture missions based on maximum use of existing spacecraft hardware from the Apollo program. The report included a cursory investigation of the feasibility of a Jovian atmosphere probe launched from the orbiter spacecraft. Also, a preliminary analysis was given to indicate the Saturn V performance potential for advanced missions employing Jupiter gravity-assisted transfer trajectories.

In reference 1 it was shown that it is possible to accomplish the basic scientific objectives of a Jupiter capture mission with significantly less payload than the Saturn V launch system affords. For relatively slow Earth-Jupiter transfers and highly eccentric capture orbits, payloads of several thousand pounds are available while only several hundred pounds are required for the basic scientific package. This suggested the possibility of combining an additional payload with the orbiter to create a dual mission with one Saturn V launch. One possibility for such a mission, with considerable scientific value, is a combined Jupiter orbiter/close solar probe payload.

Section II of this report presents the results of a mission and systems analysis to determine the feasibility of a combined Jupiter orbiter/solar probe payload based on the Saturn V launch capability. The close solar probe orbit is established by a Jupiter swingby after separation of the probe from the orbiter spacecraft prior to planet encounter. Section III gives the results of studies in several related advanced mission areas including: Jovian moon exploration, outer planet missions via Jupiter swingbys, and exploration of the asteroids in conjunction with Jupiter missions.

The results of recent studies of the flight mechanics, entry heating, and systems aspects of a Jovian atmosphere probe launched from an orbiter spacecraft are reported in a separate document: "A Study of a Jovian Atmospheric Probe," TR-292/3-6-076, Northrop Space Laboratories, September 1966.

SECTION II

JUPITER ORBITER/SOLAR PROBE MISSION

2.1 MISSION ANALYSIS

The planet Jupiter and the near region about the Sun within 0.2 AU are two prime targets for unmanned solar system missions during the next decade. Jupiter, the nearest of the outer planets and the largest planet in our solar system, has long been of great scientific interest but beyond existing mission capabilities. Scientific investigations of the very heart of the solar system, the Sun, have been limited to Earth-based studies and experiments conducted with probes at relatively large solar distances. Several important solar experiments, however, will require a very close flyby of the Sun at a distance on the order of 0.1 AU. Unfortunately, the launch energy required to achieve a 0.1 AU solar flyby directly from the Earth is prohibitive for existing chemical launch systems.

The mission considered in the present study utilizes the high-energy launch capability of the Saturn V vehicle and the strong gravitational field of Jupiter for solar probe trajectory shaping to accomplish both a Jupiter capture and a close flyby of the Sun with a single launch. Thus, it is possible to satisfy the objectives of two key solar system missions with a single mission and the potential scientific payoff is quite attractive.

In the mission analysis to follow, the Jupiter orbiter/solar probe concept is defined in terms of the overall space vehicle concept, flight profile, and sequence of events. The flight mechanical and performance characteristics of the mission are established within the constraints imposed by communications requirements, launch and parking orbit operations, launch vehicle performance capability, spacecraft design characteristics, and scientific experiment requirements. During the study the flight mechanical and performance data were correlated with the spacecraft systems analyses (presented in subsection 2.2) to arrive at conceptual orbiter and solar probe designs satisfying all mission requirements and constraints.

2.1.1 Mission Ground Rules

The ground rules given as a basis for this study are as follows:

1. All missions are to be unmanned.
2. Launch opportunities are to be considered during the 1970-1980 decade.
3. The basic mission is to be a straightforward capture into an elliptical orbit about Jupiter with a probe continuing on a swingby through the Jovian gravitational field to achieve a near flyby of the Sun.
4. The launch vehicle is to be the basic Saturn V as developed for the Apollo program.
5. Utilization of Apollo spacecraft hardware is desirable. As other systems are required, maximum use is to be made of existing hardware.

2.1.2 Mission Concept

2.1.2.1 Space Vehicle Concept. The space vehicle configuration for the mission is shown in Figure 2-1. The launch vehicle is the three-stage Saturn V as developed for the Apollo lunar landing program. The spacecraft is composed of the Jupiter orbiter and solar probe attached together and mounted above the Saturn Instrument Unit by an adapter truss structure. The spacecraft is shrouded by standard 260-inch MSFC nose fairing during boost through the atmosphere. Figure 2-2 illustrates the spacecraft configuration just after separation of the solar probe from the orbiter prior to Jupiter encounter. The details of the spacecraft conceptual designs are covered in subsection 2.3.

2.1.2.2 Mission Profile. The mission is initiated with launch of the Saturn V vehicle from the Atlantic Missile Range. After a short coast in low Earth parking orbit, a second burn of the S-IVB third stage injects the combined Jupiter orbiter/solar probe spacecraft into a fast (typically 500-550 days) Earth-Jupiter transfer trajectory. During the heliocentric coast to Jupiter, measurements of the interplanetary environment are made and transmitted to Earth in addition to the spacecraft systems monitoring data. Two, or possibly three, midcourse corrections aim the spacecraft at the planned planetary approach point at Jupiter's sphere of influence. At this point the solar probe is separated from the orbiter and continues on a swingby trajectory passing Jupiter at several planet radii. The midcourse propulsion system aboard the orbiter is used to maneuver the vehicle in for a relatively close approach to Jupiter. At the periapsis of the approach hyperbola, the main braking engine is fired to place the orbiter into a highly elliptical capture orbit about the planet. The orbiter begins its programmed experiments in orbit. Meanwhile the solar probe has continued on its pass through the Jovian gravitational field to emerge from the sphere of influence on a reshaped heliocentric trajectory designed to send the probe by the Sun at a very close distance. The probe coasts on the post-encounter trajectory, generally with relatively large inclination to the ecliptic plane, transmitting experimental and systems data on command. During the close solar flyby, at a perihelion on the order of 0.1 AU, key experimental measurements are made and transmitted to Earth.

Figure 2-3 illustrates the mission profile. A detailed sequence of events is given in the next subsection.

2.1.2.3 Sequence of Events. The operational aspects of the nominal mission profile are outlined by the following sequence of events:

1. Launch from the Atlantic Missile Range with Saturn V to a 185-km circular Earth parking orbit. The vehicle flies a two-dimensional ascent trajectory utilizing a sub-orbital start of the S-IVB third stage.
2. Coast in parking orbit up to one orbital period until the proper position is attained relative to the outgoing geocentric asymptote of the required escape hyperbola.
3. Re-ignite the S-IVB stage for injection into the heliocentric transfer trajectory. Jettison S-IVB, Instrument Unit, and spacecraft adapter and initiate automatic attitude stabilization. Search and target acquisition mode is initiated for Earth sensors and star trackers. Interplanetary experiments are initiated.

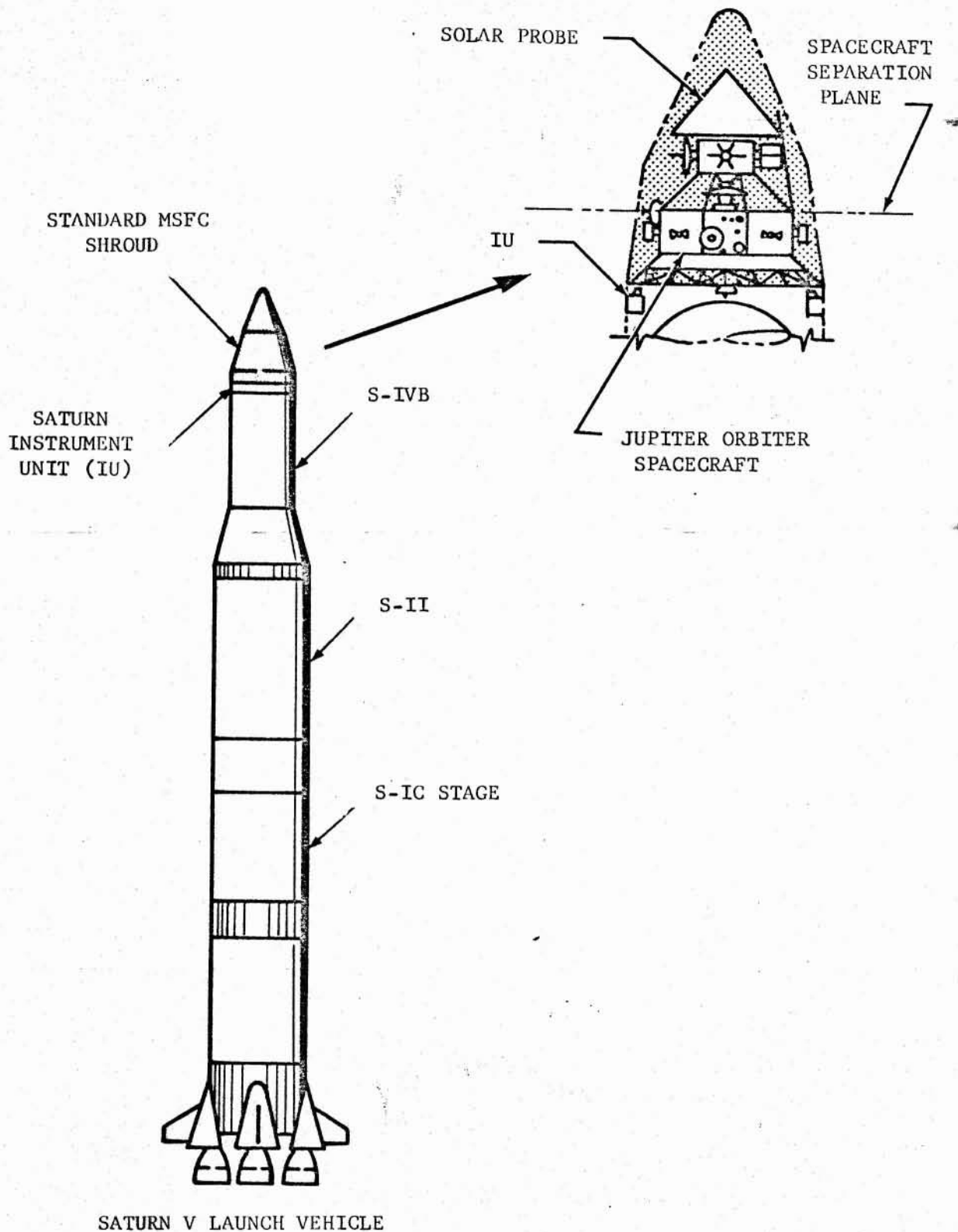


Figure 2-1. SPACE VEHICLE CONFIGURATION

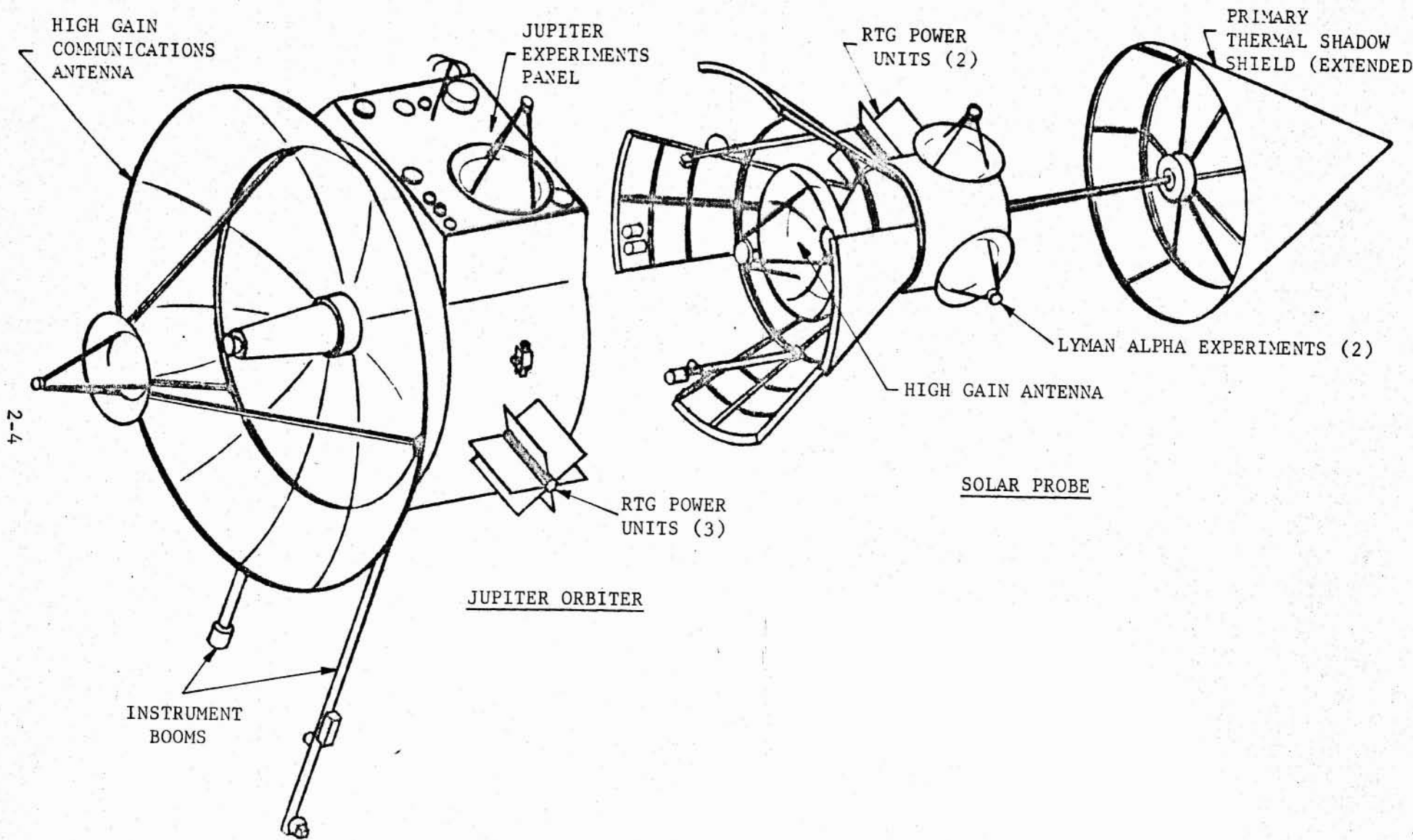
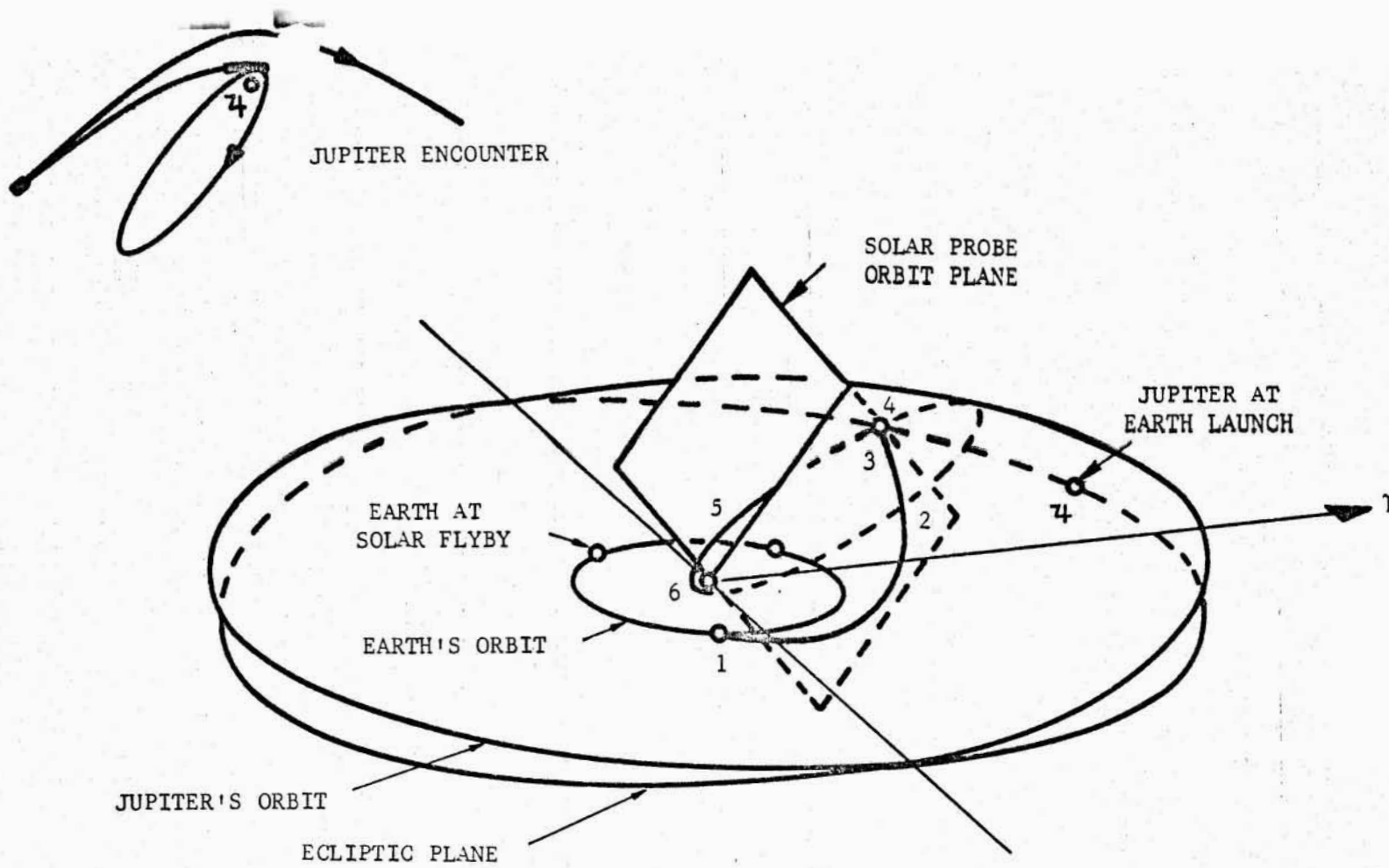


Figure 2-2. JUPITER ORBITER/SOLAR PROBE CONCEPT



2-5

1. LAUNCH FROM AMR THROUGH 185-KM PARKING ORBIT
2. EARTH-JUPITER TRANSFER; 500-550 DAYS
3. SEPARATION OF SOLAR PROBE FROM ORBITER; MANEUVER ORBITER FOR CLOSE APPROACH TO JUPITER
4. ESTABLISH CAPTURE ORBIT; SOLAR PROBE CONTINUES ON SWINGBY
5. JUPITER-SUN TRANSFER; 500-1000 DAYS
6. SOLAR FLYBY AT .1 AU

Figure 2-3. JUPITER ORBITER/SOLAR PROBE MISSION PROFILE

TR-292/3-6-075

September 1966

4. Regular transmission is made of housekeeping data for orbiter and solar probe and interplanetary experiments data during heliocentric coast mode.
5. The first midcourse correction is executed at 10 days after injection. Spacecraft returns to heliocentric coast mode.
6. Canopus cone angle is up-dated at 100-day intervals.
7. Second midcourse correction is executed at approximately 330 days after injection.
8. Transmit from Earth the separation maneuver data to spacecraft computers and initiate separation sequence programmer and times upon arrival at the Jovian sphere of influence.
9. Perform separation including Jupiter orbiter approach maneuver using midcourse propulsion system.
10. Solar probe establishes heliocentric coast orientation with solar and Canopus lock. During Jupiter swingby, Sun occultation may occur and solar lock must be reacquired.
11. Activate main braking propulsion system aboard the orbiter vehicle for Jovian capture. Ignite mainstage propulsion for retro maneuver. Tracking from Earth verifies Jovian orbit.
12. On-station experimentation is initiated in capture orbit and data is stored for later transmission. On-board sensors maintain proper vehicle orientation with respect to Jupiter.
13. At pre-programmed time (probably near apojove) the orbiter terminates experiments, initiates search mode, acquires Earth, and transmits stored data. Experiment-on mode is re-established.
14. If, for a particular mission it is determined that a close approach to a Jovian moon will occur, the orbiter will be commanded to proper attitude and the television system activated for a specified period of time during moon encounter. Automatic return to coast mode is followed by transmission of images to Earth.
15. Depletion of attitude control propellants marks end of useful orbiter life.
16. After Jupiter encounter the solar probe begins return heliocentric coast and regularly transmits housekeeping and experiments data.
17. At approximately 0.6 AU from the Sun, the solar probe breaks Canopus lock and begins a controlled orientation toward the Sun.
18. Experiments data are transmitted during favorable geometric constellations throughout solar flyby. Depletion of attitude control propellants after closest solar approach marks end of probe usefulness.

2.1.3 Heliocentric Trajectory Analysis

The Jupiter orbiter/solar probe mission, from a flight mechanics standpoint, can be analyzed in four phases:

1. The geocentric or Earth-launch phase,
2. The Earth-to-Jupiter heliocentric phase,
3. The planetocentric phase at Jupiter, and
4. The post-encounter, Jupiter-Sun phase of the solar probe heliocentric orbit.

This subsection presents an analysis of the heliocentric phase of flight (2. and 4. above). The heliocentric trajectories are considered first since their characteristics must be known before the geocentric and planetocentric flight for the mission can be completely analyzed.

2.1.3.1 Earth-Jupiter Transfers. As will be shown later, the characteristics of solar probe orbits based on Jupiter swingbys are dependent essentially on two factors:

1. The Jupiter arrival conditions in the Earth-Jupiter transfer trajectory, and
2. The aiming point at the Jovian sphere of influence.

The complete Earth-Jupiter transfer trajectory, including arrival conditions, may be determined for a specified pair of Earth-departure and Jovian-arrival dates. The procedure is to analytically determine the Keplerian heliocentric ellipse that: (1) contains the positions of the planets on the specified dates, and (2) satisfies the timing defined by the difference between the two dates (transfer time). This procedure is ideally suited to high-speed computer handling.

Reference 2 contains the tabular results of extensive, systematic computer computations of Earth-Jupiter transfer trajectories for the 1970-1980 time period. This work was used as a source for the basic transfer data required to analyze the Earth-Jupiter leg of the Jupiter orbiter/solar probe mission.

Of fundamental importance to the mission analysis are the Earth-departure and Jupiter-arrival energies associated with the heliocentric trajectories. During each launch opportunity that occurs once for each synodic period (approximately 13 months), a period of consecutive days exists during which the departure energy requirements are within the Saturn V capability. A direct measure of the departure energy is the so-called hyperbolic-excess speed, V_{HE} , at Earth escape. This quantity is the speed the spacecraft must have relative to the Earth in excess of that required to escape onto a given transfer trajectory. The departure energy is sometimes expressed by the parameter C_3 defined as twice the total spacecraft energy per unit mass where $C_3 = V_{HE}^2$.

The energy of the spacecraft with respect to Jupiter at arrival is measured by the hyperbolic-excess speed at arrival, V_{HP} . This is the speed of the spacecraft relative to Jupiter at entry into the planet's sphere of

influence. The performance requirements for Jovian capture and the characteristics of the post-encounter solar probe orbit are dependent on the magnitude of V_{HP} .

Based on the data of reference 2, Figure 2-4 presents the variation of the departure and arrival hyperbolic-excess speeds over the 1970-1980 decade for 500-day Earth-Jupiter transfers and typical 20-day launch periods. As will be shown later, relatively fast (typically 500 550-day) transfers are required for the combined Jupiter orbiter/solar probe mission. The hyperbolic-excess speeds are shown in Figure 2-4 as a fraction of the Earth mean orbital speed (EMOS = 29.78 km/sec). The variation of arrival speeds is seen to be much more pronounced over the decade than the departure speed variation. For 500-day transfers, the combined effects of departure and arrival energies are such that the best mission performance opportunities occur during the 1972-1976 time period. The latter years in the decade are the most demanding from the mission performance standpoint. However, the effect of higher arrival energies early and late in the decade permits the use of longer Earth-Jupiter transfers times to achieve the 0.1 AU solar flyby. The longer transfer times tend to ease the performance requirements for the latter years. These tradeoffs will be discussed in more detail in subsequent sections of the mission analysis.

Figures 2-5, 2-6, and 2-7 show the Earth-departure and Jupiter-arrival hyperbolic-excess speeds as functions of departure date and transfer time for the 1972, 1975, and 1978 opportunities, respectively. For each opportunity, the departure speed is seen to reach a minimum during the launch period for a given transfer time, whereas the arrival speed continually decreases across the period. The effect of this trend in arrival energy across the launch period on the solar probe orbit characteristics will be shown later.

Communication Distance. An important parameter in the mission analysis is the communication distance between the spacecraft and Earth for which the onboard communication system must be designed. The distance between the Earth and Jupiter at opposition varies because of the eccentricities of the planetary orbits but has a minimum possible value of 3.93 AU. The maximum possible Earth-Jupiter distance is 6.47 AU. For the fast Earth-Jupiter transfers under consideration the Earth-spacecraft distance at Jupiter arrival will be typically 4 to 4.5 AU. However, because the Jupiter orbiter will be designed for an operational life in capture orbit of typically 90 days, the communication distance for orbiter system design purposes will be approximately 6 AU.

Planetary Constellation at Jupiter Arrival. The Sun is a potent source of radiation that can cause blackout in communications with the spacecraft if the vehicle-Earth line-of-sight is within about two degrees of the Sun. For mission analysis purposes, this constraint on the heliocentric trajectory design is considered at time of Jupiter arrival. Figure 2-8 is a plot of the heliocentric longitude of Earth and Jupiter at Jupiter arrival as functions of departure date for the 1975 launch opportunity. Curves are shown for transfer times of 500, 540, and 600 days. The slopes of the longitude curves for the Earth are seen to be relatively large compared to the Jupiter curves. This means that a line-of-sight occultation will occur only for a brief time (on the order of two days). Therefore, if an occultation is found to occur during any chosen launch period, the problem can be avoided by planning a hold period until the launch time within the occultation deadband passes.

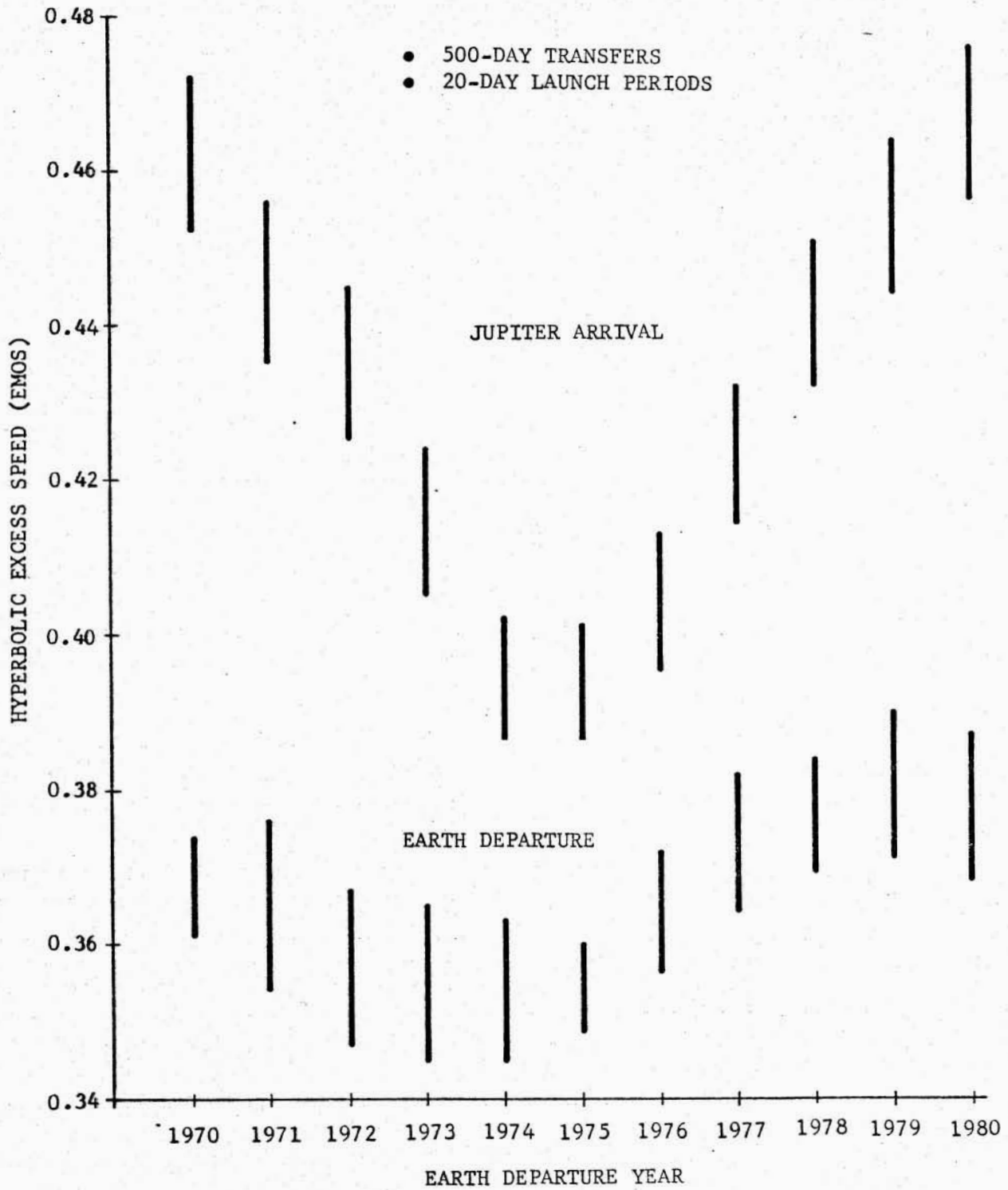


Figure 2-4. HYPERBOLIC EXCESS SPEEDS FOR FAST EARTH-JUPITER TRANSFERS DURING 1970-1980

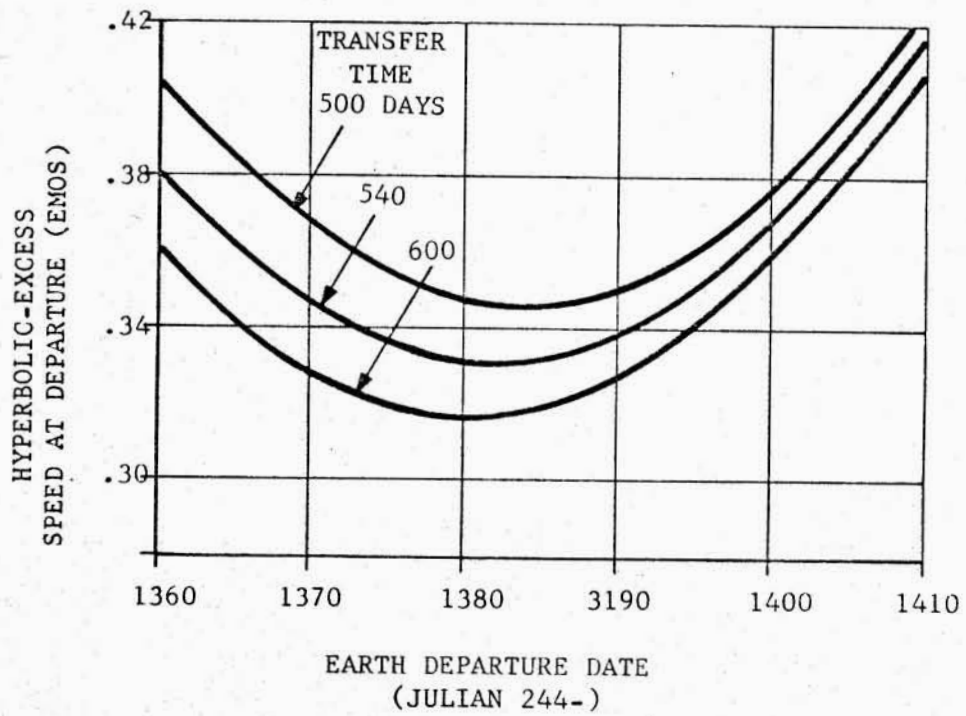
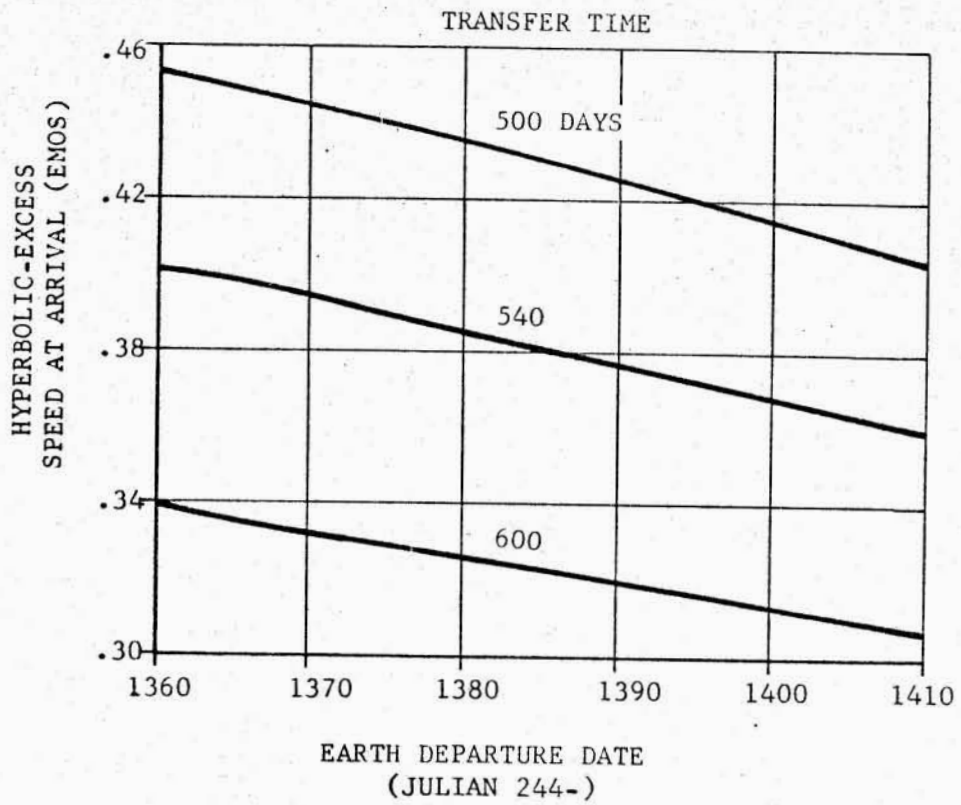


Figure 2-5. DEPARTURE AND ARRIVAL HYPERBOLIC-EXCESS SPEEDS FOR 1972 EARTH-JUPITER TRANSFERS

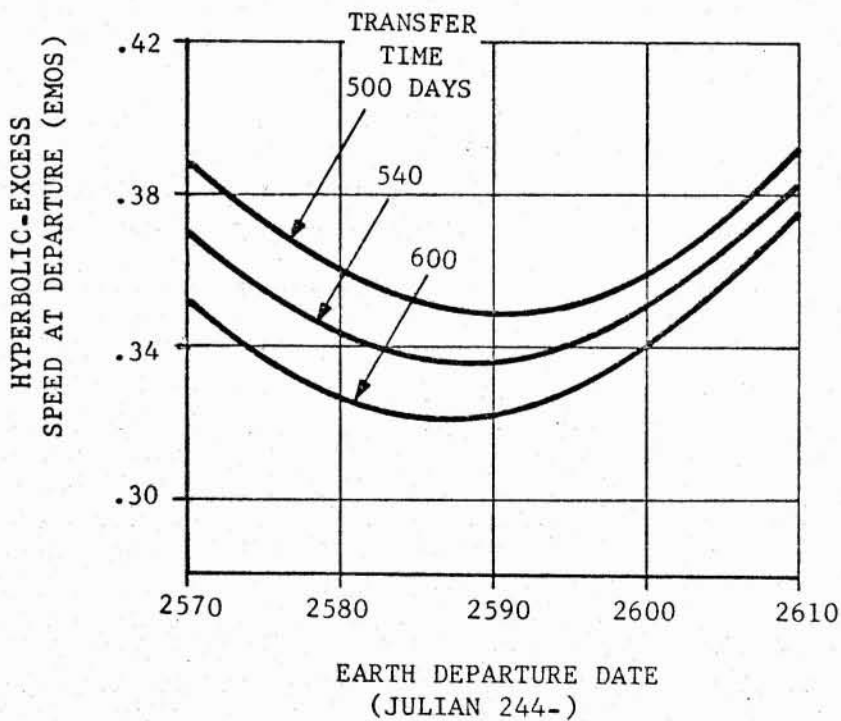
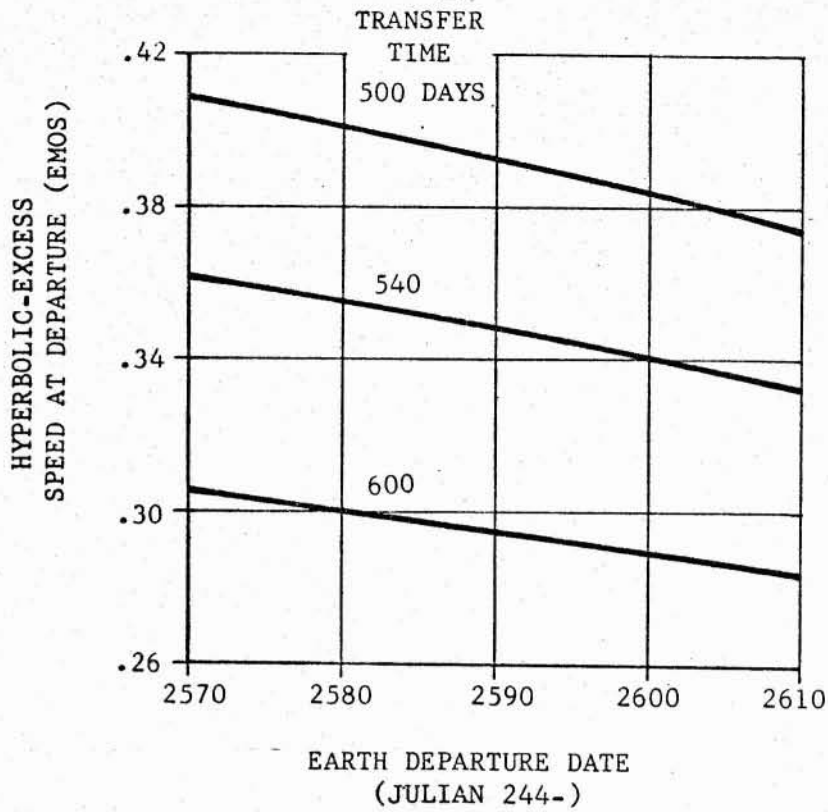


Figure 2-6. DEPARTURE AND ARRIVAL HYPERBOLIC-EXCESS SPEEDS FOR 1975 EARTH-JUPITER TRANSFERS

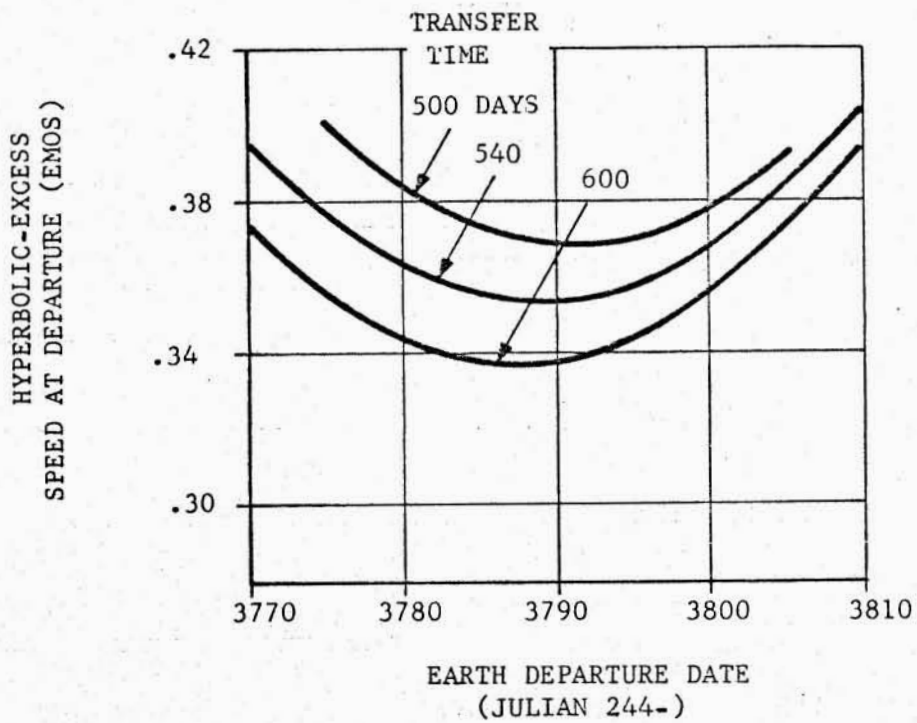
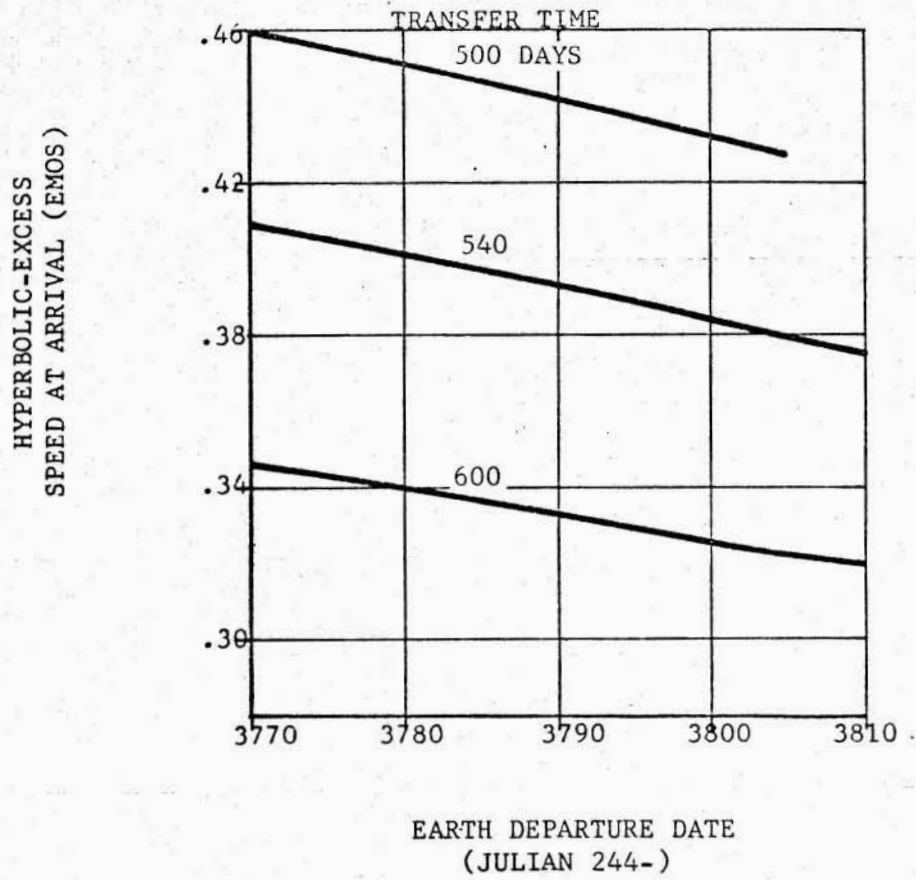


Figure 2-7. DEPARTURE AND ARRIVAL HYPERBOLIC-EXCESS SPEEDS FOR 1978 EARTH-JUPITER TRANSFERS

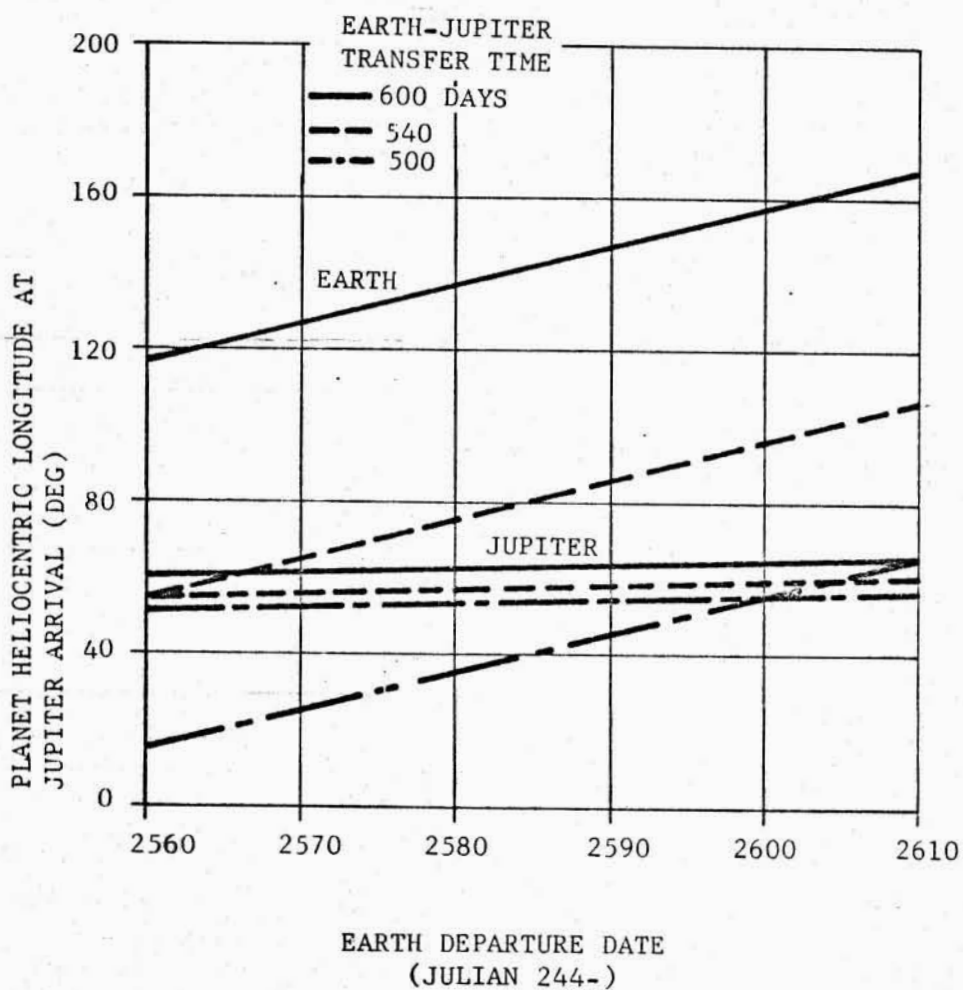


Figure 2-8. EARTH-JUPITER TRAJECTORIES 1975: PLANETARY CONSTELLATIONS AT JUPITER ARRIVAL FOR FAST TRANSFERS

2.1.3.2 Solar Probe Orbit Analysis. The heliocentric ballistic trajectory of a spacecraft can be greatly altered if the vehicle passes through the gravitational field of a planet. This influence can be employed to a very significant advantage for certain classes of missions where energy and/or time characteristics of the flight profile can be attractively improved by a "gravity-assist" trajectory.

The concept of a close solar probe as a combination payload with a Jupiter orbiter is based on the fact that the strong Jovian gravitational field can be used to radically alter the heliocentric Earth-Jupiter trajectory to allow the probe to free-fall back close to the Sun at perihelion. The effect of an encounter with Jupiter on the heliocentric trajectory is illustrated by the velocity vector diagrams in Figure 2-9. Although both direct and retrograde encounters are always possible, the retrograde swingby is necessary to produce a heliocentric orbit with a perihelion close to the Sun. The direct encounter is required for missions to the outer planets or for solar system escape. The following brief discussion of both types of encounters is helpful in understanding the necessity of retrograde swingbys for the Jupiter orbiter/solar probe mission. This discussion also aids in understanding the solar probe orbit data to be presented based on a digital computer simulation of Jupiter swingby trajectories.

First consider the case of a direct encounter. The velocity vector diagram for the direct encounter (Fig. 2-9a) shows the velocity \vec{V}_P of Jupiter about the Sun, and the velocity vector \vec{V}_A on the Earth-Jupiter transfer trajectory at arrival. The hyperbolic-excess or relative velocity V_{HP} of the probe with respect to Jupiter is determined by the vector difference,

$$\vec{V}_{HP} = \vec{V}_A - \vec{V}_P \quad (1)$$

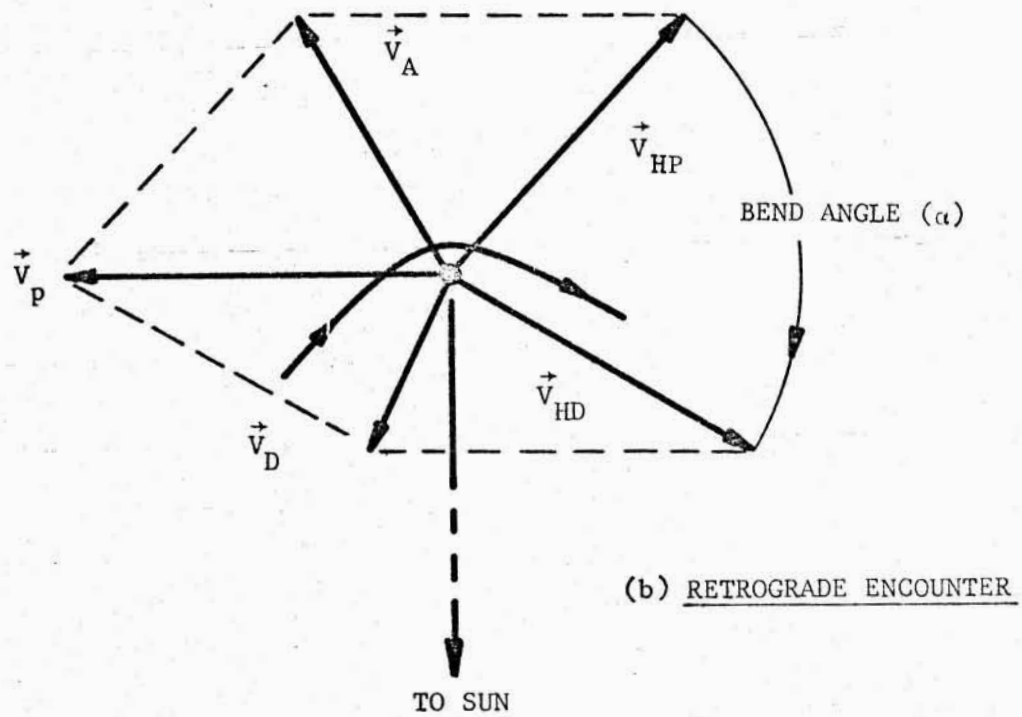
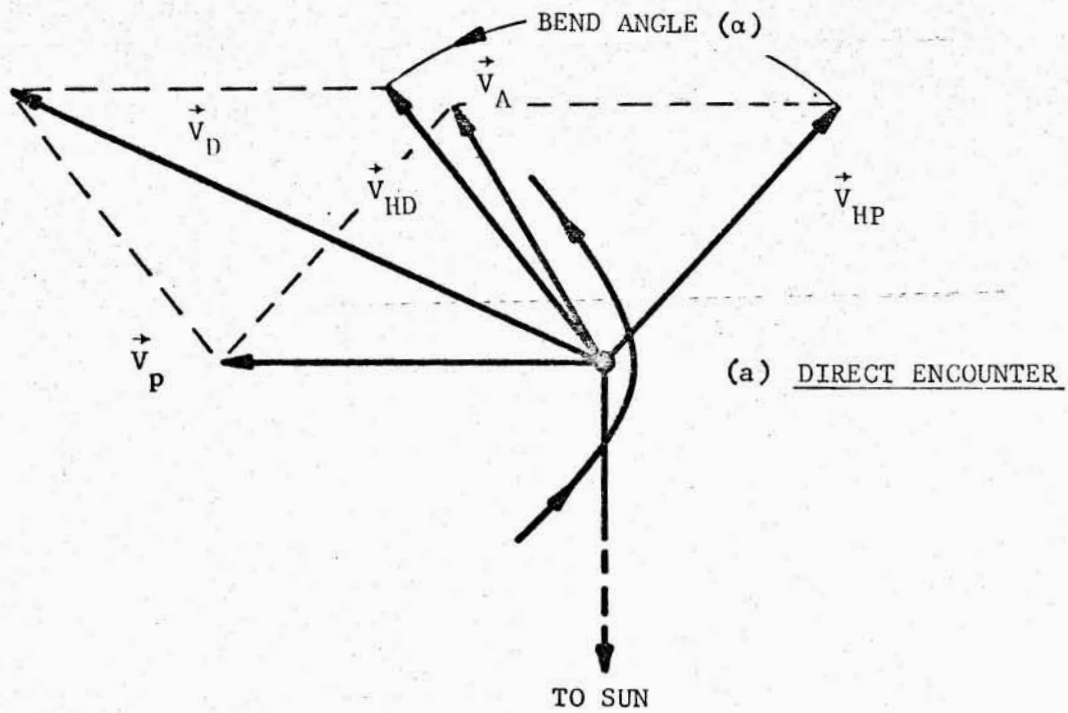
as shown in the diagram. The direction of the incoming hyperbolic asymptote is that of the \vec{V}_{HP} vector. The effect of the direct encounter is to rotate the hyperbolic-excess velocity vector in a counterclockwise direction through an angle α defined by the expression

$$\alpha = \pi - 2 \cos^{-1} \left(1 + \frac{V_{HP}^2 r_p}{GM} \right)^{-1} \quad (2)$$

where V_{HP} is the hyperbolic-excess speed, r_p is the distance of closest approach to the planet, and GM is the planet's gravitational constant. The re-directed hyperbolic-excess velocity is labeled V_{HD} in Figure 2-9a. Now the post-encounter velocity \vec{V}_D of the probe with respect to the Sun is determined by re-combining the hyperbolic-excess velocity with the planet's velocity; i.e.,

$$\vec{V}_D = \vec{V}_P + \vec{V}_{HD} \quad (3)$$

As indicated by the velocity diagram, the direct encounter results in both an increase in the heliocentric velocity of the probe and its heliocentric energy. The change in energy ΔE per unit mass with respect to the Sun is given by the equation



$$\alpha = \pi - 2 \cos^{-1} \left(1 + \frac{|\vec{V}_{HP}|^2 r_p}{GM} \right)^{-1}$$

$$\Delta E = \frac{1}{2} \left(|\vec{V}_D|^2 - |\vec{V}_A|^2 \right)$$

Figure 2-9. VELOCITY VECTOR DIAGRAMS FOR DIRECT AND RETROGRADE PLANETARY SWINGBYS

$$\Delta E = \frac{1}{2} (|\vec{V}_D|^2 - |\vec{V}_A|^2) \quad (4)$$

It is evident that the increases in heliocentric velocity and energy of the probe resulting from a direct swingby of Jupiter will not produce a post-encounter trajectory with a perihelion near the Sun. It should be noted that energy with respect to the planet during encounter is conserved; i.e., the hyperbolic-excess velocity is changed in direction but not magnitude ($|\vec{V}_{HD}| = |\vec{V}_{HP}|$).

Now consider the velocity diagram for the retrograde encounter (Figure 2-9b). In this case the rotation of the arrival hyperbolic-excess velocity \vec{V}_{HP} is in the clockwise direction. When the rotated vector \vec{V}_{HD} is combined with the planet's velocity \vec{V}_P , the resulting post-encounter heliocentric velocity, \vec{V}_D , is reduced in magnitude from the arrival heliocentric velocity \vec{V}_A . Therefore the energy of the probe with respect to the Sun is reduced according to equation(4). This means that post-encounter trajectories can be achieved with perihelion distances possibly very close to the Sun.

On the basis of the preceding discussion, it is apparent that two factors determine the characteristics of the post-encounter solar probe trajectory:

1. The Jupiter arrival conditions in the Earth-Jupiter transfer trajectory.
2. The aiming point at the sphere of influence.

First, the arrival conditions in the Earth-Jupiter transfer directly determine the hyperbolic-excess velocity \vec{V}_{HP} . The magnitude of this vector is a measure of the amount of heliocentric energy that can be taken from the probe by the swingby. This is true since \vec{V}_{HP} is rotated during the swingby to, in effect, "oppose" Jupiter's velocity vector which remains practically constant relative to a coordinate frame fixed at Jupiter's center rotating about the Sun. Theoretically, if for a given case \vec{V}_{HP} were equal in magnitude to the planet's velocity \vec{V}_P , and were directed by the swingby to exactly oppose \vec{V}_P , then the post-encounter heliocentric velocity would be zero. The probe would then fall directly into the Sun. The mission parameters that determine the magnitude of \vec{V}_{HP} are the Earth-Jupiter transfer time and the launch date.

The second factor of importance that determines the post-encounter trajectory, as stated above, is the aiming point at the Jovian sphere of influence. This point may, in effect, be defined by specifying the miss distance B and the inclination of the plane of the encounter hyperbola with respect to a reference plane such as Jupiter's orbital plane. The miss distance is defined as the perpendicular distance from the incoming asymptote to the center of the planet. The aiming point, therefore, determines: (1) the bend angle through which the hyperbolic-excess velocity vector will be rotated, and (2) the plane of rotation.

For certain kinds of interplanetary guidance laws, the aiming point may be conveniently expressed in terms of a \vec{B} vector model. The magnitude of \vec{B} is the miss distance previously discussed. Therefore, the \vec{B} vector has its origin at the center of the planet and is normal to the incoming asymptote. A rectangular

Cartesian coordinate system is established with origin at the planet's center and one axis \hat{S} (unit vector) directed along the incoming asymptote. The other two orthogonal axes, T and R, form a plane that contains the \vec{B} vector. These axes can be arbitrarily oriented with respect to some reference plane such as the ecliptic. Thus, the aiming point can be specified by the components of the \vec{B} vector given by the dot products $\vec{B} \cdot T$ and $\vec{B} \cdot R$. These components are directly related to the distance r_p of closest approach to the planet and the inclination i_h of the encounter hyperbola. The latter parameters were chosen for development of a computer program to analyze the mechanics of the solar probe orbit based on Jupiter swingbys.

Computer Program. To provide a realistic simulation of solar probe trajectories resulting from Jupiter swingbys, a digital computer program was developed under the following guidelines and assumptions:

1. A three-dimensional solar system is assumed based on non-coplanar elliptical planetary orbits.
2. The probe is assumed to be under the gravitational influence of only one body at a time.
3. Mathematically, relative to a heliocentric reference frame, the swingby at Jupiter is assumed to occur instantaneously on the date of arrival at the planet.
4. The Earth-Jupiter trajectory characteristics are based on data from reference 2 previously discussed in subsection 2.1.3.1.

The analytical approach implemented by the computer routine is outlined as follows:

1. The arrival conditions in the Earth-Jupiter transfer trajectory are specified as input parameters from the data of reference 2. For a given launch date and transfer time, the arrival conditions are defined by the heliocentric velocity magnitude and flight path angle, and the inclination of the transfer plane with respect to Jupiter's orbital plane. The position and velocity of Jupiter on the arrival date in the heliocentric ecliptic coordinate system are specified as inputs from ephemeris data. For a given case, the only remaining input parameters are the sphere-of-influence aiming point information defined, in effect, by a distance of closest approach to Jupiter and an inclination of the encounter hyperbola. Inclination is measured as viewed from the ascending node of the encounter hyperbola as an angle between 0° and 180° with respect to Jupiter's orbital plane. Therefore, first quadrant angles are direct encounters and second quadrant angles are retrograde encounters.
2. On the basis of the Earth-Jupiter transfer arrival conditions and the Jupiter position and velocity at arrival, the hyperbolic-excess vector \vec{V}_{HP} relative to Jupiter is calculated in a coordinate system shown by Figure 2-10. The rectangular Cartesian system is centered at Jupiter with the X axis directed along the Sun-Jupiter line and the Z axis in the positive angular momentum direction of the planet's motion about

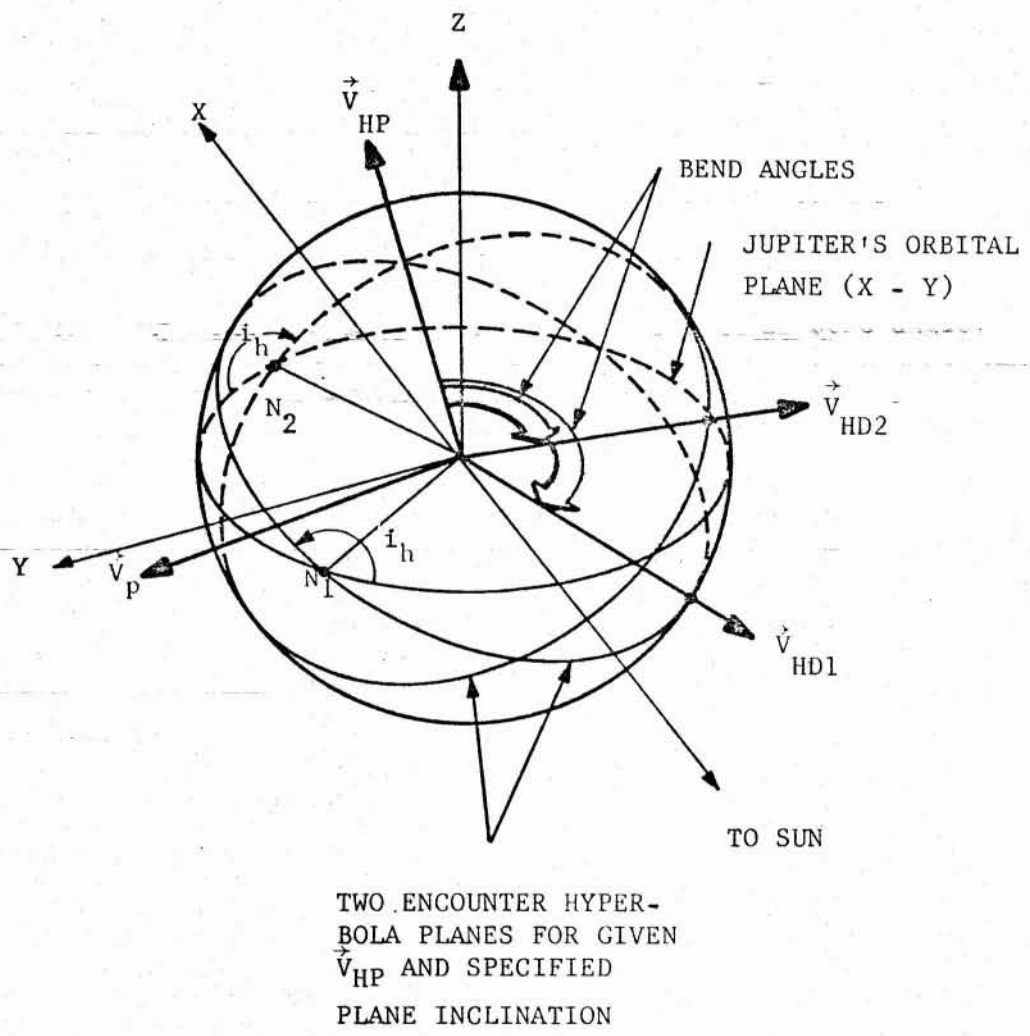


Figure 2-10. JUPITER SWINGBY TRAJECTORY MODEL

the Sun. The Y axis completes the right-handed system. Since the X axis does not move essentially during the swingby, the X, Y, Z frame is simply a heliocentric frame translated to Jupiter's center.

3. The post-encounter hyperbolic-excess velocity \vec{V}_{HD} is determined from the incoming velocity \vec{V}_{HP} by transforming the computation to a rectangular Cartesian coordinate system in the plane of the swingby trajectory. In this system one axis is directed along the incoming vector \vec{V}_{HP} , a second axis is constructed normal to the swingby plane, and the third axis completes a right-handed system. For a given encounter plane inclination there exist two hyperbola planes that contain the incoming velocity vector \vec{V}_{HP} . Therefore, there are two solutions to the swingby trajectory as shown by Figure 2-10 and illustrated by Figure 2-11. For example, an inclination of 170° , includes the two retrograde hyperbolas inclined 10° above and below Jupiter's orbital plane on the approach side of the planet. Generally these two solutions are nearly symmetrical dynamically, depending on the arrival conditions at Jupiter; therefore, one solution can be chosen for mission analysis purposes.

Thus, for a specified encounter plane inclination, the post-encounter hyperbolic-excess velocity \vec{V}_{HD} is determined in the plane of the encounter hyperbola as a function of \vec{V}_{HP} and the bend angle, equation (2), calculated from the swingby distance. Actually, as shown by Figure 2-10, the two solutions result in two post-encounter vectors, \vec{V}_{HD1} and \vec{V}_{HD2} .

4. The post-encounter vector \vec{V}_{HD} is transformed back to the Jovian X, Y, Z reference frame and combined with the planet's heliocentric velocity (transformed from the ecliptic system) to give the post-encounter heliocentric velocity. The post-encounter heliocentric position may be taken as Jupiter's position at encounter.
5. The post-encounter velocity and position vectors are transformed to the heliocentric ecliptic system and used to compute the elements of the new heliocentric trajectory. Two-body orbital mechanics are used to compute the semi-major axis, eccentricity, perihelion distance, true anomaly at post-encounter, trajectory plane inclination, transfer time from Jupiter to perihelion, and time from Earth departure to perihelion.

Numerical Results of Solar Probe Orbit Analysis. Before discussion of the characteristics of solar probe trajectories obtained for the mission analysis, it is of interest to observe the relationships among the parameters that determine the in-plane characteristics of the swingby hyperbola at Jupiter. Figure 2-12 shows the miss distance B plotted as a function of the swingby distance for a range of hyperbolic excess speeds at arrival. For an arrival speed of about 0.4 EMOS, typical of the missions under consideration, the miss distance is seen to vary from approximately 10 to 30 Jovian radii depending on swingby distance.

Figure 2-13 presents the relationship between the bend angle through which the hyperbolic-excess vector is rotated during encounter and the swingby distance. As in the case of the miss distance, the bend angle is a function of the arrival excess speed. For the typical speed of 0.4 EMOS, the bend angle varies from about 45° to 110° .

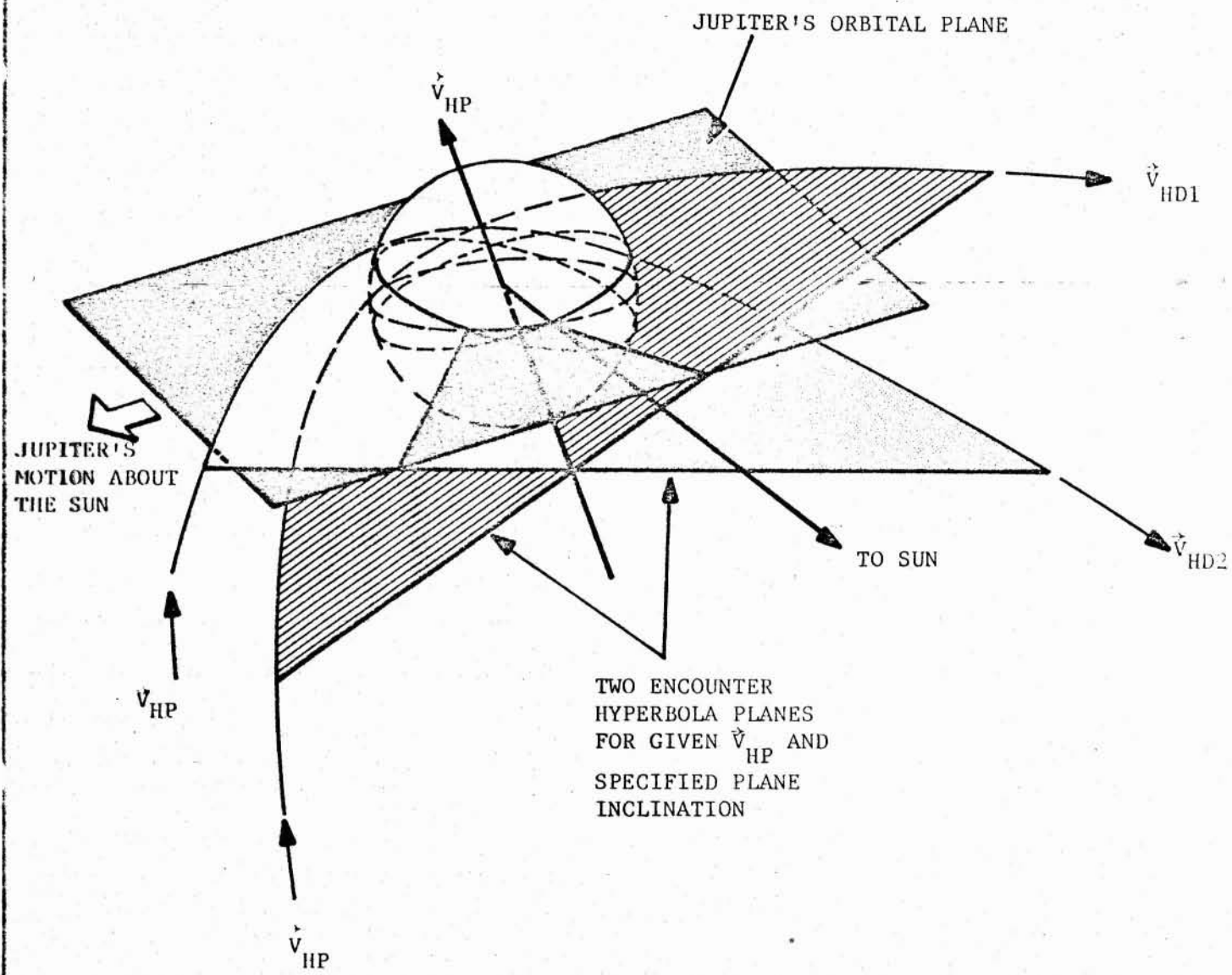


Figure 2-11. JUPITER SWINGBY GEOMETRY

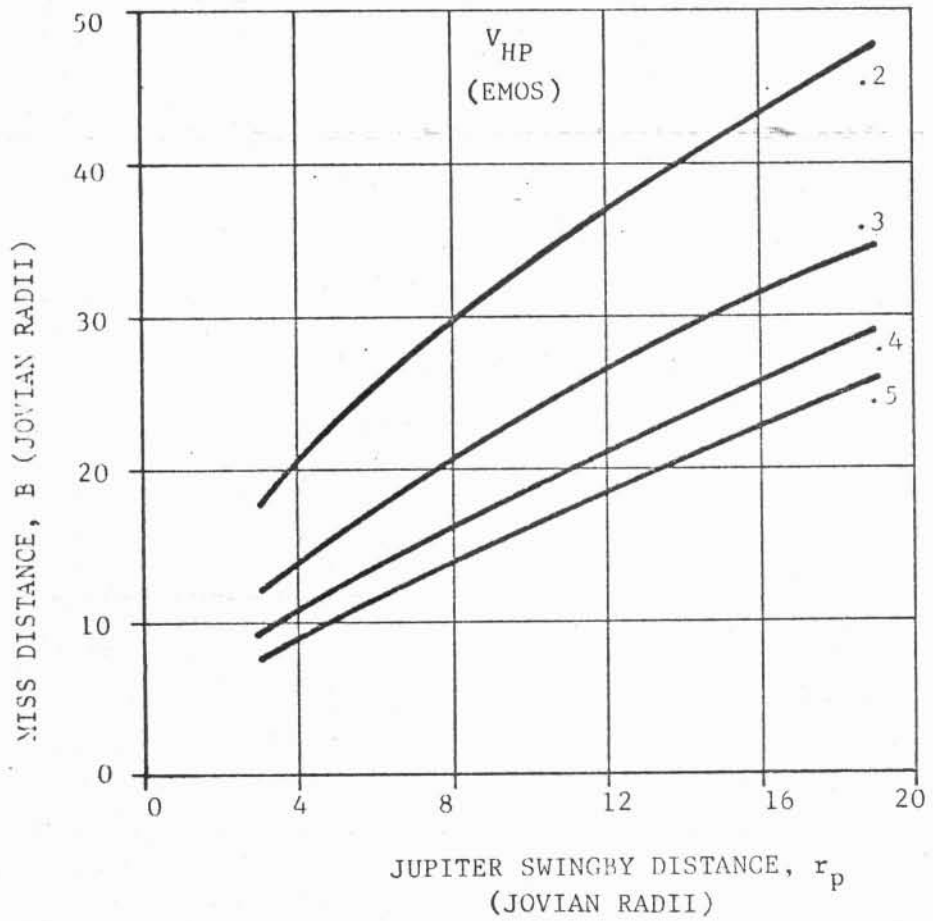
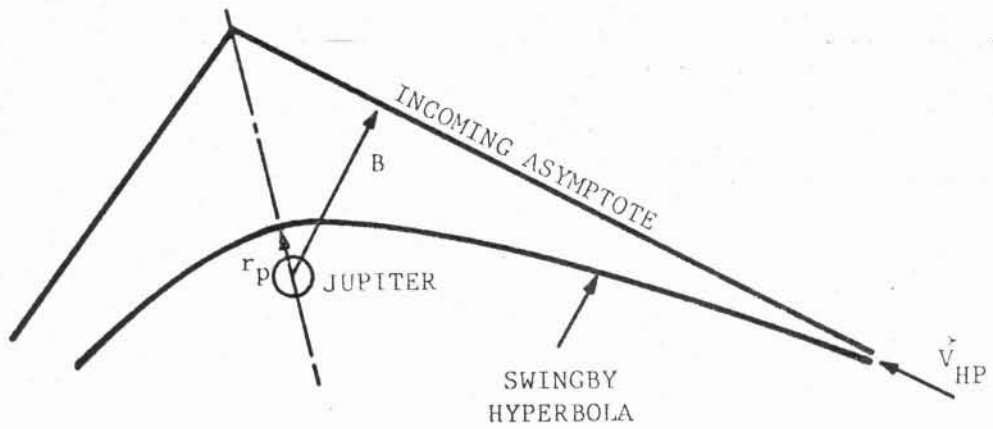


Figure 2-12. MISS DISTANCE AT JUPITER AS A FUNCTION OF SWINGBY DISTANCE

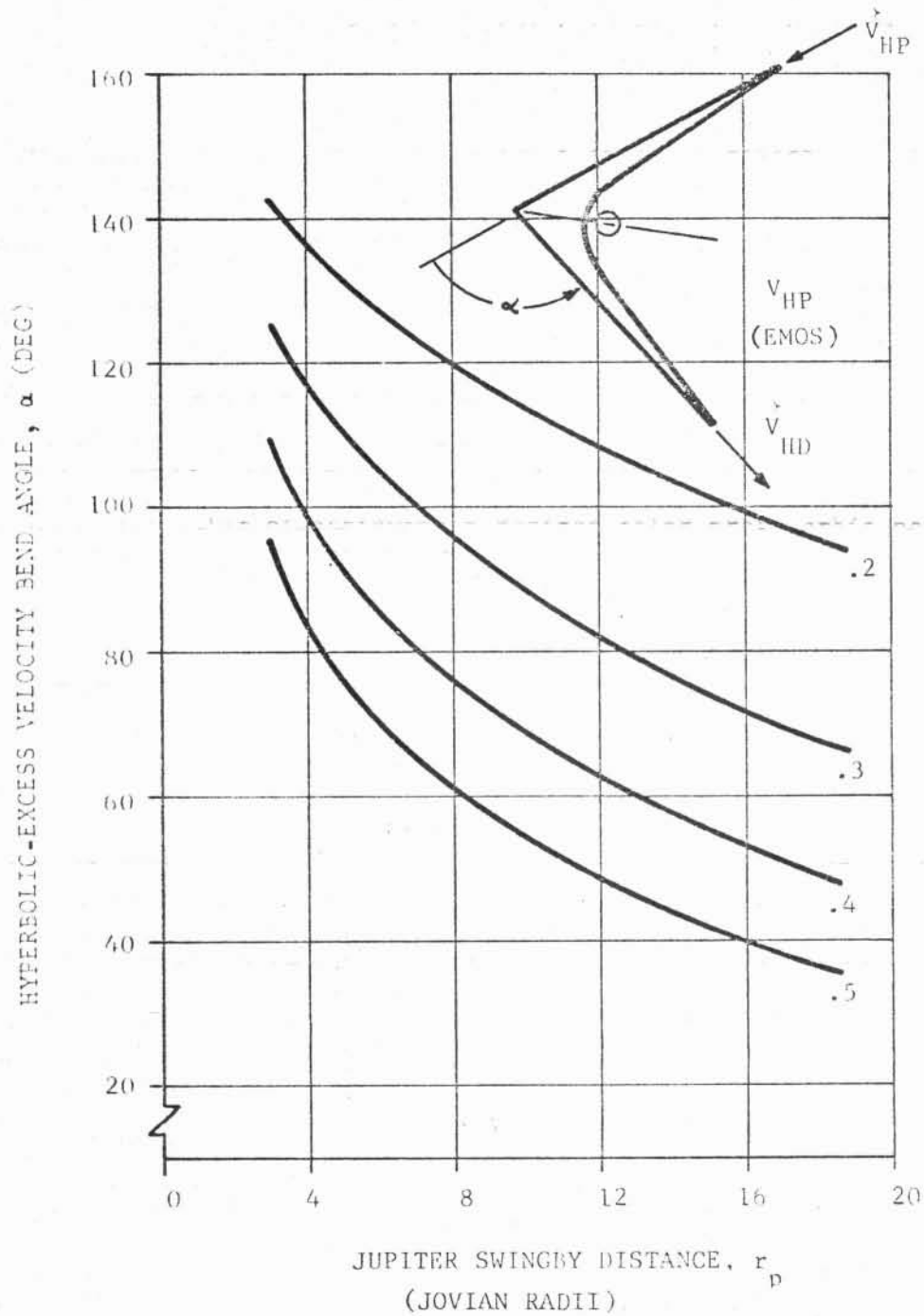


Figure 2-13. HYPERBOLIC-EXCESS VELOCITY VECTOR BEND ANGLE AT JUPITER AS A FUNCTION OF SWINGBY DISTANCE

Now consider the results of numerous swingby trajectory computations performed with the previously described computer program. First we will summarize the overall influences on the solar probe orbit by the Earth-Jupiter transfer. The general trends in mission analysis terms can be seen by investigating the effect of Earth-Jupiter transfer time on the post-encounter orbit. Throughout the presentation to follow, three solar probe orbit parameters of primary interest are considered: (1) perihelion distance, (2) trip time from Earth departure to solar flyby at perihelion, and (3) inclination of the solar probe orbit plane with respect to the ecliptic plane. Figure 2-14 shows the effect of Earth-Jupiter transfer time on solar probe orbit perihelion as a function of swingby distance at Jupiter. Although the curves are based on a specific departure date during the 1975 opportunity, the trends are typical. The figure shows one of the most important impacts that combining the solar probe with the orbiter has on the Jupiter capture mission. That is the fact that relatively fast Earth-Jupiter transfers are necessary for solar probe orbits that pass near the Sun. Therefore the choice of transfers is much more restricted for the Jupiter orbiter/solar probe mission than for a straightforward Jupiter capture mission. Figure 2-14 also indicates that for a given Earth-Jupiter transfer time, there exists a swingby distance at Jupiter that results in a minimum post-encounter perihelion distance for a given Earth departure date. The figure further gives indication of the sensitivity of errors in the post-encounter perihelion as related to errors in the Jovian swingby distance. The shape of the curves indicates that the planetary guidance problem of achieving a desired solar probe orbit perihelion by controlling the trajectory errors at Jupiter swingby is not severe.

The effect of Earth-Jupiter transfer time on the total trip time from launch to solar flyby is presented in Figure 2-15. The fast transfers result in a wider variation in total mission time over the range of swingby distances than do the slower transfers. In general, close Jovian swingby distances are desirable from a total flight time standpoint.

Figure 2-16 shows the variation of solar probe orbit inclination as a function of swingby distance for various Earth-Jupiter transfer times. The fast transfers exhibit the interesting characteristic of relatively large inclinations with a maximum value occurring at a certain swingby distance. This is an attractive feature of these orbits from the scientific experiments standpoint. It is possible, therefore, to combine the objectives of an out-of-the-ecliptic mission with those of the close solar probe mission.

The preceding figures reflect the effects of Earth-Jupiter transfer time and Jovian swingby distance on the solar probe orbit characteristics. Figures 2-17 and 2-18 show the general effect of the inclination of the encounter hyperbola on solar probe orbit perihelion and inclination to the ecliptic, respectively. A date during the 1978 opportunity was chosen for these illustrations. Figure 2-17 indicates the need for a "highly" retrograde Jovian encounter in order to get in close to the Sun at perihelion. In general a 180-degree encounter in Jupiter's orbital plane is not possible since the acute angle the encounter hyperbola plane makes with the Jupiter orbital plane cannot be less than the absolute value of the declination of the incoming asymptote. However, this declination is typically less than about 5° for the Earth-Jupiter transfers under consideration. Figure 2-17 shows that post-encounter orbits can be achieved with perihelions ranging practically from impact on the Sun to something approaching circularization at Jupiter's distance under certain conditions. An inclination of 140° would return the probe to the Earth's orbital distance. Figure 2-18

EARTH DEPARTURE DATE: 27 JUNE 1975
(JULIAN 244-2590)

INCLINATION OF ENCOUNTER HYPERBOLA AT JUPITER: 170°

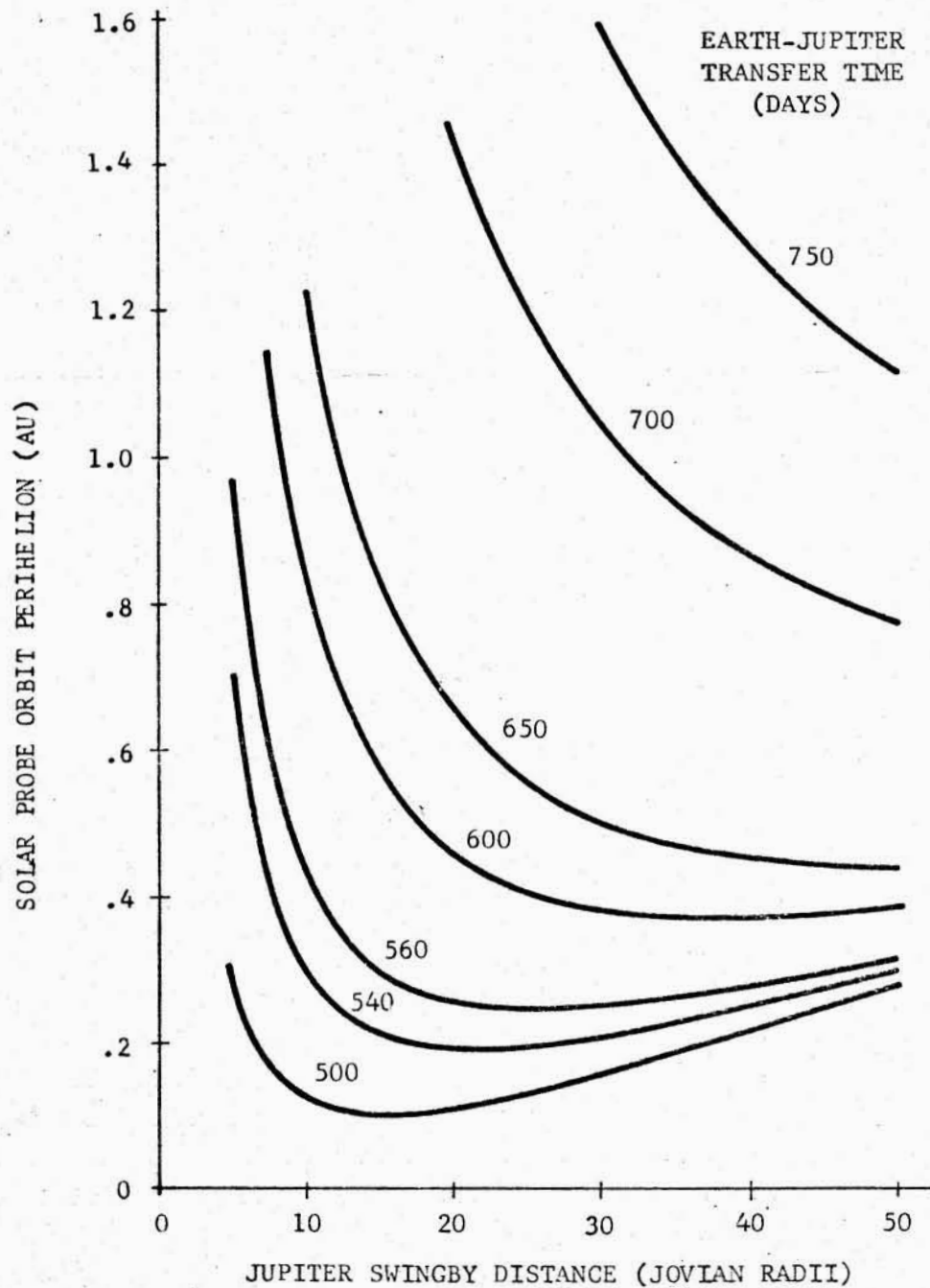


Figure 2-14. 1975 SOLAR PROBE TRAJECTORY VIA JUPITER SWINGBY:
PERIHELION DISTANCE

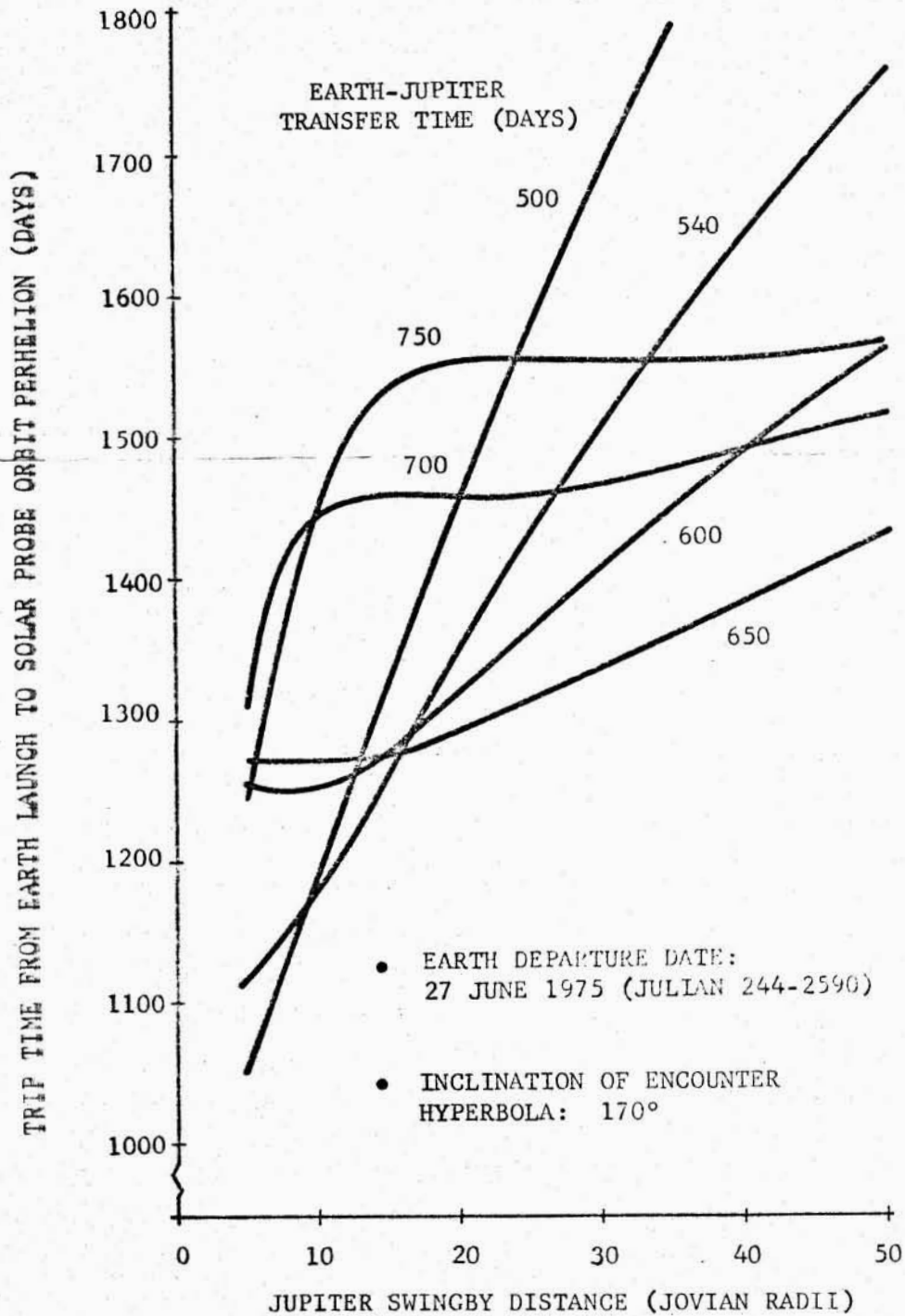


Figure 2-15. 1975 SOLAR PROBE TRAJECTORY VIA JUPITER SWINGBY:
TRANSFER TIME FROM EARTH DEPARTURE TO SOLAR FLYBY

EARTH DEPARTURE DATE: 27 JUNE 1975
 (JULIAN 244-2590)

INCLINATION OF ENCOUNTER
 HYPERBOLA AT JUPITER: 170°

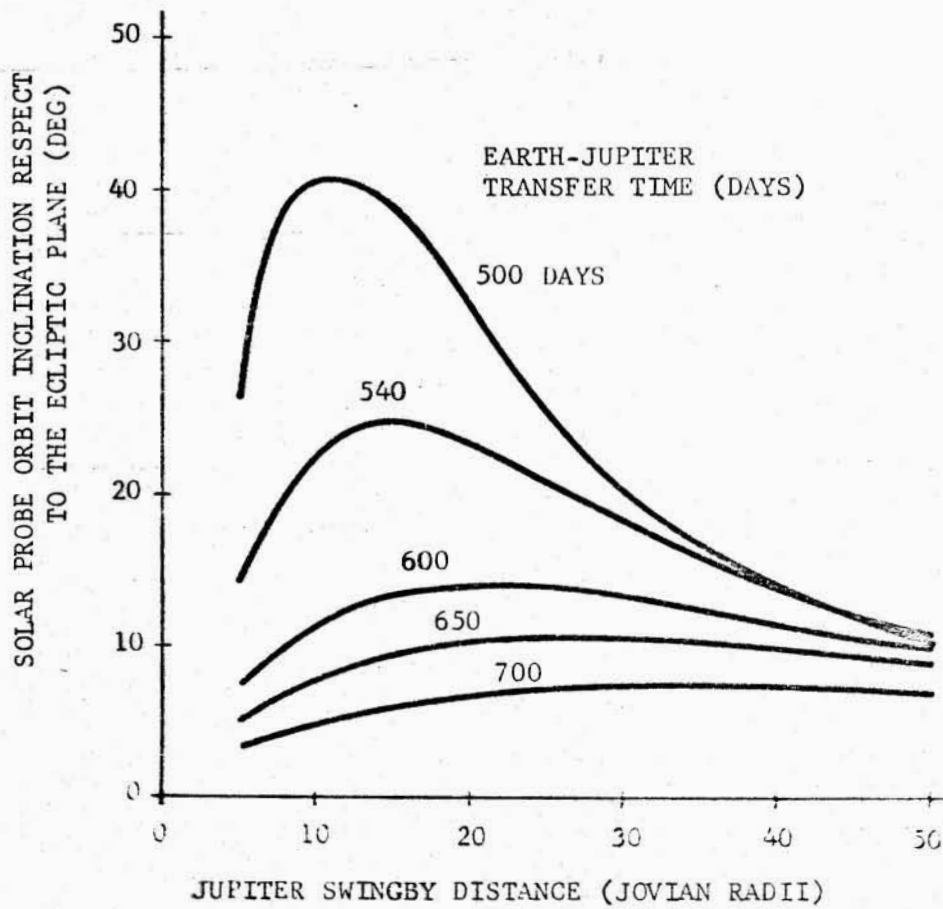


Figure 2-16. 1975 SOLAR PROBE TRAJECTORY VIA JUPITER SWINGBY:

TRAJECTORY PLANE INCLINATION

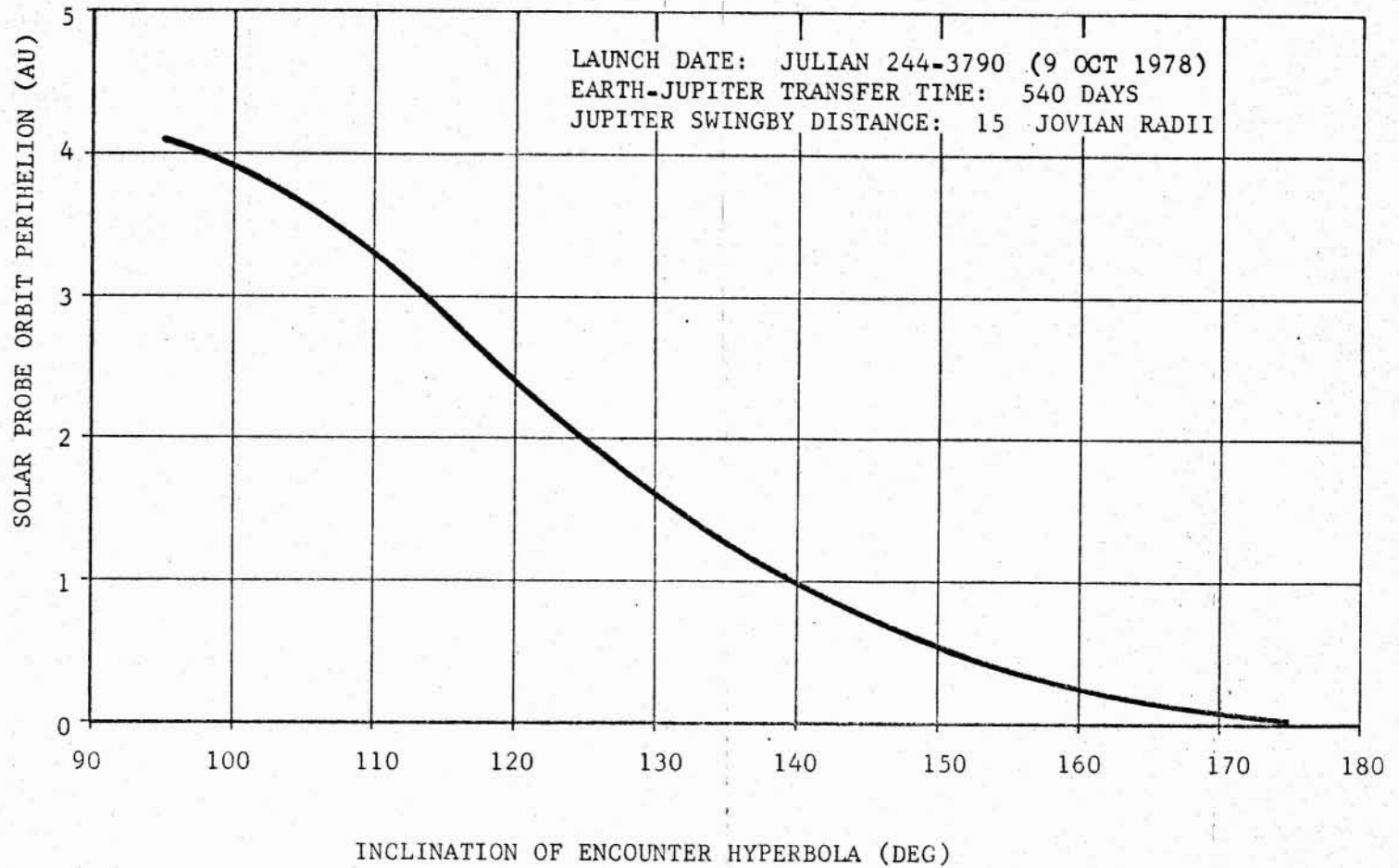


Figure 2-17. EFFECT OF INCLINATION OF JUPITER ENCOUNTER HYPERBOLA ON PERIHELION OF SOLAR PROBE ORBIT

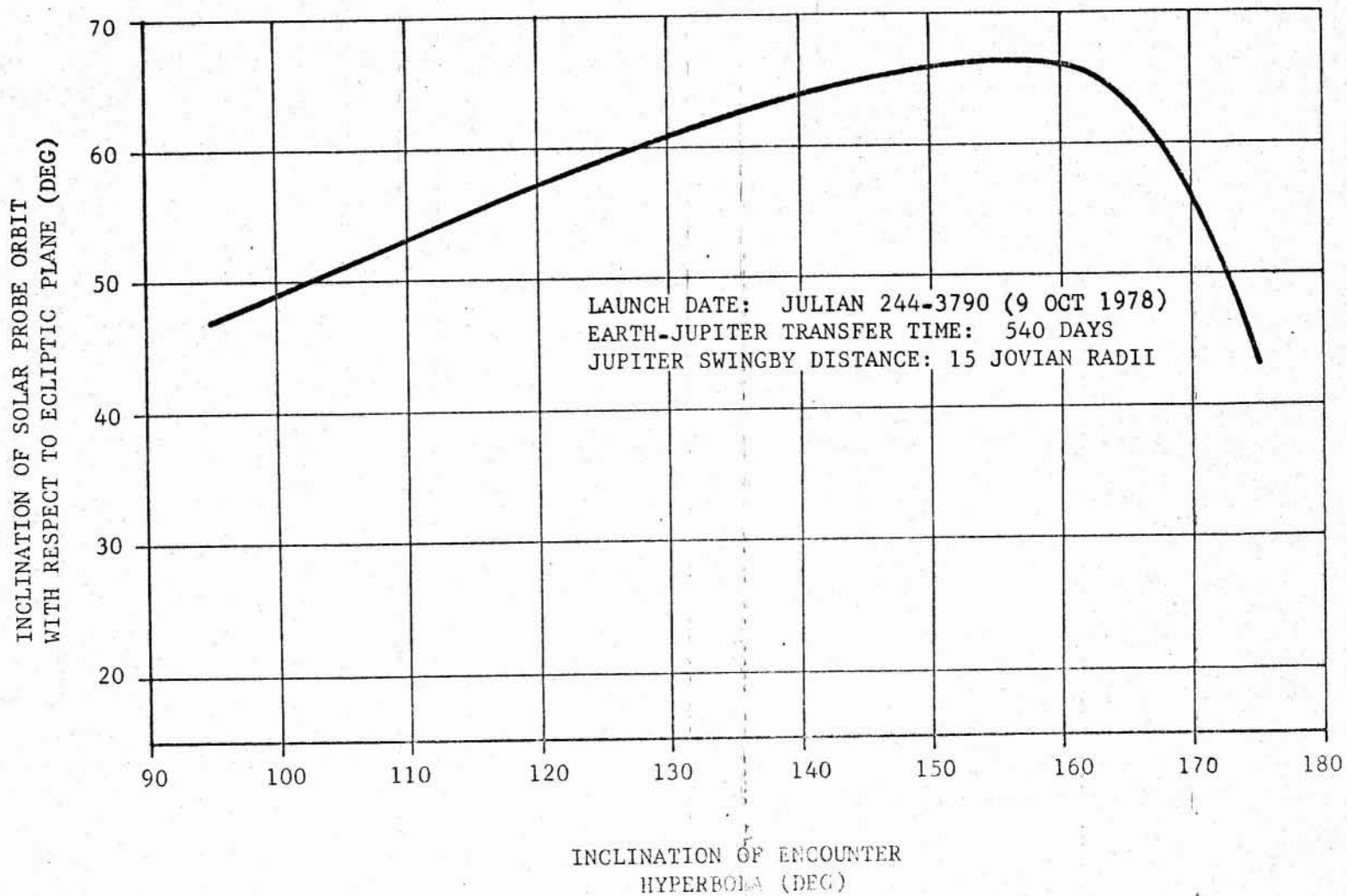


Figure 2-18. EFFECT OF INCLINATION OF JUPITER ENCOUNTER HYPERBOLA ON INCLINATION OF SOLAR PROBE ORBIT

gives a typical effect of encounter hyperbola inclination on the post-encounter orbit inclination. The encounter inclination for the very close solar flybys do not necessarily correspond to the maximum achievable post-encounter orbit inclinations.

Launch Date Effects on Solar Probe Orbit Design. The preceding discussion will now be extended to cover the effects of launch date on solar probe orbit design. Since the initial data presented was for the year 1975, the same opportunity will be discussed first here. The 1972 and 1978 launch opportunities are chosen for later discussion as representative years early and late in the 1970-1980 time period.

Figure 2-19 presents the solar probe orbit perihelion as a function of Jovian swingby distance for launch dates over a 50-day period in 1975. These curves are based on a 500-day Earth-Jupiter transfer time and a 170-degree Jovian encounter plane inclination. The 244-2590 Julian date (27 June 1975) curve corresponds to the 500-day curve of Figure 2-14 presented earlier. The effect of launch date is seen to vary the minimum achievable perihelion across the period. For example, a 0.1-AU orbit is not possible for these conditions (Earth-Jupiter transfer time and encounter plane inclination) after the date 244-2590. The effect of longer Earth-Jupiter transfer time on the launch period is shown in Figure 2-20. The transfer time of 540 days is seen to move the entire launch period above the possibility of a 0.1-AU mission. Figure 2-21 displays the effect of encounter plane inclination on the launch period situation. For 500-day transfers a 0.1-AU perihelion distance is achievable over the entire range of Earth departure dates by going to a 175-degree encounter plane inclination. For a 0.1-AU mission, the Jupiter swingby distance for a given departure date may be determined by crossing the family of curves with a horizontal line for the constant 0.1-AU perihelion distance. The swingby distance is seen to increase with later departure dates across the launch period.

Figure 2-22 presents the effect of Earth departure date on total trip time from launch to solar flyby for 500-day Earth-Jupiter transfers and a 170-degree encounter plane inclination. Generally, for a given swingby distance the total trip time decreases across the launch period. As indicated in the figure, the trip time for a 0.1-AU perihelion varies from about 1120 to 1505 days over the range of departure dates that permit a solar flyby at that distance. The effect of decreasing the encounter plane inclination, i_h , closer to Jupiter's orbital plane is indicated by Figure 2-23. For $i_h = 175^\circ$ the range of trip times for the 0.1-AU mission is reduced to approximately 1070 to 1210 days with launches possible over the complete range of dates shown. It is seen that the effect of increasing the mission perihelion distance is to further reduce the range of trip times. Times for a 0.2-AU mission range from 1010 to about 1080 days.

Figures 2-24 and 2-25 illustrate the effect of launch date on the solar probe orbit inclination with respect to the ecliptic plane. The inclination is seen to generally decrease across the launch period. The lines of constant perihelion distance show that the closer solar flybys are characterized by larger inclinations relative to the ecliptic plane. Both figures are for 500-day Earth-Jupiter transfers with the Jupiter encounter plane inclination equal to 170° in

- EARTH-JUPITER TRANSFER TIME: 500 DAYS
- INCLINATION OF ENCOUNTER HYPERBOLA AT JUPITER: 170°

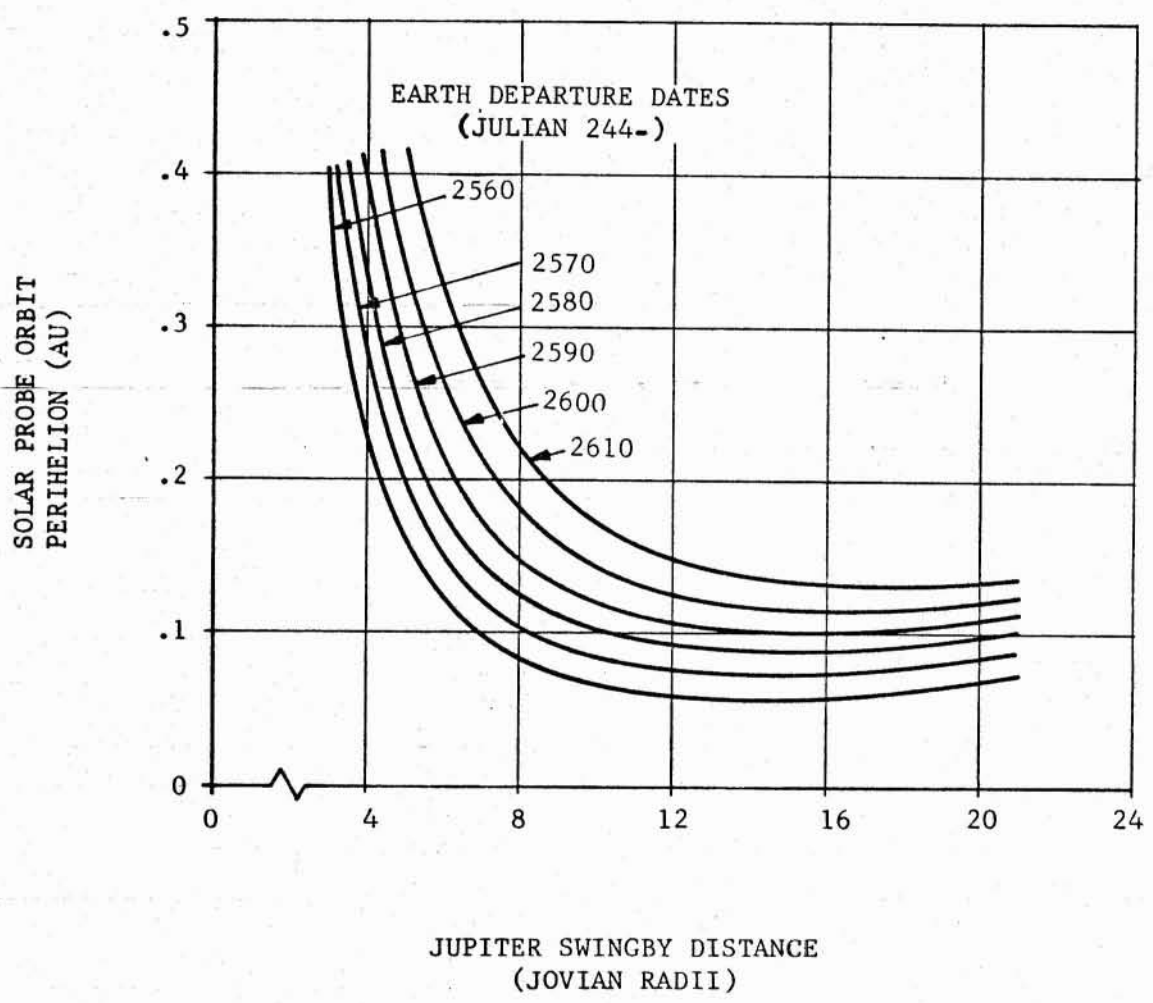


Figure 2-19. SOLAR PROBE TRAJECTORY VIA JUPITER SWINGBY:
PERIHELION DISTANCE

- EARTH-JUPITER TRANSFER TIME: 540 DAYS
- INCLINATION OF ENCOUNTER HYPERBOLA AT JUPITER: 170°

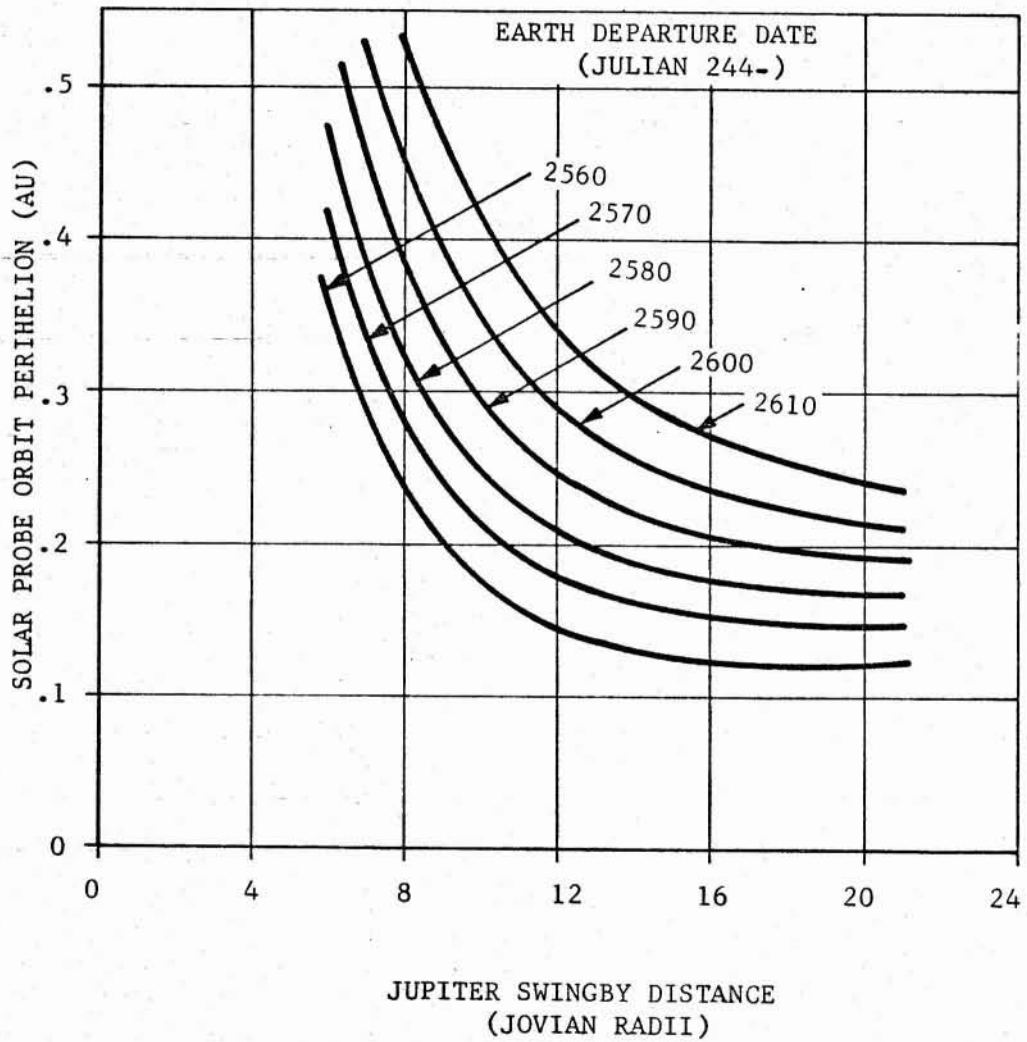


Figure 2-20. 1975 SOLAR PROBE TRAJECTORY VIA JUPITER SWINGBY:
PERIHELION DISTANCE

- EARTH-JUPITER TRANSFER TIME: 500 DAYS
- INCLINATION OF ENCOUNTER HYPERBOLA AT JUPITER: 175°

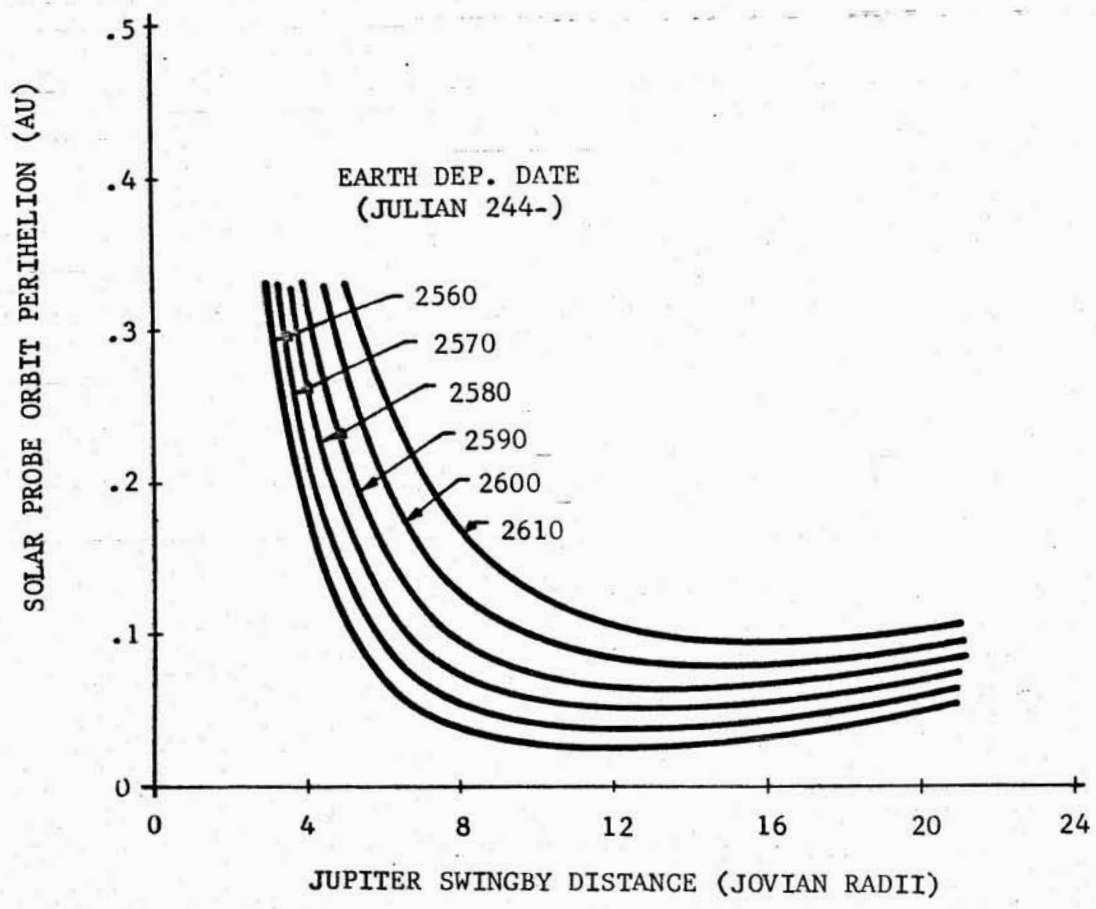


Figure 2-21 1975 SOLAR PROBE TRAJECTORY VIA JUPITER SWINGBY:
PERIHELION DISTANCE

- EARTH-JUPITER TRANSFER TIME: 500 DAYS
- INCLINATION OF ENCOUNTER HYPERBOLA AT JUPITER: 170°

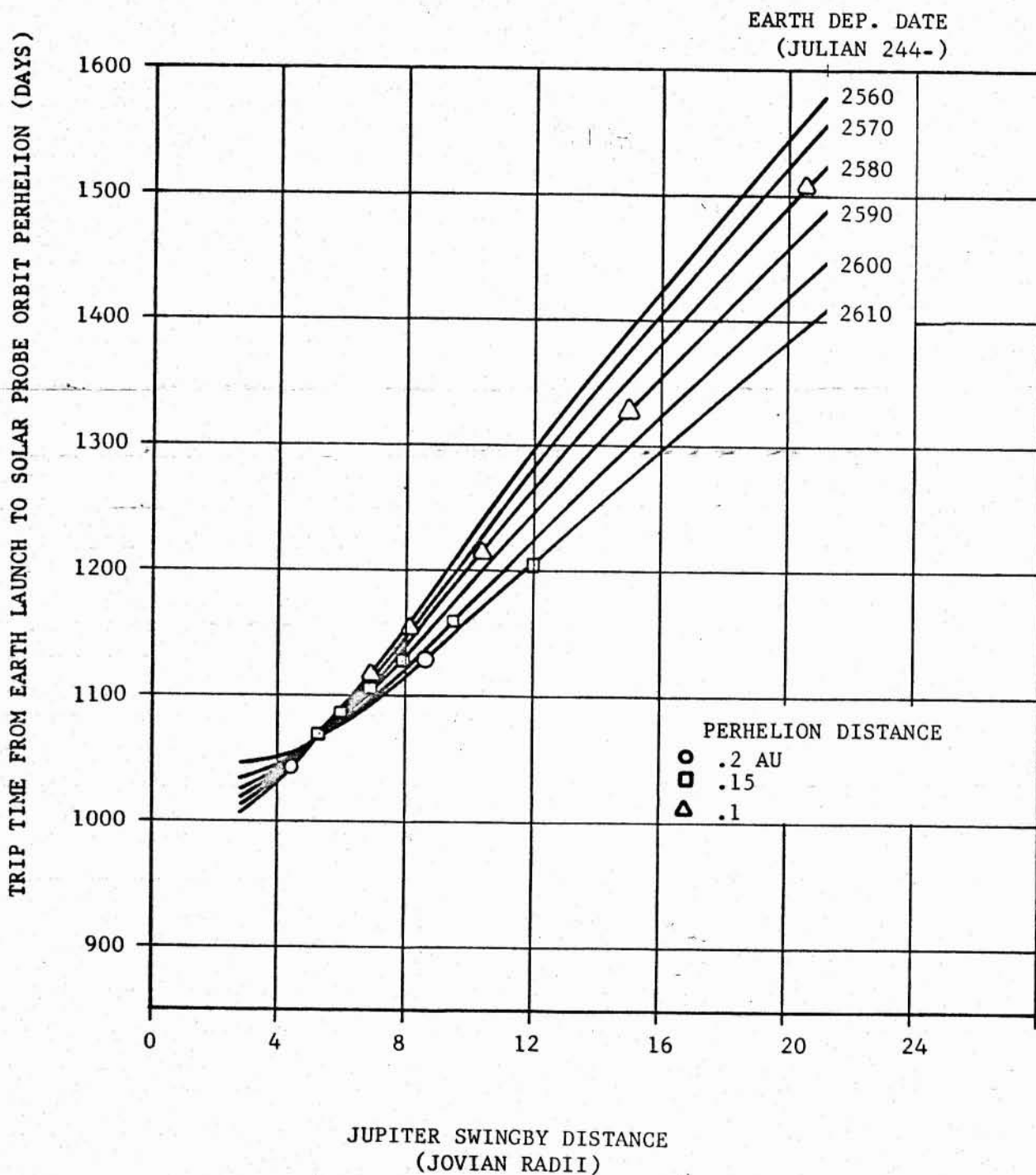


Figure 2-22. 1975 SOLAR PROBE TRAJECTORY VIA JUPITER SWINGBY: TRANSFER TIME FROM EARTH DEPARTURE TO SOLAR FLYBY

- EARTH-JUPITER TRANSFER TIME: 500 DAYS
- INCLINATION OF ENCOUNTER HYPERBOLA AT JUPITER: 175°

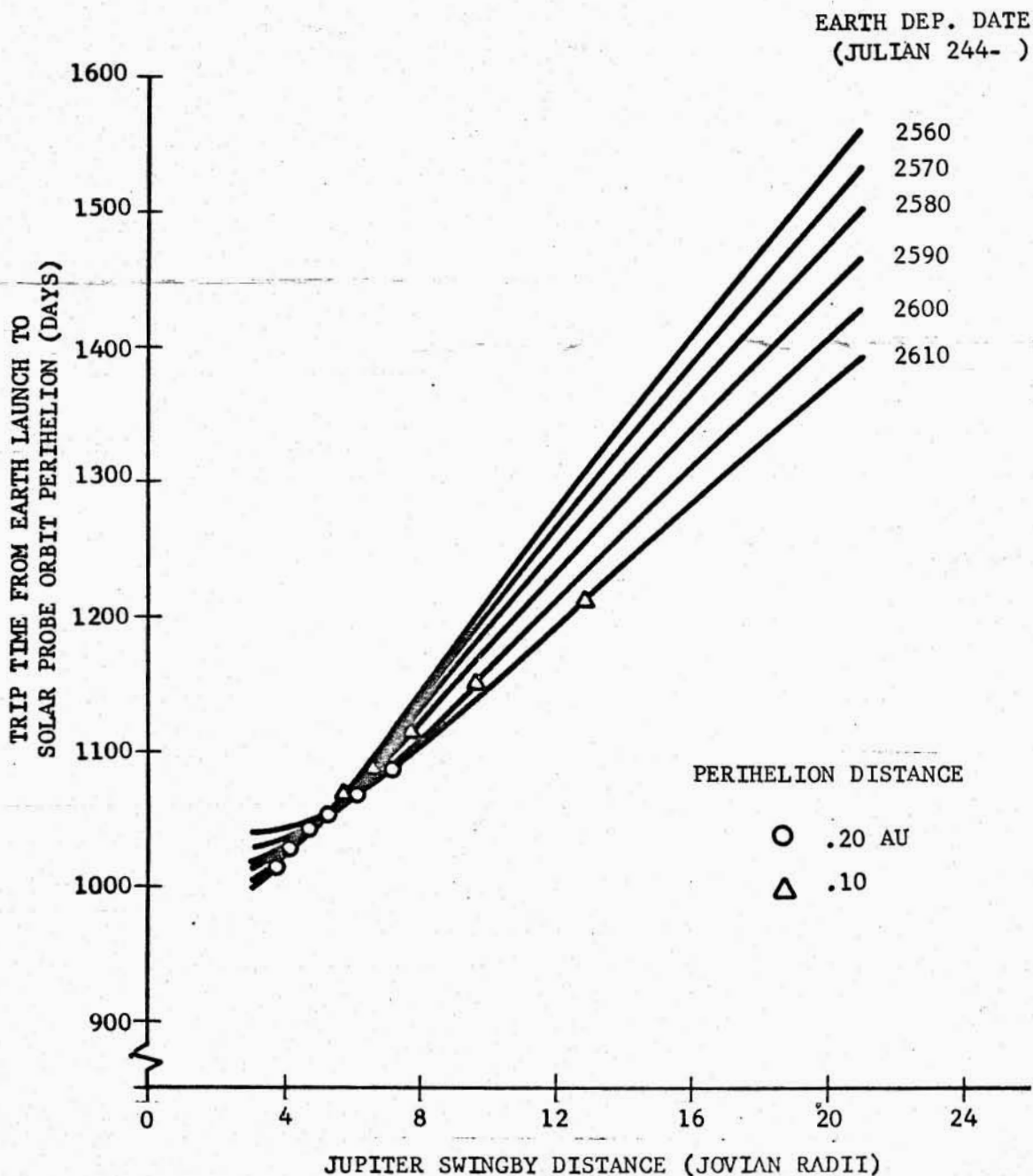


Figure 2-23. 1975 SOLAR PROBE TRAJECTORY VIA JUPITER SWINGBY:
TRANSFER TIME FROM EARTH DEPARTURE TO SOLAR FLYBY

- EARTH-JUPITER TRANSFER TIME: 500 DAYS
- INCLINATION OF ENCOUNTER HYPERBOLA AT JUPITER: 170°

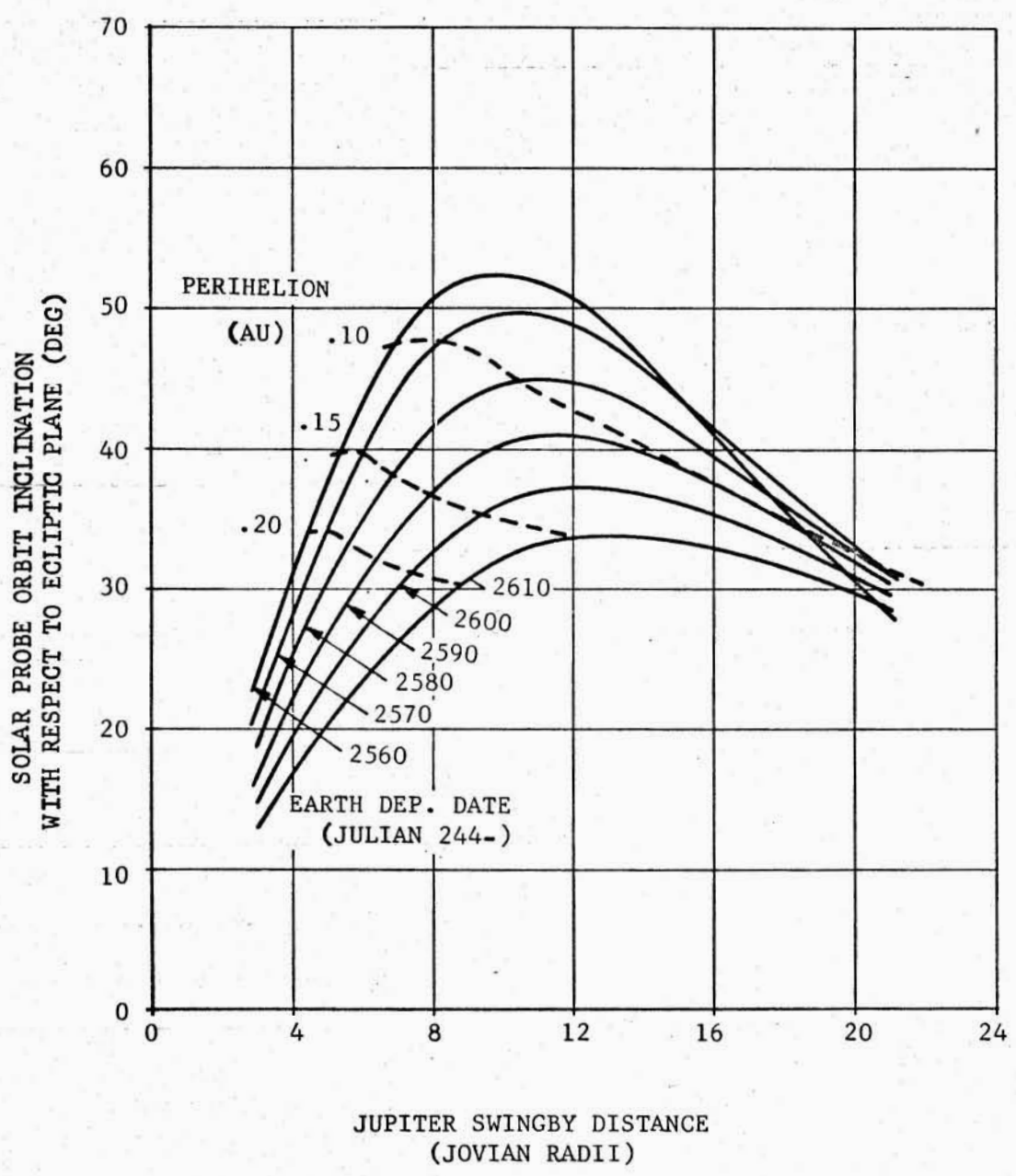


Figure 2-24. 1975 SOLAR PROBE TRAJECTORY VIA JUPITER SWINGBY: TRAJECTORY PLANE INCLINATION

- EARTH-JUPITER TRANSFER TIME: 500 DAYS
- INCLINATION OF ENCOUNTER HYPERBOLA AT JUPITER: 175°

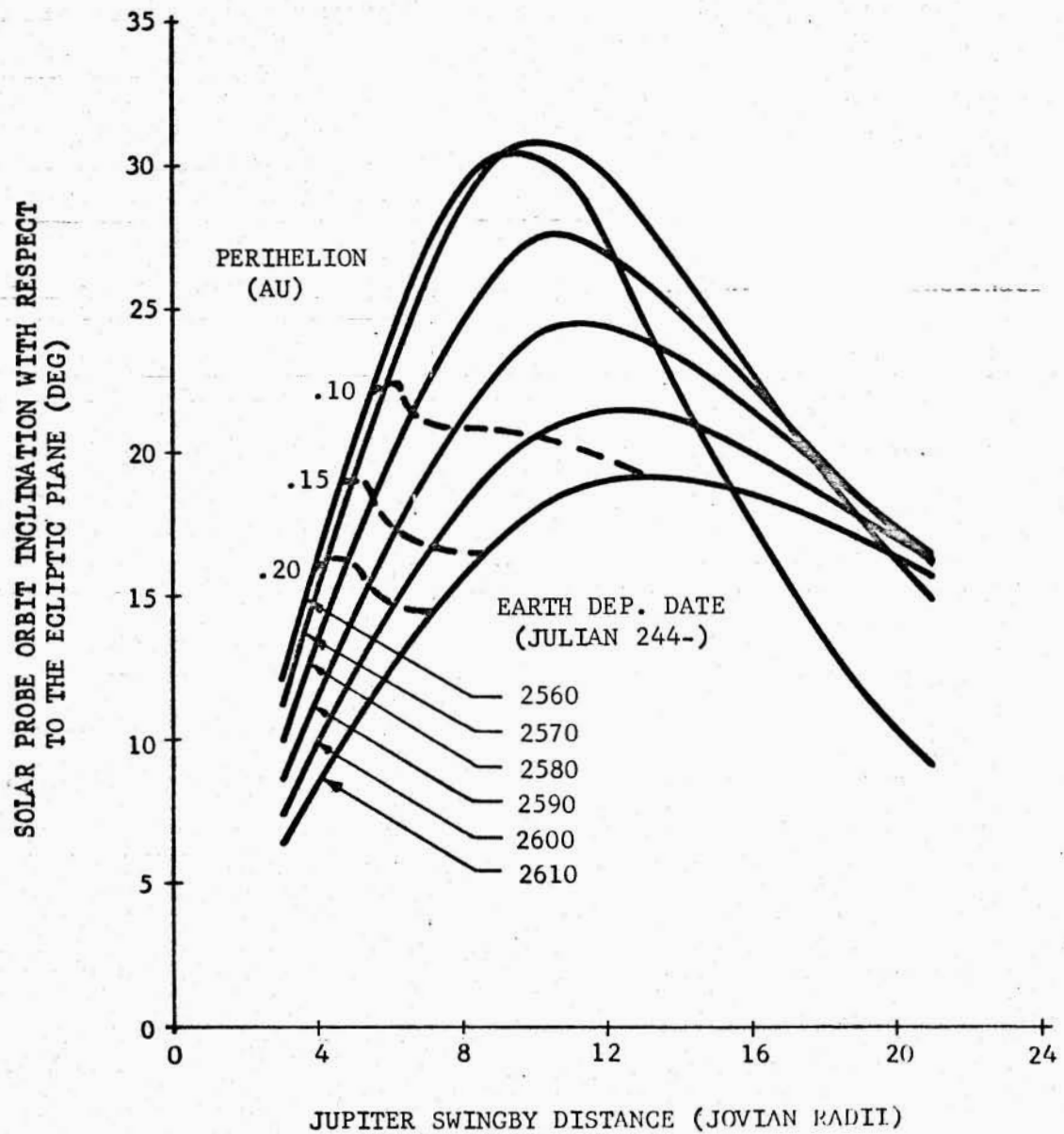


Figure 2-25. 1975 SOLAR PROBE TRAJECTORY VIA JUPITER SWINGBY: TRAJECTORY PLANE INCLINATION

Figure 2-24, and 175° in Figure 2-25. The encounter plane (175°) nearer Jupiter's orbital plane is seen to reduce the solar probe orbit inclinations significantly.

The characteristics of solar probe orbits via the Jupiter swingby mode during the 1972 launch opportunity are presented in Figures 2-26 through 2-30. The effects of launch date, Earth-Jupiter transfer time, and sphere-of-influence aiming point (represented by the swingby distance and inclination of the encounter hyperbola) are indicated. Figure 2-26 shows the perihelion achievable with 540-day Earth-Jupiter transfers and an encounter plane inclination, i_h , of 170° . Figure 2-27 is for $i_h = 175^\circ$. As shown in Figure 2-28, a 500-day Earth-Jupiter transfer with $i_h = 175^\circ$ permits solar flyby distances less than 0.04-AU throughout the range of departure dates. The flattening effect on the curves for the earlier departure dates is caused by the solar probe orbit becoming retrograde with respect to the Sun for swingby distances between about 6.5 and 11.5 Jovian radii. Figure 2-29 shows for the range of departure dates a narrow range of trip times (980-1050 days) from launch to solar flyby at a 0.1-AU perihelion for 500-day Earth-Jupiter transfers. The retrograde solar probe orbits mentioned above are shown in Figure 2-30. The inclination is seen to exceed 90° early during the launch period for a range of swingby distances centered around 9 Jovian radii. Reference back to Figure 2-28 shows that the retrograde orbits correspond to very close solar flyby distances (less than 0.04-AU). However, the inclination decreases considerably down to 25° - 30° for perihelion distances around 0.1-AU.

Figures 2-31 through 2-39 provide solar probe orbit data for a typical launch opportunity late in the decade (1978) for use in an analysis of mission trajectory and performance tradeoffs to be presented later in the report. These nine figures present the solar probe orbit perihelion, total trip time, and inclination parameters in similar format to the data previously given for the 1972 and 1975 launch opportunities. Figures 2-31 through 2-33 present data for 500-day Earth-Jupiter transfers; Figures 2-34 through 2-36 give similar data for 540-day transfers; and Figures 2-37 through 2-39 show the same parameters for 600-day transfers.

Figure 2-31 indicates a strong influence of retrograde solar probe orbits on perihelion distance for the 500-day Earth-Jupiter transfers. The perihelion curves for the range of departure dates are seen to cross over in the region of swingby distances that result in post-encounter retrograde motion about the Sun. Figure 2-33 shows the inclination as a function of swingby distance. Retrograde orbits are possible over practically the entire launch period for close perihelion distances. However, it will be shown that the performance requirements of the combined Jupiter orbiter/solar probe mission necessitate longer Earth-Jupiter transfer time than 500 days in 1978.

Operational Mode Effects on Solar Probe Orbit Design. As will be discussed in more detail in the systems analysis of subsection 2.2, it is of interest from the operational mode and vehicle design standpoint to consider the concept of a constant gross mass spacecraft designed for the end points of the launch period. This mode of operation uses the extra performance capability of the Saturn V during the launch period to decrease the Earth-Jupiter transfer time. Since the

- EARTH-JUPITER TRANSFER TIME: 540 DAYS
- INCLINATION OF ENCOUNTER HYPERBOLA AT JUPITER: 170°

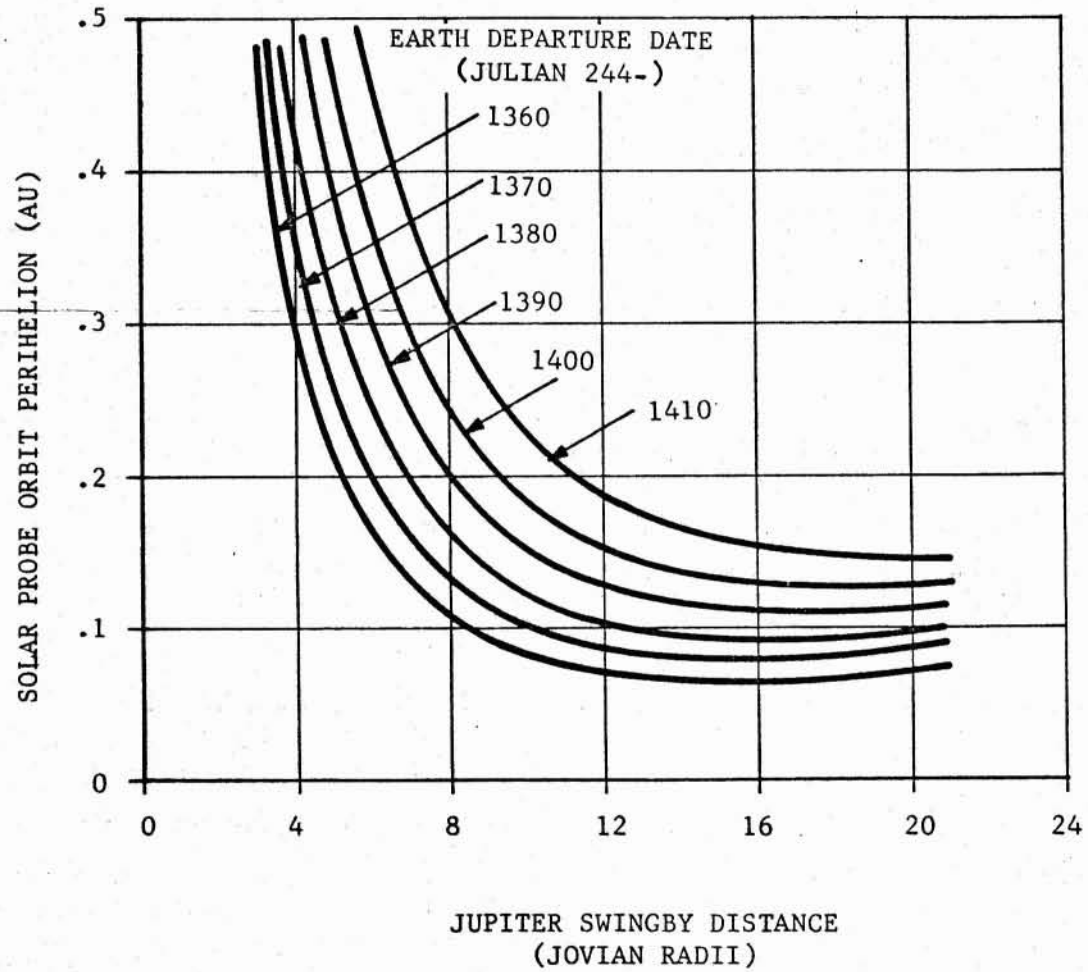


Figure 2-26. 1972 SOLAR PROBE TRAJECTORY VIA JUPITER SWINGBY: PERIHELION DISTANCE

- EARTH-JUPITER TRANSFER TIME: 540 DAYS
- INCLINATION OF ENCOUNTER HYPERBOLA AT JUPITER: 175°

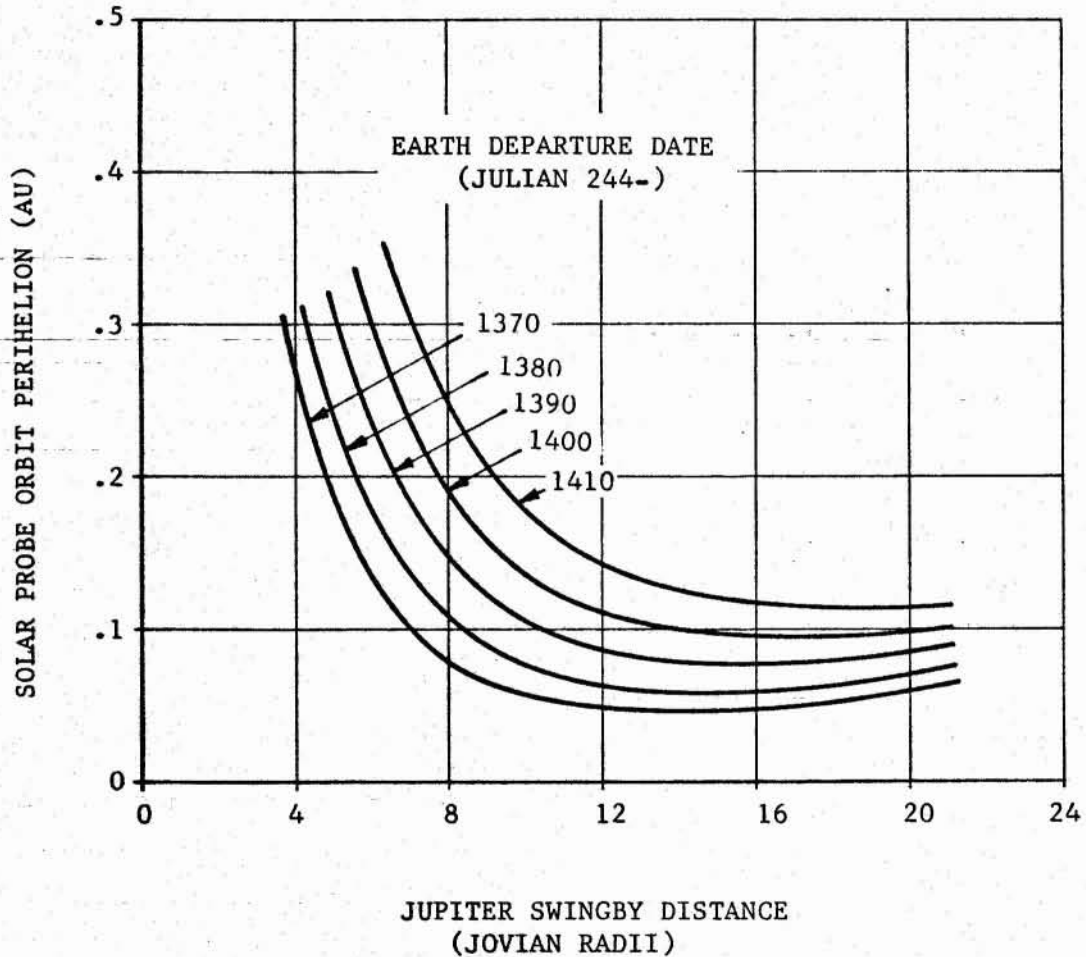


Figure 2-27. 1972 SOLAR PROBE TRAJECTORY VIA JUPITER
SWINGBY: PERIHELION DISTANCE

- EARTH-JUPITER TRANSFER TIME: 500 DAYS
- INCLINATION OF ENCOUNTER HYPERBOLA AT JUPITER: 175°

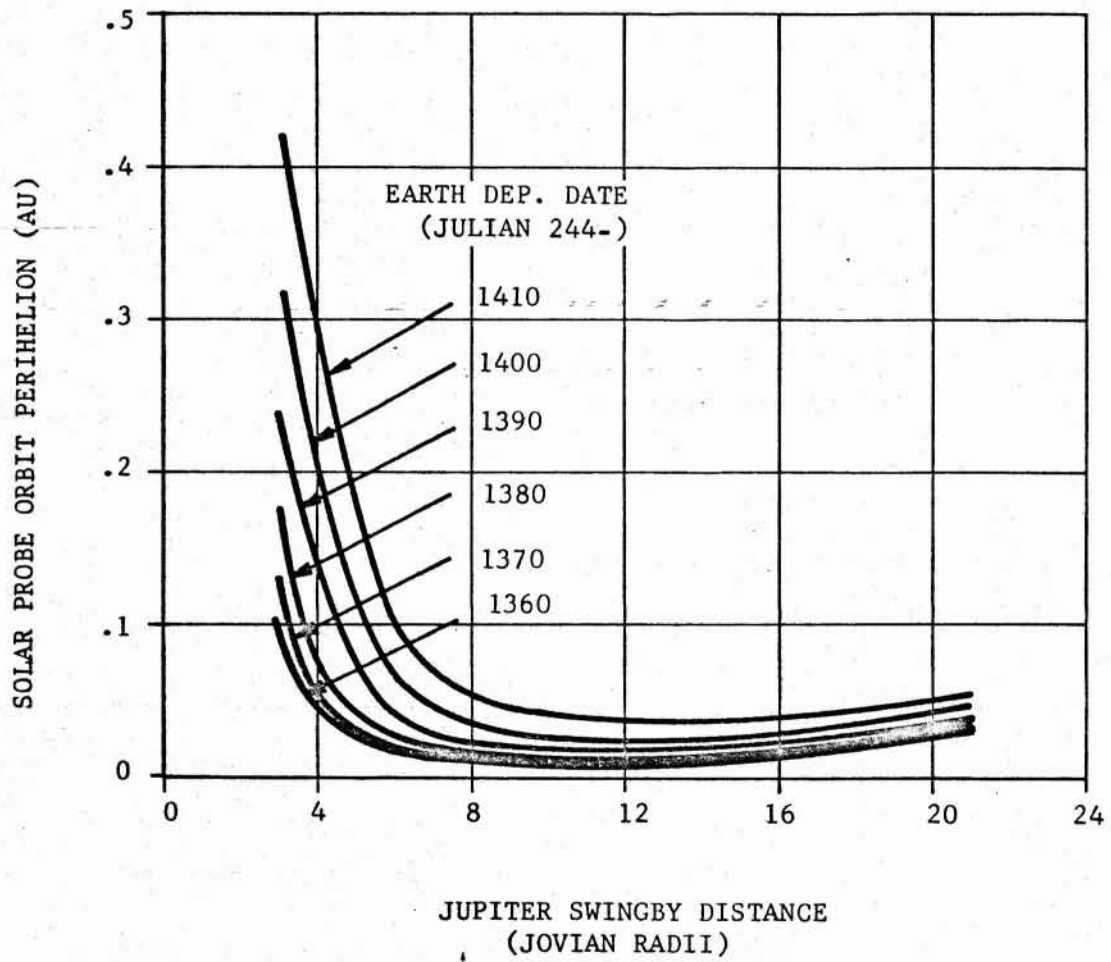


Figure 2-28. 1972 SOLAR PROBE TRAJECTORY VIA JUPITER SWINGBY: PERIHELION DISTANCE

- EARTH-JUPITER TRANSFER TIME: 500 DAYS
- INCLINATION OF ENCOUNTER HYPERBOLA AT JUPITER: 175°

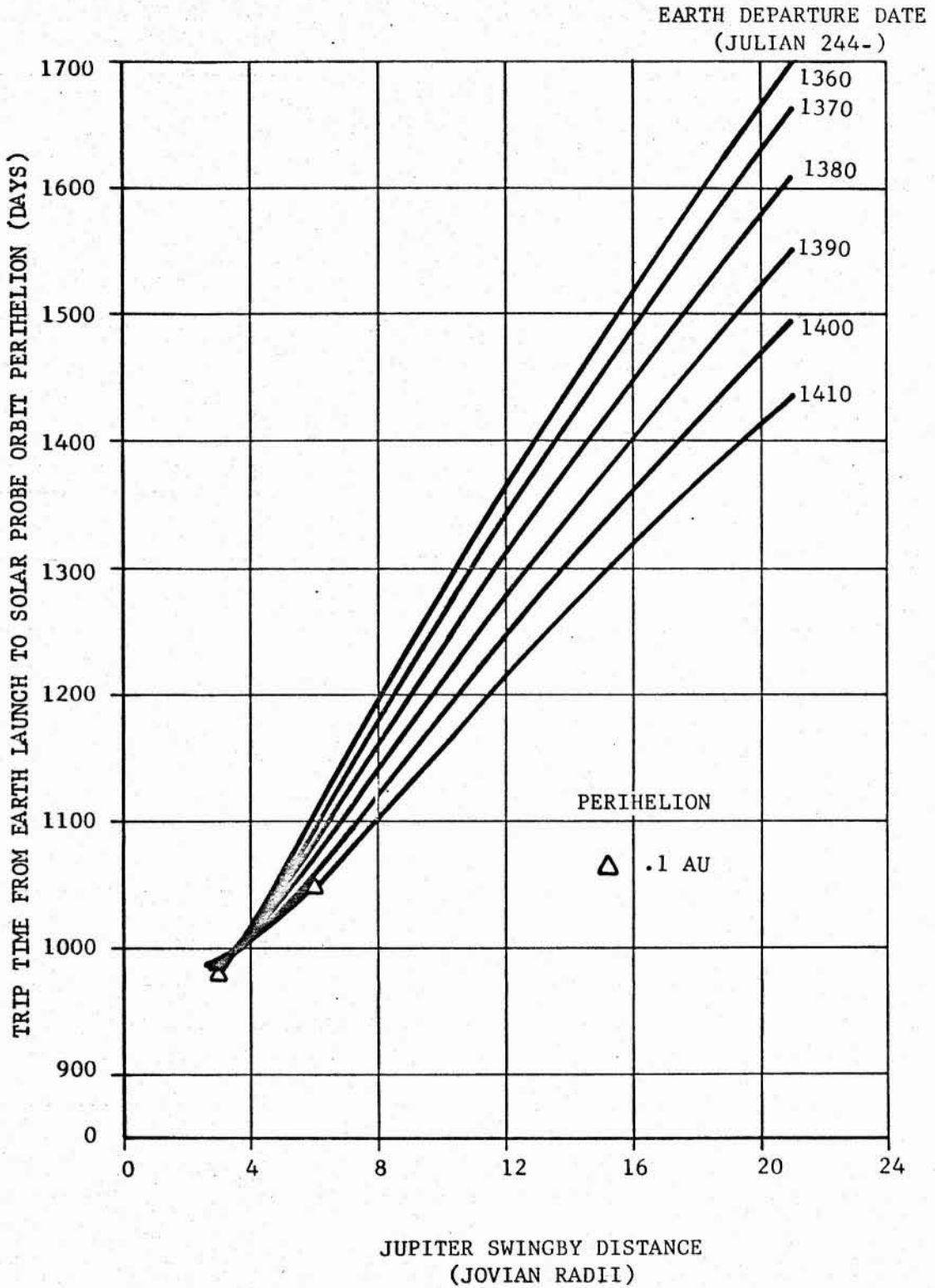


Figure 2-29. 1972 SOLAR PROBE TRAJECTORY VIA JUPITER SWINGBY: TRANSFER TIME FROM EARTH DEPARTURE TO SOLAR FLYBY

- EARTH-JUPITER TRANSFER TIME: 500 DAYS
- INCLINATION OF ENCOUNTER HYPERBOLA AT JUPITER: 175°

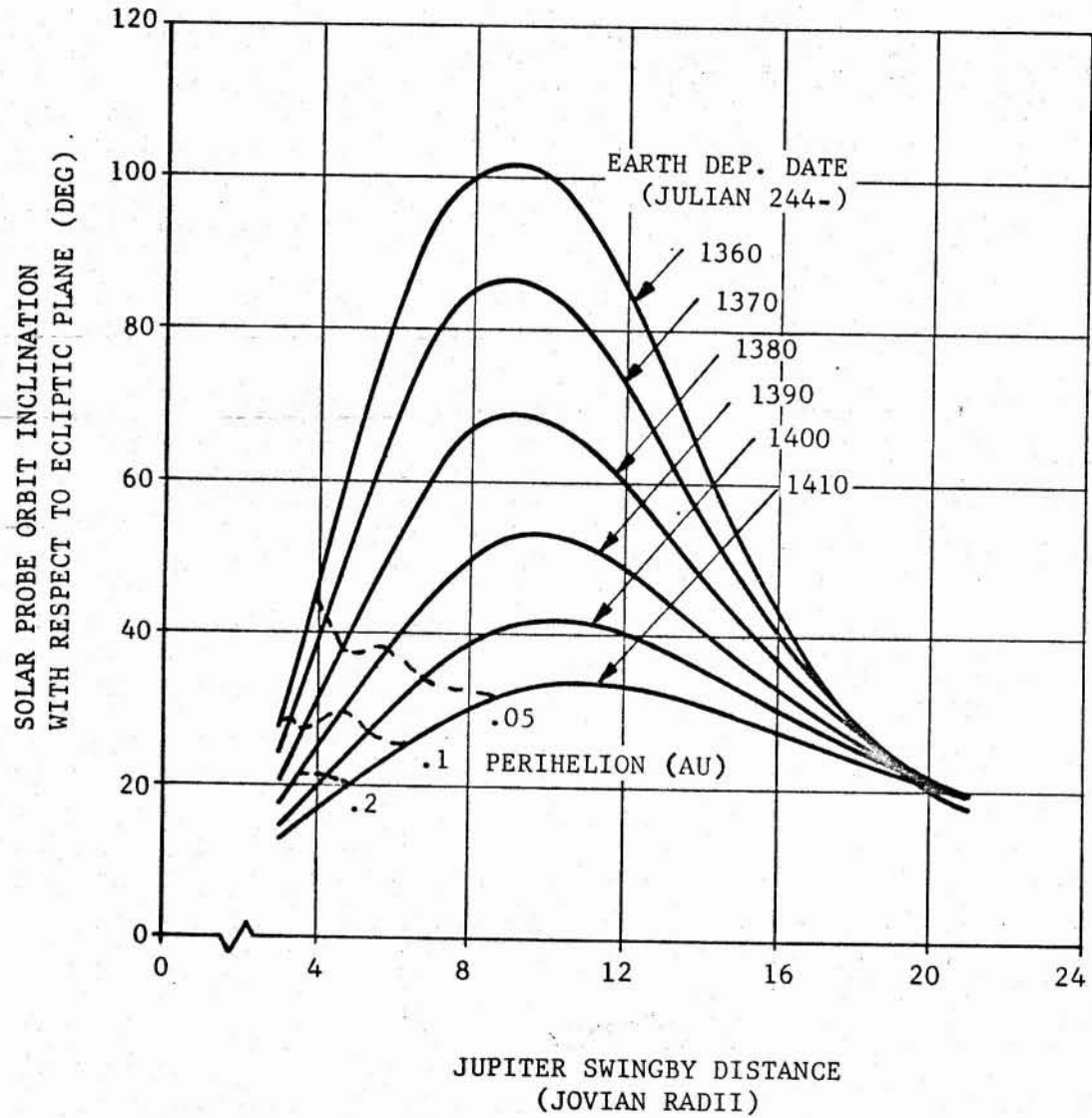


Figure 2-30. 1972 SOLAR PROBE TRAJECTORY VIA JUPITER SWINGBY: TRAJECTORY PLANE INCLINATION

- EARTH-JUPITER TRANSFER TIME: 500 DAYS
- INCLINATION OF ENCOUNTER HYPERBOLA AT JUPITER: 175°

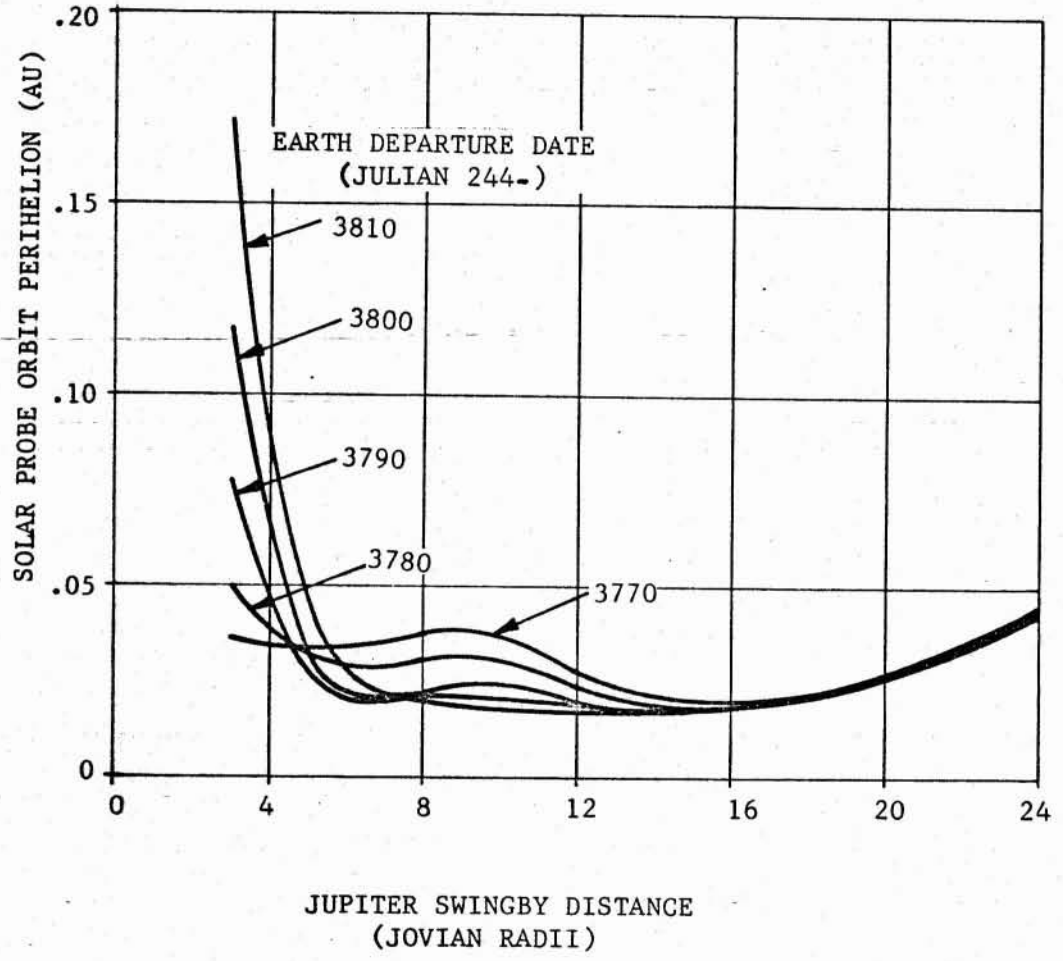


Figure 2-31. 1978 SOLAR PROBE TRAJECTORY VIA JUPITER SWINGBY: PERIHELION DISTANCE

- EARTH-JUPITER TRANSFER TIME: 500 DAYS
- INCLINATION OF ENCOUNTER HYPERBOLA AT JUPITER: 175°

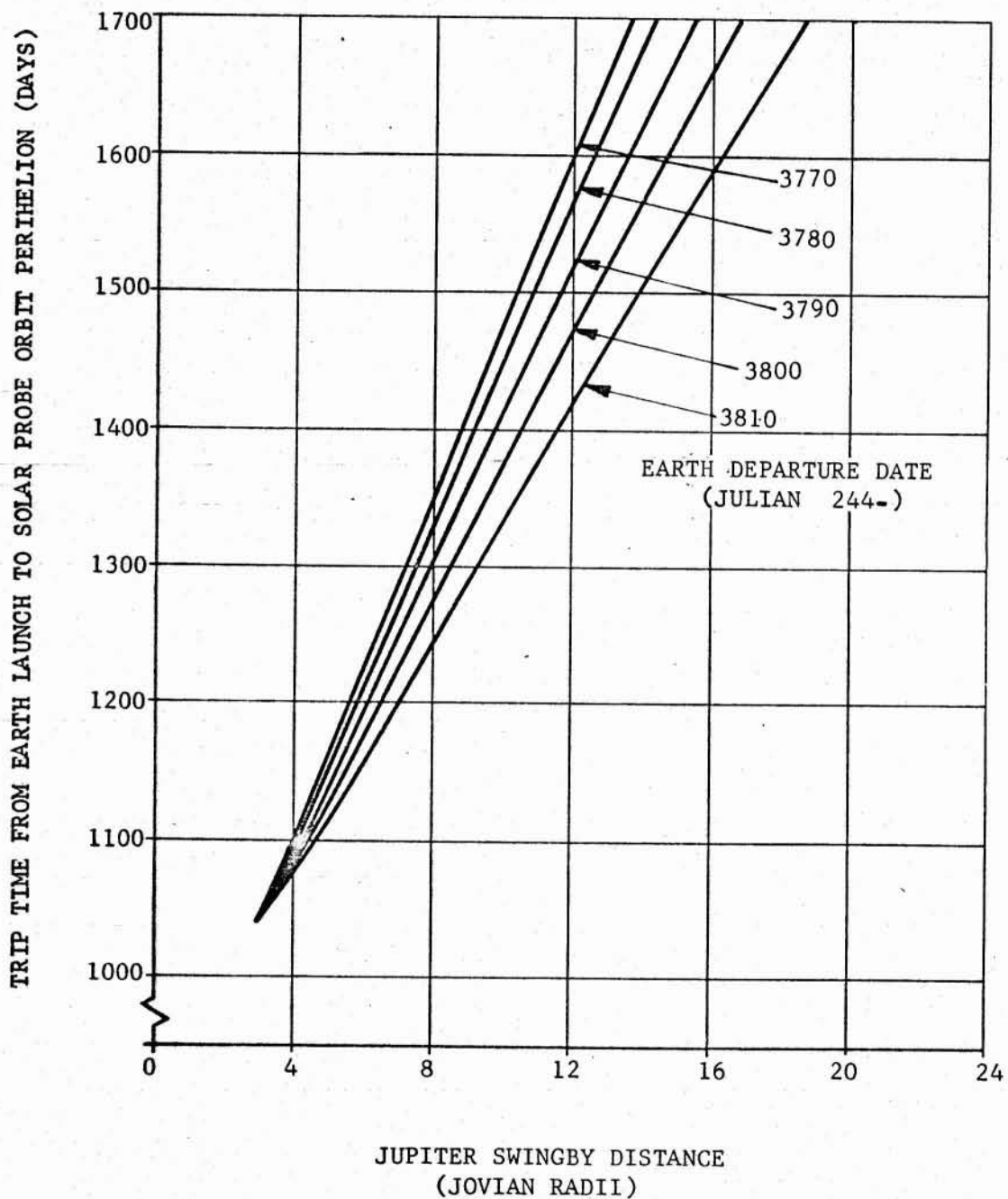


Figure 2.32. 1978 SOLAR PROBE TRAJECTORY VIA JUPITER SWINGBY: TRANSFER TIME FROM EARTH DEPARTURE TO SOLAR FLYBY

- EARTH-JUPITER TRANSFER TIME: 500 DAYS
- INCLINATION OF ENCOUNTER HYPERBOLA AT JUPITER: 175°

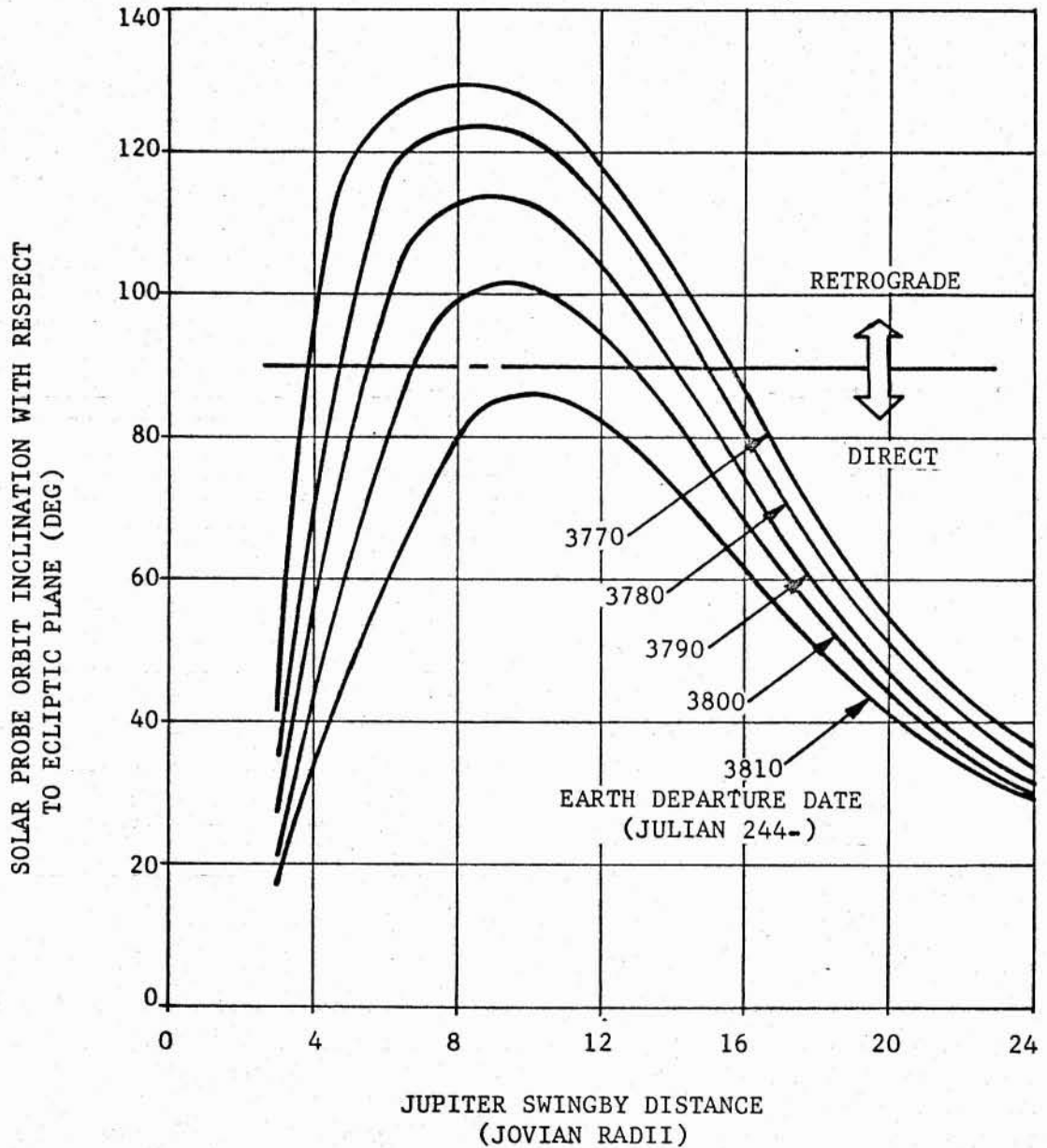


Figure 2-33. 1978 SOLAR PROBE TRAJECTORY VIA JUPITER SWINGBY: TRAJECTORY PLANE INCLINATION

- EARTH-JUPITER TRANSFER
TIME: 540 DAYS
- INCLINATION OF ENCOUNTER HYPERBOLA
AT JUPITER: 175°

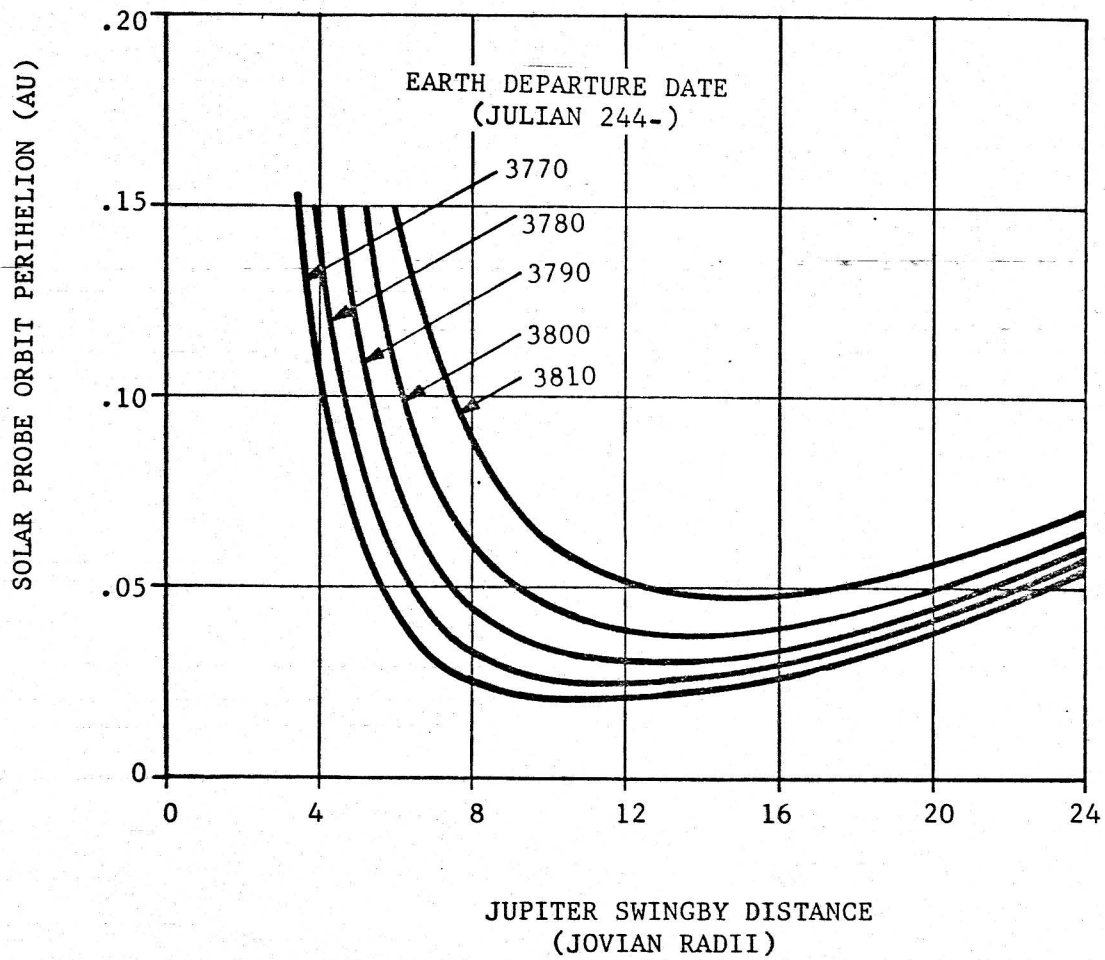


Figure 2-34. 1978 SOLAR PROBE TRAJECTORY VIA JUPITER SWINGBY:
PERIHELION DISTANCE

- EARTH-JUPITER TRANSFER TIME: 540 DAYS
- INCLINATION OF ENCOUNTER HYPERBOLA AT JUPITER: 175°

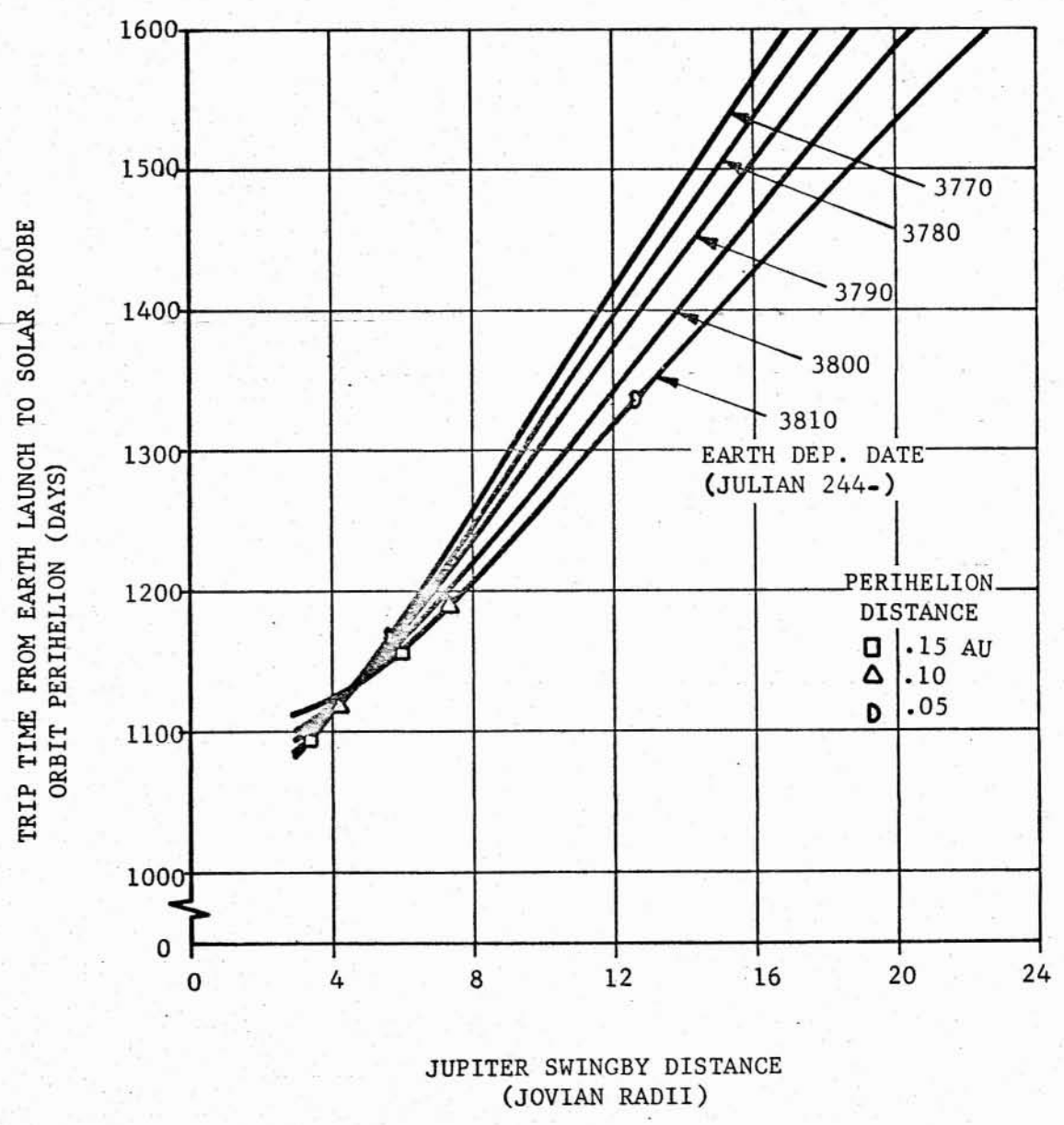


Figure 2-35. 1978 SOLAR PROBE TRAJECTORY VIA JUPITER SWINGBY: TRANSFER TIME FROM EARTH DEPARTURE TO SOLAR FLYBY

- EARTH-JUPITER TRANSFER TIME: 540 DAYS
- INCLINATION OF ENCOUNTER HYPERBOLA AT JUPITER: 175°

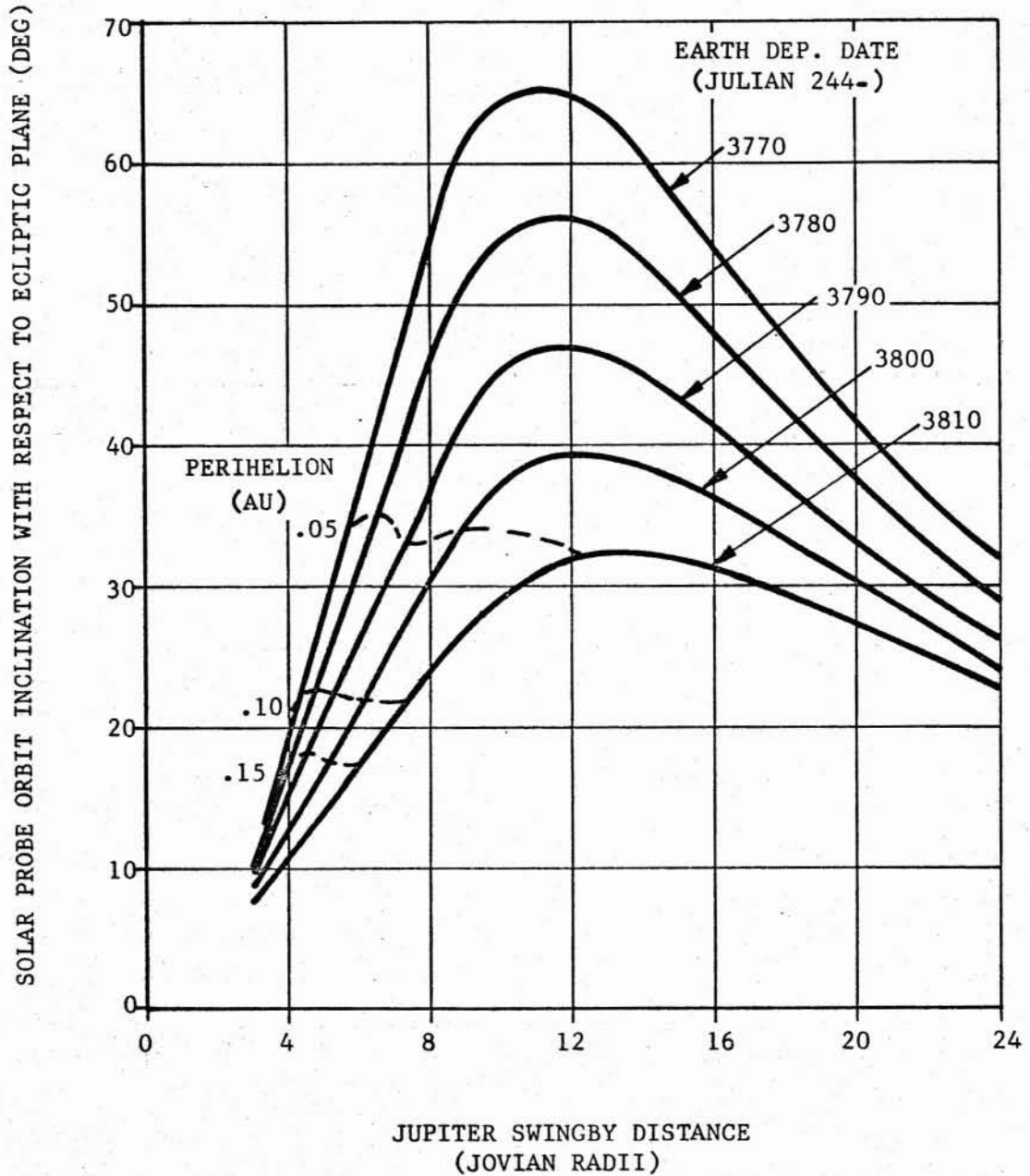


Figure 2-36. 1978 SOLAR PROBE TRAJECTORY VIA JUPITER SWINGBY: TRAJECTORY PLANE INCLINATION

- EARTH-JUPITER TRANSFER
TIME: 600 DAYS
- INCLINATION OF ENCOUNTER
HYPERBOLA AT JUPITER: 175°

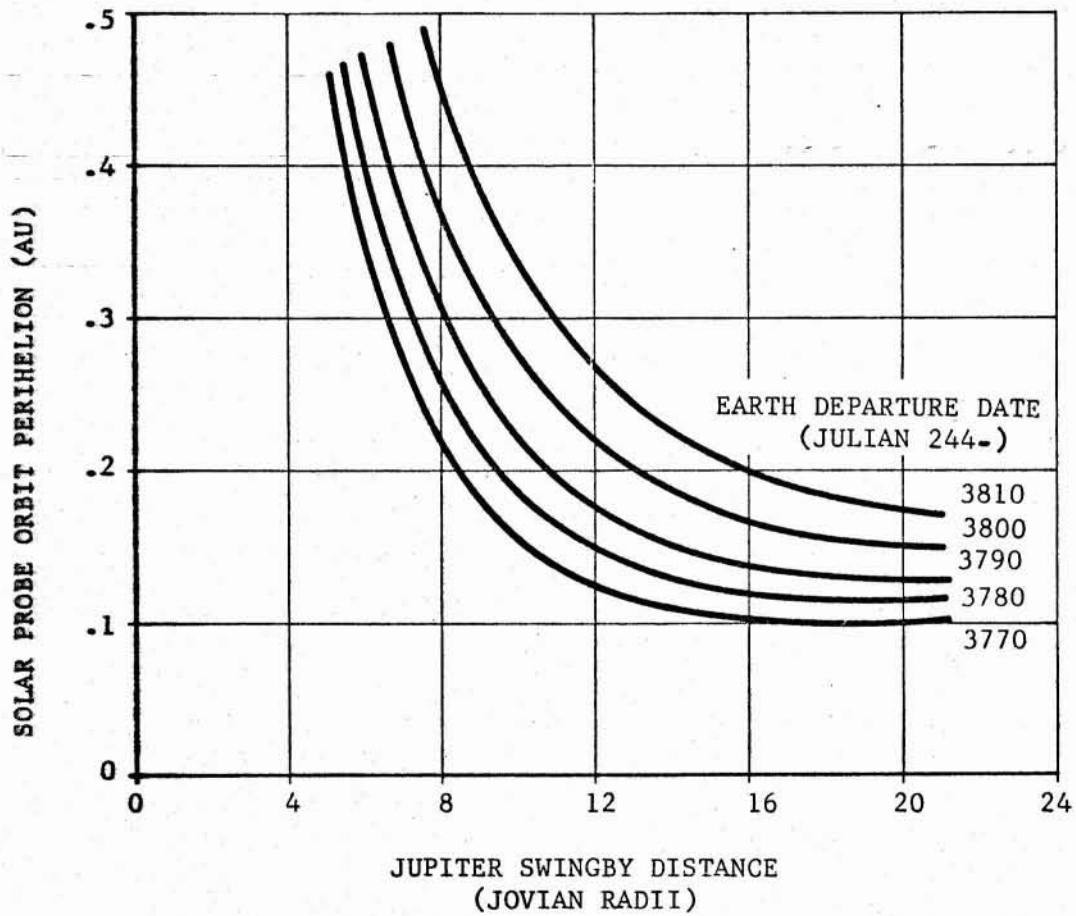


Figure 2-37. 1978 SOLAR PROBE TRAJECTORY VIA JUPITER SWINGBY: PERIHELION DISTANCE

- EARTH-JUPITER TRANSFER TIME: 600 DAYS
- INCLINATION OF ENCOUNTER PLANE AT JUPITER: 175°

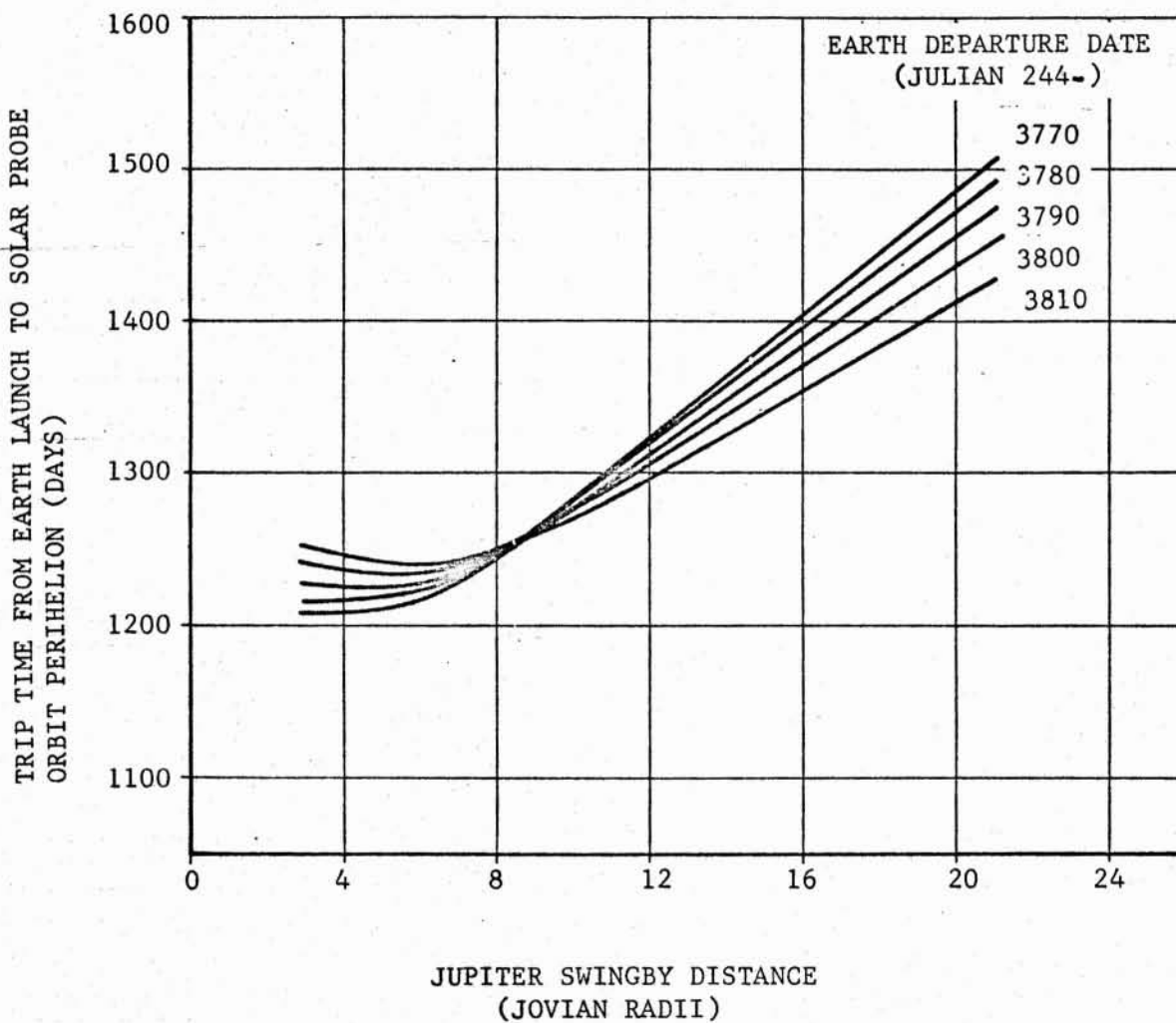


Figure 2-38. 1978 SOLAR PROBE TRAJECTORY VIA JUPITER SWINGBY: TRANSFER TIME FROM EARTH DEPARTURE TO SOLAR FLYBY

- EARTH-JUPITER TRANSFER TIME: 600 DAYS
- INCLINATION OF ENCOUNTER HYPERBOLA AT JUPITER: 175°

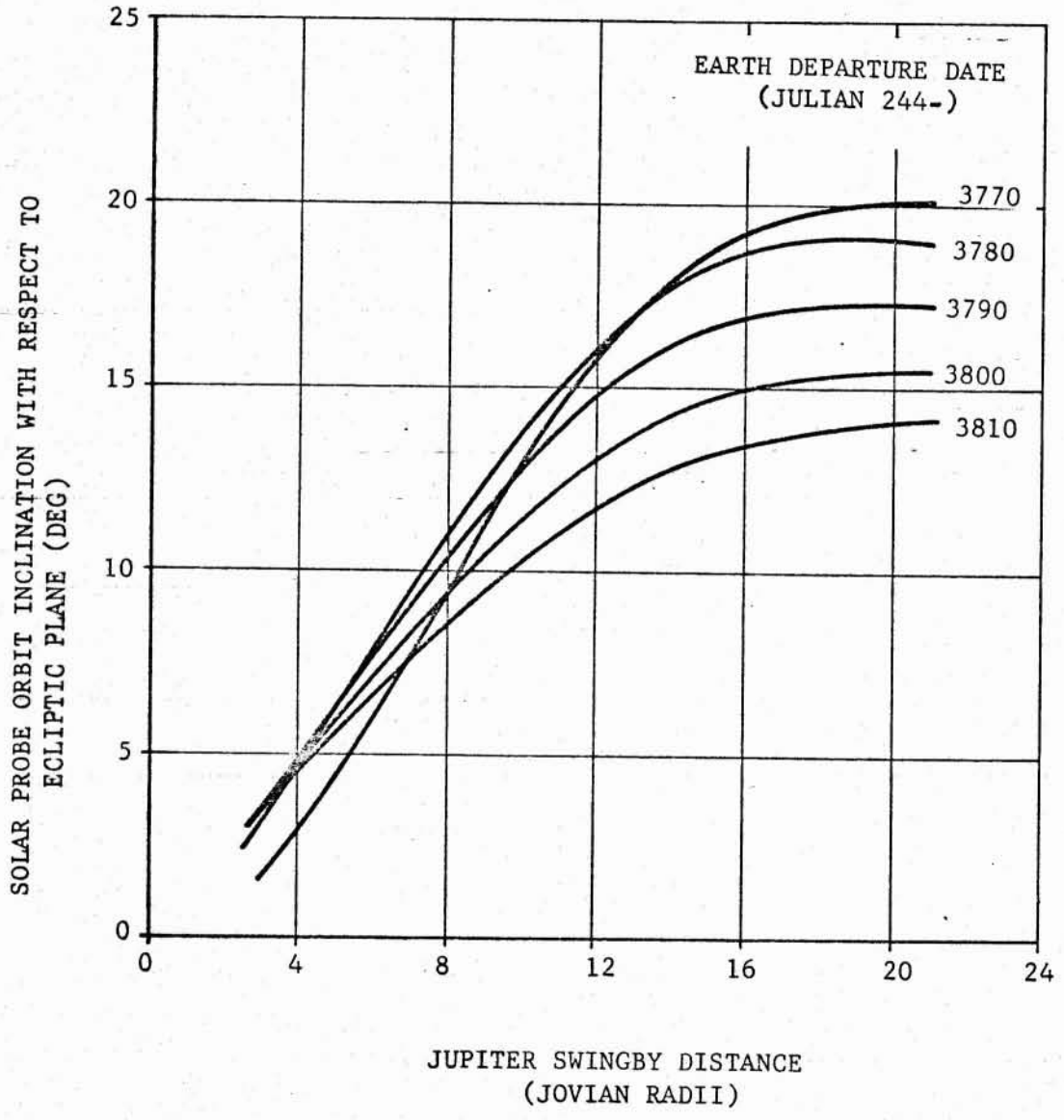


Figure 2-39. 1978 SOLAR PROBE TRAJECTORY VIA JUPITER SWINGBY: TRAJECTORY PLANE INCLINATION

arrival energy at Jupiter will vary with transfer time, the capture orbit eccentricity for a fixed perijove will have to be varied to permit capture braking with the constant propellant loading of the orbiter spacecraft. Figure 2-40 presents an example analysis of the constant spacecraft mass concept for the 1975 launch opportunity. The top figure shows the variation of Earth-Jupiter transfer time over a 20-day launch period for a 12,000-lb net injected mass (total spacecraft including launch vehicle adapter). The transfer time is seen to vary from 502 days down to 475 days, reaching the minimum near the middle of the launch period. The bottom plot of Figure 2-40 gives the solar probe orbit perihelion as a function of swingby distance at Jupiter for launch dates over the 1975 opportunity. These curves differ (relative to launch date) from the previous data presented for constant Earth-Jupiter transfer times. For a given swingby distance the perihelion distance is larger early during the launch period and decreases to a minimum for the fastest transfer at the middle of the launch period. The perihelion distance then increases later in the launch period as a result of the increasing transfer time. For a 0.1-AU perihelion mission, the required Jupiter swingby distance is about 7 Jovian radii at the beginning of the launch period. It decreases to 4.6 Jovian radii at mid-period and increases again to approximately 9.4 Jovian radii at the close of the period. Although not presented here, the total trip time from launch to perihelion for the 0.1-AU mission ranges from 1015 to 1150 days over the launch period. The inclination of the orbit with respect to the ecliptic plane varies from about 20° to 25° .

Solar Probe-Earth Communication Considerations. An analysis was performed to determine if the solar probe would be able to communicate with the Earth during solar flyby at perihelion. From the mission analysis standpoint this problem is one of determining the heliocentric position of the Earth at solar flyby relative to the "communication cone" of the probe. The communication cone is defined as the space cone, symmetrical about the longitudinal axis of the probe, inside of which the high-gain communications antenna aboard the probe can be gimbaled for pointing to the Earth. Thus, if the position of the Earth lies inside the probe communication cone during solar flyby, then line-of-sight communications can be made. For thermal control purposes, the longitudinal axis of the probe will be continually directed toward the center of the Sun.

The geometry of the communications problem can be defined in terms of four variables:

1. The heliocentric angle, λ_l , between the intersection of the probe communication cone at time of solar flyby and the projection of the solar probe orbit line of apsides onto the ecliptic plane
2. The solar probe communication cone half angle, β_c
3. The solar probe orbit perihelion radius, r_{ps}
4. The angle, μ , between the solar probe orbit line of apsides and the ecliptic plane.

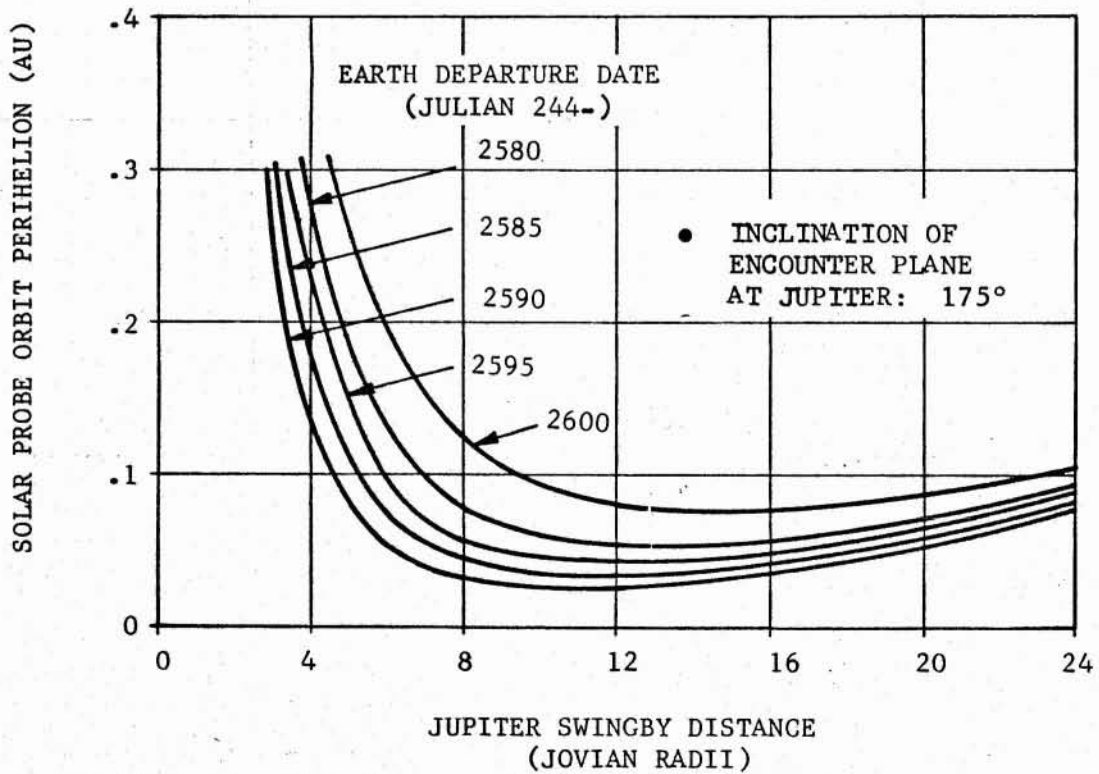
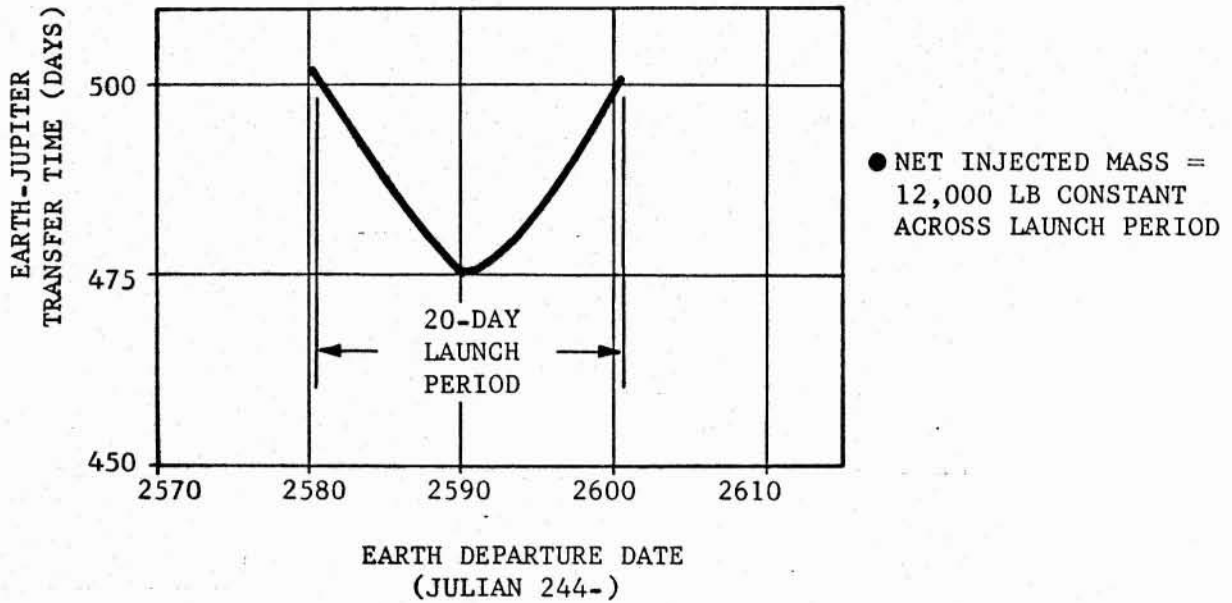


Figure 2-40. 1975 SOLAR PROBE TRAJECTORY VIA JUPITER SWINGBY: PERIHELION AND EARTH-JUPITER TRANSFER TIME FOR CONSTANT GROSS MASS JUPITER ORBITER/SOLAR PROBE

An equation may be derived to express the angle λ_ℓ as a function of β_c , r_{ps} , and μ . This relation is

$$\lambda_\ell = \arccos \frac{1 + r_{ps}^2 - \sin^2 [\beta_c - \arcsin(r_{ps} \sin \beta_c)] (\sin \beta_c)^{-2}}{2r_{ps} \cos \mu}$$

where the perihelion radius, r_{ps} , is in AU. This equation may be used to determine the angular position limits, symmetrical about the projected line of apsides of the solar probe orbit, within which the Earth must be at time of solar flyby in order to communicate with the probe. Figure 2-41 gives the value of λ_ℓ as a function of the solar probe communication cone half angle for a perihelion of 0.1 AU and a range of μ from 0° to 20° . Generally, the line of apsides of the solar probe orbit will lie close to the ecliptic plane, and μ will be small. Moreover, the value of λ_ℓ is seen to be a relatively weak function of μ . Thus, for a given perihelion, λ_ℓ is primarily a function of the probe communication cone half angle. The effect of perihelion distance on the value of λ_ℓ is shown by Figure 2-42 for a communication cone half angle of 80° . A 0.1-AU mission would require the Earth's angular position at time of solar flyby to be within $\pm 74^\circ$ of the line of apsides of the solar probe orbit for communications.

To translate the above information in terms of a typical mission trajectory, consider Figure 2-43. This figure presents the Earth's angular position, λ , relative to the solar probe orbit line of apsides at the time of perihelion passage for trajectories during the 1975 opportunity. Plots like this can be used in conjunction with the information of Figures 2-41 and 2-42 to analyze the communication geometry for given missions. For the example shown, the 0.15- and 0.20-AU missions provide excellent communication geometry at solar flyby. The trajectories during the latter portion of the 20-day launch period shown for the 0.1-AU missions result in Earth positions outside of the probe communication cone for the closer swingby distances at Jupiter. However, a favorable geometry can be achieved by going to the greater Jupiter swingby distances. For example, a trajectory with a Julian 244-2600 departure date and a Jupiter swingby distance of 22 planet radii, results in an Earth position at time of solar flyby of about -35° . This position is well within the ± 74 -degree limits for a probe communication cone half angle of 80° .

2.1.3.3 Planetary Guidance Requirements. For mission analysis purposes, the planetary guidance requirements for the Jupiter orbiter/solar probe mission were limited to consideration of:

1. Heliocentric trajectory characteristics as related to guidance requirements
2. Midcourse correction requirements
3. Approach maneuver requirements for the orbiter spacecraft after solar probe separation.

The systems aspects of guidance, navigation, and control of the spacecraft are

- PERIHELION = .1 AU
- λ_p MEASURED IN ECLIPTIC FROM PROJECTED SOLAR PROBE ORBIT LINE OF APSIDES (CLOCKWISE +)

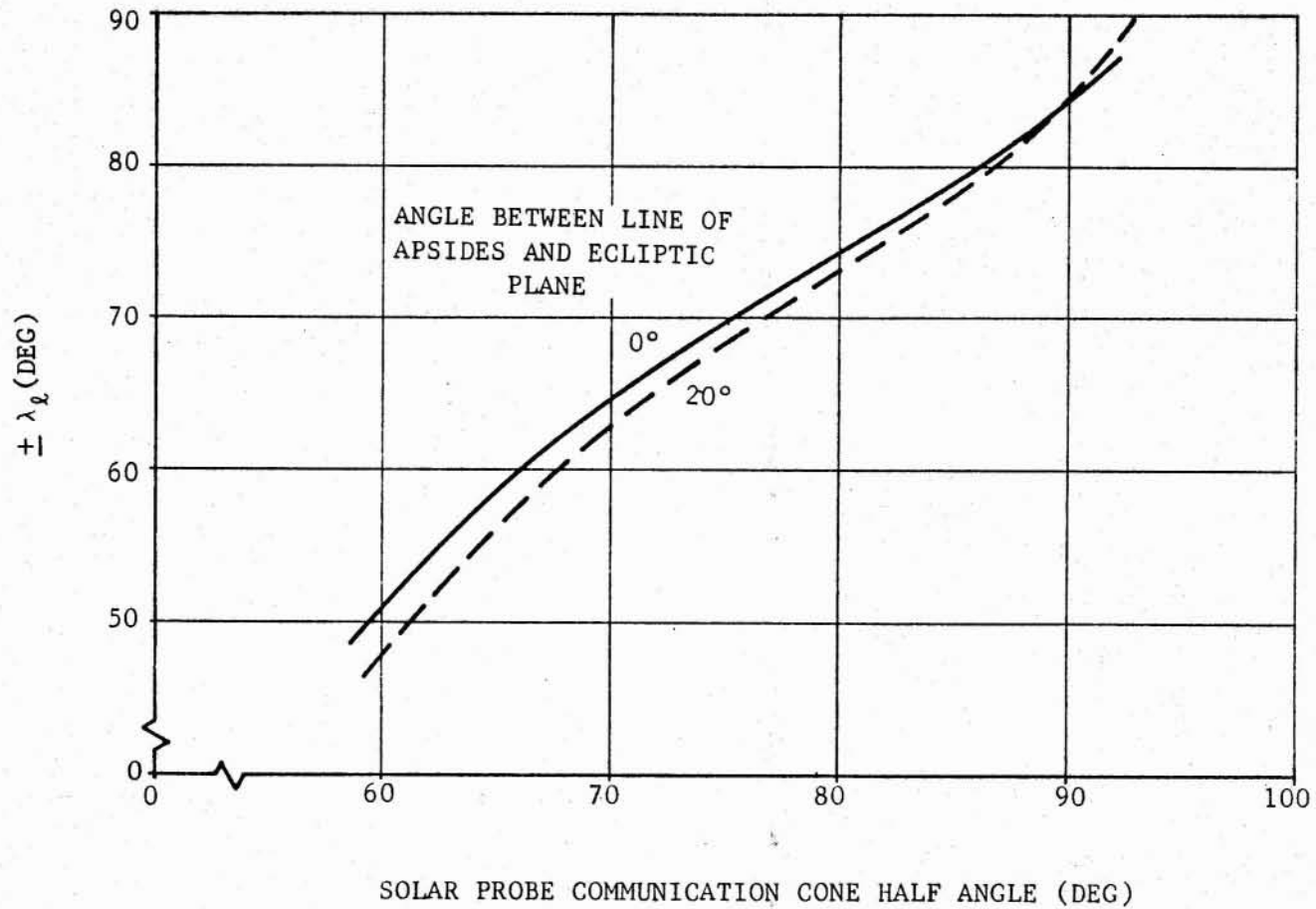


Figure 2-41. SOLAR PROBE ORBIT: REQUIRED ANGULAR POSITION LIMIT λ_p OF EARTH FOR COMMUNICATION AT SOLAR FLYBY

- λ_{ℓ} MEASURED IN ECLIPTIC FROM PROJECTED SOLAR PROBE ORBIT LINE OF APSIDES (CLOCKWISE +)
- SOLAR PROBE COMMUNICATION CONE HALF ANGLE = 80°

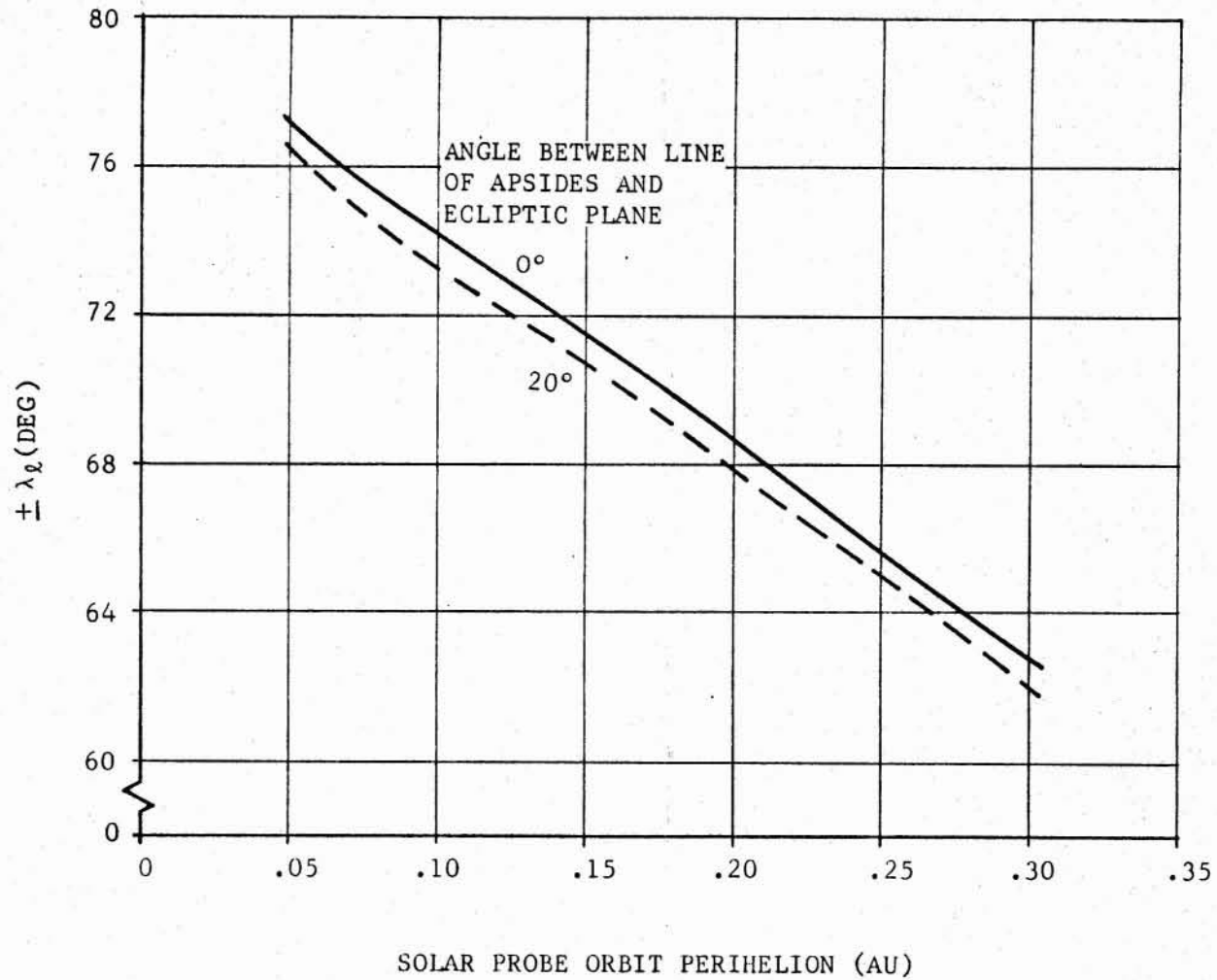


Figure 2-42. SOLAR PROBE ORBIT: REQUIRED ANGULAR POSITION LIMIT λ_{ℓ} OF EARTH FOR COMMUNICATION AT SOLAR FLYBY

• EARTH-JUPITER TRANSFER TIME: 500 DAYS

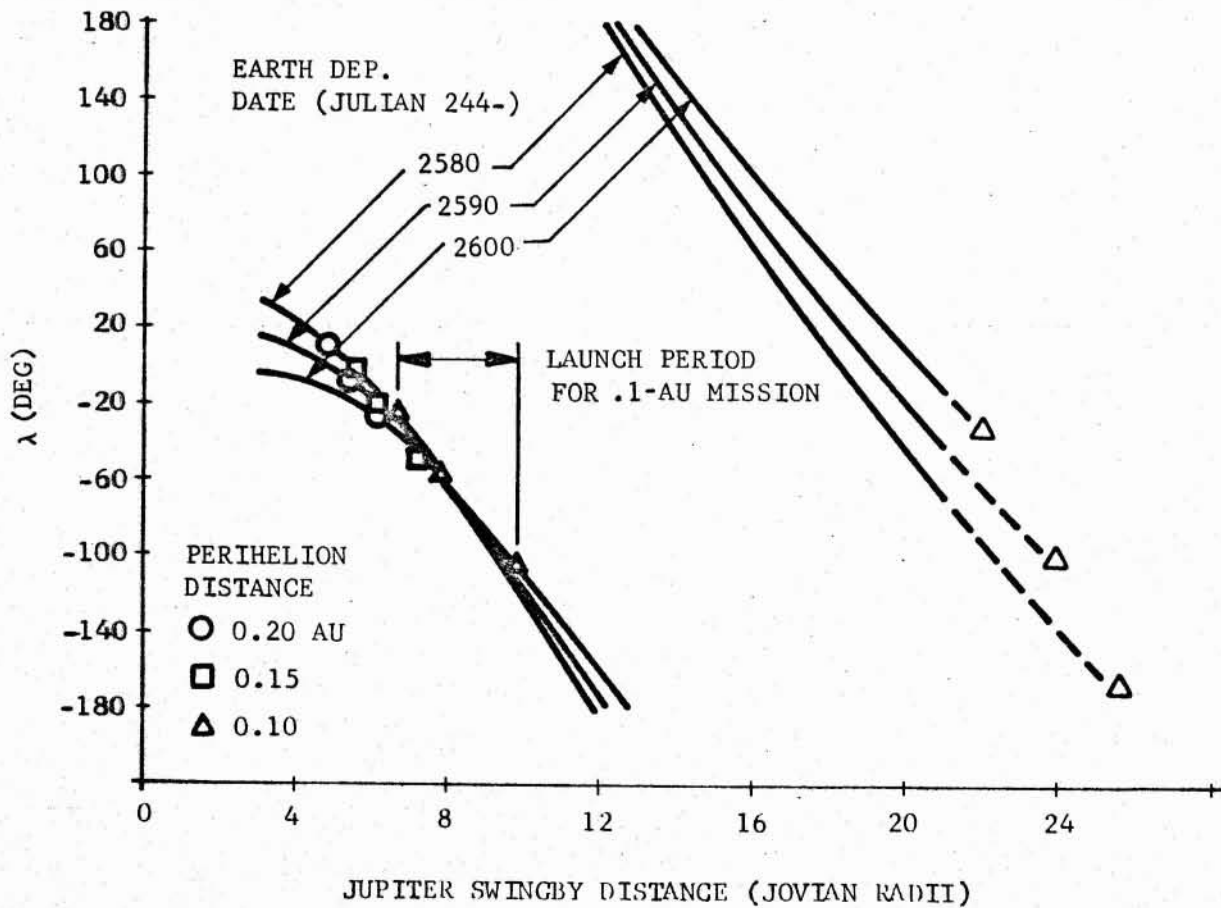
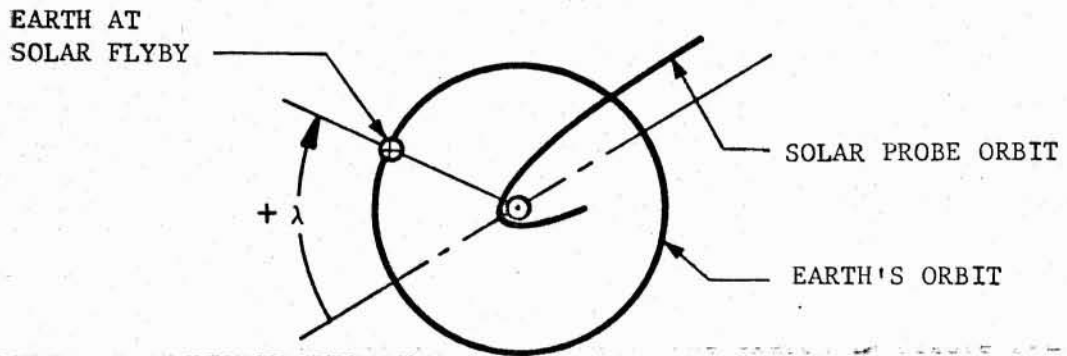


Figure 2-43. 1975 SOLAR PROBE TRAJECTORY VIA JUPITER SWINGBY: EARTH POSITION AT SOLAR FLYBY

September 1966

covered in the Systems Analysis, subsection 2.2. The solar probe is designed on the basis that no midcourse corrections will be made in the post-encounter heliocentric trajectory. Therefore, the accuracy of the solar probe orbit will be determined by the accuracy of the Jupiter swingby trajectory.

A study of the heliocentric trajectory characteristics presented in subsection 2.1.3.2 indicates that the requirements for achieving a solar probe orbit via the Jupiter swingby mode should not present any real problems in utilization of existing guidance techniques. The sensitivity of the post-encounter solar probe orbit characteristics to errors in the miss distance at Jupiter can be determined from the graphical data showing perihelion, trip time from launch to solar flyby, and orbit inclination as functions of swingby distance. The slopes of these curves around the swingby distance that gives the desired perihelion for a given departure date are direct measures of the guidance error sensitivity associated with the miss distance. As an example, consider a nominal 0.1-AU solar flyby mission in 1975 based on 500-day Earth-Jupiter transfers and an encounter hyperbola inclination of 175° . The sensitivities of the perihelion (r_{ps}), trip time (T_f) from launch to solar flyby, and solar probe orbit inclination (i) relative to errors in swingby distance (r_p) are summarized in Table 2-1.

Table 2-1.

SENSITIVITY OF SOLAR PROBE ORBIT CHARACTERISTICS
TO ERRORS IN JUPITER SWINGBY DISTANCE

Departure Date (Julian)	$\Delta r_{ps} / \Delta r_p$ (AU/Jovian radii)	$\Delta T_f / \Delta r_p$ (days/Jovian radii)	$\Delta i / \Delta r_p$ (deg/Jovian radii)
244-2580	.025	31	2.50
244-2590	.017	27	1.75
244-2600	.010	25	0.83

The sensitivity of perihelion relative to swingby distance errors can be reduced to extremely small values by proper selection of the Earth-Jupiter transfer time for each departure date. The transfer time may be chosen to place the desired mission perihelion at the minimum point on the curve of perihelion versus Jupiter swingby distance. Therefore, the slope of the curve ($\Delta r_{ps} / \Delta r_p$) at this point is zero. The typically flat characteristic of the curve near the minimum point means that a swingby distance error of 3 or 4 planet radii could be allowed with little effect on the perihelion. The associated variances in trip time and solar probe orbit inclination would be much larger; however, these parameters should not be as important to the mission objectives as the perihelion distance at solar flyby.

Perturbations on the probe trajectory caused by solar-radiation pressure were not evaluated for purposes of the mission analysis.

Midcourse Correction. For purposes of this study the velocity budget for midcourse corrections during the Earth-Jupiter transfer is based on the estimate made in reference 1 for the Jupiter capture mission. A total of 100-150 m/sec was estimated by consideration of launch vehicle guidance accuracy and the characteristics of the transfer trajectories under consideration.

With regard to the spacing of correction maneuvers during the transfer, it is desirable to make the first correction as soon as possible (5-10 days) after the injection out of Earth parking orbit. For the present study, the second correction is considered to be performed after two-thirds of the Earth-Jupiter transfer time. This should permit an adequate determination of the trajectory to justify a second maneuver. If required, a third correction is made after two-thirds of the remaining time to Jupiter arrival.

In view of the overall objectives of the Jupiter orbiter/solar probe mission analysis, a detailed study of midcourse correction requirements was not undertaken. However, for performance and mission profile design purposes, the estimates described in the preceding paragraphs are considered adequate.

Jupiter Approach Maneuver. The separation of the solar probe is made at entry into the Jovian sphere of influence. As shown by the sketch in Figure 2-44, the solar probe continues on a swingby hyperbola about the planet while the orbiter spacecraft is maneuvered onto an altered hyperbolic path. The periapsis of the altered hyperbola swings the orbiter in close to the planet for capture-orbit braking. The magnitude of the velocity change required for the approach maneuver at the sphere of influence is shown by Figure 2-44. The maneuver ΔV is plotted as a function of the arrival hyperbolic-excess speed for various solar probe swingby distances. For a typical arrival speed of 0.4 EMOS, the maneuver ΔV for a swingby distance of 10 Jovian radii is about 230 m/sec. For a 0.4 EMOS arrival speed the path angle change in the plane of the hyperbola for the approach maneuver varies from about 0.6 to 2.0 degrees for swingby distances from 5 to 20 Jovian radii, respectively.

2.1.4 Earth Launch Window Analysis. Reference 1 presented a detailed analysis of launch and parking orbit characteristics of Earth-Jupiter trajectories for Jupiter capture missions. The computer program used for that analysis was employed in the present study to determine typical surface launch window characteristics for the Earth-Jupiter trajectories associated with the combined Jupiter orbiter/solar probe mission. The program determines both the surface launch windows from AMR and Earth parking orbit coast times from parking orbit injection to interplanetary transfer injection. However, only the launch window characteristics are presented in the present study.

The computer program requires the following input parameters for the launch window analysis:

1. Launch date
2. Injection energy, $C_3 = |\vec{V}_{HE}|^2$
3. Declination of the outgoing geocentric asymptote
4. Right ascension of the outgoing asymptote.

- APPROACH MANEUVER ΔV AT JUPITER
- CAPTURE ORBIT PERIJOVE = 1.1 JOVIAN RADII

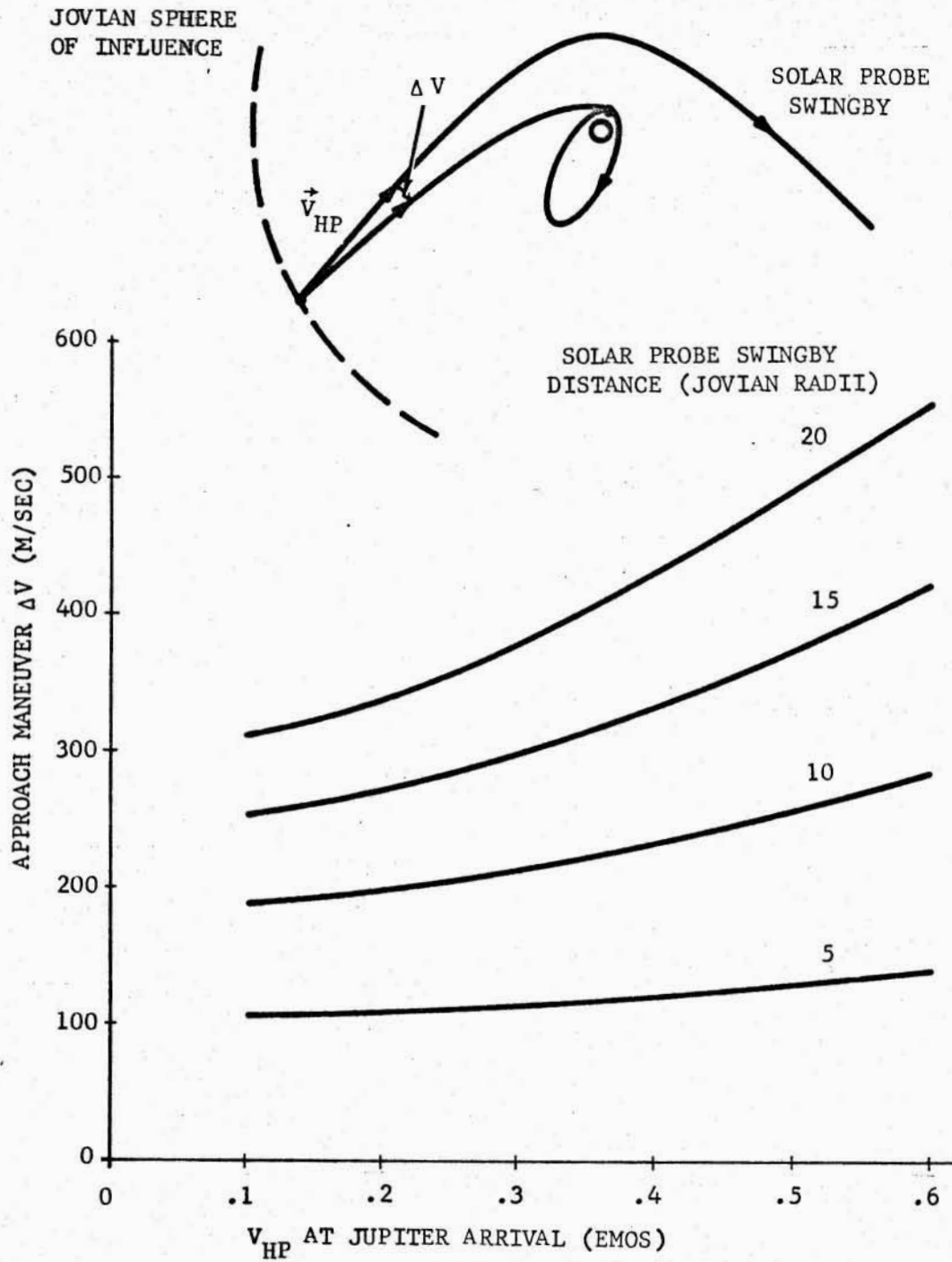


Figure 2-44. JUPITER ORBITER/SOLAR PROBE MISSION: APPROACH MANEUVER ΔV AT JUPITER

September 1966

The basic geometrical requirements on the ascent trajectory and parking orbit are primarily determined by the declination of the outgoing geocentric asymptote. The direction of the asymptote is that of the hyperbolic-excess velocity V_{HE} at departure. For two-dimensional ascent, the ascent and parking orbit plane must contain the V_{HE} vector. In general, if the absolute value of the declination is less than the launch-site latitude (28.3° at AMR), then no restrictions are placed on launch azimuth other than those imposed by range safety. If, however, the absolute value of the declination is greater than the launch-site latitude, then a band of launch azimuths symmetrical about due East (90°) are unavailable geometrically for launch by two-dimensional ascent. Figure 2-45 presents the variation of the asymptote declination over the 1970-1980 decade for 500-day Earth-Jupiter transfers and 20-day launch periods. The overall periodic pattern indicates that the 1972, 1973, 1977, and 1978 opportunities have the largest outgoing asymptote declinations; however, the absolute values do not exceed the latitude of the AMR launch site by much if any. The declination crosses through a minimum during the 1975 opportunity.

Figures 2-46, 2-47, and 2-48 give the results of a surface launch window analysis of the 1975 and 1978 opportunities as representative of the 1970-1980 time period. Figure 2-46 shows the declination and right ascension of the outgoing geocentric asymptote as functions of launch date for 500-day transfers during the 1975 opportunity. The injection energy variation over the opportunity was given previously in Figure 2-6. The surface launch window characteristics are summarized in Figure 2-47. The launch time of day in Greenwich Mean Time (GMT) is shown as a function of launch date for launch azimuths from 50° to 110° at AMR. For an azimuth range from 70° to 110° , two daily windows of 5-hours duration each are seen to exist across the entire launch period. Therefore, the launch window presents no problem to mission operations.

The daily launch windows for 540-day transfers during the 1978 opportunity are given in Figure 2-48. The figure shows that launch windows are quite satisfactory for mission operations even during a year representative of the largest asymptote declinations. As the plot of launch time of day shows, two daily windows from 2.6- to about 5-hours duration are available each day across the period.

2.1.5 Capture Orbit Analysis. This subsection presents an analysis of the characteristics of capture orbits about Jupiter and gives the necessary braking velocity increment data for sizing the orbiter mainstage propulsion system. The mission profile is based on single-impulse braking at the periapsis of the approach hyperbola.

It was shown in the Jovian Capture Analysis, subsection 2.5, of reference 1 that for a given capture orbit apsidal ratio ($n = r_a/r_p$) there exists an "optimum" perijove radius that minimizes braking velocity increment as a function of arrival hyperbolic-excess speed, V_{HP} . Figure 2-49, taken from reference 1, shows the optimum perijove radius versus arrival speed for apsidal ratios from 1 to 40. The figure shows that to achieve an optimum perijove close to the planet, which is desirable from the scientific experiment standpoint, it is necessary to have highly eccentric capture orbits. This is also desirable because the orbiter could investigate the space around Jupiter

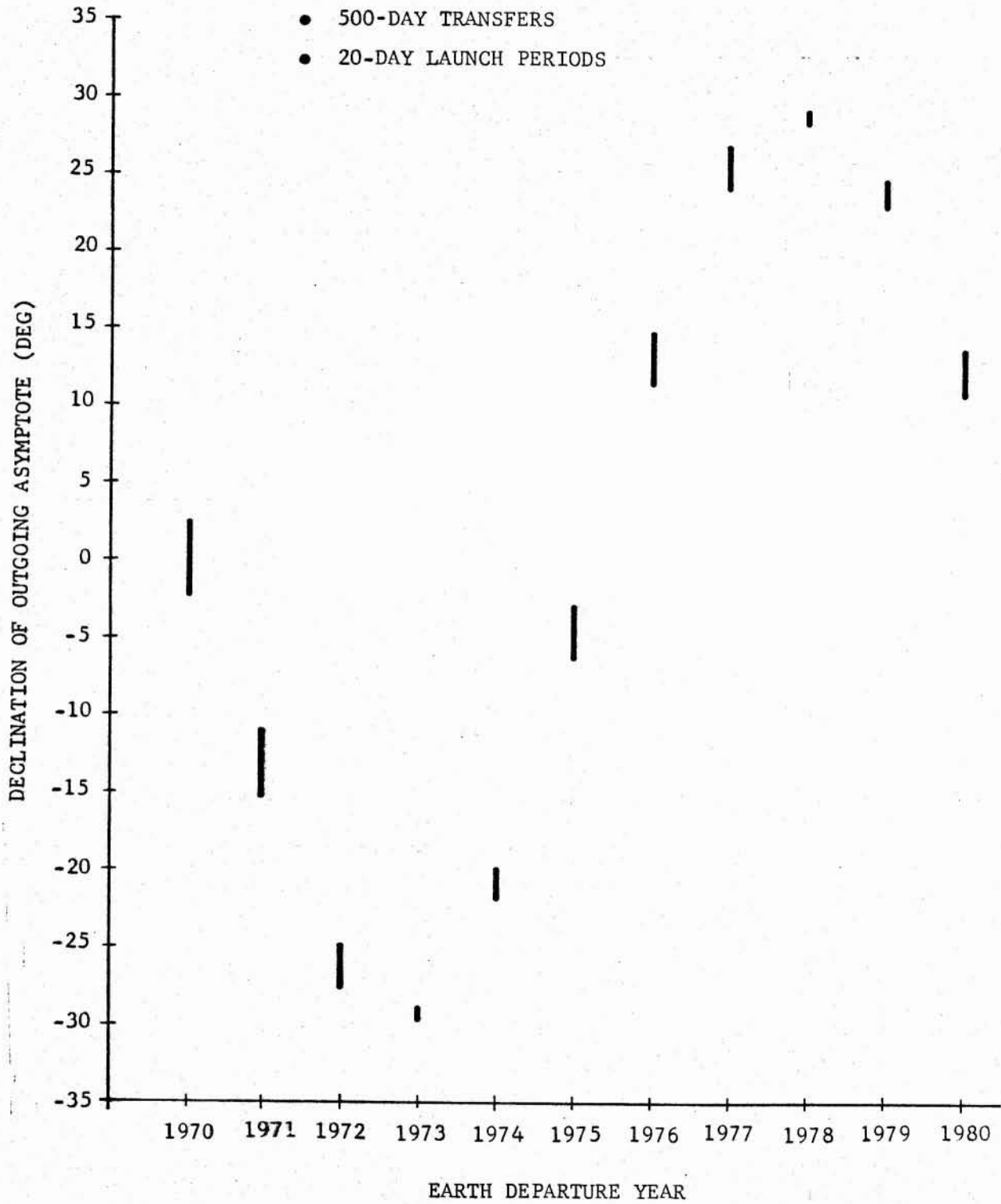


Figure 2-45. DECLINATION OF OUTGOING GEOCENTRIC ASYMPTOTE FOR FAST EARTH-JUPITER TRANSFERS DURING 1970-1980

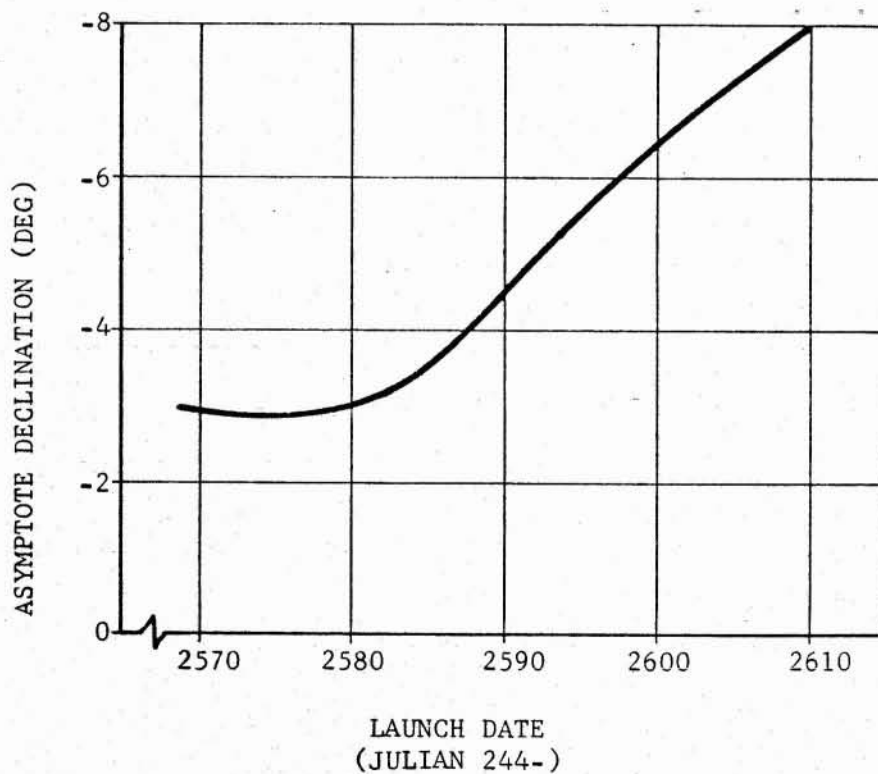
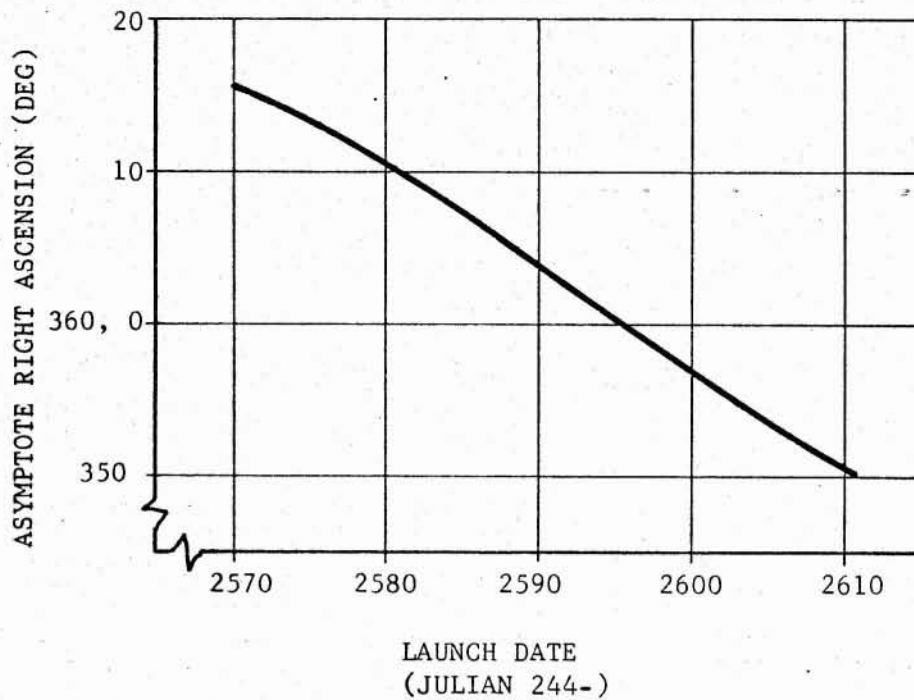


Figure 2-46. 1975 EARTH-JUPITER TRAJECTORIES: RIGHT ASCENSION AND DECLINATION OF OUTGOING GEOCENTRIC ASYMPTOTE FOR 500-DAY TRANSFERS

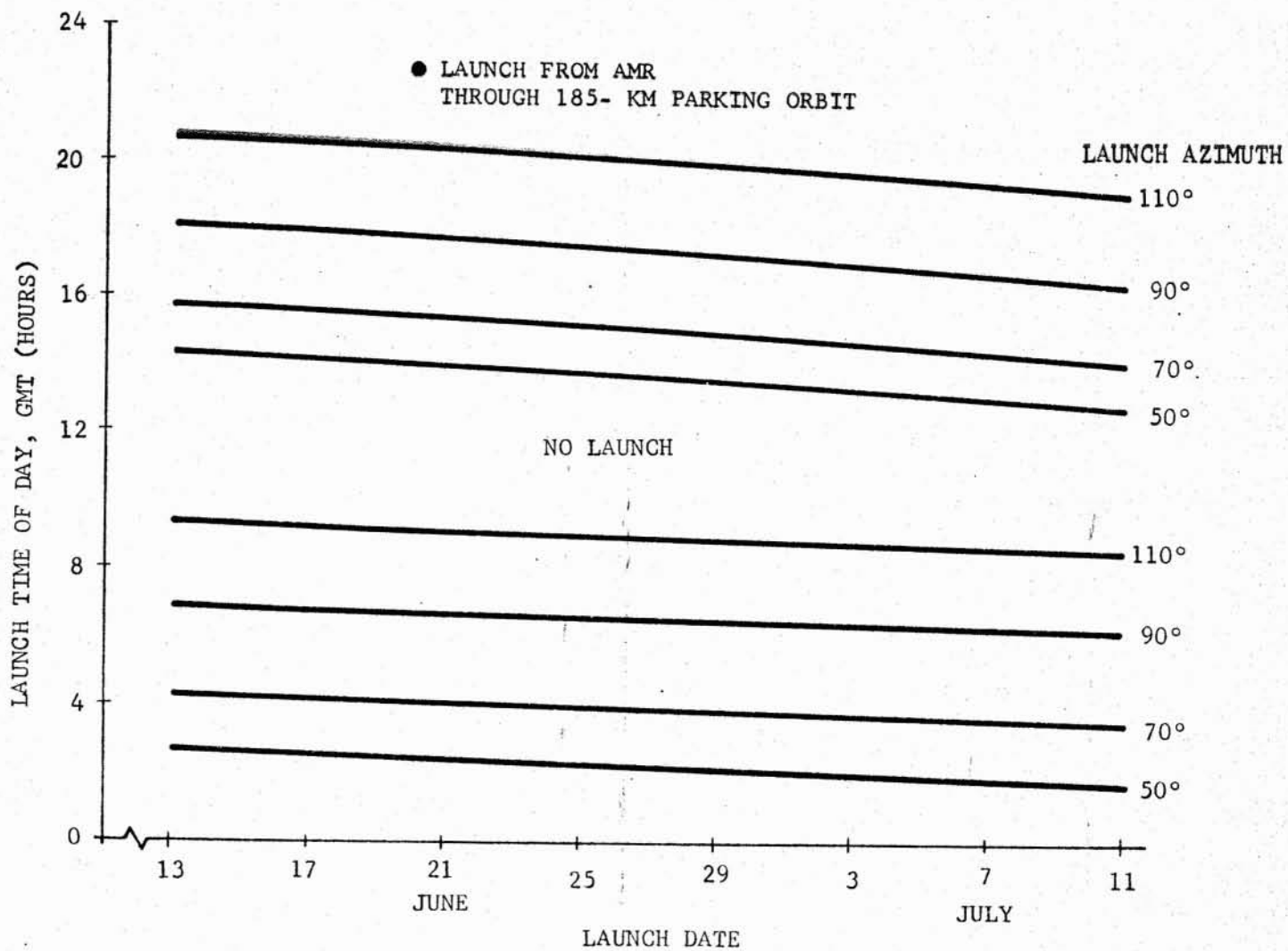


Figure 2-47. EARTH-JUPITER TRAJECTORIES 1975: DAILY SURFACE LAUNCH WINDOW FOR 500-DAY TRANSFERS

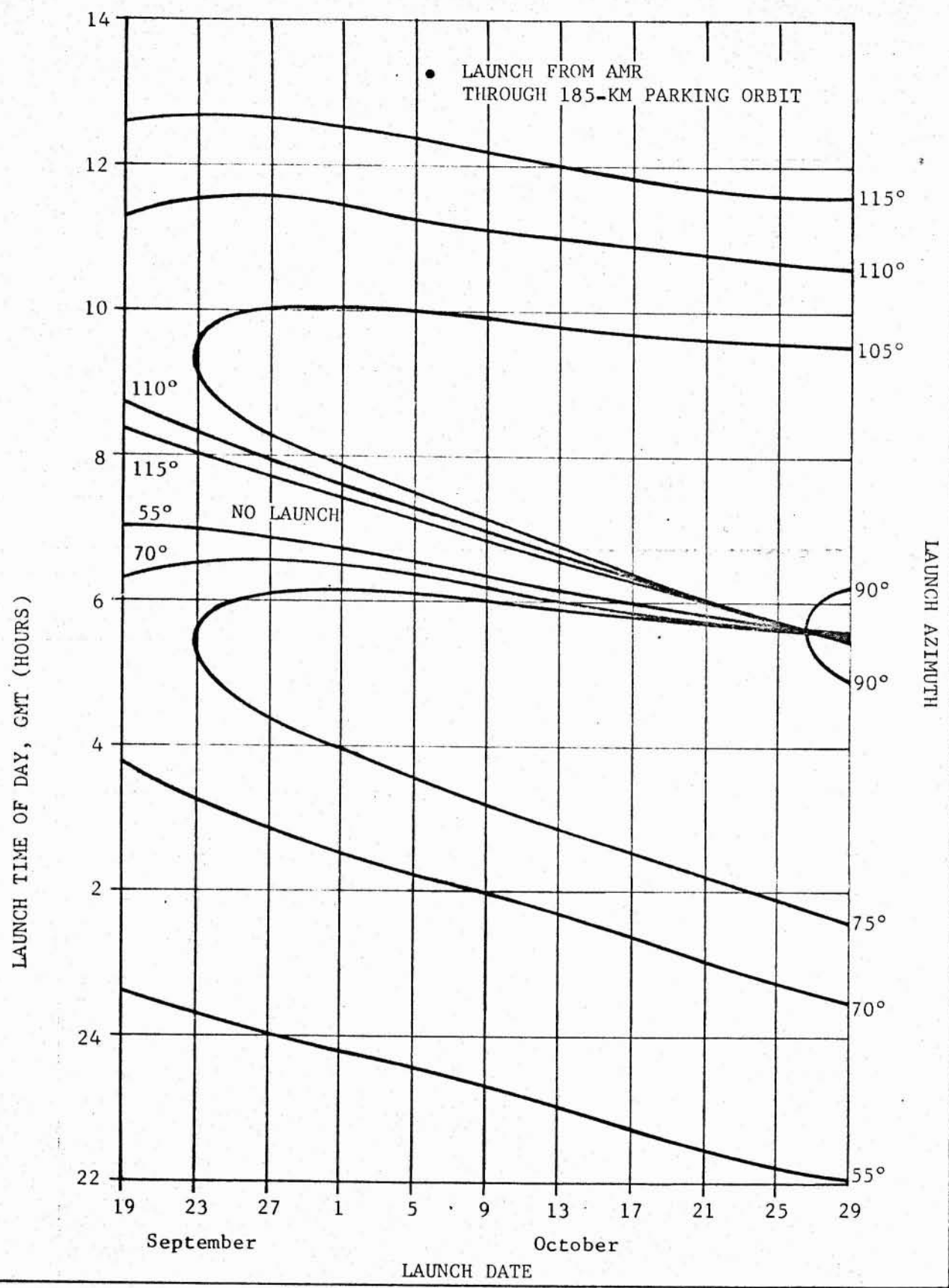


Figure 2-48. EARTH-JUPITER TRAJECTORIES 1978: DAILY SURFACE LAUNCH WINDOWS FOR 540-DAY TRANSFERS

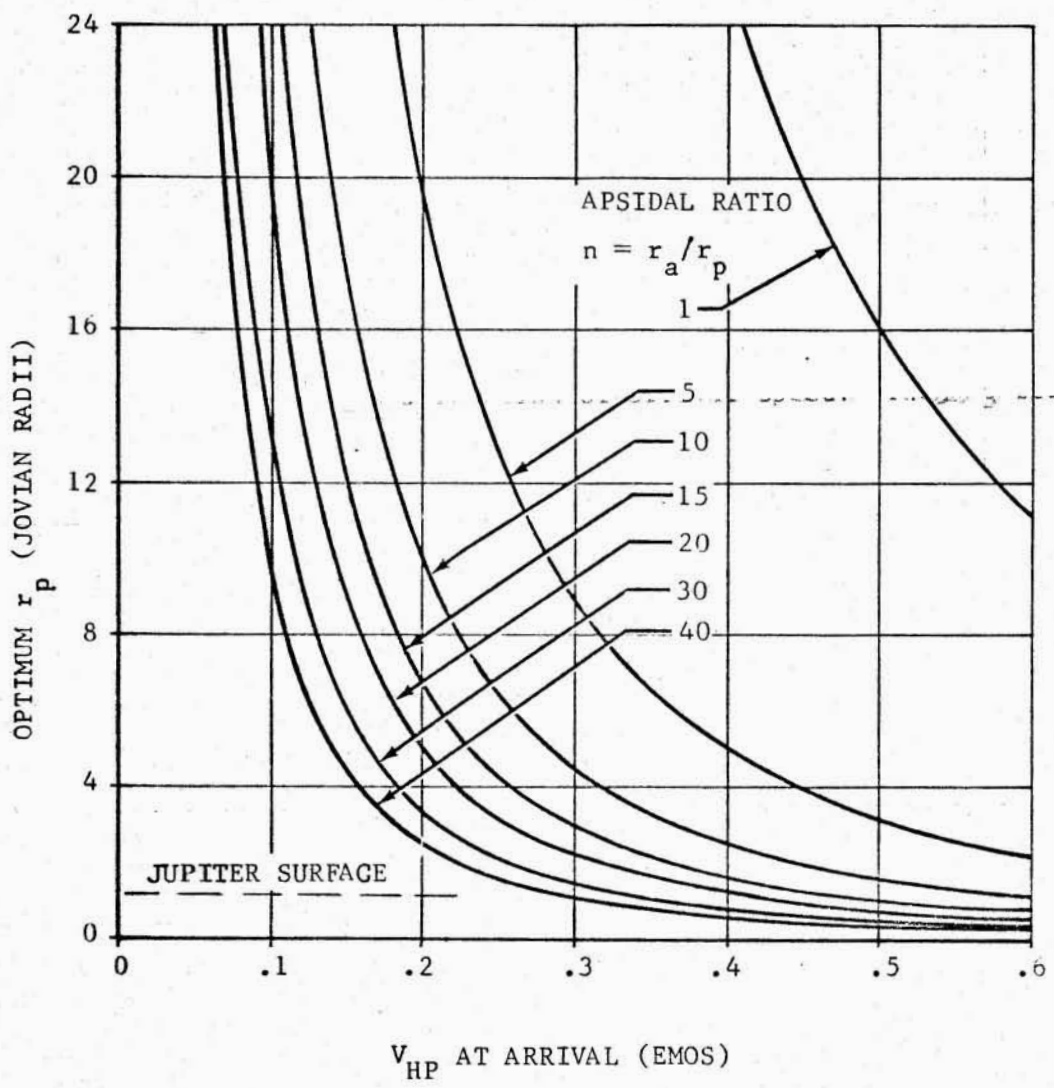


Figure 2-49. OPTIMUM JOVIAN CAPTURE ORBIT PERIJOVE FOR MINIMUM BRAKING VELOCITY INCREMENT

out to distances beyond its moons. For a typical fast-transfer arrival speed of about 0.4 EMOS and an apsidal ratio of 20, the optimum perijove is 1.25 planet radii.

The velocity increment, ΔV_B , for capture braking at the optimum perijove is given in Figure 2-50 as a function of arrival speed and apsidal ratio, n . For an arrival speed of 0.4 EMOS and $n = 20$ the minimum possible ΔV_B is 2.6 km/sec.

Figure 2-51 gives the capture braking ΔV_B required for fixed perijove radii as a function of arrival speed. These curves are for $n = 20$. Reference 1 gives similar information over a range of n from 5 to 20. Performance penalties for off-optimum values of the perijove may be determined by reference to the superimposed minimum ΔV_B curve. The penalties associated with low perijove distances are not large for the range of arrival speeds under consideration. During the mission and systems analysis it was found desirable to reduce the braking ΔV_B requirement as much as possible for the Jupiter orbiter/solar probe mission because of the limitations imposed on mission performance for some launch opportunities by the need for fast Earth-Jupiter transfers. A typical capture orbit chosen for these missions has an apsidal ratio of 40 and a perijove radius of 1.1 Jovian radii. The braking ΔV_B required for this orbit is given in Figure 2-52 as a function of arrival speed. The ΔV_B for a typical arrival speed of 0.4 EMOS is seen to be about 2 km/sec.

Orbit orientation and the effects of perturbations on the orbital elements due to Jupiter's oblateness are treated in reference 1 and will not be repeated here except to mention that the integrated orbital displacements due to secular perturbations over an orbital period will be relatively small.

Figure 2-53 presents the period of the capture orbit as a function of apsidal ratio for various perijove distances. It may be seen that for the apsidal ratios of interest, typically 20 to 40, the period will range from 4 to about 20 days for perijove radii of from 1.1 to 1.5 planet radii.

The relationship between the capture orbit and the Jovian satellite system will be discussed in Section III which considers the problems associated with exploration of the moons.

2.1.6 Mission Performance

This subsection presents the results of evaluations of the Jupiter orbiter/solar probe mission performance based on the Saturn V launch capability. Parametric performance data are given for the three representative launch opportunities, 1972, 1975, and 1978, that have been discussed in previous subsections. As will be shown, a tradeoff exists between the payload mass performance and the solar probe orbit design.

2.1.6.1 Launch Vehicle Capability. The high-energy performance capability of the three-stage Saturn V is given by Figure 2-54. The net injected mass capability is shown as a function of the hyperbolic-excess speed at Earth departure. The curve is based on two-dimensional ascent through a 185-km circular parking orbit. The net injected mass is defined as the gross injected mass, less propellants for a 60-m/sec launch window allowance, less propellants for three-fourths of one percent of total vehicle characteristic velocity for performance reserves. The Instrument Unit is subtracted but the mass of

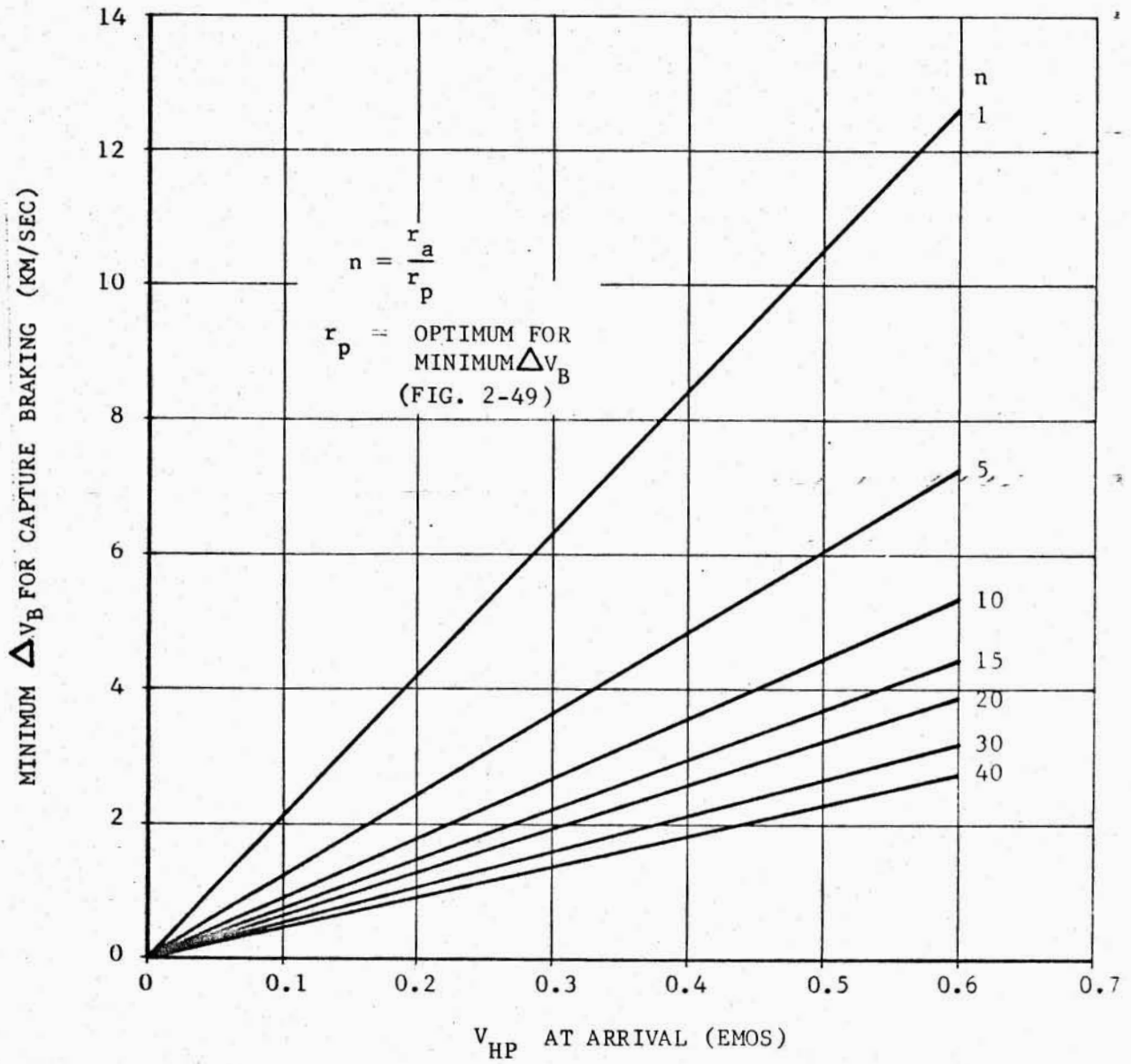


Figure 2-50. MINIMUM VELOCITY INCREMENT FOR JOVIAN CAPTURE BRAKING

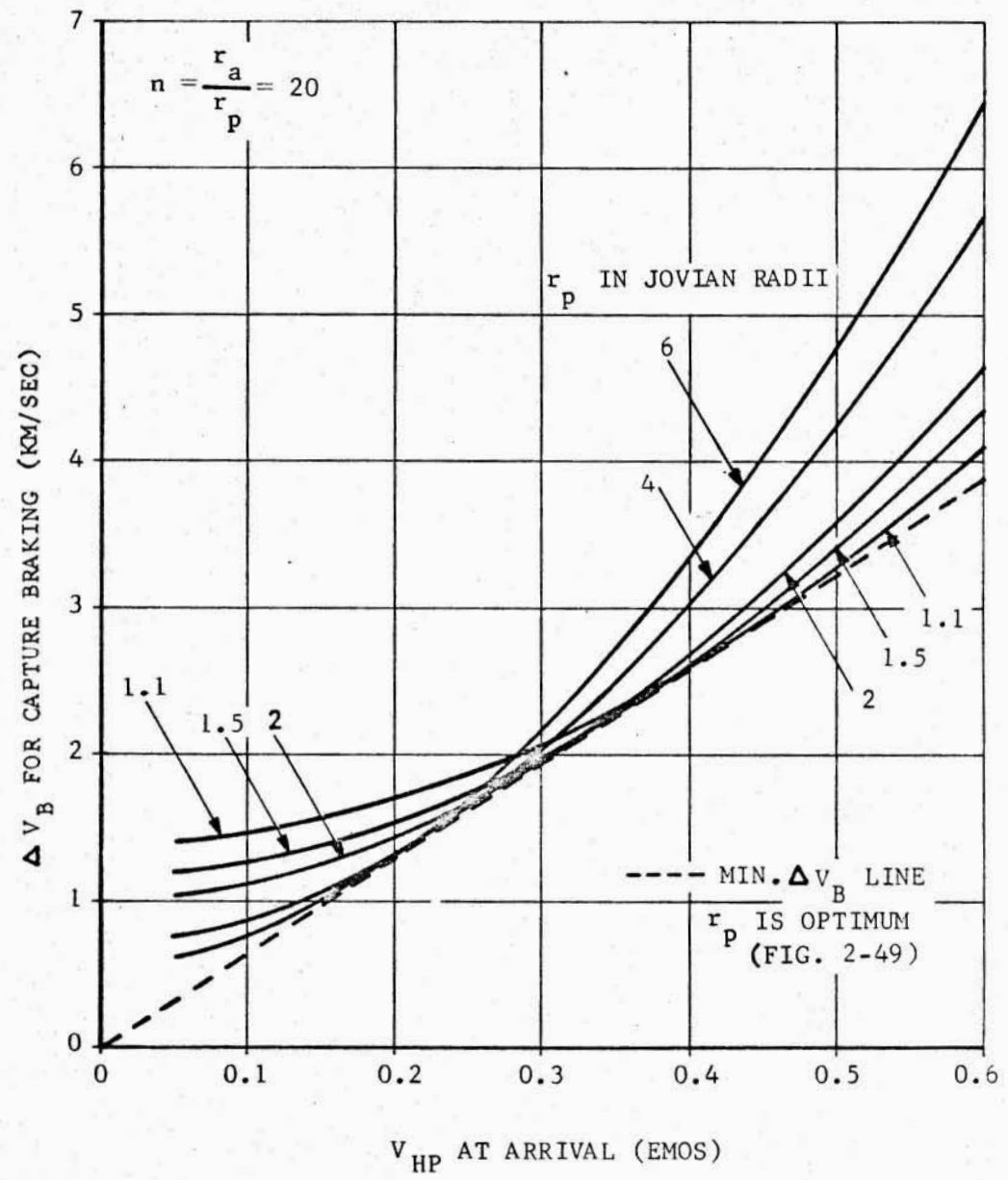


Figure 2-51. VELOCITY INCREMENT REQUIRED FOR JOVIAN CAPTURE BRAKING

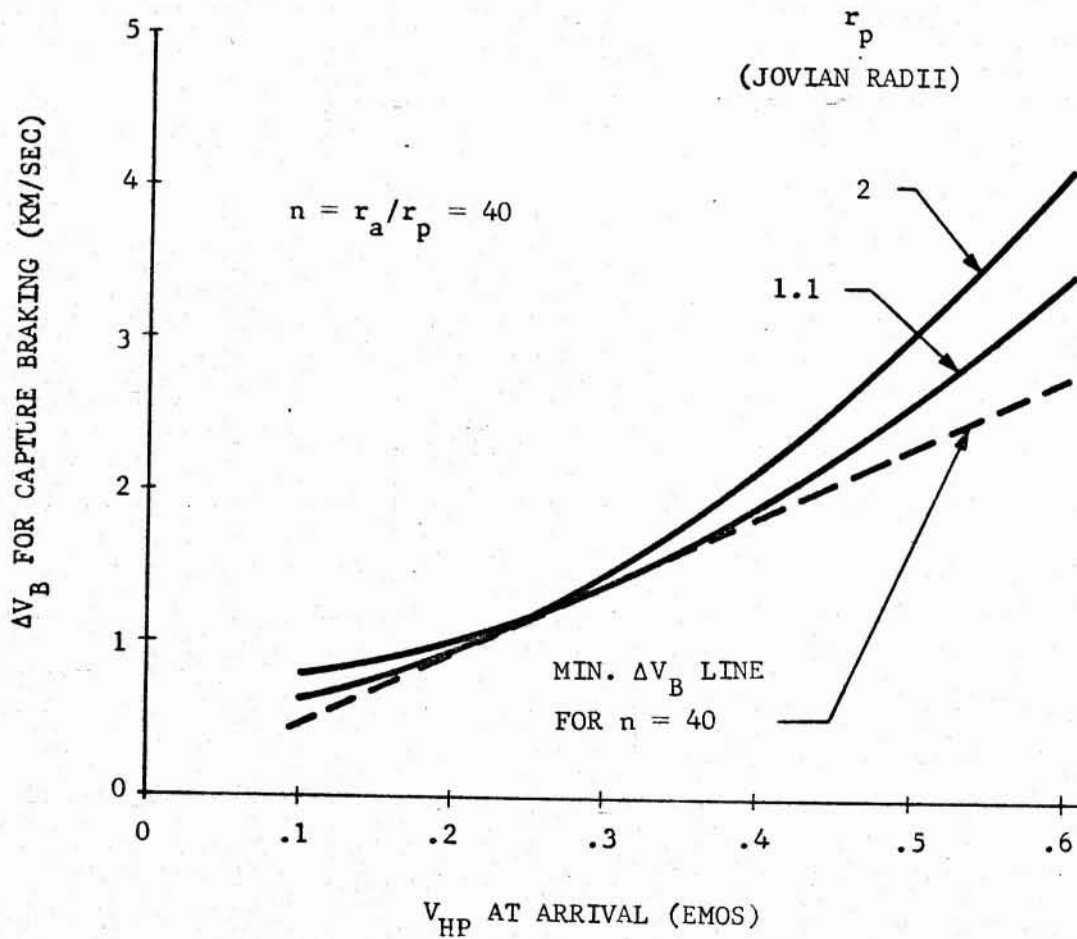


Figure 2-52. VELOCITY INCREMENT REQUIRED FOR JOVIAN CAPTURE BRAKING

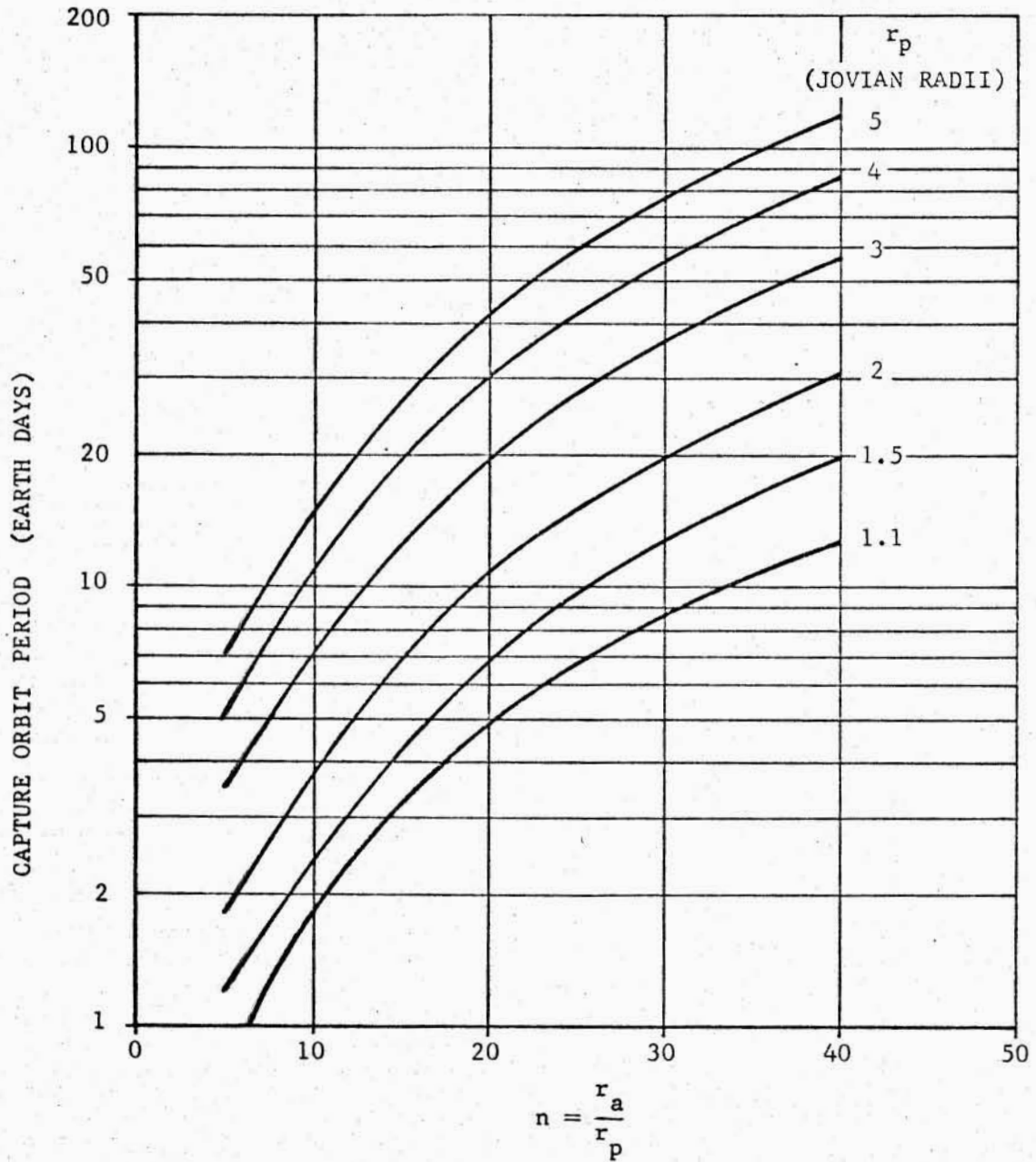


Figure 2-53. PERIOD OF JOVIAN CAPTURE ORBIT AS A FUNCTION OF APSIDAL RATIO

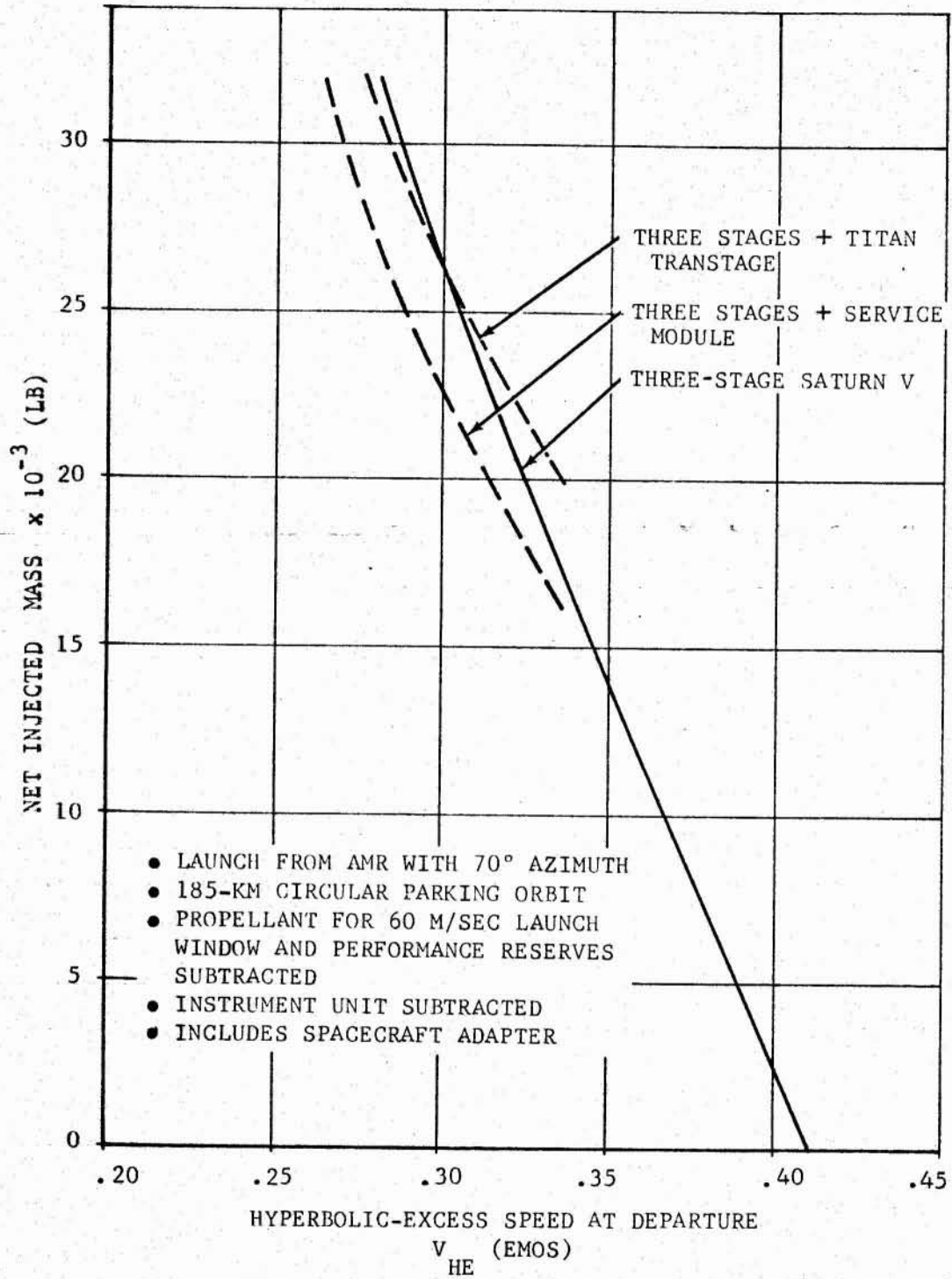


Figure 2-54. THREE-STAGE SATURN V PERFORMANCE CAPABILITY FOR HIGH-ENERGY MISSIONS

September 1966

the spacecraft adapter is included. Launch is from AMR with a 70-degree launch azimuth. Since the maximum azimuth variation from due East (90°) for the missions under consideration is 70° , the performance curve given by Figure 2-54 is satisfactory for mission analysis purposes.

2.1.6.2 Mission Mass Histories. On the basis of the Earth departure and Jupiter arrival energies for given transfer times, and the braking velocity increment requirements presented earlier, the mass history for given missions can be developed. The mass histories for the present study were calculated using a digital computer program. For specified Earth-departure and Jupiter-arrival dates and the associated hyperbolic-excess speeds, the program determined the mass histories for the Jupiter orbiter/solar probe mission based on a given solar probe mass and capture orbit defined by r_p and n . The inputs built into the program included:

1. The Saturn V performance curve (Figure 2-54)
2. A 500-lb spacecraft adapter that is jettisoned with the S-IVB stage after interplanetary injection
3. An allocation of 150 m/sec for midcourse velocity corrections and 200 m/sec for the orbiter planetary approach maneuver after separation of the solar probe
4. A specific impulse of 310 sec for midcourse corrections and the planetary approach maneuver
5. Attitude control propellants as specified by the system analysis (typically 660 lb for the missions under consideration)
6. Mass allocated to the solar probe based on the systems studies presented in subsection 2.2. (Nominal mission performance was based on a 1400-lb probe.)
7. A mainstage orbiter propulsion system based on the Apollo Lunar Excursion Module (LEM) ascent engine.

It should be noted that the capture braking performance is based on impulsive velocity increments applied at periapsis of the planetary approach hyperbola. This assumption provides an accurate performance simulation because of the negligible gravity losses associated with propulsive braking at Jupiter.

2.1.6.3 Parametric Mission Performance. This subsection summarizes the mission performance analysis in terms of net injected mass and gross Jovian capture mass as functions of Earth departure date and Earth-Jupiter transfer time during the 1972, 1975, and 1978 launch opportunities. These data must be correlated with the solar probe orbit data presented earlier to arrive at missions that satisfy performance, trajectory, and systems requirements and constraints.

Figure 2-55 shows the net injected mass for the 1972 opportunity as a function of Earth departure date. Curves for 500-, 540-, and 600-day transfers are shown. Net injected mass for 20-day launch periods varies from about 12,500

- LAUNCH FROM AMR
- 70° LAUNCH AZIMUTH
- 185-KM PARKING ORBIT

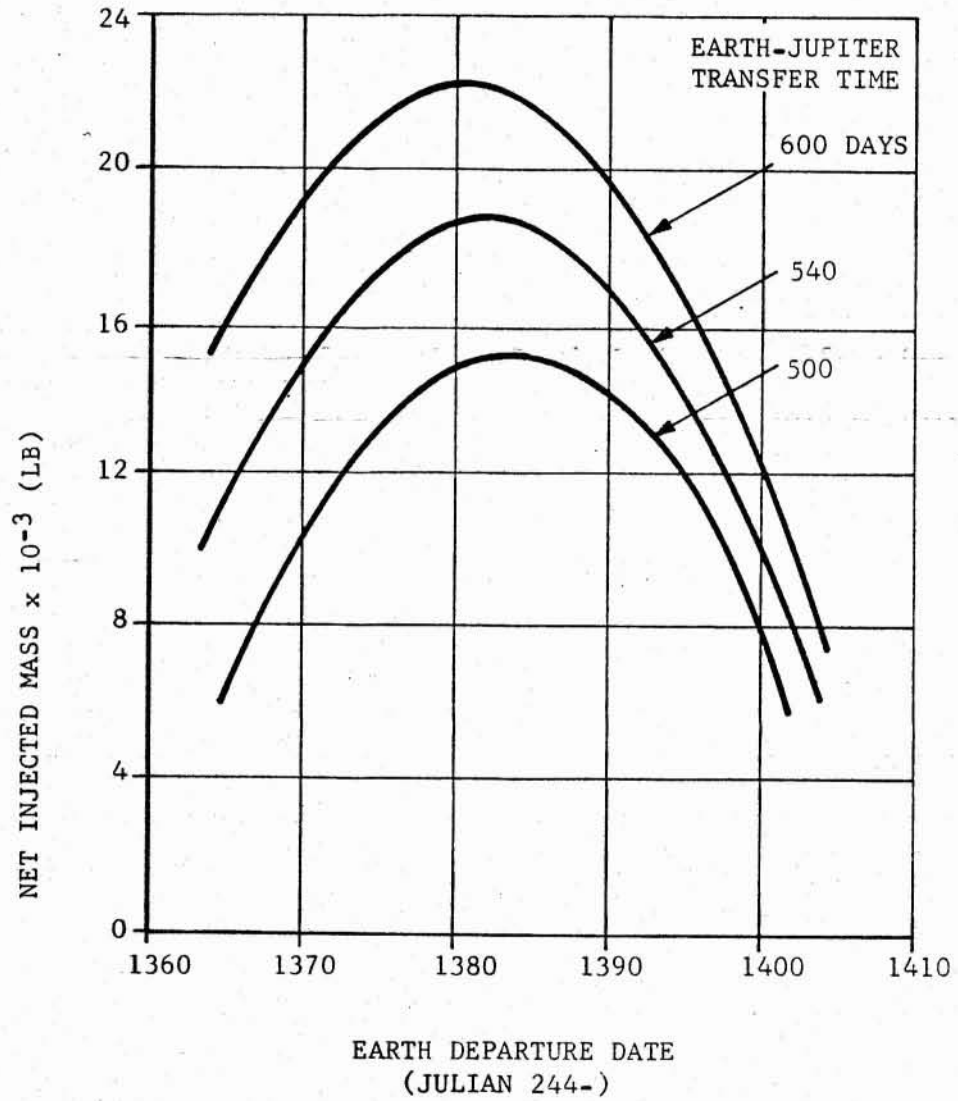


Figure 2-55. SATURN V PERFORMANCE FOR 1972 JUPITER ORBITER/SOLAR PROBE MISSION

lb to 19,500 lb for 500- to 600-day transfers, respectively. Figure 2-56 translates these data into gross mass in capture orbit about Jupiter as a function of Earth departure date. The curves are based on a 1400-lb solar probe mass and a capture orbit with $n = 40$ and $r_p = 1.1$ Jovian radii. For 20-day launch periods the capture mass is seen to vary from about 4300 lb to 9000 lb for 500- and 600-day Earth-Jupiter transfers, respectively.

The effect on mission performance of varying the solar probe mass is shown in Figure 2-57. The gross capture mass is plotted versus Earth departure date for 540-day transfers and solar probe masses of 1000, 1800, and 3000 lb.

Data similar to that given for 1972 is presented in Figures 2-58 and 2-59 for the 1975 opportunity. The injected masses shown in Figure 2-58 are seen to be slightly less than the 1972 capability for given transfer times. The capture performance given in Figure 2-59 is very similar to the 1972 data. The figures show a 20-day launch period for a 0.1-AU Jupiter orbiter/solar probe mission based on 500-day Earth-Jupiter transfers and a 4400-lb orbiter spacecraft developed later in the systems analysis of subsection 2.2.

Figures 2-60 and 2-61 give the parametric performance data for 1978. Figure 2-60 shows net injected mass capability for the 1978 opportunity to be typically 30 to 50 percent less, for a given Earth-Jupiter transfer time, than the 1972 capability. Similarly, Figure 2-61 indicates significantly less capture mass performance potential for the 1978 as compared with the 1972 or 1975 opportunities. These trends in performance can be predicted by referring back to the departure and arrival energy trends across the decade (Figure 2-4).

2.1.6.4 Mission Performance/Solar Probe Orbit Tradeoffs. The 1978 opportunity offers less performance potential for given Earth-Jupiter transfer times than do the earlier years represented by 1972 and 1975. However, in terms of the combined Jupiter orbiter/solar probe mission characteristics and requirements, there are tradeoffs which make 1978 as usable as the 1972 opportunity and possibly more attractive than the 1975 missions. Like 1972, the 1978 Earth-Jupiter transfer trajectories are characterized by large arrival energies at Jupiter. This means that longer Earth-Jupiter transfer times are permissible for achieving the close solar flyby via the swingby mode. Thus, the longer transfer times and associated gains in Saturn V launch capability tend to make the 1978 opportunity compare favorably with the 1975 missions. This is true because of the smaller arrival energies, for given Earth-Jupiter transfer times, associated with the 1975 opportunity; i.e., faster transfers are required to achieve close solar flybys.

The tradeoff between performance and solar probe orbit characteristics was performed for the 1978 opportunity. The results are shown in Figure 2-61 by the dashed curves superimposed on the capture mass performance curves. The dashed curves represent the optimum selection of Earth-Jupiter transfer time as a function of departure date to achieve the solar probe orbit perihelion distances shown. The optimum transfer time for a given departure date is determined by finding the transfer time that produces a minimum perihelion (as a function of swingby distance) equal to the desired solar flyby distance. These transfers were obtained for the 1978 opportunity by cross plotting the perihelion versus swingby distance data for various transfer times given by Figures 2-31, 2-34, and 2-37. Figure 2-61 shows that the 0.1-AU solar probe orbit can be achieved with Earth-Jupiter transfer times that approach 600 days. Therefore, the capture masses available are comparable to 500-day Earth-Jupiter transfer time missions during 1975 (see Figure 2-58) where the faster transfer is required

- SATURN V LAUNCH FROM AMR
- 1400-LB SOLAR PROBE
- CAPTURE ORBIT: $n = 40$, $r_p = 1.1$ JOVIAN RADII
- LEM/A BRAKING PROPULSION

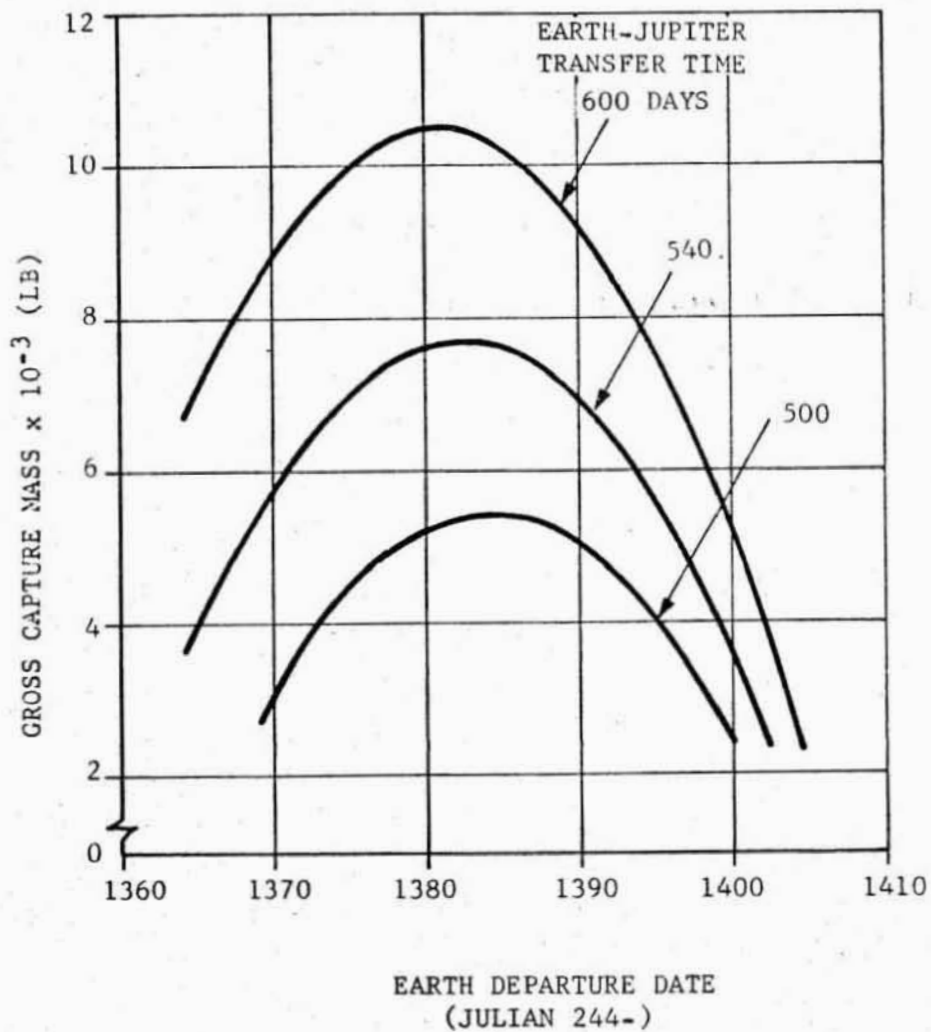


Figure 2-56. 1972 JUPITER ORBITER/SOLAR PROBE MISSION PERFORMANCE

- SATURN V LAUNCH FROM AMR
- CAPTURE ORBIT: $n = 40$, $r_p = 1.1$ JOVIAN RADII
- LEM/A BRAKING PROPULSION
- EARTH-JUPITER TRANSFER TIME: 540 DAYS

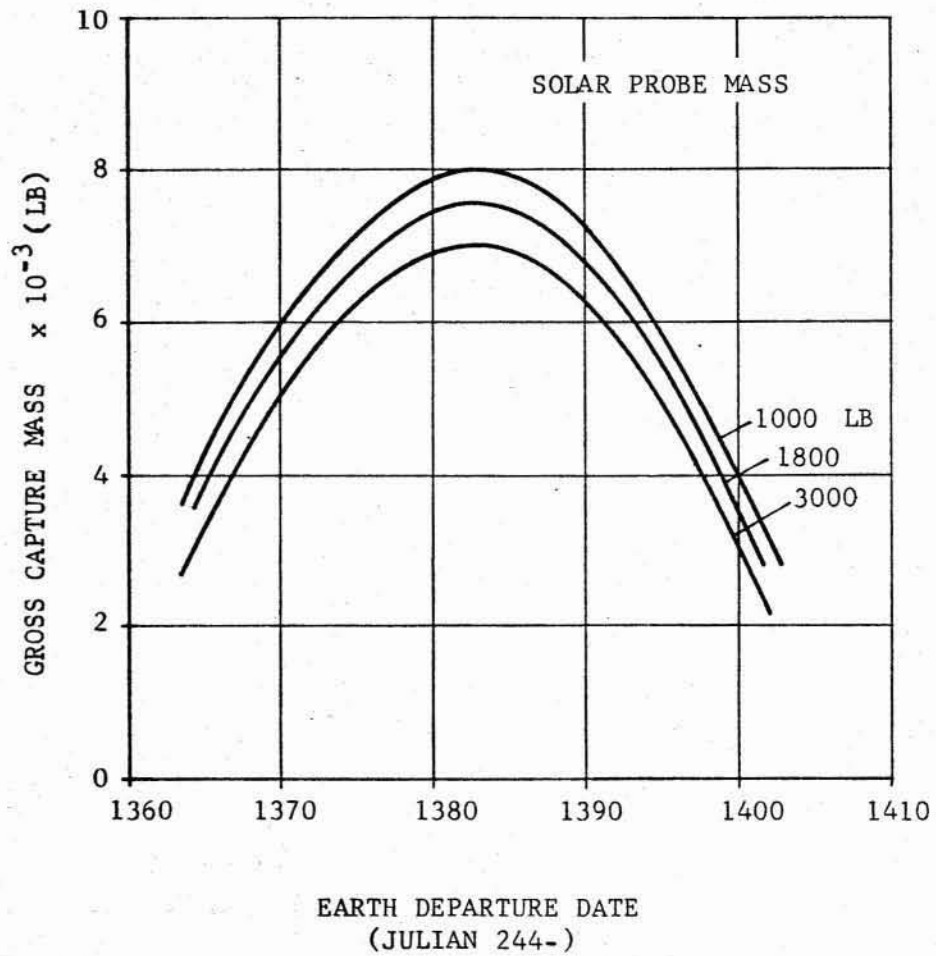


Figure 2-57. 1972 JUPITER ORBITER/SOLAR PROBE MISSION PERFORMANCE: EFFECT OF VARIATION OF SOLAR PROBE MASS

- LAUNCH FROM AMR
- 70° LAUNCH AZIMUTH
- 185-KM PARKING ORBIT

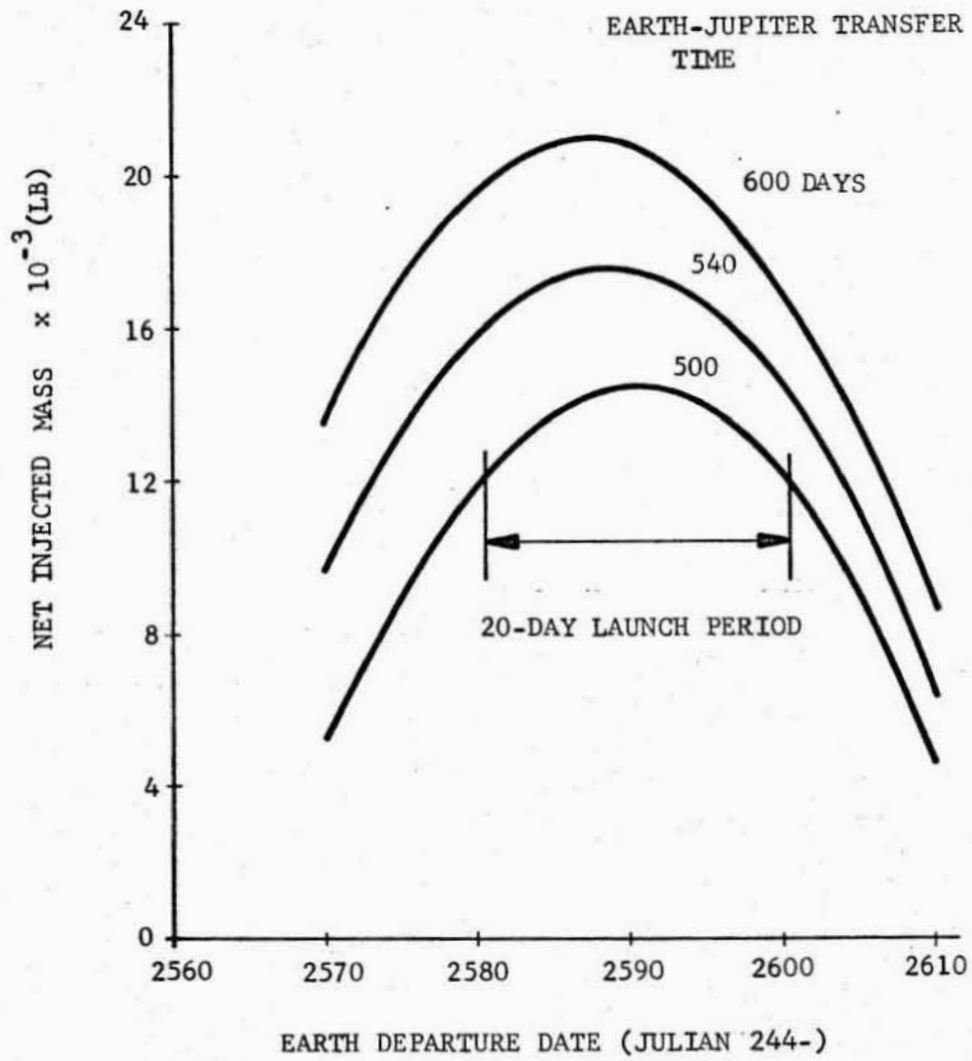


Figure 2-58. SATURN V PERFORMANCE FOR 1975 JUPITER ORBITER/SOLAR PROBE MISSION

- SATURN V LAUNCH FROM AMR
- 1400 -LB SOLAR PROBE
- CAPTURE ORBIT: $n = 40$, $r_p = 1.1$ JOVIAN RADII
- LEM/A BRAKING PROPULSION

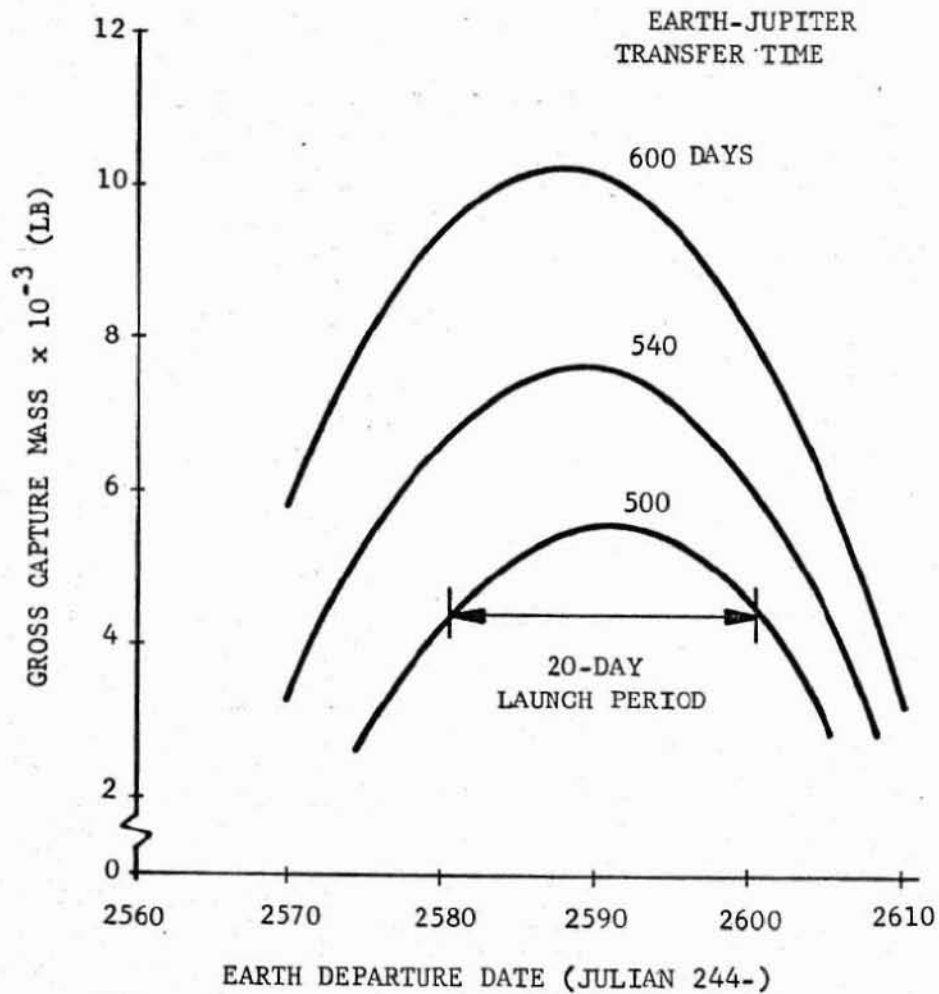


Figure 2-59. 1975 JUPITER ORBITER/SOLAR PROBE MISSION PERFORMANCE

- LAUNCH FROM AMR
- 70° LAUNCH AZIMUTH
- 185-KM PARKING ORBIT

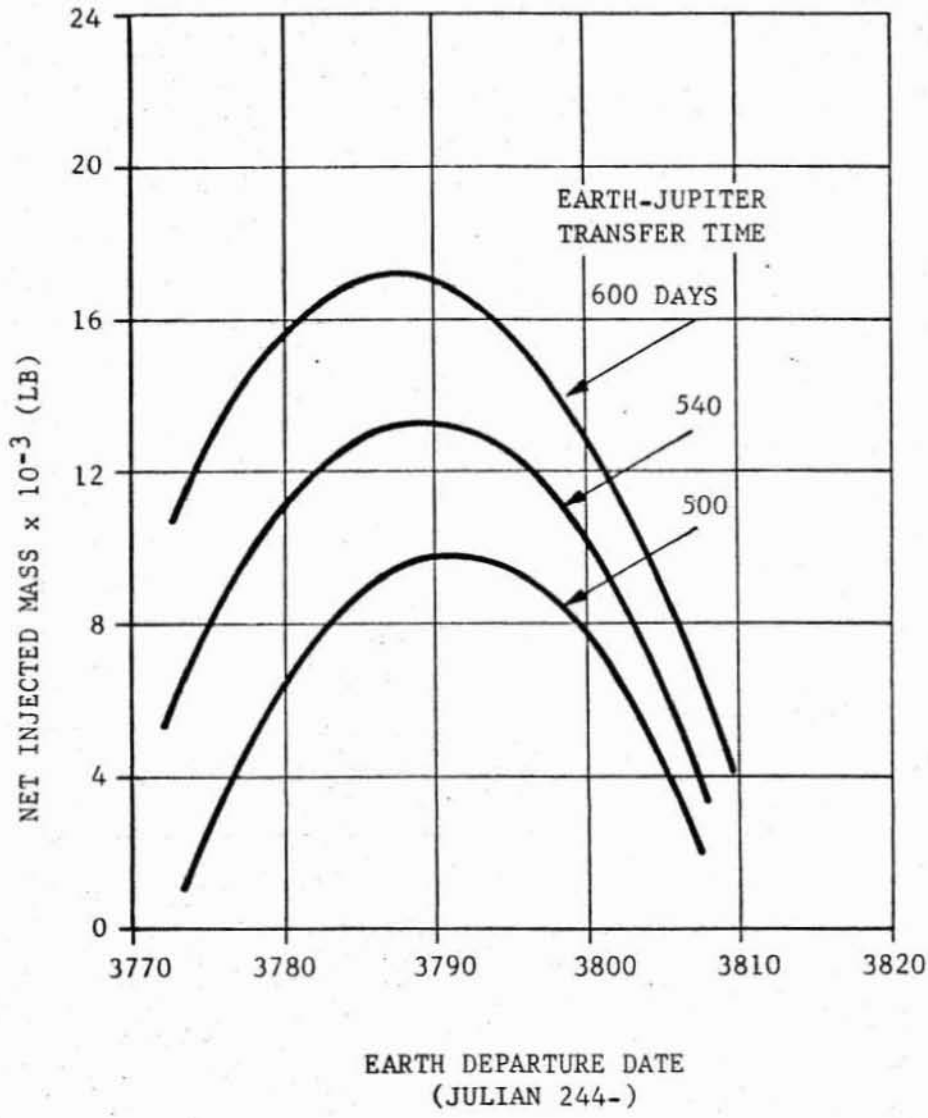


Figure 2-60. SATURN V PERFORMANCE FOR 1978 JUPITER ORBITER/SOLAR PROBE MISSION

- SATURN V LAUNCH FROM AMR
- 1400-LB SOLAR PROBE
- CAPTURE ORBIT: $n = 40, r_p = 1.1$ JOVIAN RADII
- LEM/A BRAKING PROPULSION

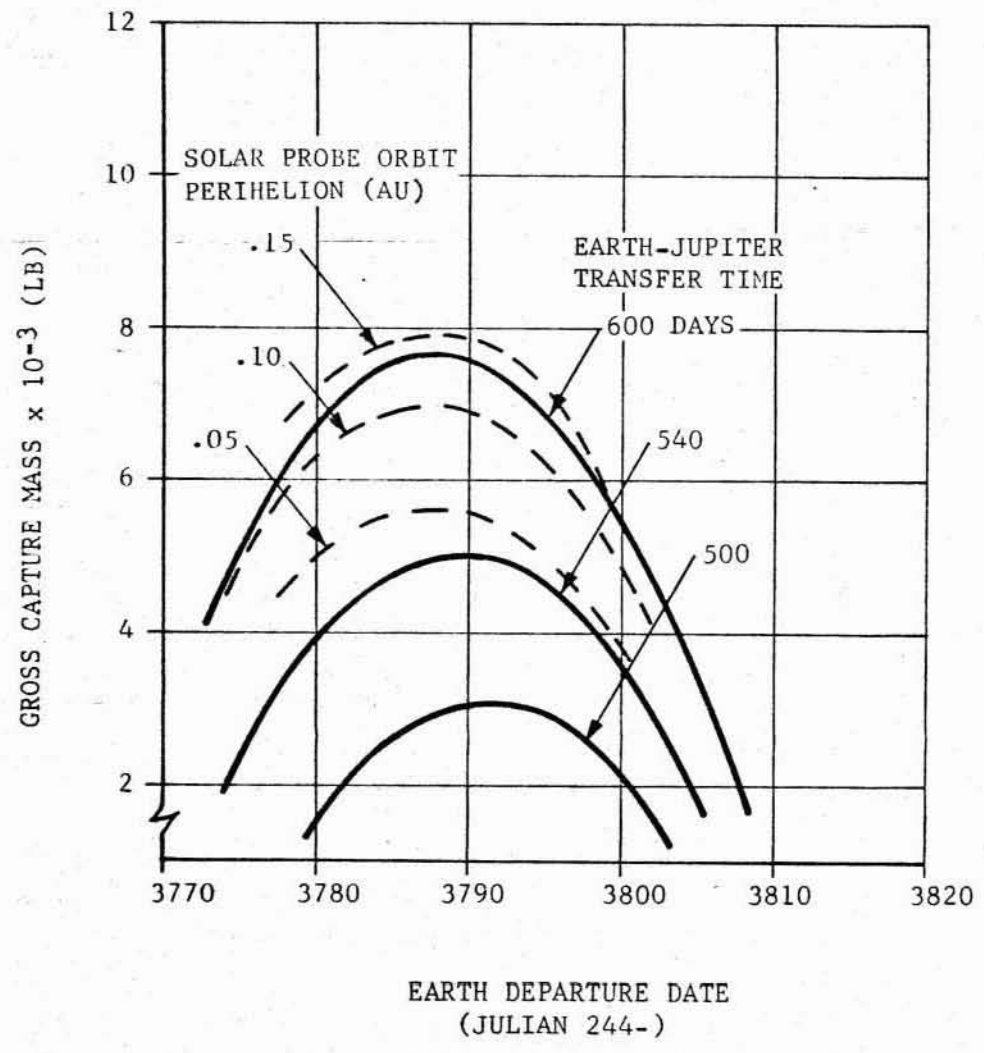


Figure 2-61. 1978 JUPITER ORBITER/SOLAR PROBE MISSION PERFORMANCE

to achieve a 0.1-AU perihelion.

2.1.6.5 Mission Summaries. On the basis of the parametric data which has been presented throughout the mission analysis, the characteristics of representative Jupiter orbiter/solar probe missions may be determined. Sufficient data are presented to analyze primary mission parameter tradeoffs within the constraints that may be imposed on the mission.

Two missions are selected here for presentation in summary form. Table 2-2 summarizes the characteristics of a typical 0.1-AU mission during the 1975 opportunity. Table 2-3 gives a summary of the same mission but for the constant-gross-spacecraft-mass operational mode concept. This operational mode will be covered in detail in the systems analysis subsection to follow. The orbiter gross mass in capture orbit shown in Tables 2-2 and 2-3 includes the scientific payload and is based on the conceptual design developed in the following subsections. Also the 1400-lb solar probe is based on the systems and conceptual design studies that follow.

Table 2-2

1975 SATURN V JUPITER ORBITER/SOLAR PROBE
TYPICAL MISSION SUMMARY

LAUNCH PERIOD:

20 Days, 17 June - 7 July 1975
(Julian 244-2580.5 -244-2600.5)

DAILY WINDOW:

Two Daily 5-Hr Windows with 70-110°
Launch Azimuths from AMR

EARTH-JUPITER TRANSFER: 500 Days

Net Injected Wt: 12,000 - 14,400 Lb
(Across Launch Period)

JUPITER ENCOUNTER:

Capture Orbit: $n=40$, $r_p = 1.1$ Jovian Radii
Gross Capture Wt: 4400 Lb
Solar Probe Swingby Distance: 6.7-9.9 Jovian Radii
Solar Probe Wt: 1400 Lb

JUPITER-SUN TRANSFER: 590-655 Days

Perihelion Distance: 0.1 AU
Inclination to Ecliptic: 21 Deg
Total Time from Earth Departure To Perihelion:
1090-1155 Days

Table 2-3

1975 SATURN V JUPITER ORBITER/SOLAR PROBE
TYPICAL MISSION SUMMARYLAUNCH PERIOD:

20 Days, 17 June - 7 July 1975
(Julian 244-2580.5 -244-2600.5)

DAILY WINDOW:

Two Daily 5-Hr Windows with 70-110°
Launch Azimuths from AMR

EARTH-JUPITER TRANSFER: 475-500 Days

Net Injected Wt: 12,000 Lb
(Constant Across Launch Period)

JUPITER ENCOUNTER:

Capture Orbit: $n = 40-52$, $r_p = 1.1$ Jovian Radii
Gross Capture Wt: 4400 Lb
Solar Probe Swingby Distance: 4.6-9.4 Jovian Radii
Solar Probe Wt: 1400 Lb

JUPITER-SUN TRANSFER: 540-650 Days

Perihelion Distance: .1 AU
Inclination to Ecliptic: 20-25 Deg
Total Time From Earth Departure To Perihelion:
1015-1150 Days

2.2 SYSTEMS ANALYSIS

The primary emphasis in the systems analysis portion of this study was placed on a combined Jupiter orbiter/solar probe. The two separate spacecraft are launched together on one Saturn V vehicle. During the outbound heliocentric coast, both spacecraft remain attached to each other. Earth communication is maintained with the Jupiter orbiter which reports on the condition of the solar probe and relays its scientific data. The two spacecraft are umbilically connected for this purpose. Before encounter with the planet Jupiter, the two spacecraft are separated. The solar probe swings by the planet and starts its heliocentric coast for a close approach to the sun. The Jupiter orbiter uses its onboard propulsion to brake into a Jupiter capture orbit.

This subsection presents the operational, reliability, and subsystem considerations for the probes. These analyses were developed parametrically to cover the entire range of requirements expected for the next decade.

2.2.1 Mission and Trajectory Selection

For the purpose of orienting and conducting the systems analysis of the Jupiter orbiter/solar probe, a typical mission and operational mode was selected. The Saturn V performance in the 1972 launch window was used to define the total spacecraft ejected mass. Heliocentric transfer times of up to 600 days were considered reasonable. The typical case represents a compromise between the greater spacecraft masses of other annual launch periods and a reasonable mission duration. Figures 2-55 and 2-56 present typical Saturn V performance for the 1972 mission including Earth injected mass and Jupiter capture orbit mass for various trip times and capture orbit parameters. The mass allocated for the close solar probe is indicated in Figure 2-57 for a typical Jupiter capture orbit.

These data are examples of the possible trade offs and a family of curves exists for each of the vast number of possible capture orbits, trip times, and spacecraft masses.

2.2.1.1 Operational Mode. Various alternatives exist in the operational assumptions for selecting design points. Over a 30-day launch period, a significant variance occurs in Saturn V injected mass and therefore in the Jupiter orbiter/solar probe masses. A Jupiter capture spacecraft can thus be designed to either of the following criteria:

- Fix the spacecraft inert mass, payload mass, and heliocentric trip time. Then vary the spacecraft propellant loading at launch to match the Saturn V capability for the constant trip time. The resultant Jupiter capture orbit parameters are then the dependent variables.
- Fix the vehicle inert, payload, and propellant mass for the opening of the launch window. Then use the excess Saturn V capability during the window to reduce trip times. The Jupiter capture orbit parameters are still the dependent variables but will be different than those above.

To investigate these concepts, a typical Jupiter capture vehicle, launch window, and trajectory were selected and the performance of each of the above modes analyzed and compared. The configuration chosen for this study is not necessarily the recommended or optimum design but was selected as a typical spacecraft. The operational results of this analysis should not change with the selection of a different vehicle.

Fixed Trip Time/Variable Propellant Mode. The Saturn V performance capability for this mode is summarized in Figure 2-62 for the trajectory and vehicle selected for analysis. It can be seen that for a 30-day launch period and 600-day trip time, spacecraft propellant loading could vary from 8500 to almost 15,000 pounds for a Jupiter capture vehicle of the fixed launch mass indicated. Such extremes in propellant loading could cause significant problems with ground operations during the launch window. Large quantities of propellants must be loaded or unloaded for each daily launch opportunity resulting in complicated launch and checkout procedures.

Shown also on Figure 2-62 are the Jupiter capture orbit parameters for minimum ΔV braking capture maneuvers. As an alternative to minimum ΔV braking, a fixed perijove radius could be selected and the eccentricity of the Jupiter capture orbit considered as the variable parameter. Figure 2-63 shows a typical example of this approach for $r_p = 1.5$ as compared to the minimum ΔV braking. The modes are quite different, but the capture orbit variances are not significant enough to affect the selection and installation of the spacecraft's experiments.

During this launch window, the declination of the outgoing geocentric asymptote varies as shown in Figure 2-64 as the "Constant 600-day Trip Time" curve.

Fixed Propellant/Variable Trip Time Mode. This mode will use the same Saturn V total performance capability and launch window. The propellant loading will be that required at the opening of the launch window and will be held fixed throughout the 30-day increment. The excess payload capability of the Saturn V booster can then be used to reduce trip times. Figure 2-65 shows the resultant mission time decreases for this mode and the assumptions of this analysis.

While this concept offers advantages in operational procedures due to the fixed propellant loading, the faster trip times result in higher spacecraft energies at Jupiter arrival. The fixed propellant loading, and thus a fixed ΔV capability, imposes different restrictions on the Jupiter capture orbit parameters which can be achieved. Figure 2-63 shows the Jupiter capture orbits which can now be achieved with optimum braking maneuvers. It can be seen that only very highly elliptical orbits are possible throughout the launch window if close approaches to the planet are desired. Actually, an elliptical orbit of large eccentricity may be desirable for a Jupiter capture probe in order to investigate the widest possible spectrum of the Jupiter environment. Thus, this mode of operation may be the most advantageous.

The declination of the outgoing geocentric asymptote for this mode is shown in Figure 2-64 as the "Constant Gross Mass" curve.

Mode Comparison and Conclusions. Based on this brief study it can be seen that for the range in parameters of the Jupiter capture orbit studied herein, little

- 500-LBM PAYLOAD MASS
- 600-DAY TRIP TIME
- MINIMUM BRAKING ΔV

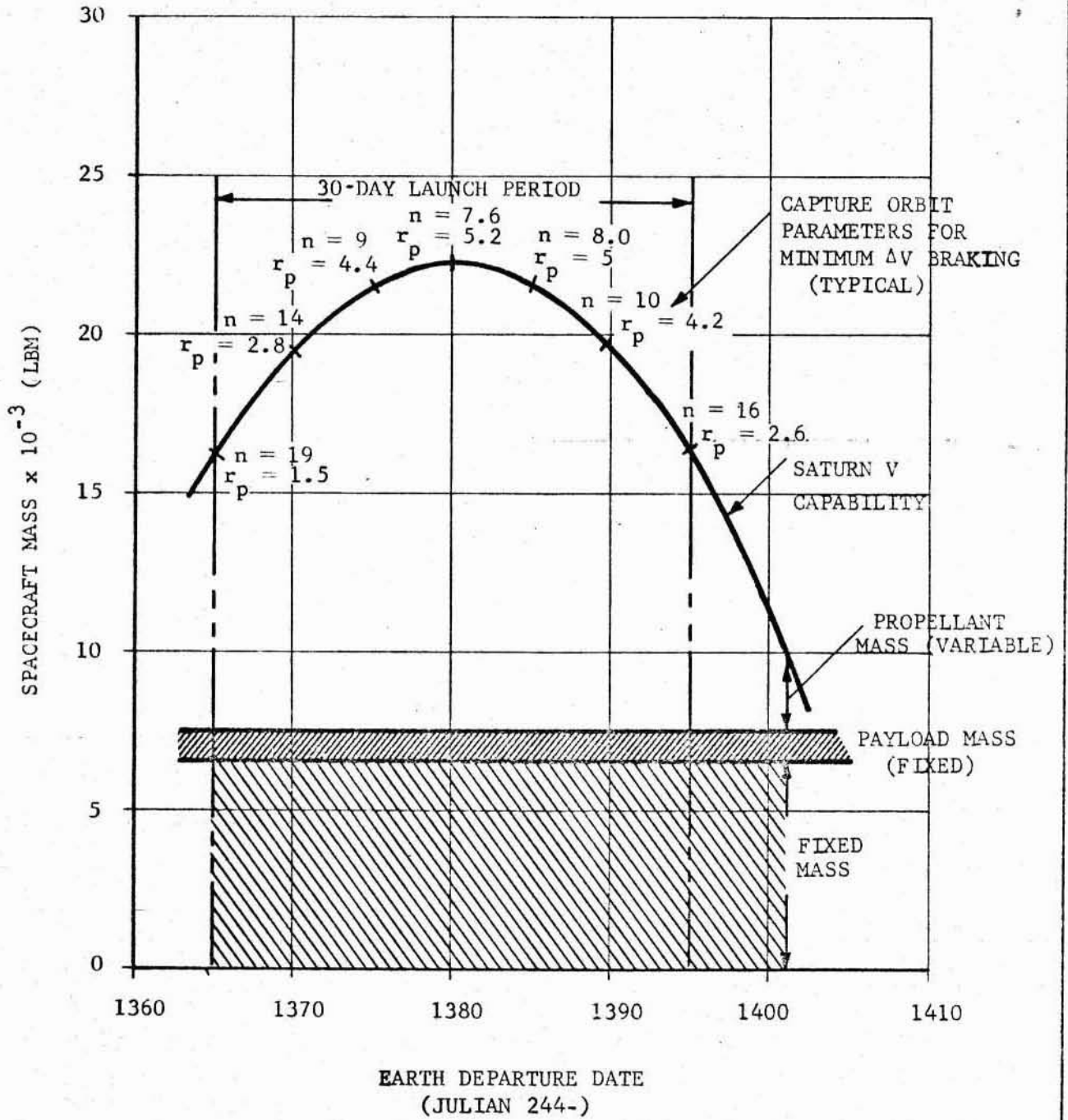


Figure 2-62. SPACECRAFT MASS VS EARTH DEPARTURE DATE

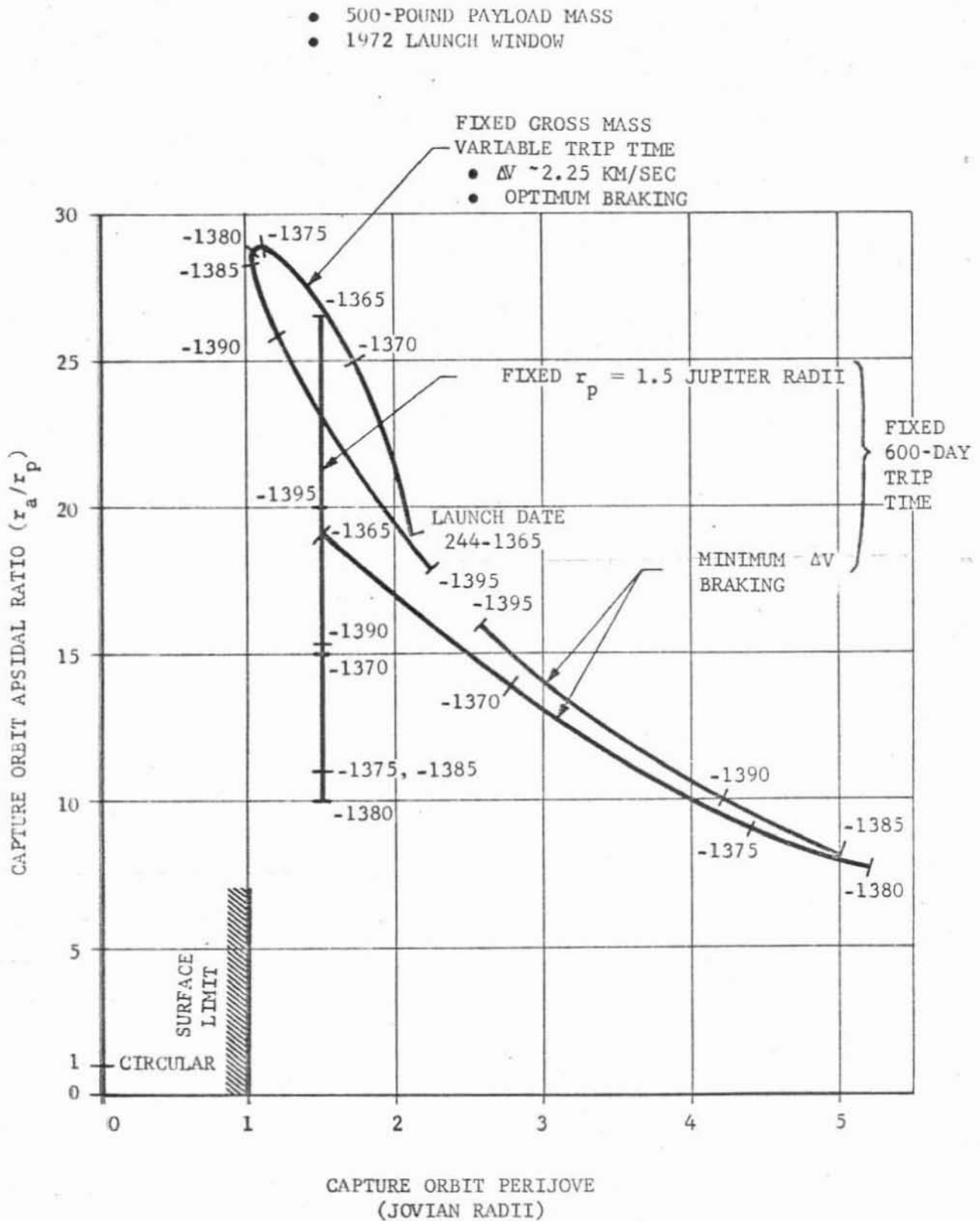


Figure 2-63. COMPARISON OF CAPTURE ORBIT APSIDAL RATIOS VS PERIJOVE DISTANCE

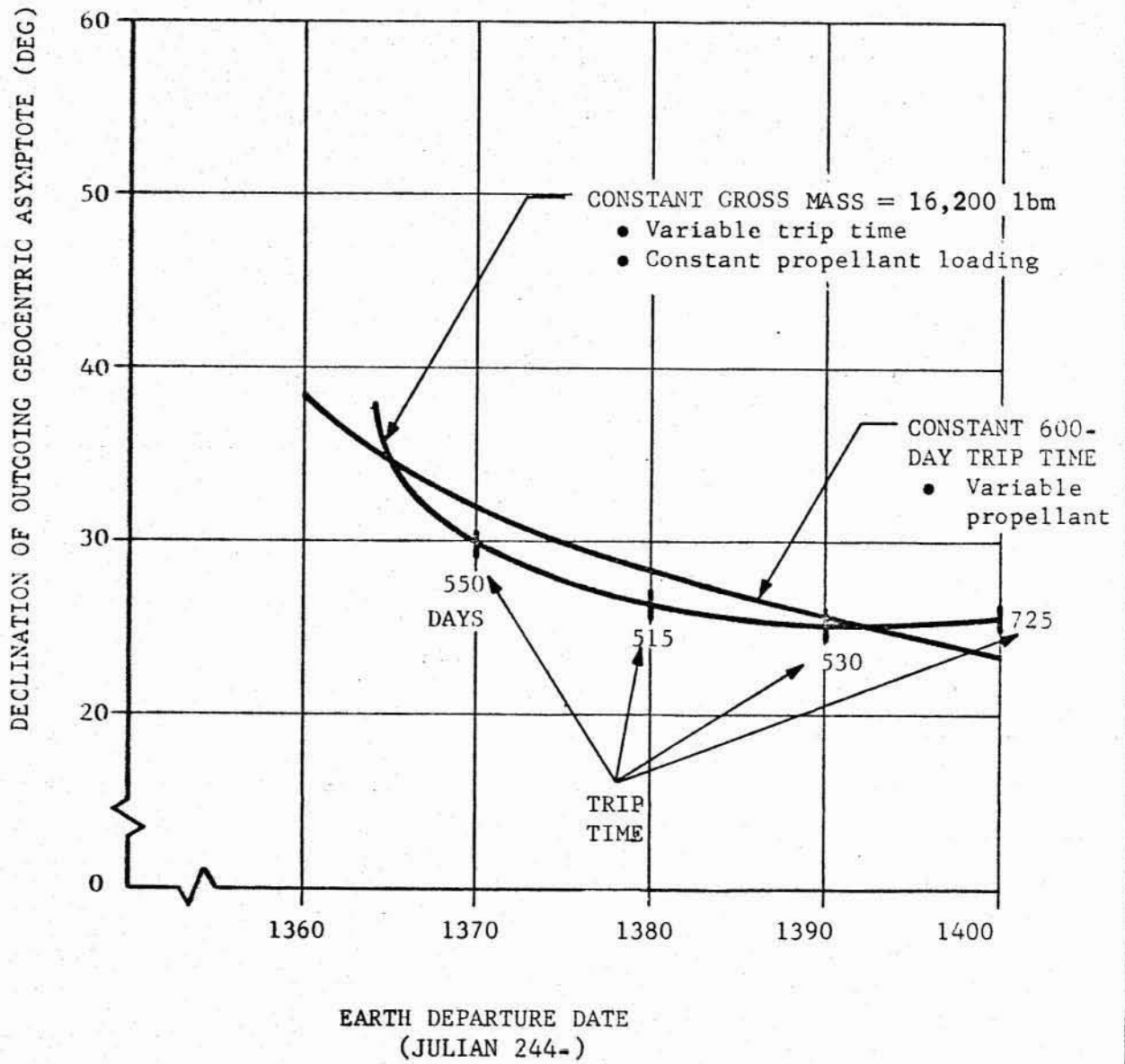


Figure 2-64. DECLINATION OF OUTGOING GEOCENTRIC ASYMPTOTE FOR JUPITER PROBE VS EARTH DEPARTURE DATE

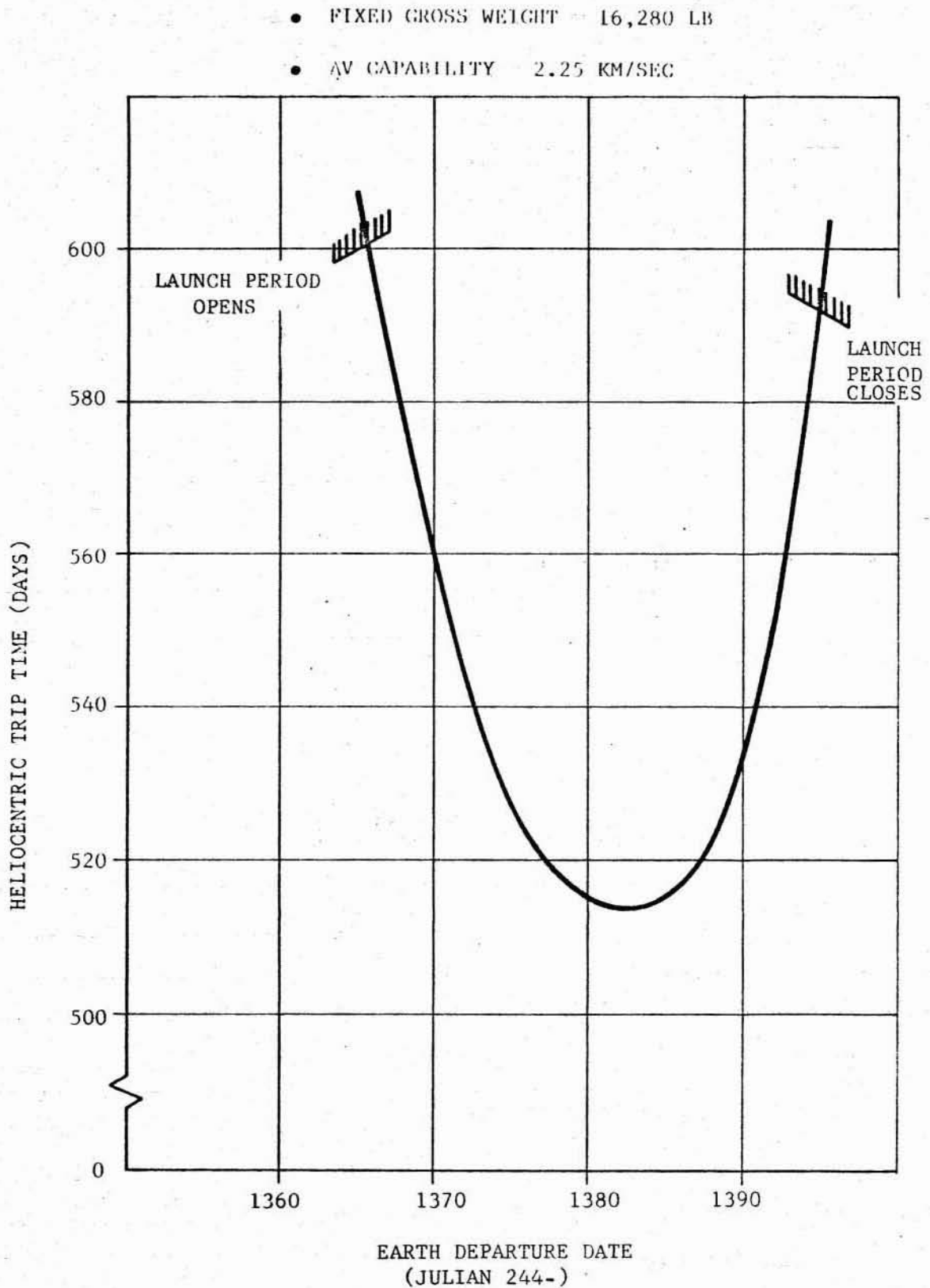


Figure 2 -65. JUPITER PROBE TRIP TIME REDUCTION - HELIOCENTRIC TRANSFER TIME VS EARTH DEPARTURE DATE

significant differences can be noted. The best operational mode is the fixed ΔV /variable trip-time concept. This mode results in highly elliptic capture orbits, but may actually be desirable from the viewpoint of the scientific experiment requirements. Also, it permits the design of a spacecraft with a constant propellant loading which reduces the complexity of system development, testing, and launch operations. No practical difference in the outgoing geocentric asymptote can be noted implying that the launch guidance techniques, daily launch windows, and other factors related to the Saturn V boost guidance function are essentially identical for these two modes.

It is therefore concluded that the fixed propellant loading concept can be considered without compromising mission results.

2.2.1.2 Scientific Investigations. Man's knowledge of the solar system until recent years was limited to terrestrial observations. Through the use of Earth satellites and interplanetary spacecraft, much data (although incomplete) has been collected concerning the environment between 0.8 AU and 1.5 AU. The purpose of this mission is to extend man's knowledge of the solar system from about 0.1 AU out to 5.2 AU via a Jupiter orbital spacecraft and solar flyby probe. Both vehicles are launched simultaneously on one booster. Near the planet Jupiter, the probes separate; one achieving a capture orbit, the other establishing a trajectory to bring it close to the Sun using Jupiter's gravitational assistance. As a further refinement, the Jupiter orbital spacecraft could launch a probe into the atmosphere of Jupiter. Also, by proper selection of the capture orbit, a close approach to one of Jupiter's moons might be achieved.

The selection of scientific investigations for this mission is dependent on a large number of factors. Among these are the scientific value; uniqueness to the mission; data acquired from previous missions; mass, power, configuration, telemetry, and time constraints; trajectory and orbital considerations; availability of instrumentation; reliability under mission environment; and the influence of future missions. All of these factors are interdependent and are influenced primarily by the state-of-art and knowledge of the subjects to be investigated. It is expected that priorities will shift as man's knowledge of the solar system and his technical capabilities increase so that the experiments suggested herein must be considered preliminary.

A detailed analysis and selection of experiments for various phases of this mission has been completed and documented. Brief descriptions of the environment to be expected in different space regimes are summarized in this report and possible experiments are discussed for investigating scientific phenomena. Table 2-4 summarizes the experiments investigation and presents power and mass requirements for various phases of the Jupiter capture/solar probe mission. A normal and emergency power mode are shown to indicate which experiments would be shut down in the event of a partial power supply loss. This is discussed more fully in subsection 2.2.5 of this report.

The instruments for observing the Jupiter moons are of value only if close approaches to those bodies can be achieved. Section III of this report discusses the analyses conducted for the Jupiter moon flybys. Data in Figure 2-66 is presented summarizing the closest approach to the moons. It can be seen that by proper selection of the capture orbit, reasonable approaches may be made to

Table 2-4. EXPERIMENT REQUIREMENTS

JUPITER ORBITER/SOLAR PROBES

a/Heliocentric Phase:

Phenomenon	Instrument	Quantity used on:			Unit Power (watts)	Experiment Power on:			Total Mass	
		Jupiter Probe	Solar Normal	Probe Emer.		Jupiter Probe (watts)	Solar Normal (watts)	Probe Emer. (watts)	Jupiter Probe (kg)	Solar Probe (kg)
Solar Plasma	Hydrogen Lyman- α	2	—	—	0.5	1.0	—	—	6.0	—
	Plasma Probe	2	2	1	3.0	6.0	6.0	3.0	7.2	7.2
	Faraday Cup	1	2	1	10.0	10.0	20.0	10.0	2.3	4.6
Magnetic Fields	Helium magnetometer	1	1	1	7.3	7.3	7.3	7.3	3.4	3.4
	Tri-axial flux gate magnetometer	1	1	1	6.0	6.0	6.0	6.0	1.0	1.0
Trapped Radiation	Radiation detector	2	2	1	0.4	0.8	0.8	—	2.0	2.0
Solar Neutrons	Neutron detector	—	2	1	1.0	—	2.0	1.0	—	6.8
Cosmic Radiation	Cosmic ray telescope	2	2	1	1.0	2.0	2.0	1.0	6.8	6.8
Electromagnetic Fields	VHF occultation	2	2	1	2.0	4.0	4.0	2.0	4.6	4.6
	VLF occultation	2	2	1	0.5	1.0	1.0	0.5	4.0	4.0
Particulate Matter	Gas Chromatography	1	—	—	30.0	30.0	—	—	6.3	—
	Photometer and Polarimeter	1	—	—	5.0	5.0	—	—	2.7	—
	Direct impact devices	2 sets	2 sets	1 set	2.5/set	5.0	5.0	2.5	4.6	4.6
TOTALS						78.1 w	54.1 w	33.3 w	50.9 kg	45.0 kg

2-91

TR-292/3-6-075

Table 2-4. (Concluded)

EXPERIMENT REQUIREMENTS

JUPITER ORBITER SPACECRAFT

b. Jupiter Capture Orbit Additions:

Phenomenon	Instrument	Quantity on Probe:		Unit Power (watts)	Total Power		Total Mass (kg)
		Normal Operation	Emer. Operation		Normal (watts)	Emer. (watts)	
Ionosphere	Swept frequency monitor	2	2	2.0	4.0	4.0	2.8
	Topside sounder	1	1	10.0	10.0	10.0	11.3
Atmosphere	Spectrometers	1 set	1 set	15.0 set	15.0	15.0	42.0
	Microwave radiometer	1	—	200.0	200.0	—	45.4
	IR Television	1	—	10.0	10.0	—	4.5
	Visual Television	1	1	8.0	8.0	8.0	5.1
TOTALS					247.0 w	37.0 w	111.1 kg

2-92

c. Jupiter Moon Fly-by Additions:

Phenomenon	Instrument	Quantity on Probe:		Unit Power (watts)	Total Power		Total Mass (kg)
		Normal Operation	Emer. Operation		Normal (watts)	Emer. (watts)	
Surface	IR imager	1	—	100.0	100.0	—	30.0
	Radar imager	1	—	340.0	340.0	—	181.8
	Altimeter-scatterometer	1	—	29.0	29.0	—	22.7
TOTALS					469.0 w	0	234.5 kg

TR-292/3-6-075

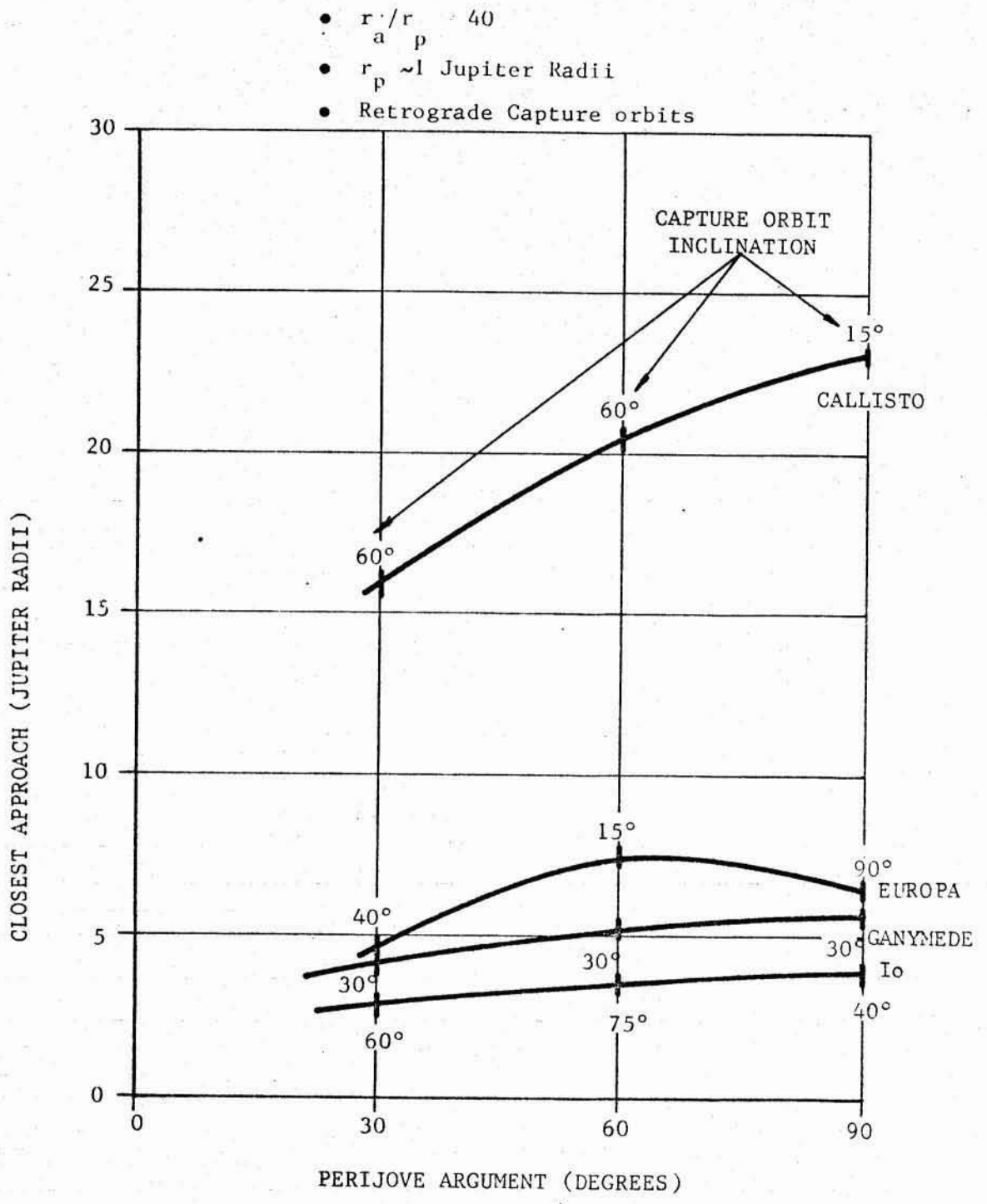


Figure 2-66. JUPITER MOON FLYBY SHOWING CLOSEST APPROACH VS PERIJOVE ARGUMENT

the innermost moons. If desired, capture orbits could be selected specifically to result in extremely close approaches to the moons.

2.2.2 Sterilization

NASA and the scientific community in general have adopted a policy of planetary quarantine to prevent the transport of Earth life to other regions of the solar system. While a specific requirement for sterility has not yet been agreed upon by all the international scientific agencies, the NASA policy for preventing contamination of Mars by the Voyager and subsequent spacecraft is that the probability of landing one live organism is less than 10^{-4} . This means that the Voyager landing capsule will be assembled under sterile conditions and then be subjected to a sterilization treatment. Also, the capsule must be transported, handled, assembled to the spacecraft bus, erected on the launch vehicle, and launched without further contamination. This imposes severe requirements on every aspect of the design, development, assembly, test, and launch of the spacecraft. New fabrication techniques and launch procedures must be developed to meet these requirements.

While the Jupiter orbiter/close-solar probe mission is not designed to contact any interplanetary body except with a Jupiter atmospheric probe, there are some phases of the mission in which accidental contamination could occur. Thus, both the Jupiter orbiter and the solar spacecraft must conform to the stated policy of non-contamination. The following events may occur in this mission which would transport Earth life to other regions of the solar system if the spacecraft were not sterile:

- In passage through the asteroid belt, collision with a large asteroid may occur. Contamination of this body may be spread to others through subsequent collisions and/or fragmentation.
- After separation of the Jupiter orbiter/solar probe spacecraft, either vehicle may accidentally impact with one of Jupiter's moons.
- The braking maneuver for the Jupiter orbiter may inadvertently insert the spacecraft into a planet impact trajectory.
- Long time orbital decay of the Jupiter orbiter may cause the spacecraft eventually to enter the planet atmosphere.
- A Jupiter atmospheric probe, launched from the orbiter will enter the Jupiter atmosphere and may impact the planet.
- The solar probe, on its return heliocentric coast, may impact a large asteroid or one of the planets.

If it can be shown that the probability of contamination by any one of these events is greater than 10^{-4} , means must be taken either to reduce the probability of the event or provide for spacecraft sterilization.

It has been shown that a spacecraft manufactured and assembled using contemporary clean room practices has a number of live organisms of the order

of 10^9 . If this number is not reduced in any way during the mission, then the probability for the occurrence of any of the above events must be less than $10^{-4}/10^9$ or 10^{-13} to meet the current NASA contamination policy.

The best sterilization medium which can be expected in space is heat which is the prime sterilization technique used on Earth. In space, this concept is limited since the spacecraft systems must be thermally controlled within certain operating limits. This precludes consideration of heating the vehicles in space with solar or generated heat to high temperatures. However, other studies are currently underway which may show that very high temperatures are not necessary.

Various time-temperature relationships have been developed for heat-sterilization cycles on Earth which have been shown to be effective. For example, heating to about 378°K for 336 hours is equivalent to heating to about 433°K for 3 hours. Both of these conditions lead to acceptable sterility. With the extremely long mission durations associated with the Jupiter orbiter/solar probe, the time-temperature cycle may be quite reasonable. Excess heat may be used from the RTG units to heat the spacecraft to its upper temperature tolerance limit during the heliocentric coast phases to achieve sterilization.

Figure 2-67 shows the current requirements and a postulated extrapolation. If this extrapolation is valid, the Jupiter orbiter must be heated to about 330°K during its heliocentric coast to be sterile at Jupiter encounter. While this temperature does not exceed the usual limits of conventional systems, continuous operation at this level seriously affects the lifetime of electronics. Also, it does not seem probable that absolutely all elements of the spacecraft could be maintained at this temperature. Unless a very compact design was developed, appendages such as antennas, instrument booms, etc., would be difficult to heat properly. Little confidence could be placed in this concept of heating enroute to insure a completely sterile spacecraft at planetary encounter, although the biological count could probably be reduced over most of the spacecraft.

A sterilization technique under consideration for the Voyager mission is the use of a microbiological barrier around the landing capsule. Upon approach to the planet, the barrier will be opened and the sterile capsule ejected onto its landing trajectory. This concept has many advantages:

- The barrier can be made impervious to contamination after encapsulation of the sterile landing probe permitting conventional handling during transport, assembly, and launch operations.
- The barrier provides a means of connecting the landing capsule to the spacecraft bus so that cross contamination during the heliocentric coast will not occur.
- The barrier can be filled with a sterilizing gas such as ethylene oxide or Freon 12 to maintain sterility and provide a long term decontamination exposure during the heliocentric coast.

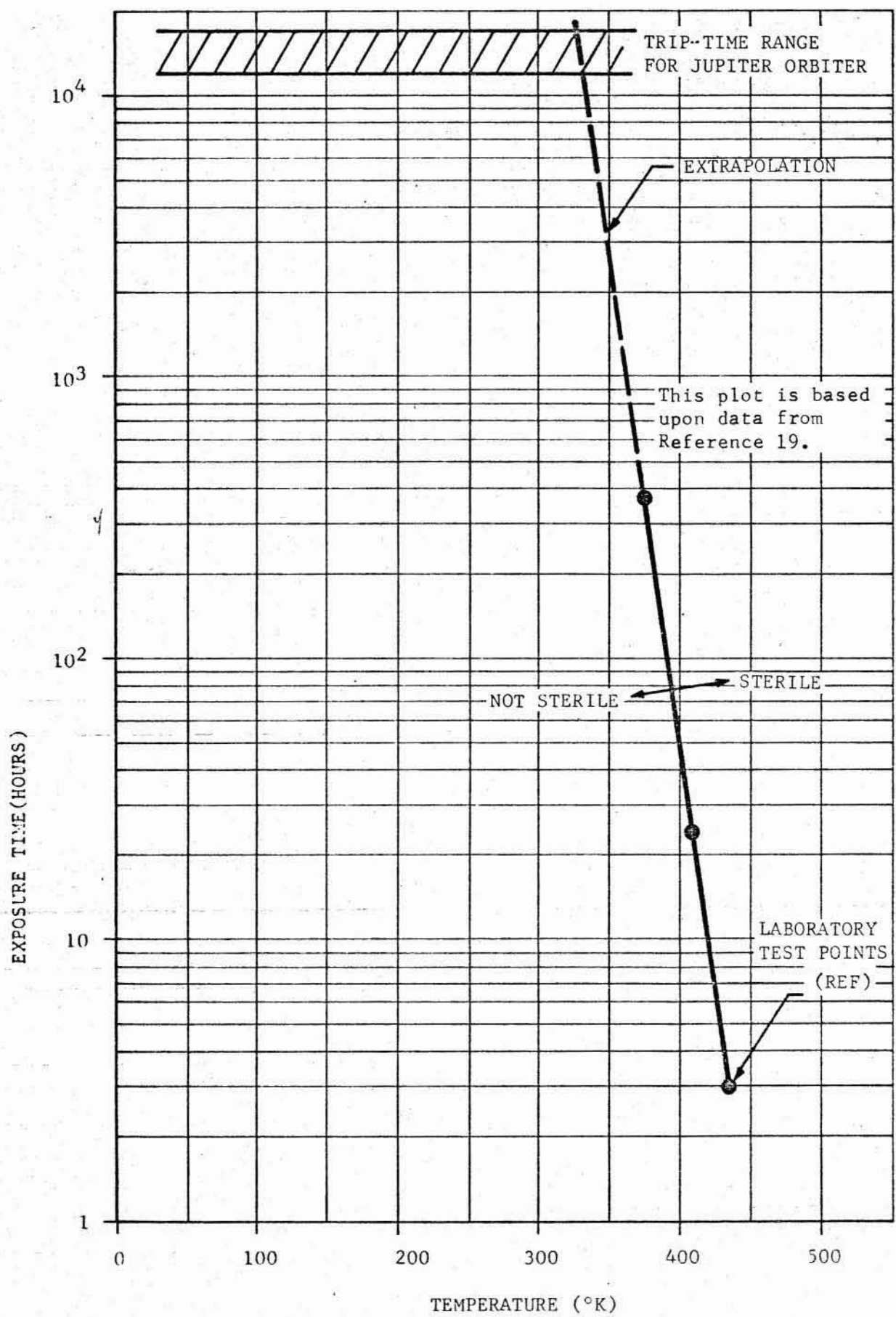


Figure 2-67. STERILIZATION TIME-TEMPERATURE CYCLES

2.2.3 Communication Subsystem

The functions of the communication subsystem on interplanetary unmanned spacecraft can be summarized as follows:

- **Command and control:** provide system command in real time; provide a means of relaying information from Earth to be stored in the spacecraft control system or data handling system; and provide for verification readouts of commands stored on the spacecraft upon interrogation from Earth. The required transmission rates are low, but accuracy requirements are severe.
- **Tracking:** provide for precise determination of the spacecraft velocity vector and range to correctly interpret scientific data and compute course corrections.
- **Telemetry:** provide for transmission to Earth of scientific data and engineering status of the spacecraft (housekeeping data). To minimize system power requirements, the data handling system must be highly flexible in programming and routing capabilities and must incorporate adaptive techniques, data compression techniques, and storage devices.

The most sophisticated of the above functions is telemetry. Before scientific or engineering data can be transmitted from a spacecraft, it must be sampled, encoded, and modulated. By these techniques, a message is transformed from its original form into a signal suitable for transmission and processing.

The following subsections present discussions of these functions together with subsystem requirements, state-of-the-art capabilities where appropriate, and spacecraft subsystem descriptions.

2.2.3.1 Command and Control. To provide the proper command and control function, the spacecraft command receiver subsystem must be operated continuously. This is necessary to permit ground communications with the spacecraft at the ground controllers' option during the flight phases of the mission. The command and control receiver is fed by an omnidirectional antenna on the spacecraft to allow Earth-to-spacecraft communications even if a failure in the attitude control system or guidance and navigation system has deoriented the high-gain antenna. In the event of such a failure, the spacecraft will be able to receive command signals from the Earth through its omnidirectional antenna in an effort to correct malfunctions or establish emergency modes of operation.

The command and control link is usually designed for about 1 BPS data rate operation. To preclude the transmission of erroneous commands, this subsystem requires a low bit error rate of approximately 1 in 10^5 bits. The unique requirements of this subsystem lead to consideration of a ground-to-spacecraft communications link separate from the telemetry link. Thus, for the Jupiter orbiter/solar probe mission under study herein, the 25.9-meter (85-foot) DSIF ground antenna could be used for the command link at the low bit rates. For data telemetry, the 64-meter (210-foot) ground antenna must be used. This concept will also help relieve the utilization load on the large DSIF antennas which will be in great demand in the next decade.

A spacecraft-to-Earth communications link for the command and control subsystem is necessary to verify the receipt of commands and to transmit the stored commands upon interrogation from the Earth. This can be accomplished with the spacecraft high-gain telemetry system independent from the omnidirectional command receiving subsystem.

For both the Jupiter orbiter/solar probe, communications out to about 6.5 AU must be provided. Thus, the two spacecraft may well use identical command and control receiving systems. Based on data to be presented in following paragraphs of this report, the characteristics of this system can be determined. Table 2-5 summarizes the important data relating to the command and control communications at S-band operation.

2.2.3.2 Tracking. Doppler frequency shift and range measurements are required for accurate trajectory reconstruction. Doppler information is obtained by a flight transponder which coherently tracks the incoming radio frequency carrier from the ground station and radiates back a carrier whose frequency relationship to the received carrier is set and known. The ground station observes the Doppler shift in their received carrier frequency and computes the spacecraft velocity. Existing systems permit an accuracy of one foot per second or less.

Range information is obtained by noting the signal round-trip propagation time and correlating pseudo-random codes. At interplanetary distances, the spacecraft must detect, reconstruct, and retransmit the ranging pseudo-random codes. Advanced systems under development also correlate the phase of the coded signal and of the carrier, providing a fine vernier determination of spacecraft range.

The equipment to perform these functions is an integral part of the spacecraft high-gain communications system discussed below. Only a very small portion of the bit rate is used for tracking data and the bit error rate is not critical. Trajectory reconstruction entails the utilization of many range and velocity points and one data sample out of tolerance can be noticed and discarded.

2.2.3.3 Telemetry. The primary purpose of an interplanetary mission is the return to Earth of scientific data. Sampling and preselection of spacecraft data is desirable as it is not efficient nor necessary to transmit all the information collected during the mission. Postulated techniques which would significantly affect the communication system requirements of the Jupiter orbiter/close solar probe will be discussed in the following paragraphs.

Self Adaptive Telemetry Systems. These systems perform an onboard selecting function and reduce the transmitted data bits. A simple concept uses a programming technique to routinely select data transducers. A controlling sequencer is located between the encoder and data transducers which sequentially selects the data to be transmitted. Thus, during one spacecraft interrogation only a portion of the total onboard stored data is relayed to the Earth. On the next interrogation data of a different nature is transmitted. For example, housekeeping data may be relayed only every tenth interrogation and the various scientific data divided between the other nine transmissions.

Associated with the above approach may be programming of an increase in transmitter power at predetermined points in the flight to maintain a desired

Table 2-5. COMMAND AND CONTROL GROUND-TO-SPACECRAFT LINK
(JUPITER ORBITER/SOLAR PROBE)

COMMUNICATIONS COMPONENT	REMARKS	SYSTEM GAINS	SYSTEM LOSSES
GROUND STATION	DSIF 25.9-m (85-ft) antenna gain	52.5 db	
	DSIF transmitter gain @ 1 BPS and 100 kw input power	73.0	
SPACECRAFT	Omni-antenna gain	3.5 db	
	Receiver gain @ 1 BPS and 10 db noise figure	164.0	
	Internal system losses		18.0 db
SPACE PROPOGATION	Transmission losses from 6.5 AU		234.0 db
	Sky noise losses		15.0
	Jupiter background noise losses		22.0
TOTALS		293.0 db	289.0 db

signal-to-noise ratio over the entire trajectory. An effective system can be developed wherein the measured signal received by the ground station from the spacecraft serves as the controlling parameter. At a predetermined minimum signal level, the spacecraft transmitter power is increased in increments.

A new development in self-adaptive telemetry which may be considered is the use of an onboard device to examine each of the measurements taken and reduce only those data segments which exceed stipulated tolerances. In this way, the system telemeters out-of-tolerance data and the gaps between such information implies within-tolerance conditions.

The ideal self-adaptive telemetry system would monitor all data before transmission and select only that information of interest. This requires sophisticated data processing onboard the spacecraft and establishing criteria to make the selection decisions. Such criteria may account for the occurrence of an event, duration of an event, and exceeding a predetermined threshold. Advanced telemetry systems of this nature have not yet been developed for operational use, but may be available in the next decade for use on a Jupiter/solar probe.

Feedback systems. These systems can improve the reliability of the received data by automatically monitoring the communications link. A number of automatic feedback techniques can be considered:

- Decision feedback employs a means for the ground receiver to request additional data from the spacecraft if the information symbol received is unclear or appears to be erroneous.
- Information feedback allows the spacecraft to obtain information from the ground station regarding the quality of the received signal and to send additional adjustments in doubtful cases.
- Power control feedback adjusts the radiated transmitter power upon feedback from the ground station so that the received signal strength is always above a certain threshold.

The advantages of feedback telemetry systems are 1) the feedback function improves the reliability of the data, and 2) the feedback function can be employed to change the data rate in response to fluctuating system signal-to-noise conditions. These advantages are in contrast to normal telemetry systems which are designed for the worst case signal-to-noise ratio at which the system is expected to operate.

2.2.3.4 Spacecraft Antennas . An important aspect of interplanetary spacecraft communication systems is the configuration and design of antennas. These have a strong influence on the design of the spacecraft in terms of weight, power, and attitude stabilization. This analysis considered the following factors to properly size the telemetry antennas for the Jupiter orbiter/solar probe:

- Antenna and system gains
- Propagation losses
- System noise losses
- Ground system characteristics

September 1966

The following subsections present a discussion of these subjects and indicate the process utilized in selecting the telemetry system characteristics.

Antenna and system gains will be considered first. The various common antenna configurations which can be used on interplanetary spacecraft and the restrictions on their use are as follows:

- Stub antennas: a rod which is one quarter the wave length of the carrier frequency. Four of these stubs placed in a plane and located 90° apart can be made to provide a nearly omnidirectional radiation pattern.
- Dipole antennas: used on spin-stabilized spacecraft with the antenna axis collinear with the spin axis of the probe. The radiation pattern is doughnut shaped with a gain of a little more than 2 db on the plane perpendicular to the dipole axis.
- Directional antennas: usually paraboloids, these antennas provide a beam radiation pattern which must be accurately pointed to the receiver.

Directional antennas collect and focus a great deal of radiative energy into a beam permitting greater transmission distances for any given power level. For this reason, they are used almost exclusively on interplanetary spacecraft. The feed to the parabolic reflector is usually tapered from maximum illumination at the center to zero at the edge. This is done to eliminate side lobes in the radiative pattern and create a more uniform beam. The efficiency of such an antenna lies between 50 and 80 percent.

Because of the collecting and focusing feature of these antennas, a system gain over omnidirectional antennas can be expected for any given power level. In addition, the half-power beam width of parabolic antennas can be calculated in terms of its gain. The graphic presentation of the functions is shown in Figure 2-68 for operation at DSIF S-band frequencies with an efficiency of 50 percent. The dotted line on the plot indicates the method of using this data. It can be seen that large antennas, while providing great system gain, must be pointed very precisely. This is a disadvantage which must be considered in the selection of antennas for interplanetary spacecraft. Another disadvantage associated with the large parabolic antennas is the requirement for close mechanical fabrication tolerances. Surface irregularities limit the coherence of the collected energy which degrades the antenna gain. When the irregularities approach one-quarter of the wavelength, there is complete loss of antenna gain.

In addition to the gain of directional antennas, system gain is achieved in the transmitting devices. The general tradeoff of system gain in decibels vs rf power is shown in Figure 2-69. This is a costly method of achieving gain as is evidenced by the drastic increase in required power to achieve minor increases in gain. The usual approach to increasing communications capability is to increase the antenna size.

The major system propagation losses are due to attenuation in space and absorption in the atmosphere and ionosphere. For the former case, it can

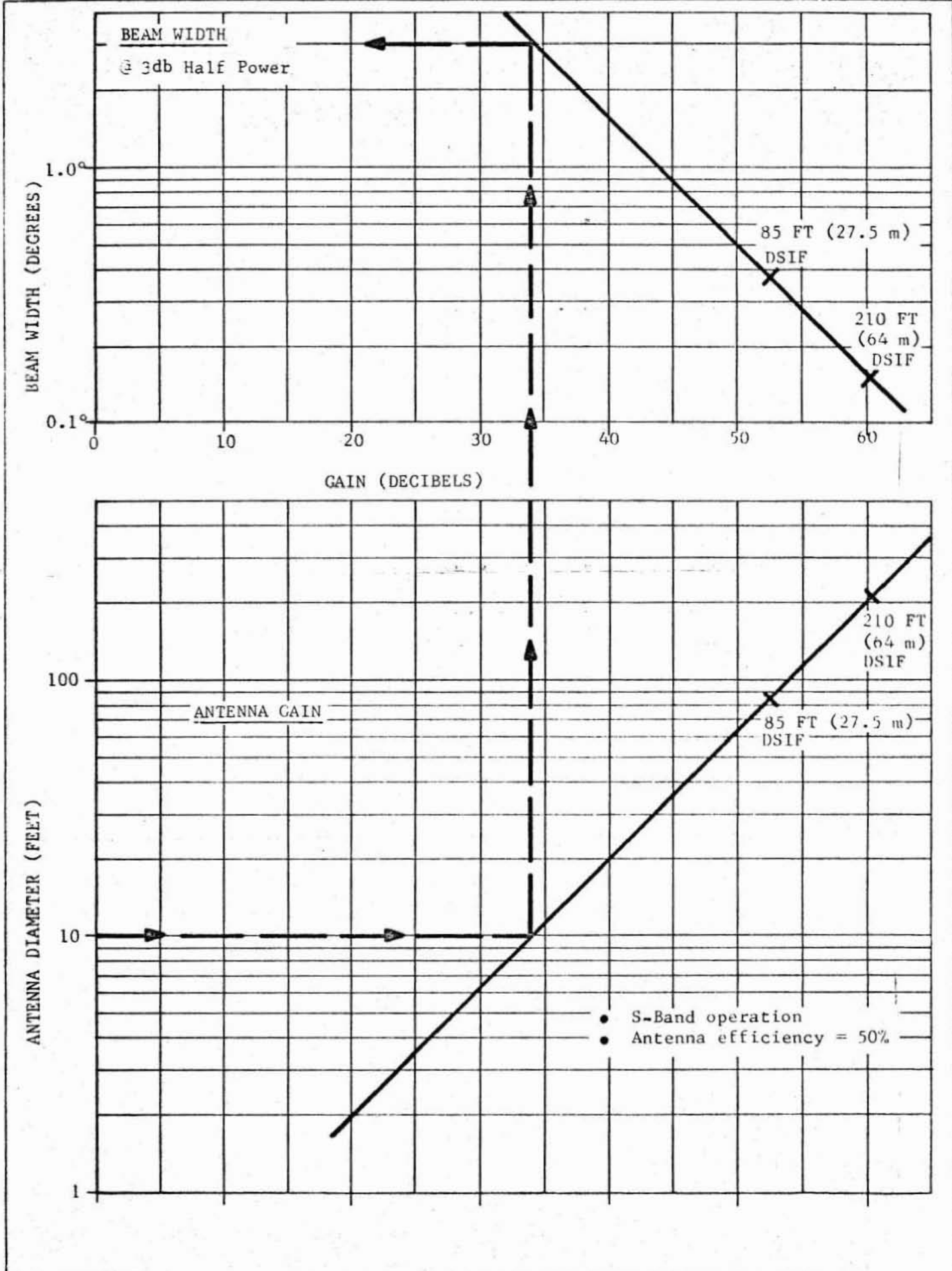


Figure 2-68. PARABOLIC ANTENNA CHARACTERISTICS

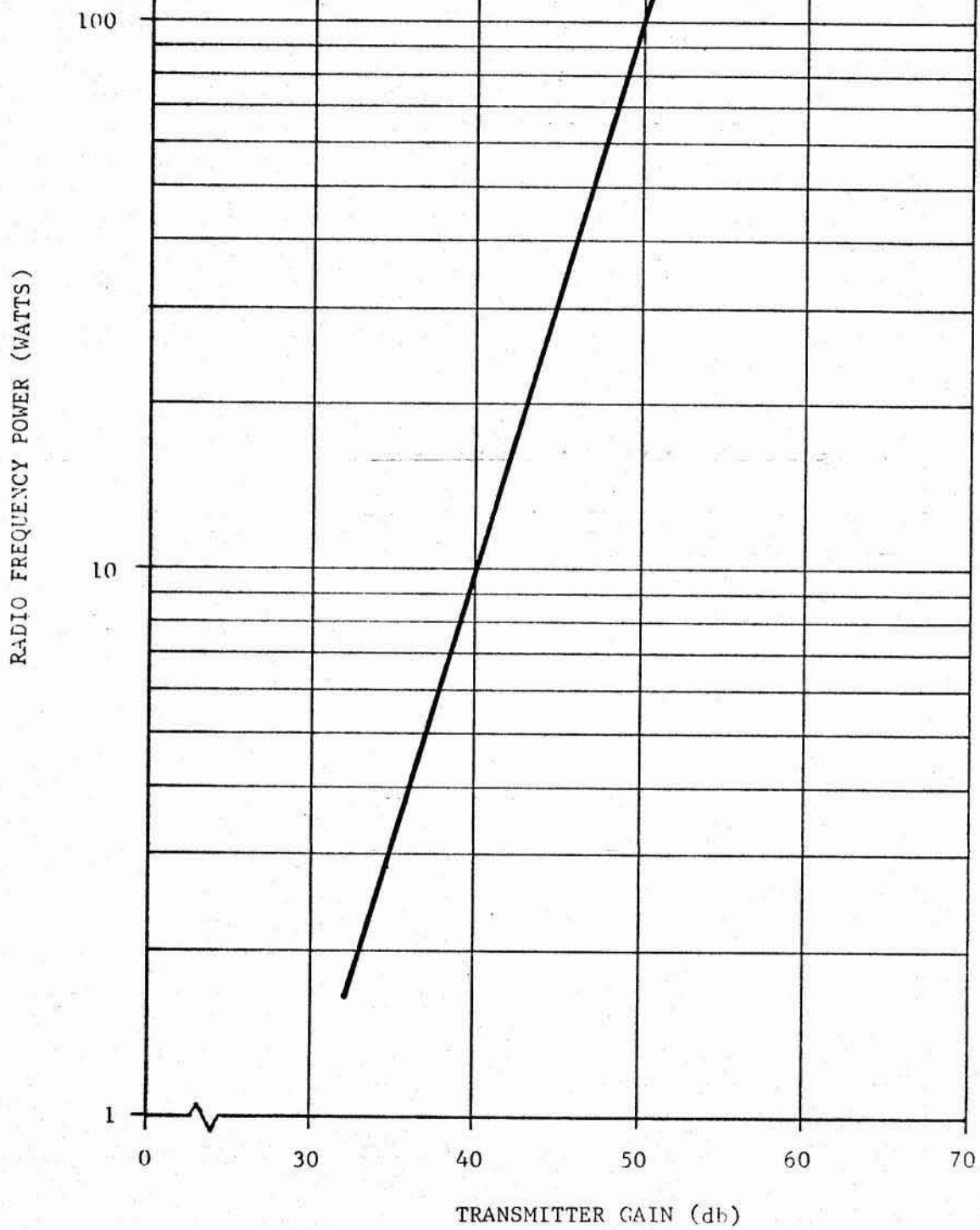


Figure 2-69. TRANSMITTER POWER REQUIREMENTS VS TRANSMITTER GAIN

be shown that the total space loss between two parabolic antennas is as plotted in Figure 2-70 assuming the utilization of the 64-meter (210-foot) Goldstone antenna at S-band frequencies. For reference purposes, the space propagation losses for a half-wave dipole (omnidirectional) antenna are also shown. These curves clearly indicate the advantages of using large diameter antennas at interplanetary distances. However, a tradeoff of size and pointing accuracy is necessary and the larger diameters must be stabilized to very close tolerances as indicated in Figure 2-70 for 3-decibel half-power beam widths.

In addition to losses due to propagation through space, absorption in the Earth's atmosphere and ionosphere occurs. In the atmosphere, losses are caused almost entirely by the molecular absorption of oxygen and water vapor. This absorption decreases sharply with increasing elevation angle of the signal source because of the decrease in path length through the atmosphere. Ionosphere losses are caused by the transfer of energy from the propagating electromagnetic waves to the electrons of the ionosphere layers. These losses exhibit daily, seasonal, and sporadic variations due to oscillations and changes in the ionosphere. Absorption losses are very small at S-band frequencies and can be ignored in the conceptual design stages. Other effects listed below are also small but will be accounted for.

- Faraday effect - rotation of the plane of polarization of the propagated wave due to the combined presence of the ionosphere and magnetic field of the Earth. The apparent losses due to this effect are less than 3 db.
- Polarization - induced in the propagated wave by the relative aspect and orientation of the spacecraft antenna with respect to the ground station. System losses are less than 3 db.
- Interference - spurious signals in the transmitter and transmitter-receiver space link, input circuitry of receiver, and receiver local rf power generating circuitry.

A study will now be made of the system noise losses. The ground receiving station for an interplanetary probe, in addition to acquiring normal transmitter signals, acts as a radio telescope and picks up radiations from the Sun, galaxy, stars, Moon, and other planetary bodies. The most isotropic source of this background noise is the galaxy. The Sun and planets are stronger emitters but are discrete or localized sources affecting communications only in specified directions. The Sun is a strong noise source and communications with interplanetary probes close to or in front of the Sun will be difficult.

Noise sources in the sky have been extensively studied by radio astronomers. Maps of the celestial sphere have been prepared showing equivalent noise temperature in great detail. For the purposes of this study, these data can be summarized as shown in Figure 2-71. The line labeled "average" in this figure represents the background noise which is independent of direction. It can be seen that at S-band frequencies, galactic noise is an approximate 5°K source, while the nominal background noise is negligible. The energy absorbed by the atmosphere of the Earth is partly reradiated as thermal energy giving rise to a thermal noise spectrum surrounding the Earth. The energy level of

- S-Band frequency (2.2 GHz)
- Goldstone 64 antenna (210 ft)
- Antenna efficiency = 50%

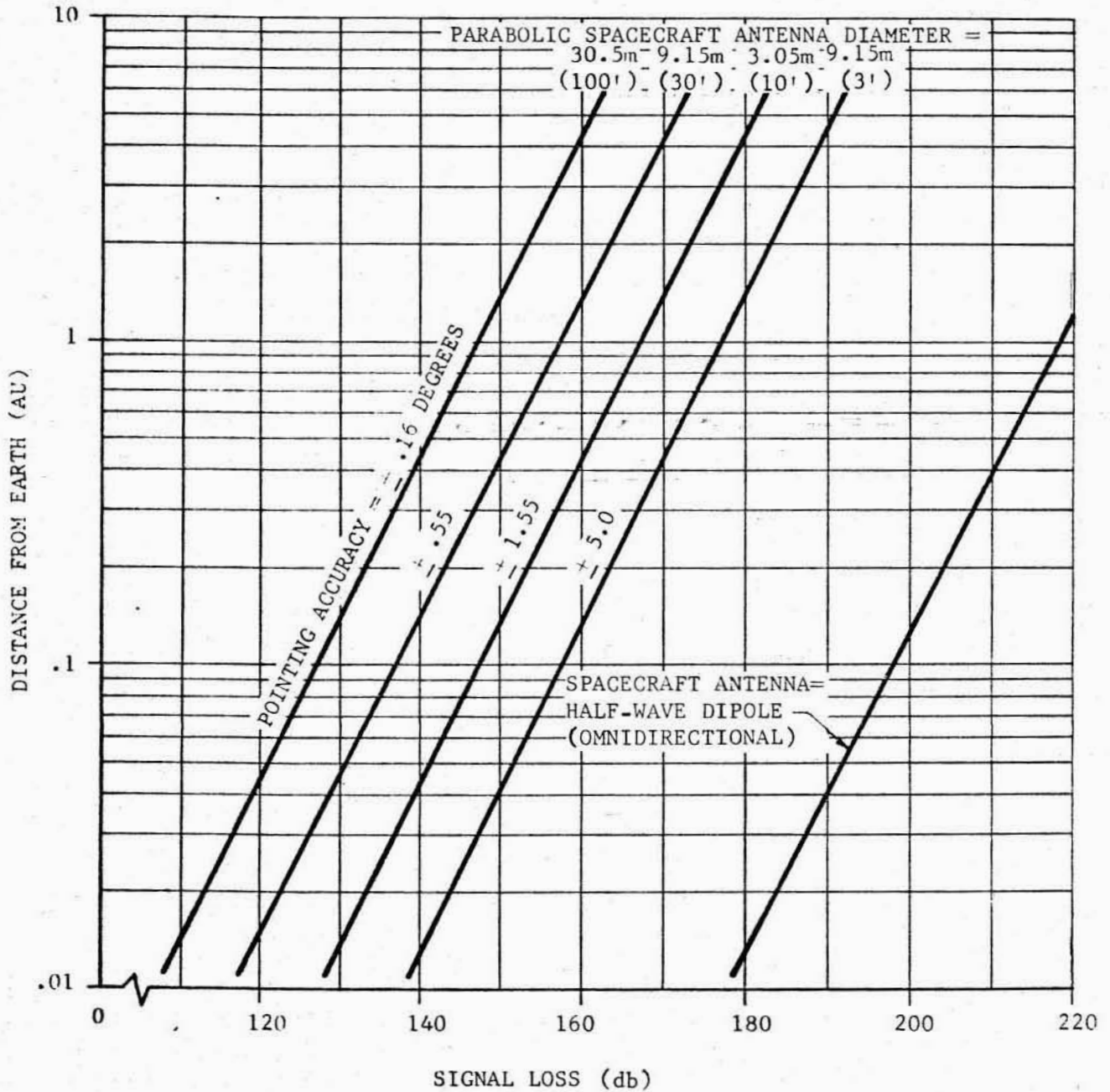


Figure 2-70. DISTANCE FROM EARTH VS SIGNAL LOSSES

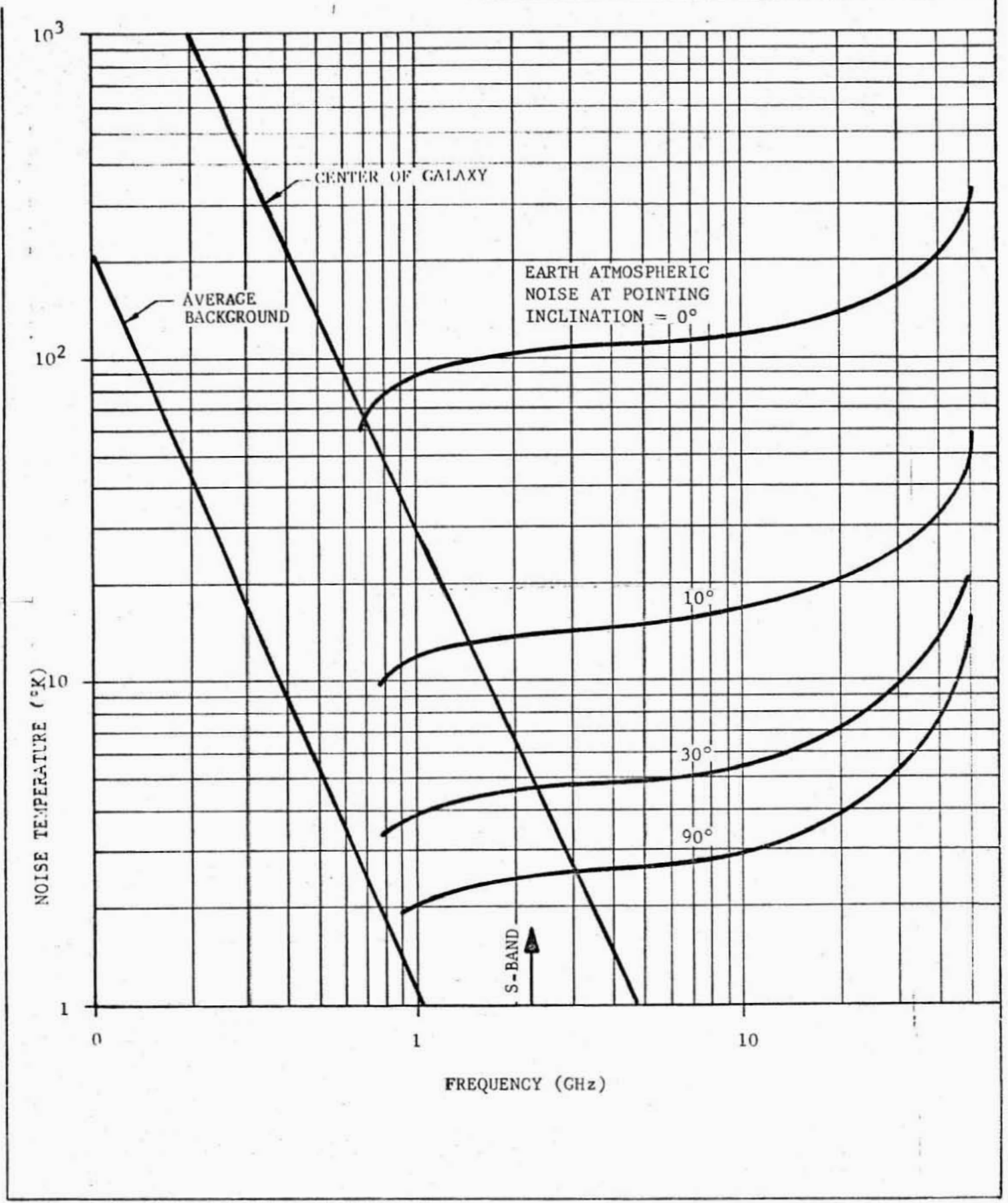


Figure 2-71. SKY NOISE TEMPERATURE VS TRANSMISSION FREQUENCY

this noise is low and is a strong function of elevation. This noise source is also indicated in Figure 2-71 .

The surface of the Earth also acts as a noise source with a noise temperature of 290°K. This radiation usually enters the communication loop through side lobes of the ground antenna. However, properly designed equipment has been able to reduce the Earth's surface equivalent noise source temperature to about 20 - 50°K. When the ground antenna is operating at high inclinations, this noise is greatly reduced. Of course, the interplanetary probes's antenna when pointed at the Earth for data transmittal sees a 290°K noise source.

The radiation from the Sun has a complex spectrum, but it is primarily composed of a basic thermal component, a slowly varying component, and various types of sudden bursts. Because of the complexity of this spectrum, it is not possible to establish exact noise values. However, at S-band frequencies, the solar noise corresponds almost entirely to the 6000°K black body thermal emission of the Sun's photosphere.

The planet Jupiter is a relatively strong noise emitter. Thermal emission occurs at a wavelength approximately 3-cm long corresponding to an equivalent noise temperature of 130°K. The planet also exhibits a non-thermal radiation spectrum with a continuous emission in the decimeter wavelength region and noise-storm type emission in the decameter range. The latter occur in bursts of a second or two duration in groups lasting 5 to 10 minutes and continuing intermittently over a period of hours. These bursts are inversely related to sunspot activity and can thus be roughly predicted. Because of the short duration and rarity of these events, they will not be accounted for in the development of the communications system for the Jupiter orbiter/solar probe.

The effect of this background noise on system operation is shown in Figure 2-72 . On this graph, the equivalent temperature of the noise sources expected for the Jupiter orbiter/solar probe is indicated. To accurately calculate the signal loss expected, the trajectory for the probe must be examined to determine the relative location of the noise sources with respect to the Earth-to-probe communication line of sight. A constant background signal noise loss of at least 22 db should be expected for the Jupiter orbiter. A greater signal loss can be anticipated for the solar probe as the spacecraft approaches the Sun leading up to complete signal loss during passage across the solar disc.

In addition to noise losses due to propagation phenomena, internal sources of noise power generated in the transmitting and receiving equipment must be accounted for. The type of equipment has a strong influence on the internal noise. Table 2-6 below summarizes some typical values for receivers operating at S-band frequencies.

Table 2-6. EFFECTIVE NOISE TEMPERATURE

TYPE OF RECEIVER	NOISE TEMP., °K	NOISE FIGURE, db
Crystal mixer	1500	8
Traveling-wave	750	5.5
Parametric amplifier	100	1.3
Maser	3 to 10	.04 to .2

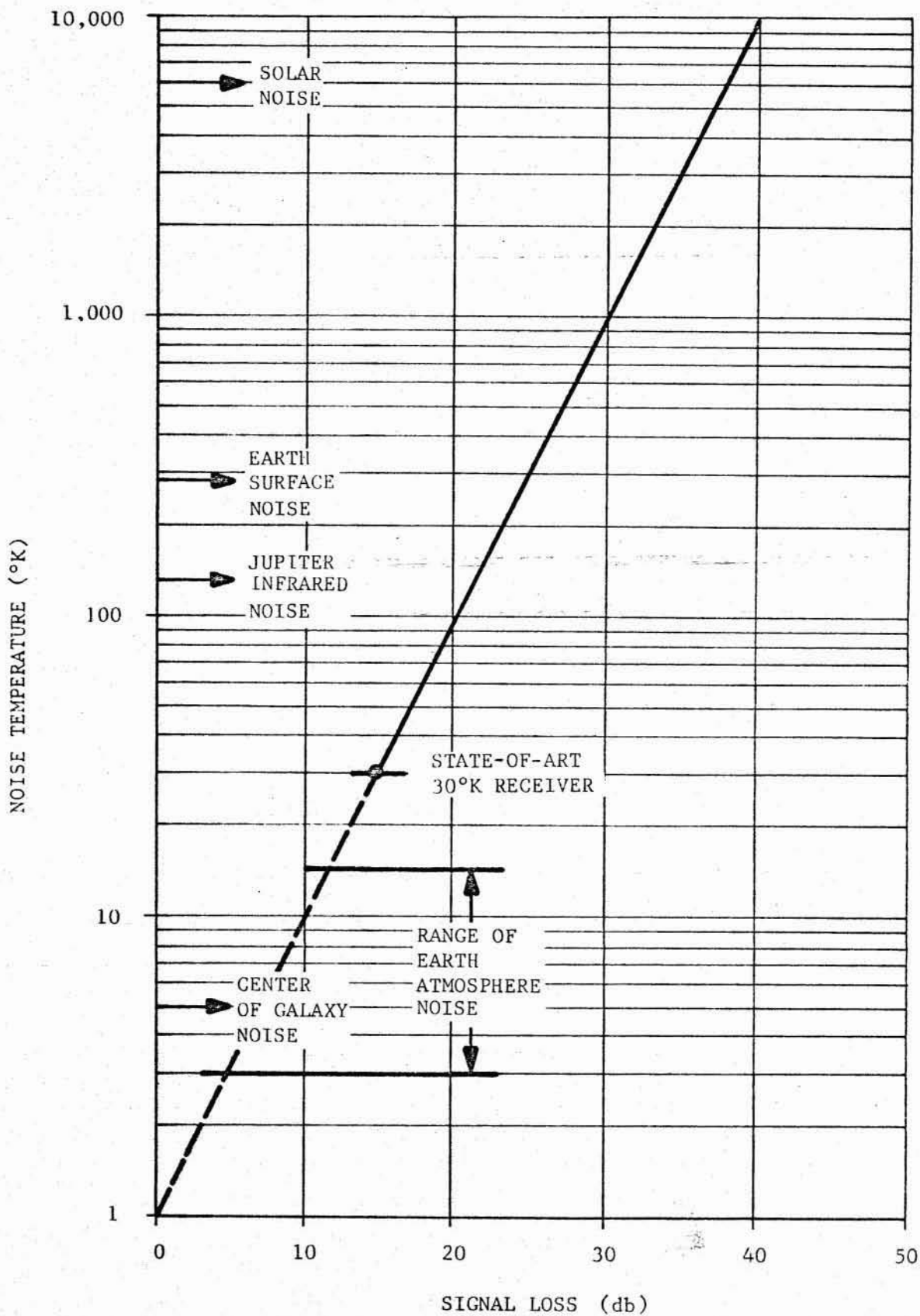


Figure 2-72. BACKGROUND NOISE LEVELS VS SIGNAL LOSSES

The superiority of the modern maser systems is readily apparent. Other onboard losses related to antenna feeds will account for another 1 or 2 db loss over that shown in Table 2-6.

The only ground system characteristics which can be considered are the DSIF network of NASA. In the next decade, the 64-m (210-foot) antenna will be the primary ground antenna in use for telemetry. This system will have an equivalent noise temperature of about 30°K which is a receiver noise figure of about -10 db. This is an excellent receiving system approaching theoretically perfect limits. To achieve this performance, the preamplifiers are cooled with liquid hydrogen to obtain superconductivity in the system circuits and minimize thermal noise losses. The system gain which this ground station contributes to the communications subsystem is a function of the data bit rate. In terms of decibels over a milliwatt, this tradeoff is shown in Figure 2-73 for a range of receiver noise figures. In this study it will be conservatively assumed that the 0 db noise level will be achieved in the next decade.

The significant gain contribution by the ground system can be noted from the data in Figure 2-73. This performance is all that can reasonably be expected in the next decade although interest has been expressed in the X-band (10GHz) for future development. At this time significant improvements cannot actually be realized over the S-band performance due to practical fabrication problems. Two typical S-band and X-band systems were compared in a previous Jupiter probe study (reference 1).

2.2.3.5 Telemetry System Summary. Tables 2-7 and 2-8 were prepared to summarize the primary characteristics of a typical spacecraft-to-Earth telemetry communication link. The selection of the features shown is, to some extent, arbitrary, and exchanges of antenna size, power, and bit rate can be made to obtain a reasonable system. However, for use in conceptual spacecraft designs, the characteristics shown on these tables will be used. A number of explanatory comments are in order:

- **Ground Station** - A receiver noise figure of zero db is assumed. If a -10 db noise figure is achieved in the next decade, the ground receiver gains for the bit rates shown will be increased by that 10 db. To maintain similar operating margins, this gain may be compensated for by decreasing either the spacecraft power, the antenna size, or both.
- **Space Propagation** - Omnidirectional transmission antennas are shown for use at distances close to Earth. This antenna configuration used out to about 2 AU for the Jupiter probe will reduce the attitude control requirements of the spacecraft during the critical ejection and stabilization maneuvers. Also, during the early phases of the mission, the relative change in the angle between the Earth-to-spacecraft line and spacecraft-to-Sun line is high. These problems are discussed more fully in subsection 2.2.7 (Guidance and Navigation), of this report.

For the solar probe, an omnidirectional system is used if the spacecraft passes within 0.75 AU of the Earth. For the Jupiter gravity assist trajectories under consideration herein, this does not occur until the solar encounter has

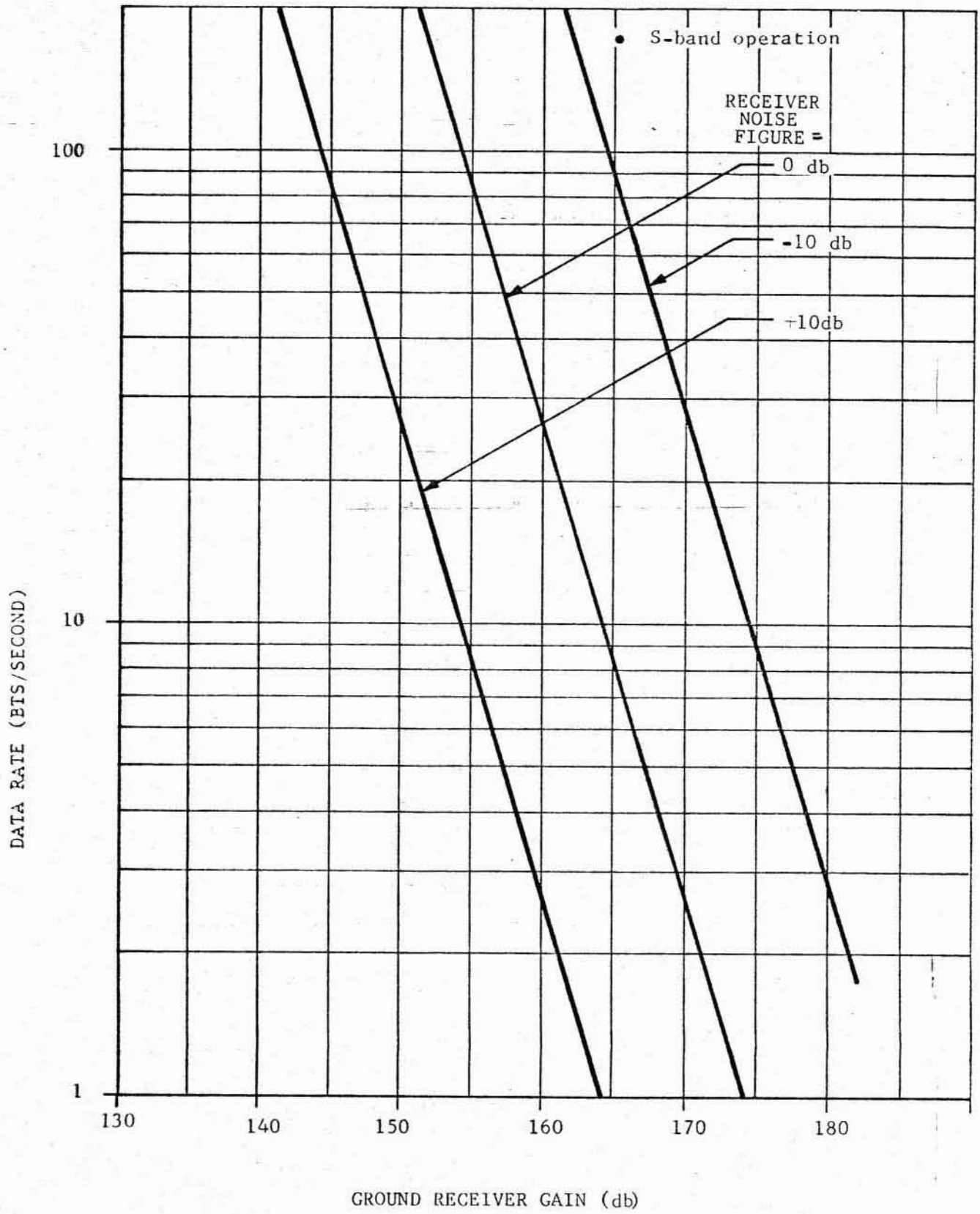


Figure 2 -73. DATA RATE VS DSIF RECEIVER GAIN

Table 2-7. TELEMETRY SYSTEM PERFORMANCE

JUPITER ORBITER

COMMUNICATIONS COMPONENT	REMARKS	OMNI. ANTENNA	HIGH GAIN ANTENNA
GROUND STATION	DSIF 64m(210-ft) antenna gain	+ 60 db	+ 60 db
	DSIF receiver gain @ 90 BPS	—	+ 155
	DSIF receiver gain @ 9 BPS	+ 165	—
		+ 225 db	+ 215 db
SPACE PROPOGATION	Space transmission loss from ~2 AU	- 224	—
	Space transmission loss from ~6.5 AU	—	- 180
	Jupiter background noise loss	—	- 22
	Earth atmospheric and surface noise loss	- 15	- 15
		- 239 db	- 217 db
SPACECRAFT	Antenna gain @ 4 m (15 ft)	—	+ 37 db
	Omnidirectional antenna gain	+ 12	—
	Transmitter gain @ 40-w. rf power	+ 46	+ 46
	Antenna feed losses	- 2	- 2
	Internal system noise losses	- 2	- 2
	Polarization loss	- 3	- 3
	Faraday effect loss in ionosphere	- 3	- 3
	Modulation bandwidth loss	- 20	- 20
	FM improvement and phase lock tracking losses	- 10	- 10
		+ 18 db	+ 43 db
NET OPERATING MARGIN		+ 4 db	+ 41 db

2-111

TR-292/3-6-075

Table 2-8. TELEMETRY SYSTEM PERFORMANCE

CLOSE SOLAR PROBE

COMMUNICATIONS COMPONENT	REMARKS	OMNI. ANTENNA	HIGH GAIN ANTENNA
GROUND STATION	DSIF 64 m (210-ft) antenna gain	+ 60 db	+ 60 db
	DSIF receiver gain @ 90 BPS	—	+ 155
	DSIF receiver gain @ 9 BPS	+ 165	—
		+ 225 db	+ 215 db
SPACE PROPAGATION	Space transmission loss from 6.5 AU	—	- 190 db
	Space transmission loss from 0.75 AU	- 214 db	—
	Jupiter background noise loss	- 11	- 28
	Earth atmospheric and surface noise loss	- 15	- 15
		- 240 db	- 233 db
SPACECRAFT	Antenna gain @ 1.2 m (4 ft)	—	+ 26 db
	Omnidirectional antenna gain	+ 12 db	—
	Transmitter gain @ 40-w. rf power	+ 46	+ 46
	Antenna feed losses	- 2	- 2
	Internal system noise losses	- 2	- 2
	Faraday effect in ionosphere	- 3	- 3
	Polarization loss	- 3	- 3
	Modulation bandwidth loss	- 20	- 20
	FM improvement and phase lock tracking losses	- 10	- 10
		+ 18 db	+ 32 db
NET OPERATING MARGIN		+ 3 db	+ 14 db

2-112

September 1966

been achieved.

- Net operating margin for the omnidirectional antenna systems, the signal-to-noise margin shown is relatively low corresponding to the values expected at distances where this antenna becomes useless. Due to modern filtering techniques and ground system improvement, it may be later possible to receive signals beyond these distances with close to one db operating margin. For the high-gain systems, a considerable margin is maintained at the limits of the communications line of sight. This will account for any contingencies, spurious noise, or other unexpected system losses. With these relatively high margins and the reasonable estimates for system gains and losses indicated in the tables, it is believed that a very conservative system has been developed for this mission.

2.2.3.6 Communications Geometry. To locate the antennas on the conceptual spacecraft designs and define the antenna gimbal requirements, the heliocentric geometry of the Jupiter orbiter/solar probe must be analyzed. For the Jupiter capture mission, a typical trajectory is shown in Figure 2-74. During the heliocentric coast beyond 2 AU, when the omnidirectional antenna is no longer useful, the high-gain antenna must be capable of gimbaling about $\pm 20^\circ$ from the spacecraft-to-Sun axis. The Earth appears never to be more than 12° away from the Sun when viewed from Jupiter orbit. However, the orbiting spacecraft must now keep one axis pointed toward the planet for scientific measurements. During one Jupiter orbit the Earth appears to the planet-oriented spacecraft to traverse the entire sky. Therefore, complete 360° gimbaling capability must be provided if communications are desired throughout each Jupiter orbit.

For the close-solar spacecraft, the communications geometry during the inbound heliocentric coast is not critical. Again, the Earth appears to traverse approximately $\pm 20^\circ$ about the Sun during most of the trajectory. As the spacecraft nears Earth and then passes through perihelion, the geometry becomes more complex. Figure 2-43 summarizes the results of a parametric line-of-sight study for a variety of trip times and close solar approaches during a particular launch window. It can be seen that communications with the solar probe during its perihelion can be readily accomplished.

2.2.3.7 Communications Subsystem Description. The Jupiter orbiter/solar probe communications system is diagrammed in Figure 2-75. This system can operate in several modes. Under normal conditions ground commands select the desired mode including switching to redundant units. If communications to Earth are lost, the spacecraft central computer and sequencer will automatically prevent transmissions and wait for commands from the Earth command antenna. If no signal is received after a predetermined length of time, the spacecraft will automatically switch to a redundant command receiver. If communications are restored, the data-handling system will provide the necessary information to permit determination of the nature of the malfunction. Corrective procedures could then be sent from Earth.

During the launch and initial operational phases, spacecraft performance can be transmitted on a real-time basis. Data from the attitude control, power supply, and other systems are required in order to verify that the spacecraft is operating properly and has been oriented correctly. The omnidirectional antennas

1972 MISSION

LAUNCH 244-1380 JULIAN
 ENCOUNTER 244-1980 JULIAN

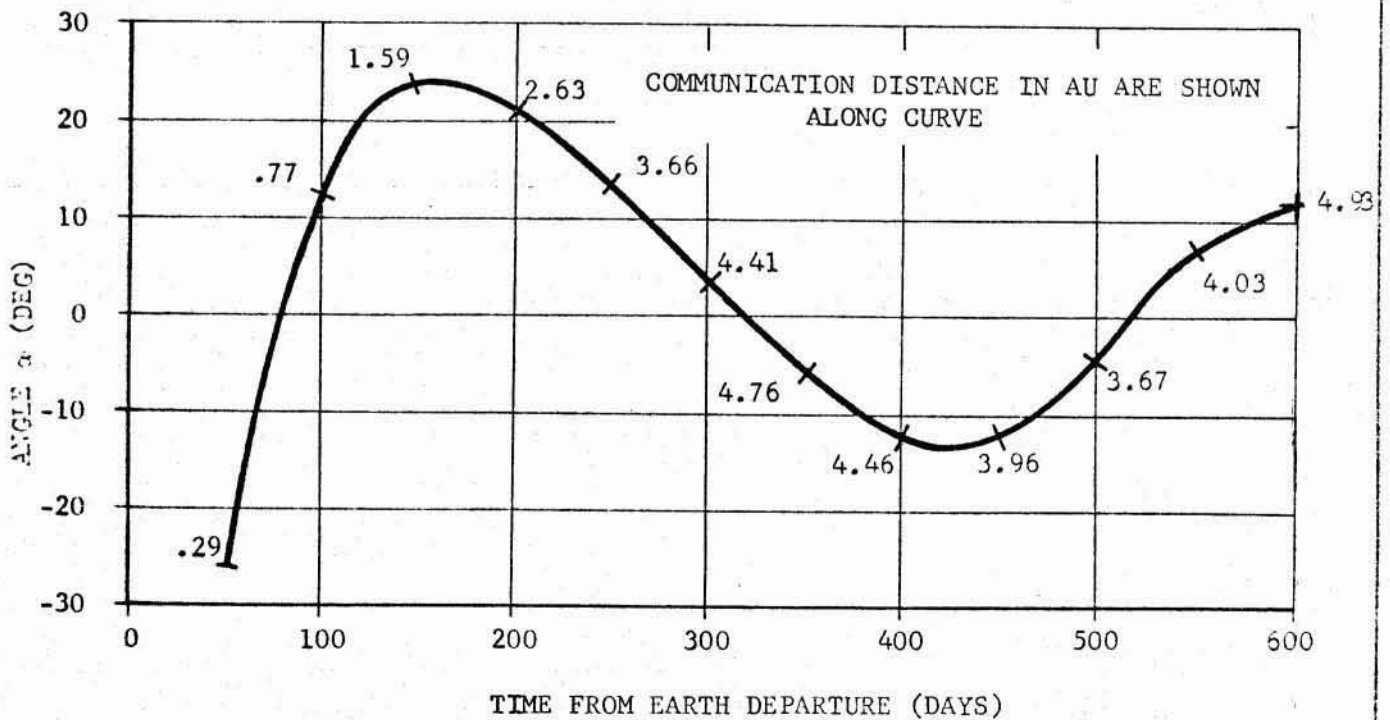
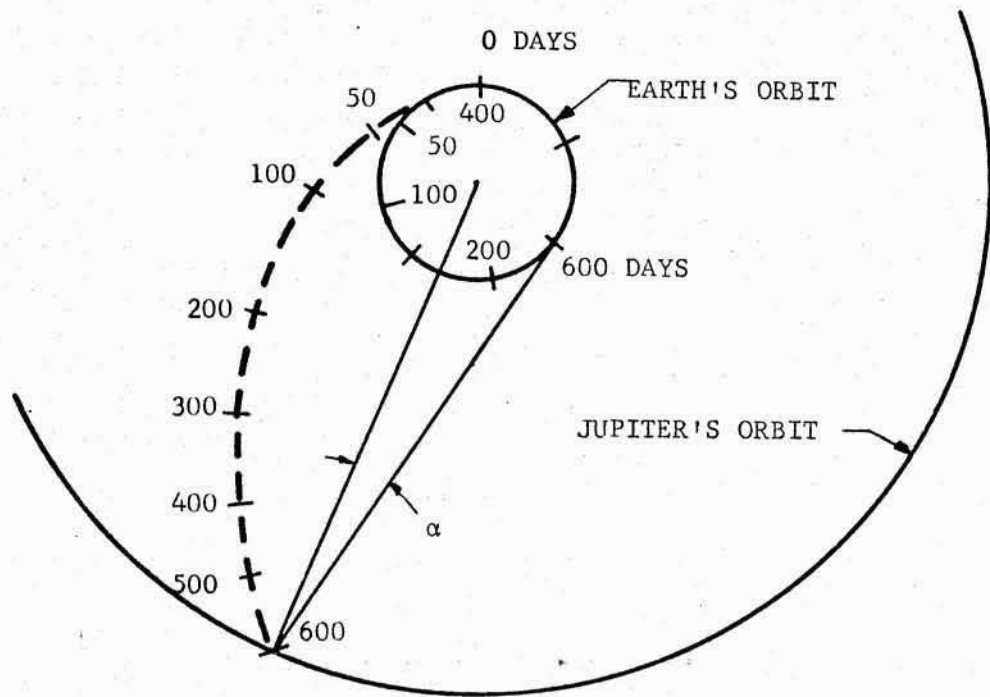


Figure 2-74. TYPICAL COMMUNICATIONS GEOMETRY FOR JUPITER ORBITER VS DAYS FROM EARTH DEPARTURE

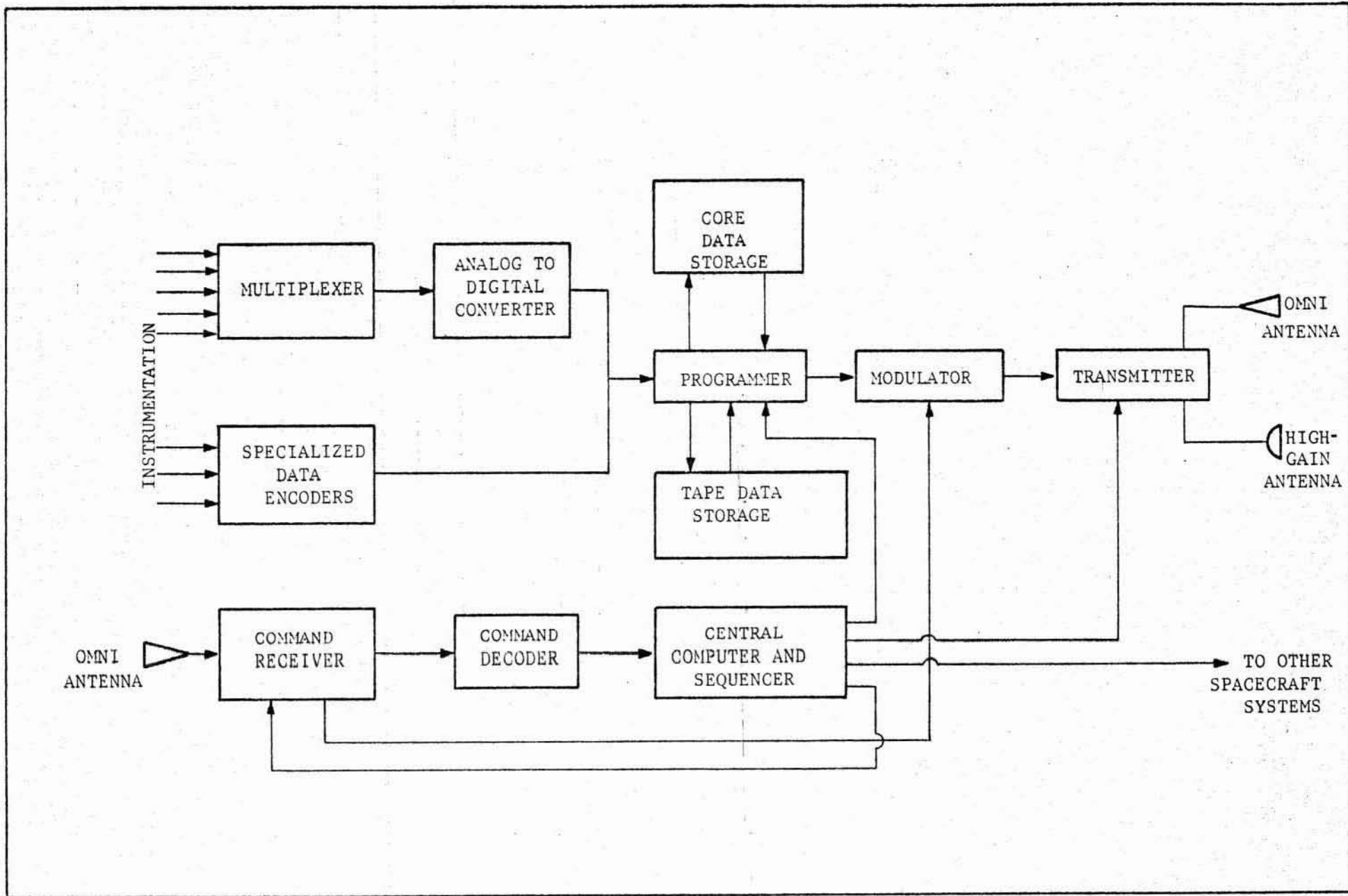


Figure 2-75. COMMUNICATION SYSTEM BLOCK DIAGRAM FOR JUPITER ORBITER/SOLAR PROBE

September 1966

would be used in these phases.

The data-handling subsystem provides multiplexing of the spacecraft and instrumentation system parameters, converts the input data to a digital representation, and formats the specialized digital encoder output with other scientific data acquired directly in digital form or from special purpose encoders included with the instrumentation. A storage capability must be furnished for transmission of data collected at the communications interrogations during the long duration heliocentric coast.

The magnetic tape storage system can record data at very high bit rates permitting storage of TV data. A maximum record-to-playback speed ratio of about 500 to 1 will be possible in the next decade so that for transmission at 100 BPS bit rates, the tape storage system can record at about 50 KBS if necessary. It is postulated that the tape system will operate in a start-stop mode, recording blocks of data of 15,000 to 20,000 bits. A tape length necessary to store about 20 frames of TV pictures at 2.5×10^5 bits/frame appears reasonable at this time.

The mass and power requirements of this system including redundancy are listed in Table 2-9. These must be considered nominal values at this time and may be substantially changed with technology advances in the next decade.

2.2.4 Spacecraft Thermal Control

The requirements of thermal control for this mission vary considerably with the mission phase. The space probe will start from the Earth's surface at 1 AU and travel away from the Sun to ~ 5 AU for the first phase of the mission, consisting of Jupiter flyby and capture of part of the payload into Jupiter orbit. During this phase the system and surface equilibrium temperature will continue to drop and will be the lowest in the vicinity of Jupiter. Hence, internal heat generation with an insulation shield should maintain the internal spacecraft temperature above the lowest tolerance limit of the spacecraft components. In the second phase of the mission the solar probe will swing by the planet Jupiter and will proceed towards the Sun on a close solar approach mission. During this phase the increased solar radiation will cause the surface temperature to rise, and will impose the need of a heat dissipation system to maintain the spacecraft instruments and other sensitive components below the maximum permissible temperature. Figure 2-76 shows the variation of a spacecraft surface equilibrium temperature as a function of its distance from the Sun. The extreme temperature excursion can be noted as well as the very unacceptable temperatures at close solar distances. The following paragraphs discuss various phases of this mission and the associated thermal control systems selected for use on the Jupiter orbiter/solar probe.

2.2.4.1 Deep Space Control. For operations in the far regions of the solar system, spacecraft systems and propellants must be kept heated. Subsection 2.2.6.1 discusses thermal control and heating of liquid propellants during the long, cold heliocentric coast phases of this mission, and subsection 2.2.5.3 presents concepts of waste heat utilization from RTG power supply units.

Without a detailed spacecraft design, the thermal control requirements of each system cannot be analyzed in great depth. Such a study must account

Table 2-9.

COMMUNICATION SYSTEM CHARACTERISTICS FOR JUPITER ORBITER/SOLAR PROBE

COMPONENT	JUPITER ORBITER		SOLAR PROBE	
	INPUT POWER	APPROX MASS	INPUT POWER	APPROX MASS
High-gain antenna	--	7.0 kg	--	4.5 kg
Omni antennas	--	1.0	--	1.0
Transmitter	93 watts	7.0	93 watts	7.0
Modulator	4	2.5	4	2.5
Programmer	8	3.5	8	3.5
Data Storage	45	25.5	45	25.5
CC and S	10	7.0	10	7.0
Command receiver and decoder	16	8.5	16	8.5
Analog to digital converter	8	9.0	8	9.0
Multiplexer and encoder	16	18.0	16	18.0
Chassis and cables	--	15.0	--	15.0
TOTALS	200 watts	104.0 kg	200 watts	101.5 kg

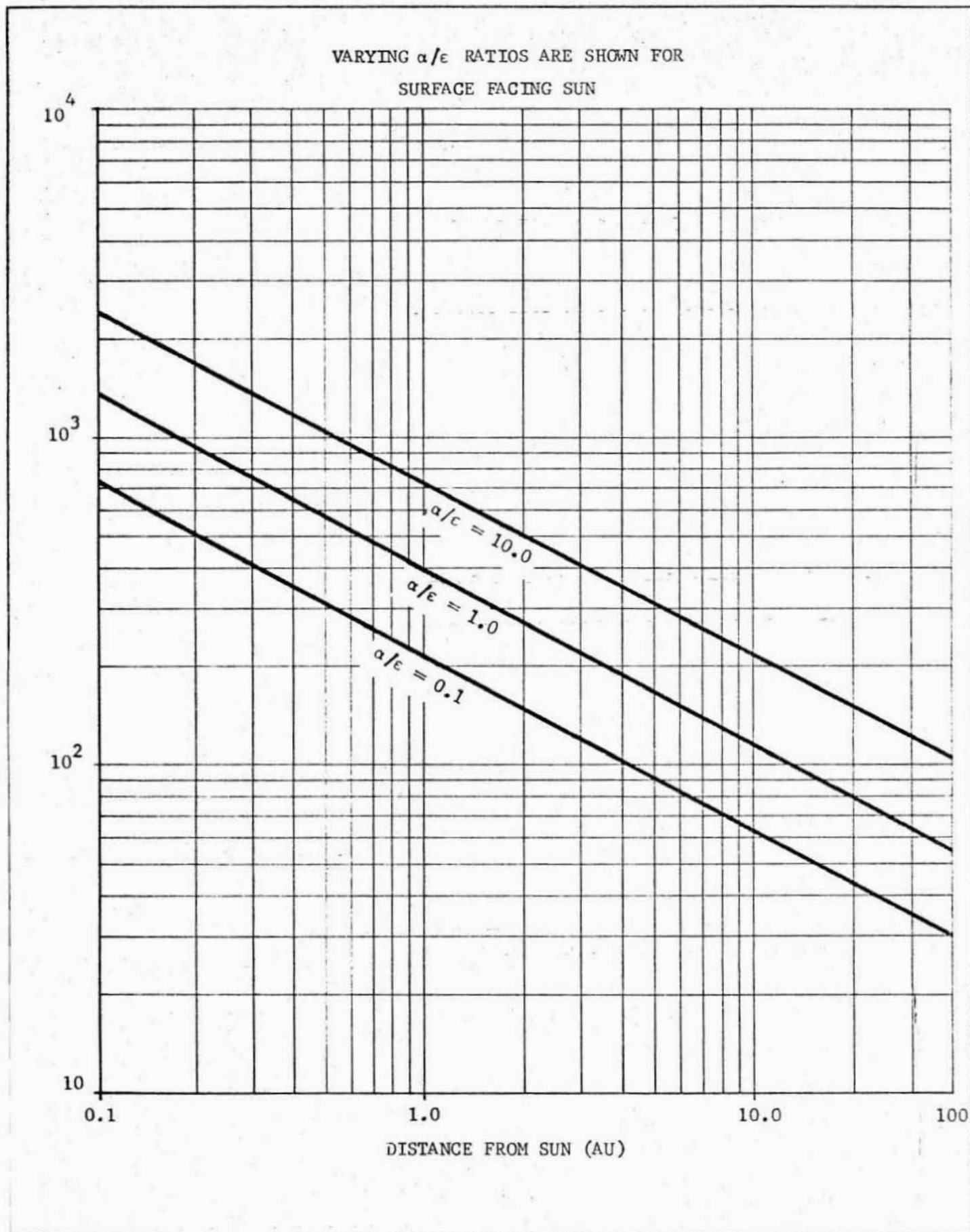


Figure 2-76. TEMPERATURE vs. DISTANCE FROM SUN FOR AN INSULATED FLAT PLATE FACING SUN

for the heat input and loss from internal generation, solar radiation, radiation to space, planet albedo, and RTG-unit radiation. Data regarding materials and heat transfer paths are required to accurately predict the temperature profile of any system or component. This is not possible at this stage of the development of the Jupiter orbiter/solar probe configurations. Based on past experience, it is anticipated that proper thermal control can be maintained in deep space using electrical heaters for critical systems and super insulation. Considerable excess heat and power is available from the RTG units as discussed in subsection 2.2.5.3. To indicate that enough heat is available, a preliminary energy balance was completed for a typical spacecraft configuration. Assuming a spacecraft radiating surface area of 50 m^2 , the total heat make-up required is as shown in Figure 2-77. This data corresponds to a range of superinsulation thickness up to about 10 cm around the spacecraft. Based on the power profiles of subsection 2.2.5.1, the excess energy available for thermal control is noted also on Figure 2-77. From this data it can be seen that insulation is usually required for the Jupiter orbiter/solar probe.

2.2.4.2 Close-Solar Protection. A number of concepts can be considered for dissipating heat at close solar distances. An ablative shield pointed at the Sun, a circulating fluid conducting heat from the hot to cold surfaces, and passive shadow shield are examples. The use of an active control system may be unreliable or may impose a prohibitive weight penalty (in the form of expendable materials) on the payload. A passive thermal control system has significant advantages. First, because it is a passive system, its inherent reliability is high. This is especially important when it is realized that 1100 to 1200 days elapse between launch and close solar encounter. Dormancy and activation of an active thermal control system for this trip lifetime is a challenging design problem which may not be possible with the state-of-the-art to be expected in the next decade.

A simple shadow-shield concept which may be considered is a series of flat plates separated by a low-conductivity structure. Figures 2-78 through 2-80 show the features of such a shield for various materials, solar distances, and number of plates. It is evident that multiple-shield thermal control is not extremely sensitive to α/ϵ variation. This is advantageous since spectrally selective coatings degrade very rapidly when exposed to the UV radiation and particle radiation of the solar environments. However, the surface temperatures at close-solar approaches are still very high. This can be improved by the utilization of a conical front shield. Analysis has shown that this configuration offers greater potential for thermal control. This is because the conical inclined surface will reflect more energy and the larger surface area for a given base diameter is capable of absorbing more heat for a unit volume of space.

Assuming the shield reached equilibrium temperatures, Figure 2-81 shows the shield temperature for different shape configurations and distances from the Sun when the absorptivity and emissivity are equal. In the actual mission being flown, the spacecraft passes by the Sun at a very high velocity and it is not certain that it will reach the calculated equilibrium temperature. The data shown are conservative and will be used in this study. This figure indicates the advantages of using a conical configuration. The temperatures at $l/d=0$ correspond to flat plate values. At an l/d of 4 or more it can be seen that the conical shield equilibrium temperatures are about 60 to 70 percent of these flat plate

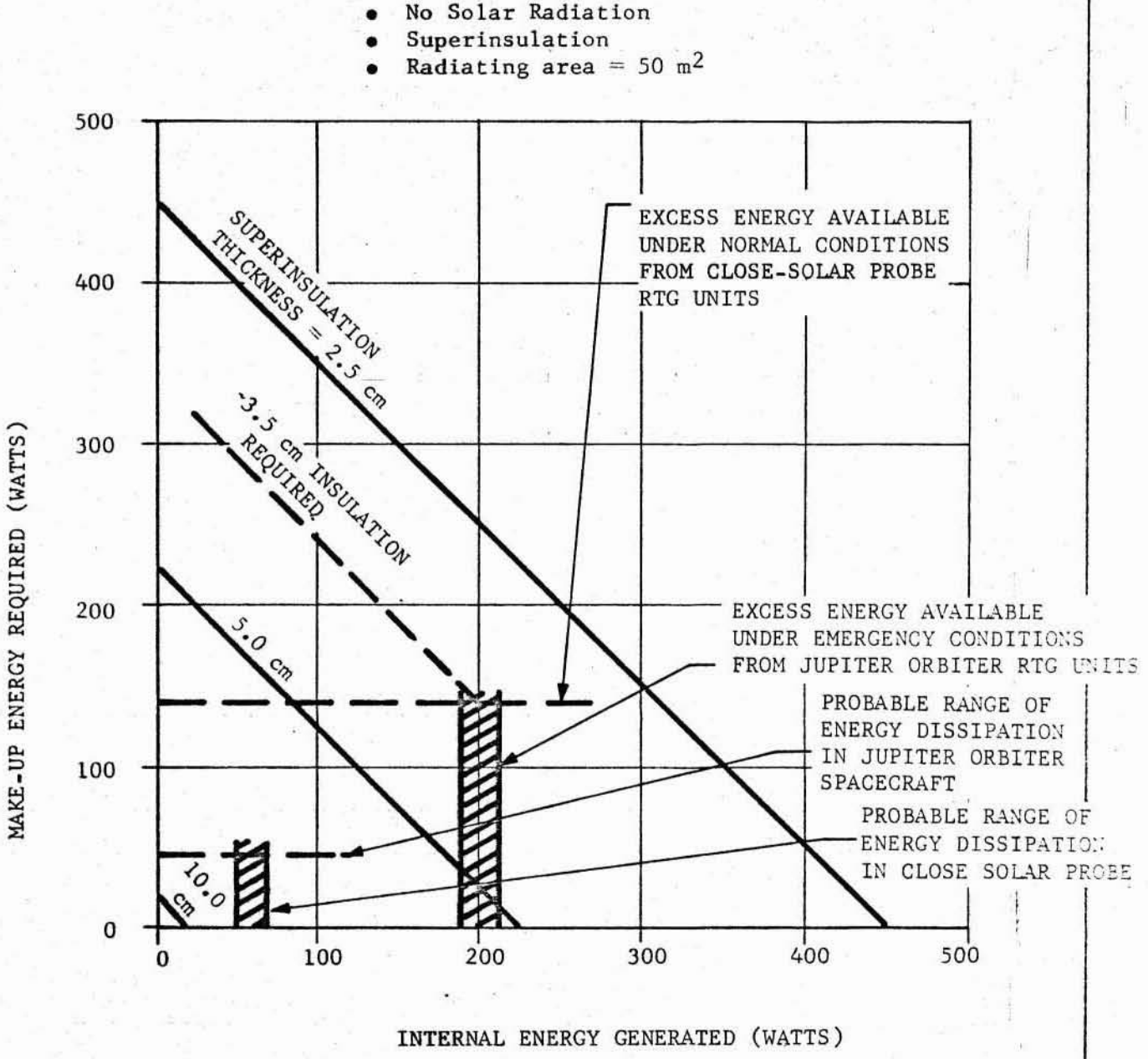


Figure 2-77. SPACECRAFT HEAT ENERGY BALANCE

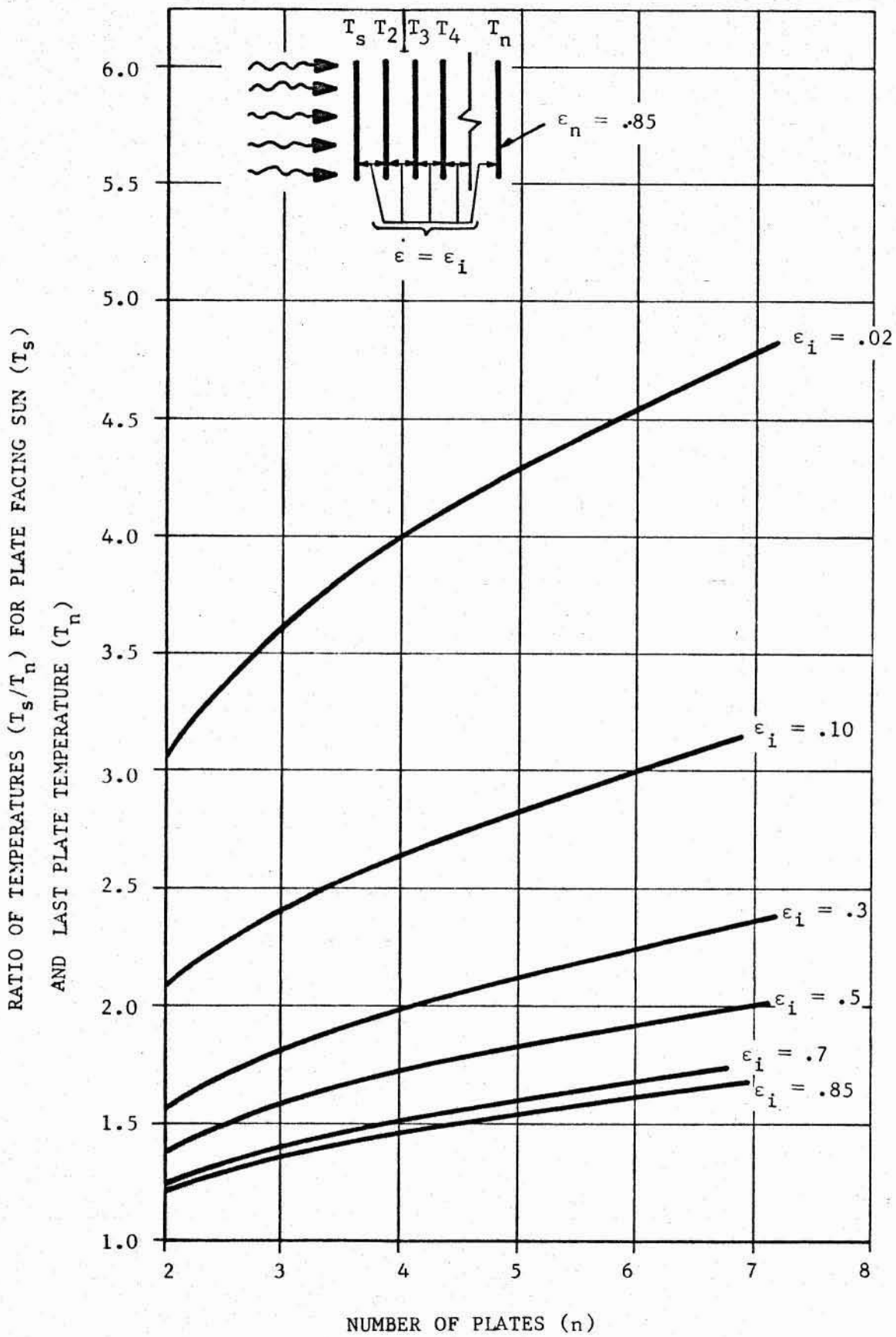


Figure 2-78. VARIATION OF T_s/T_n WITH NUMBER OF THERMAL SHIELDS

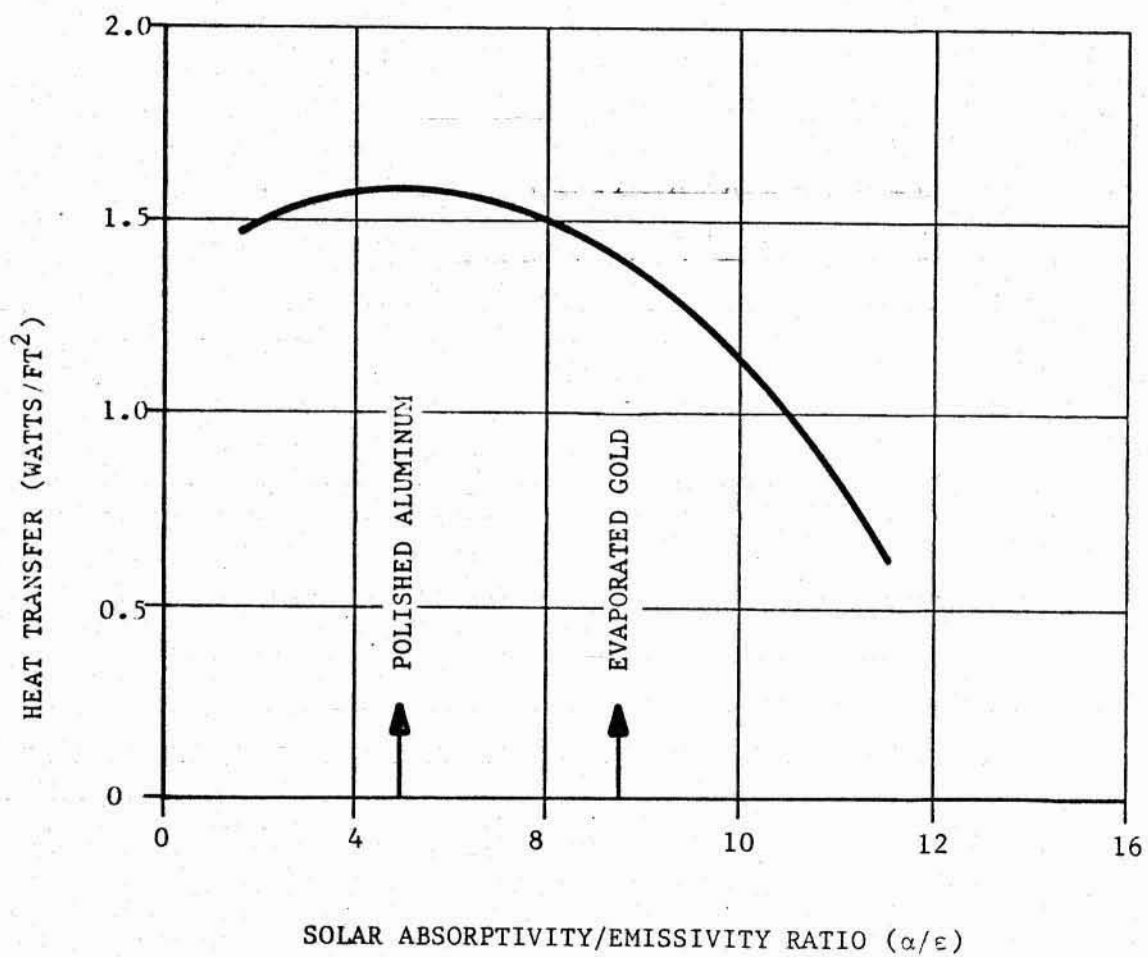


Figure 2-79. HEAT TRANSFER BETWEEN TWO FLAT PLATES FOR VARIOUS α/ϵ RATIOS

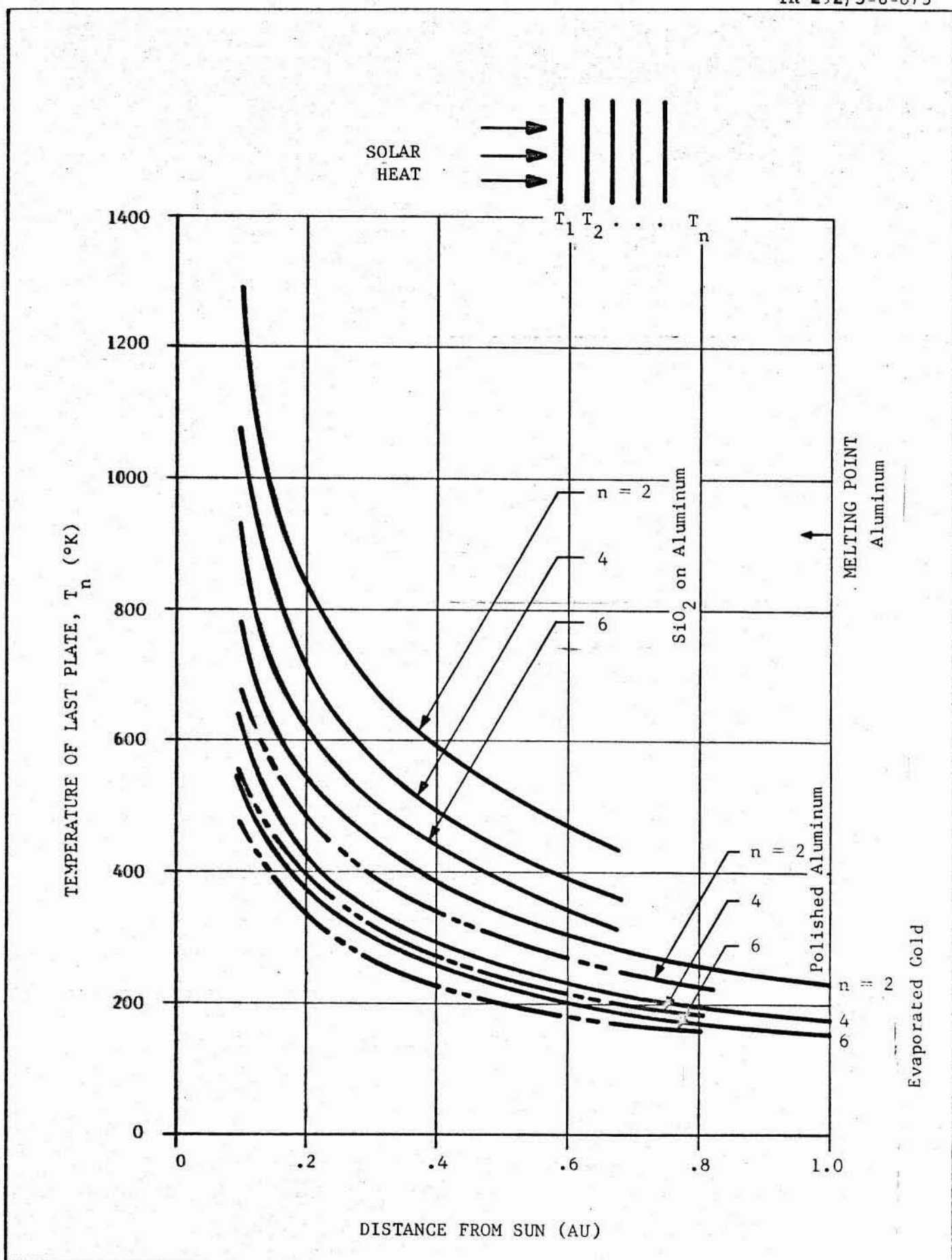


Figure 2-80. TEMPERATURE OF LAST PLATE IN FLAT PLATE SHADOW SHIELD VS DISTANCE FROM THE SUN FOR VARIOUS MATERIALS

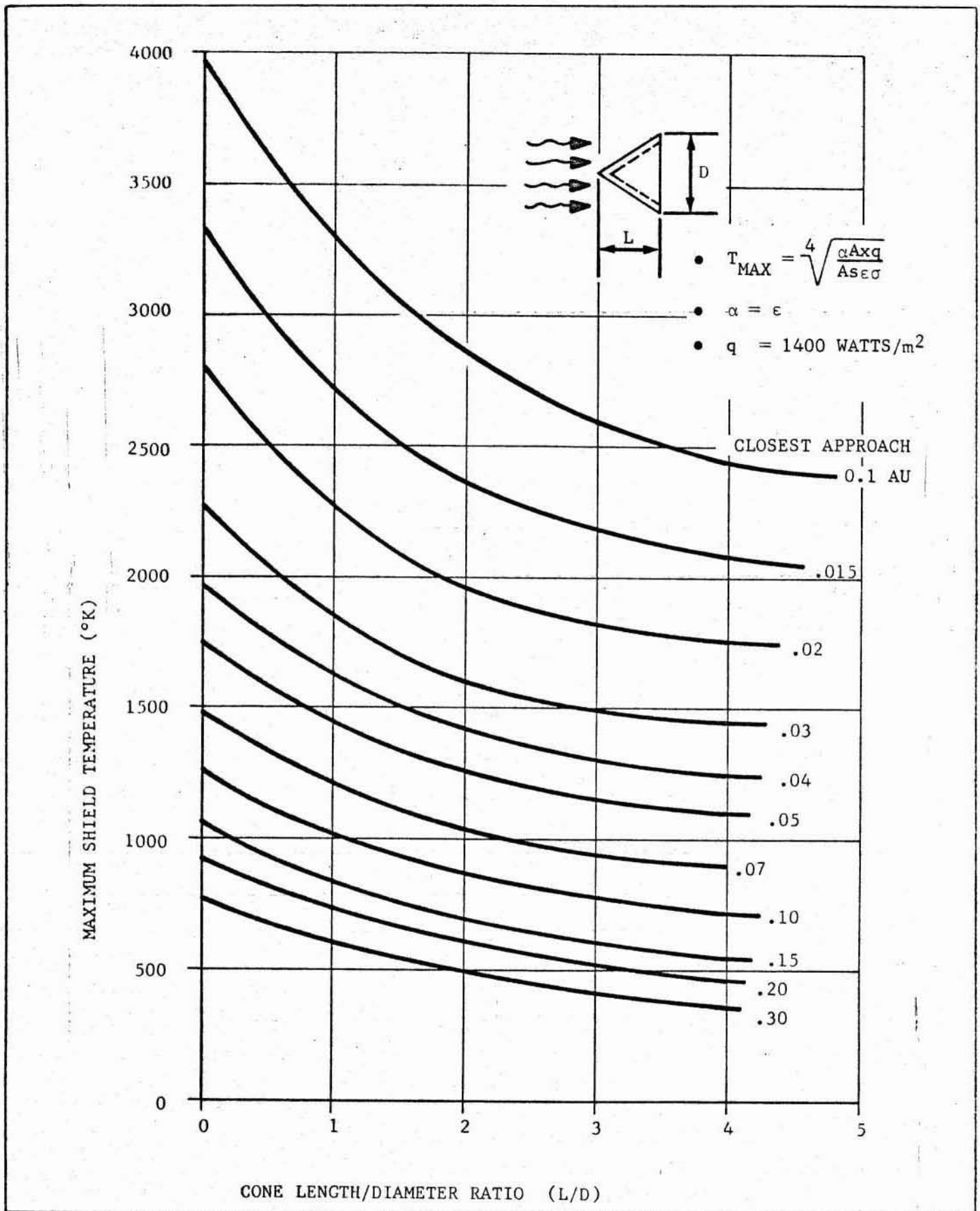


Figure 2-81. CONICAL SHADOW SHIELD TEMPERATURE VS LENGTH TO DIAMETER RATIOS FOR VARYING SOLAR DISTANCES

values. It should be noted that a further reduction in temperature over those shown in this figure is theoretically possible by the utilization of a surface coating on the shield with an α/ϵ ratio less than one. However, this effect is minor compared with the improvements due to increased shield area alone. For example, for the lowest expected α/ϵ of about .2, corresponding to white paint, the maximum temperature for the shields will be reduced to about 2/3 the values shown in Figure 2-81. However, under the effects of the high heat flux at the close distances to the Sun being considered here, the white paint would not maintain its characteristics for any period of time. Other surface coatings are available which will provide permanent α/ϵ ratios close to one and these can be considered for use on the probe.

The temperatures of Figure 2-81 are still high for very close solar approaches implying there is a requirement for a secondary shield. Figure 2-82 shows the shadow geometry and the placement of a secondary shield associated with the spacecraft. The temperature of this shield is a function of its distance from the primary shield and its surface emissivity characteristics. Figure 2-83 presents the secondary shield equilibrium temperatures for a given primary shield configuration and $\alpha/\epsilon=.2$. These curves also show the effect of the solar closest approach achieved. It can be seen that acceptable secondary shield temperatures can be achieved if the probe is kept as small as possible and the separation between shields is maximized.

To further reduce the heat transfer to the spacecraft, the secondary shield can include superinsulation. It offers reduced mass and lower shroud volume over metallic radiation shielding. The variation of the superinsulation shield heat transfer is plotted in Figure 2-84 as a function of α/ϵ at 0.3 AU. The solid lines assume no edge radiation while the dashed lines take edge radiation into account. It is evident that relatively thin insulation is required to thermally isolate the spacecraft at 0.3 AU, and that over a wide range of α/ϵ the front surface optical properties are less important than the edge radiation effects.

The influence of spacecraft angular displacement around the yaw or pitch axis for an open compartment design is shown on Figure 2-85. Maximum vehicle displacement in the yaw or pitch axis was assumed to be 5° and 15° . The expected increase in temperature is as shown. It can be seen that if the vehicle is stabilized to less than $\pm 5^\circ$, the temperatures are acceptable.

The temperature limits indicate that passive thermal control of a solar probe can be provided within the state-of-the-art in terms of both design techniques and materials. A titanium plate meets the temperature requirements for the outer shield surface and the secondary shield concept includes multifoil insulation on aluminum plates at an appropriate distance between the outer shield and payload.

2.2.4.3 Closest Solar Approach. Based on the properties of the thermal control shield materials and configurations, the limits of the solar approach can be tabulated. Figure 2-86 summarizes the data showing the characteristics of various shadow shields. This curve also indicates the capabilities of solar-cell panels for reference. From this data, Table 2-10 was prepared to define the closest solar approach possible with different shadow shields and solar-cell-panel designs.

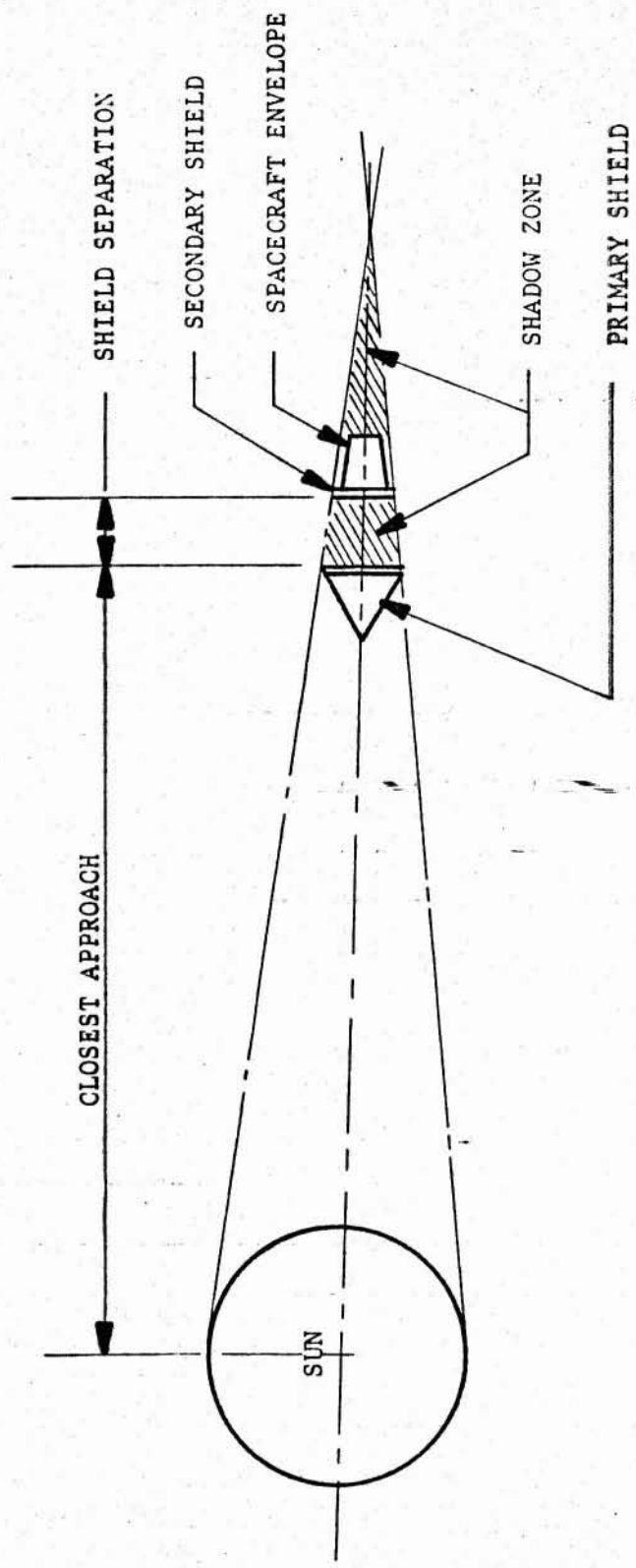


Figure 2-82. SHADOW SHIELD GEOMETRY
2-126

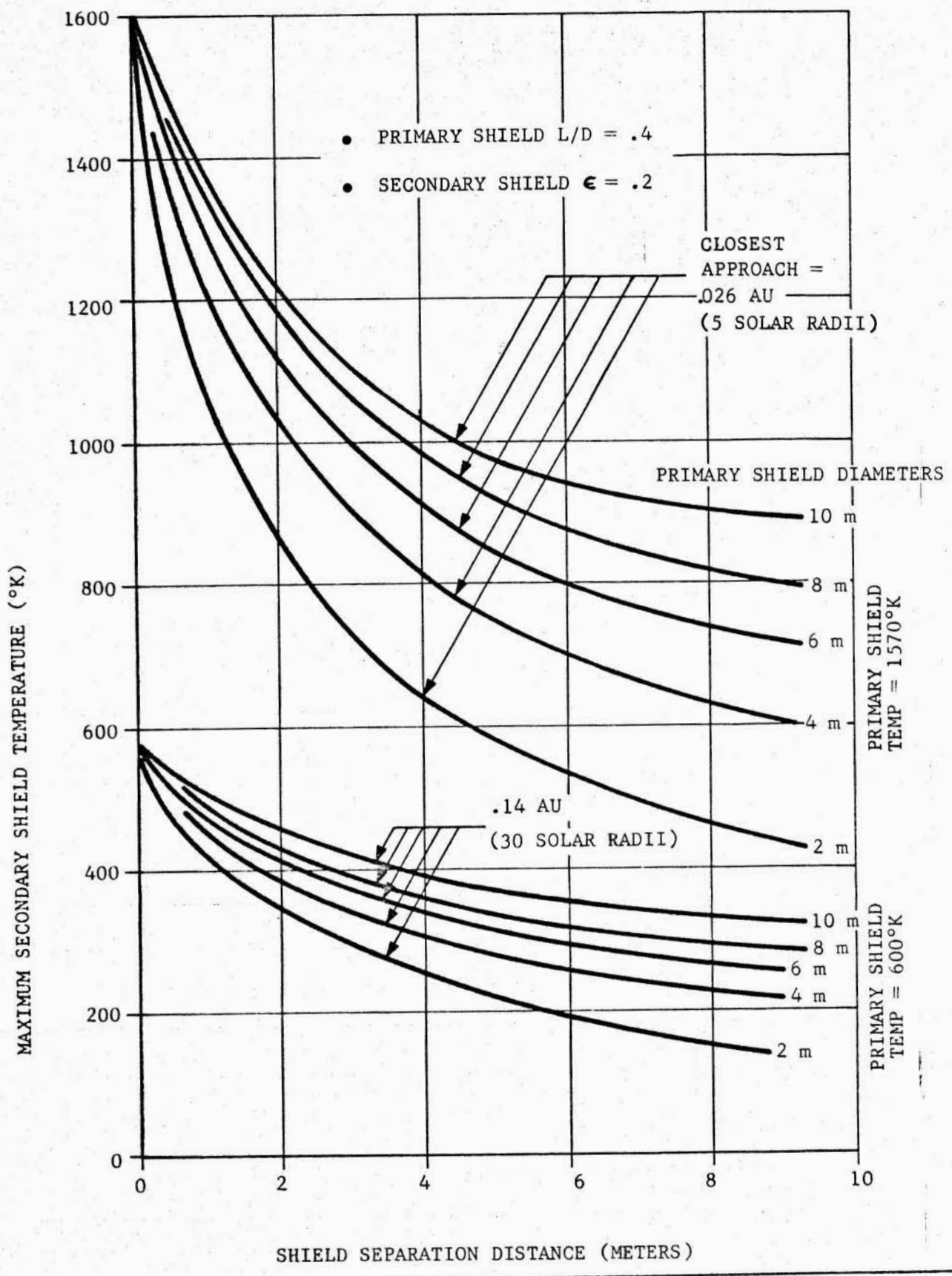


Figure 2- 83. SECONDARY SHIELD TEMPERATURE VS SEPARATION DISTANCE IN METERS

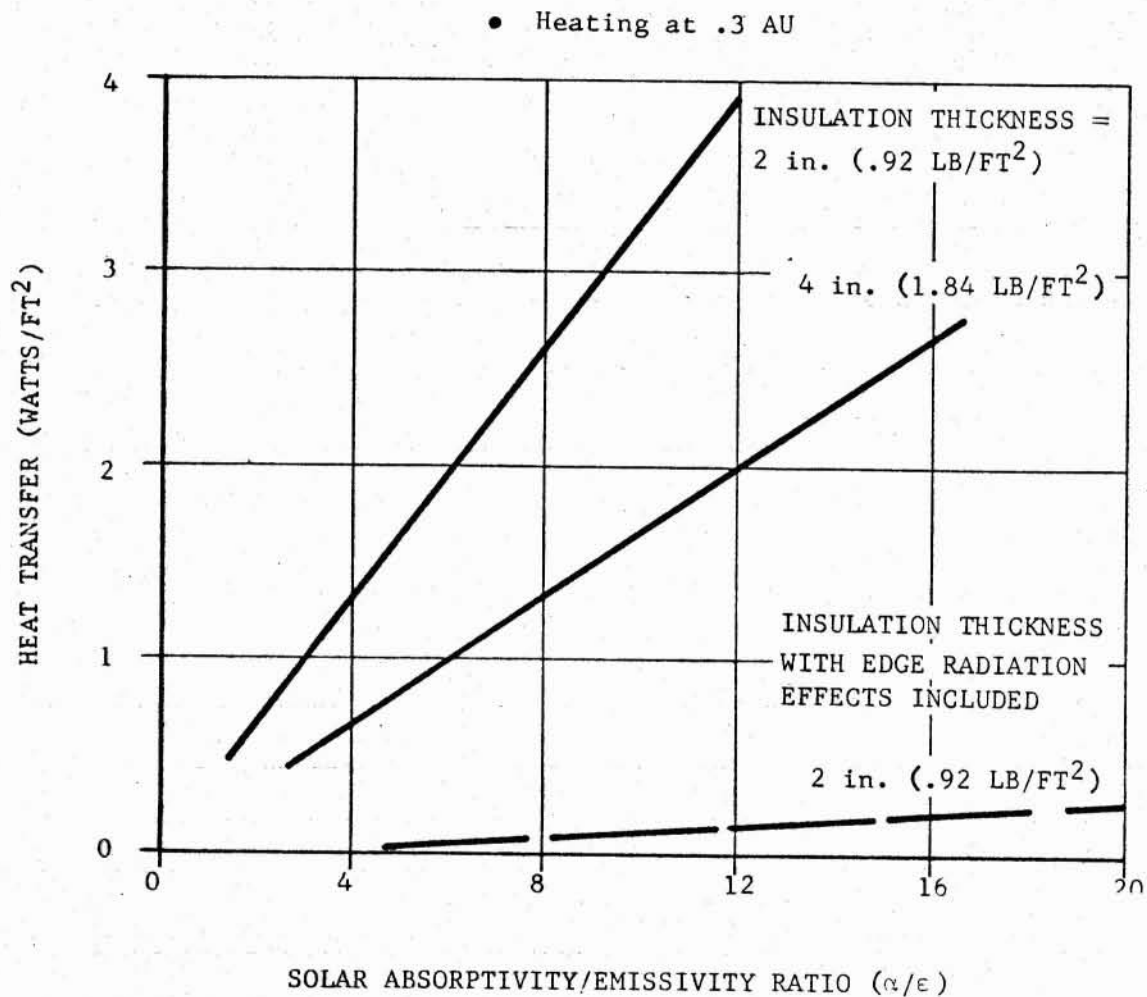


Figure 2-84. HEAT TRANSFER FOR SECONDARY SHIELD WITH SUPERINSULATION FOR VARIOUS α/ϵ RATIOS

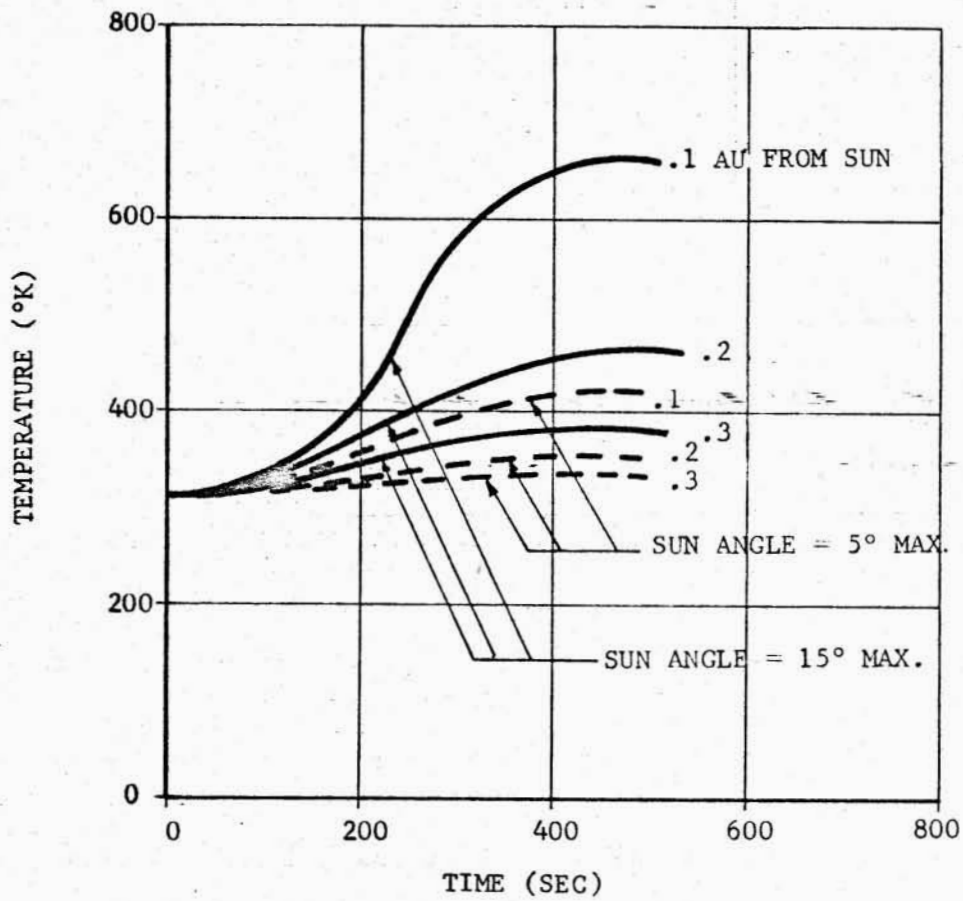


Figure 2-85. EFFECT OF SPACECRAFT-SUN MISALIGNMENT ANGLE UPON SHIELD TEMPERATURES FOR VARYING DISTANCES FROM THE SUN

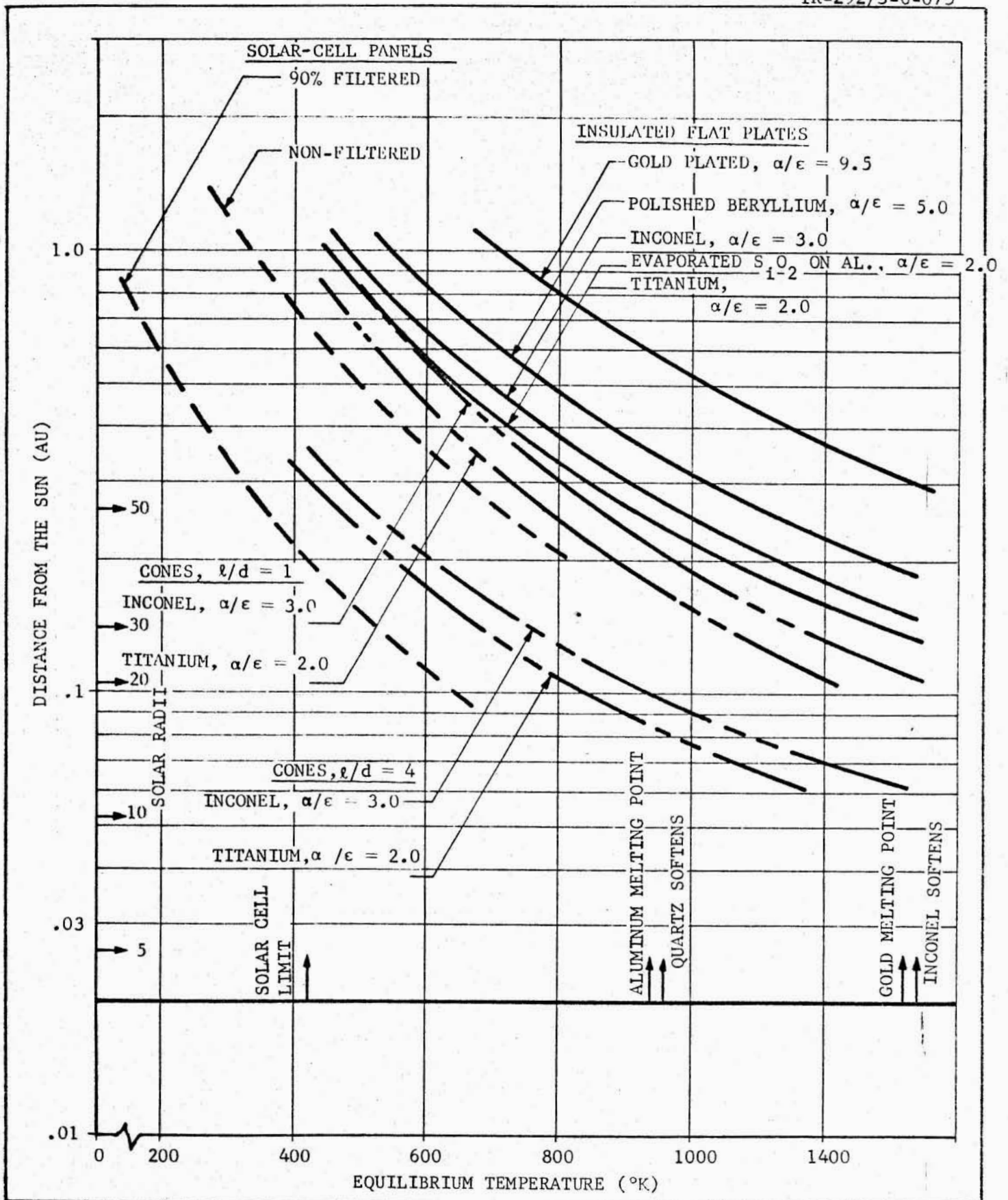


Figure 2-86. MATERIAL TEMPERATURE LIMITATIONS AS A FUNCTION OF VARIOUS SHAPES AND PROXIMITY TO THE SUN

Table 2-10.
SOLAR DISTANCE LIMITATIONS
SHADOW SHIELD MATERIAL LIMITATIONS

Shadow Shield		α / ϵ Ratio	Limiting Parameter	Closest Solar Approach
Material	Configuration			
Gold plated	Flat Plate	9.5	Gold melting point	.3 AU
Beryllium	" "	5.0	Softening & loss of strength	.2
Inconel	" "	3.0	" "	.15
Aluminum	" "	2.0	" "	.33
Titanium	" "	2.0	" "	.1
Inconel	Cone, $l/d = 1$	3.0	" "	.11
Titanium	" , $l/d = 1$	2.0	" "	.055
Inconel	Cone, $l/d = 4$	3.0	" "	.06
Titanium	" , $l/d = 4$	2.0	" "	.04

SOLAR CELL LIMITATIONS

System	Limitations	Closest Solar Approach
Solar cells	Overheating and power drop off	.68 AU
.90 filtered Solar Cells	" " " " "	.2 AU
.99 filtered Solar Cells	" " " " "	.032 AU

For solar cells, the temperature rise with distance to the Sun precludes their use unless filtering techniques are used. Figure 2-87 shows the optimum continuous filtering required to maintain a constant design temperature. If the solar cells are permitted to cycle up to their maximum operating temperature, a stepped filtering scheme can be envisioned as noted on Figure 2-87. It can be seen that with extensive filtering, solar cells can be considered for close solar distances. However, a number of factors pose doubts as to the practicality of this concept.

- The filtering medium must be capable of withstanding a very high surface temperature at close solar distances without destruction or alteration of its filtering properties. Such a material is not common and some analysis and development is necessary before a design could be evolved.
- The use of a continuous or stepped filtering technique requires a mechanical system to operate as a function of time as the spacecraft approaches the Sun. This introduces a reliability parameter into the power supply system which is not normally there.
- Because the solar probe in this mission is transported to 6.5 AU for the Jupiter gravitational swingby, radioisotopic units are installed for power during the 1100- to 1200-day heliocentric transfer. Since these units are already onboard, it is not clear why these should not be used close to the Sun also. Switching to another power system close to the Sun raises a question of reliability, especially since the second system must be exposed to a space environment for up to 3 years prior to its use.

Based on the data in Table 2-10, solar approaches of less than 0.1 AU are possible if conical shadow shields of Inconel or titanium are used.

2.2.5 Power Supply System

Because of the extremely long mission durations in this study, only nuclear power sources are considered for the Jupiter orbiter/solar probe. RTG units offer the best compromise of availability, cost, shielding, life time, and power density. The units currently under development or study by the AEC were considered in this analysis, which include both thermoelectric and thermionic systems.

Thermoelectric systems use thermocouples to convert heat generated in the fuel source to electricity. Waste heat is removed by active or passive means, depending on the power level of the unit. Cooling fins can be used to radiate excess heat to space up to 250 watts electrical power. For larger units, a circulating fluid and radiator are used. A combination active and passive cooling system may also be considered. Figure 2-88 schematically represents the basic thermoelectric unit concepts.

Thermionic systems convert the energy liberated by the fuel elements to electricity through the use of thermionic diodes. These units operate at higher temperatures, have about double the thermoelectric units efficiencies, and are thus more compact for a given power level. The current state-of-the-

● SOLAR CELL DESIGN CONDITIONS = 325°K @ .45 VOLTS

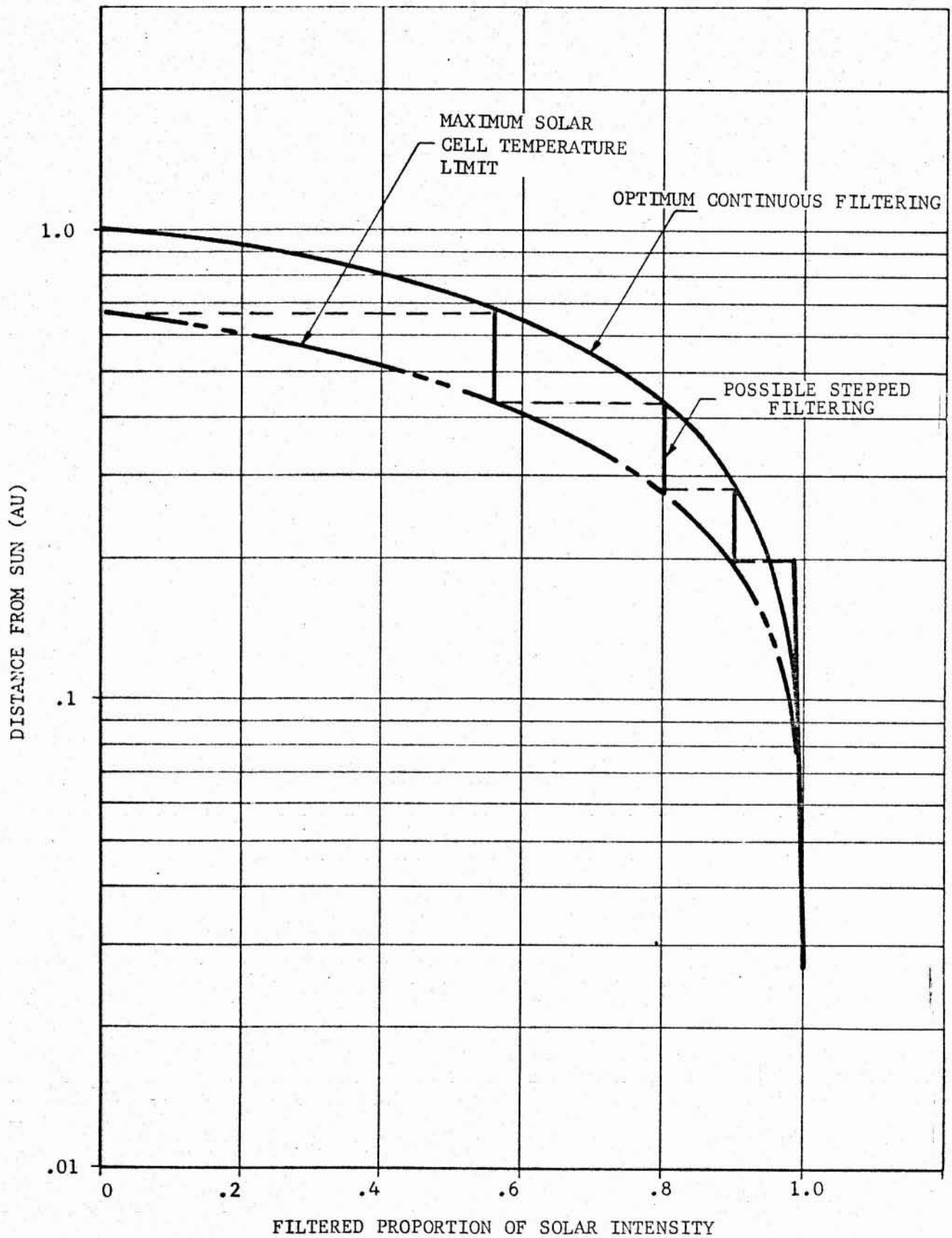
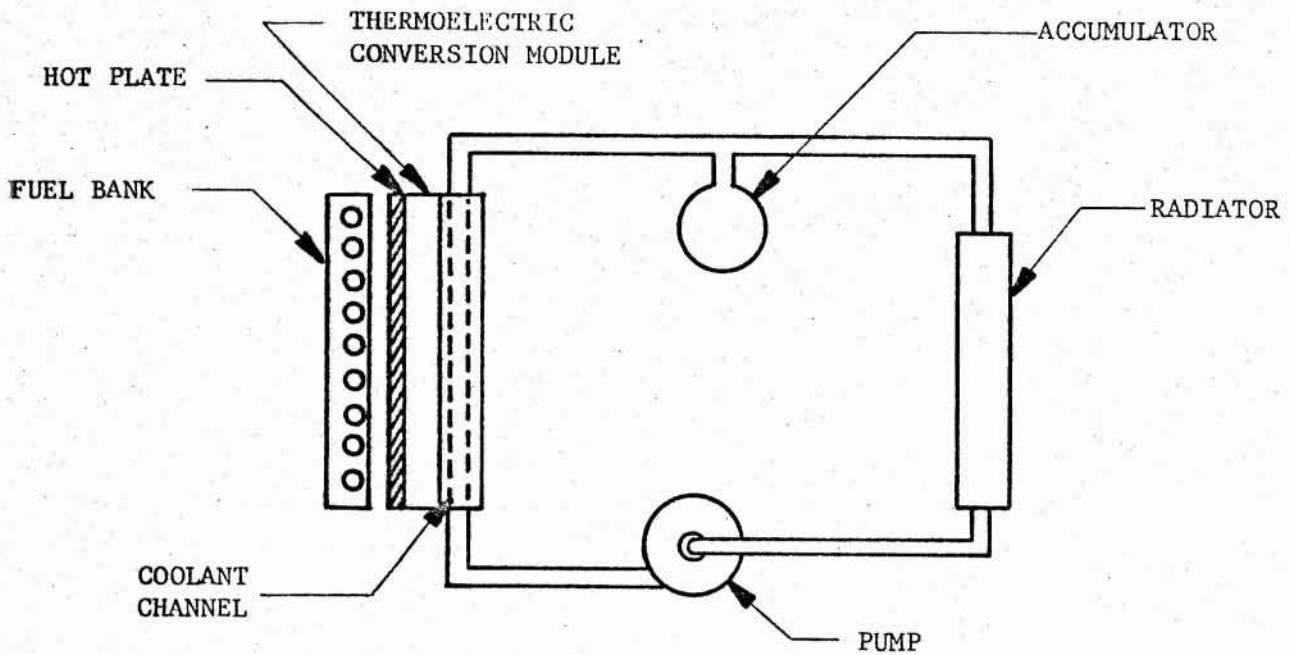
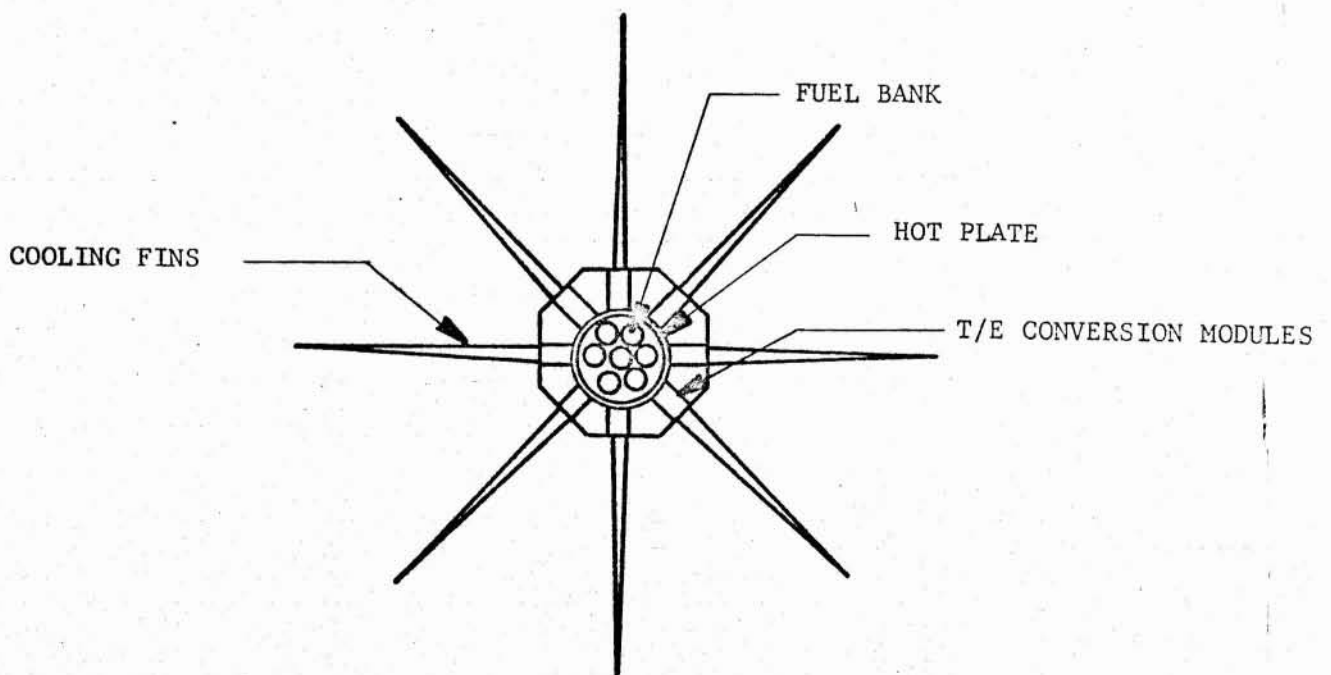


FIGURE 2- 87. DISTANCE FROM SUN VS SOLAR INTENSITY FILTERING AND RESULTANT EFFECT UPON SOLAR CELL OPERATION



a. ACTIVE THERMAL CONTROL



b. PASSIVE THERMAL CONTROL

Figure 2- 88. RTG THERMOELECTRIC SYSTEMS

September 1966

art in thermionic generator systems is considerably behind that of the thermoelectric. Prototype hardware for a 100-watt system may be available from the AEC by 1970. Unless a specific program is initiated by the AEC at an early date, higher power thermionic production units cannot be considered for use on the Jupiter orbiter/solar probe.

The thermoelectric units of appropriate size now under consideration are summarized in Table 2-11. Because of the trip-life-time requirements, only the Pu-238-fueled units can be considered. It can be seen that both actively and passively cooled systems may be available. The selection of the unit to be used on the Jupiter orbiter/solar probe depends on the spacecraft power requirements, utilization of waste heat for thermal control, total system mass and reliability, and power subsystem handling. These factors will each be considered below.

2.2.5.1 Spacecraft Power Requirements. The mission power requirements shown in Table 2-12 were developed for this analysis. This data indicates a number of features that must be considered in the selection of the power systems, including:

- The Jupiter orbiter spacecraft requires a minimum power level of 553 watts during normal heliocentric transfer. This is more than adequate for the execution of midcourse and braking maneuvers.
- The Jupiter orbiter spacecraft requires an additional 47 watts of power while in Jupiter orbit if all experiments are operated simultaneously and an additional 269 watts of power if infrared and radar imagers are used at Jupiter moon flybys.
- The solar probe requires a minimum of 529 watts of power to cover all phases of its mission.

Based on these observations, it can be concluded that the Jupiter orbiter could utilize two of the 500-watt actively cooled Pu-238 units or three 250-watt passively cooled units. During heliocentric coast, almost half the total power generated would then be available for thermal control. Also, the installation of multiple units offers a system redundancy so that in the event of one unit failing, the mission can be continued by proper sequencing of loads. Figure 2-89 summarizes the Jupiter orbiter power profiles including emergency operations with one RTG unit not providing any power.

The use of three 250-watt passively-cooled Pu-238 units better matches the normal power requirements if the Jupiter spacecraft experiments are properly sequenced during a Jupiter moon flyby to eliminate the high peak during that mission phase. Emergency operations due to one RTG-unit failure would be as shown in Figure 2-89.

The solar probe requires a minimum of 529 watts power to cover all phases of its mission. This indicates that one actively cooled RTG unit or two passively cooled units closely match the power requirements. The use of two passive units can be seriously considered based on the ideas previously discussed for the Jupiter orbiter. Two 250-watt units offer the following significant advantages:

Table 2-11.

THERMOELECTRIC POWER SYSTEMS

Fuel	Power (electric)	Design Life	Active Cooling		Passive Cooling Fin Area	Approximate Dimensions	Approx. Mass	Remarks
			Coolant	Radiator Area				
Po-210	500 W. @ end of design life	104 days	NaK and Water	8.9 m ²	—	.3 x .75 x .9 m	130 kg	Design life ~ 100 days.
Po-210	400 W. @ end of design life	104 days	NaK and Water	7.1 m ²	—	.2 x .23 x .86 m	110 kg	Compact, high temperature design. To be used on MOL for 90-day missions.
Pu-238	500 W.*	Years	NaK and Water	8.9 m ²	—	.25 x .75 x .9 m	156 kg	
Pu-238	250 W.*	Years	—	—	6 fins @ .17 m ² each	.2 m hexagon x .64-m long .27-m Fins (6 places)	76 kg	Highest power passive cooling system possible

* Due to the 90-year half life of Pu-238, power levels of these units will be 97.5% of the fueled power level at the end of 3.5 years.

Table 2-12. MISSION POWER REQUIREMENTS
(NORMAL OPERATION)

	Jupiter Probe	Solar Probe
<u>Heliocentric Coast:</u>		
Experiments	78 watts	54 watts
Guidance and ACS**	50	40
Thermal Control	25	20
	<u>153</u> watts cont.	<u>114</u> watts continuous
Communication (including omni-directional)	400	400
	<u>553</u> watts peak	<u>514</u> watts peak
<u>Jupiter Moon Flyby:</u>		
Experiments	547 watts	
Guidance and ACS**	50	
Thermal Control	25	
	<u>622</u>	
Communication	200	
	<u>822</u> watts peak	
<u>Propulsion Maneuvers:</u> (Midcourse corrections or braking into capture orbit)		
Experiments	78 watts	
Guidance and ACS**	50	
Thermal Control	25	
Propulsion	75	
	<u>228</u> watts @ each maneuver	
<u>Jovian Capture Orbit:</u>		
Experiments	325 watts*	
Guidance and ACS**	50	
Thermal Control	25	
	<u>400</u> watts cont.	
Communications	200	
	<u>600</u> watts peak	
<u>Close Solar Approach:</u>		
Experiments		54 watts
Guidance and ACS**		50
Thermal Control		25
		<u>129</u> watts continuous
Communication (including omni-directional)		400
		<u>529</u> watts peak

* Under emergency conditions, to compensate for a partial power loss, this can be reduced to 115 watts without seriously compromising mission objectives. See Table 2-4.

** Attitude and Control System

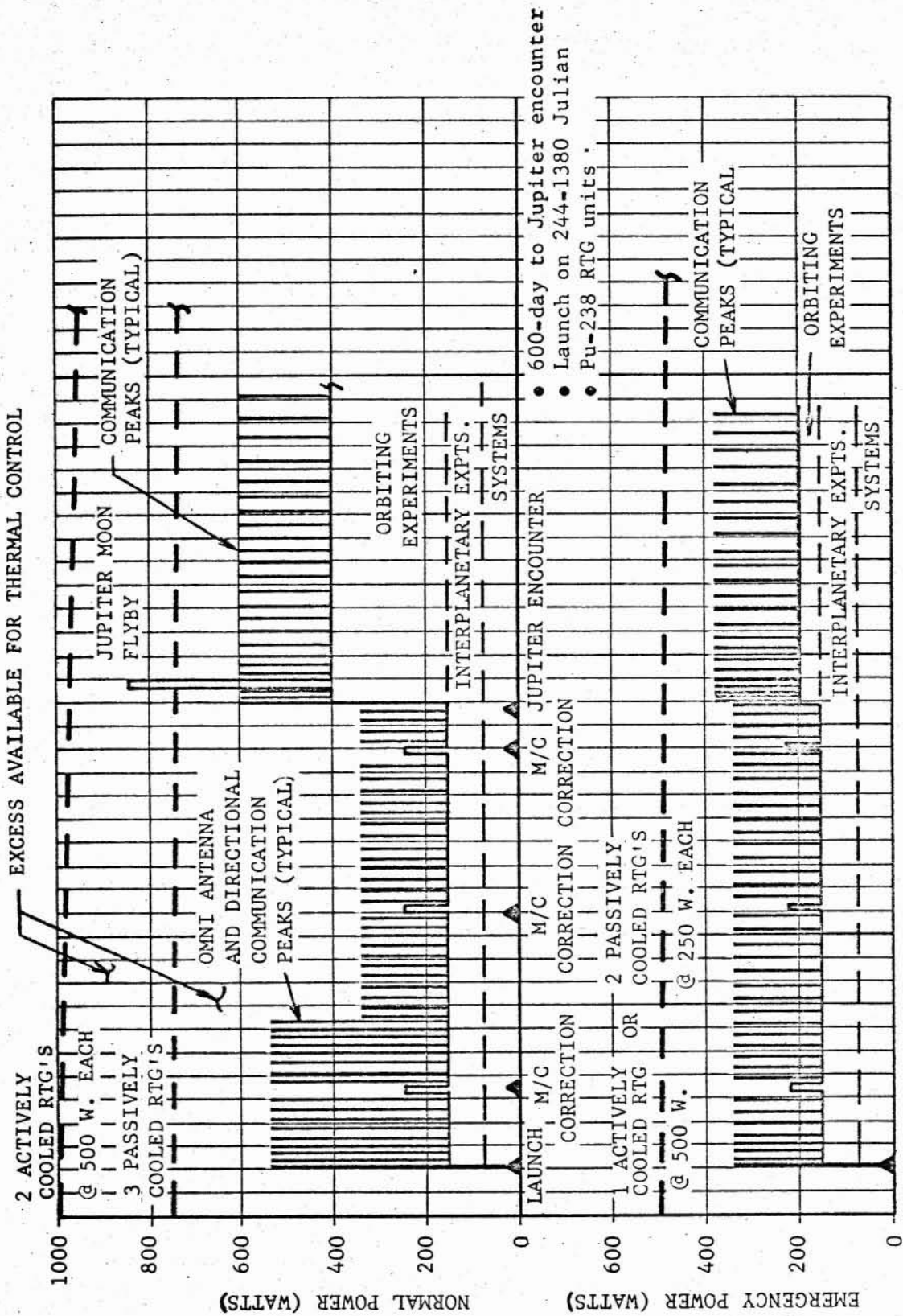


Figure 2-89. JUPITER TYPICAL MISSION POWER PROFILES

- In case of one unit failing, the mission can still be completed on the remaining RTG. The logical emergency mode of operation would be to shut down one of the communications systems (reducing the power requirements by 200 watts), operate only those experiments listed under the emergency solar probe column in Table 2-4, subsection 2.2.1.2, and use batteries for the small excess loads.
- The active-thermal-control RTG units require a large radiator area which has to be designed for the high temperature environment close to the Sun. Because the solar probe is anticipated to be a relatively small spacecraft, the inclusion of the radiator will present a difficult design problem.
- The selection of the 250-watt passively cooled units for the Jupiter orbiter, based on the mass and reliability considerations of subsection 2.2.5.2, dictates that the same units be used on the solar probe to eliminate parallel RTG development programs and reduce cost and design integration problems.

2.2.5.2 Power Subsystem Mass and Reliability. As noted above, the use of three 250-watt or two 500-watt RTG units on the Jupiter orbiter offers a system redundancy of significant value to mission success. The choice between these systems can be analyzed as follows using the range of expected failure rates discussed in subsection 2.2.8.8 of this report.

Consider the alternate systems sketched in Figure 2-90. For the active thermal control scheme, more than one system component failure results in the loss of the power supply. Conversely, the passive units, installed as shown, still provide a duplicate system if any one component fails. Further, the active system relies on a pump for the circulating fluid which is inherently an unreliable device for long mission durations. To determine the pump reliability necessary for the first two concepts to have equal system probability of success, the data in Figure 2-91 was prepared. It can be seen that the pump in the active system degrades the system success significantly unless the pump reliability is greater than about .96. This may be possible in the next decade.

An additional system refinement would be the addition of batteries to accommodate peak loads or surges. Over the long heliocentric coast, the batteries could be recharged between communication periods. It is anticipated that fully charged batteries would thus be available in Jupiter capture orbit to operate the extra experiments power load in that phase of the mission. The orbiting spacecraft lifetime, assuming no system failure, would then be a function of the battery life as well as attitude control gas depletion. A disadvantage in using batteries is the requirement for careful thermal control to prevent freezing at deep space distances. If it can be assumed that temperature limits will not be exceeded, the power subsystem using batteries offers a lower, although acceptable, overall system probability of success.

To analyze the mass relationships of these concepts, Table 2-13 was prepared summarizing the system features of interest. The disadvantage of using an active-thermal-control RTG unit is apparent. Also, the use of batteries in conjunction with the 250-watt units offers identical subsystem mass if a 30-hour battery power supply is acceptable.

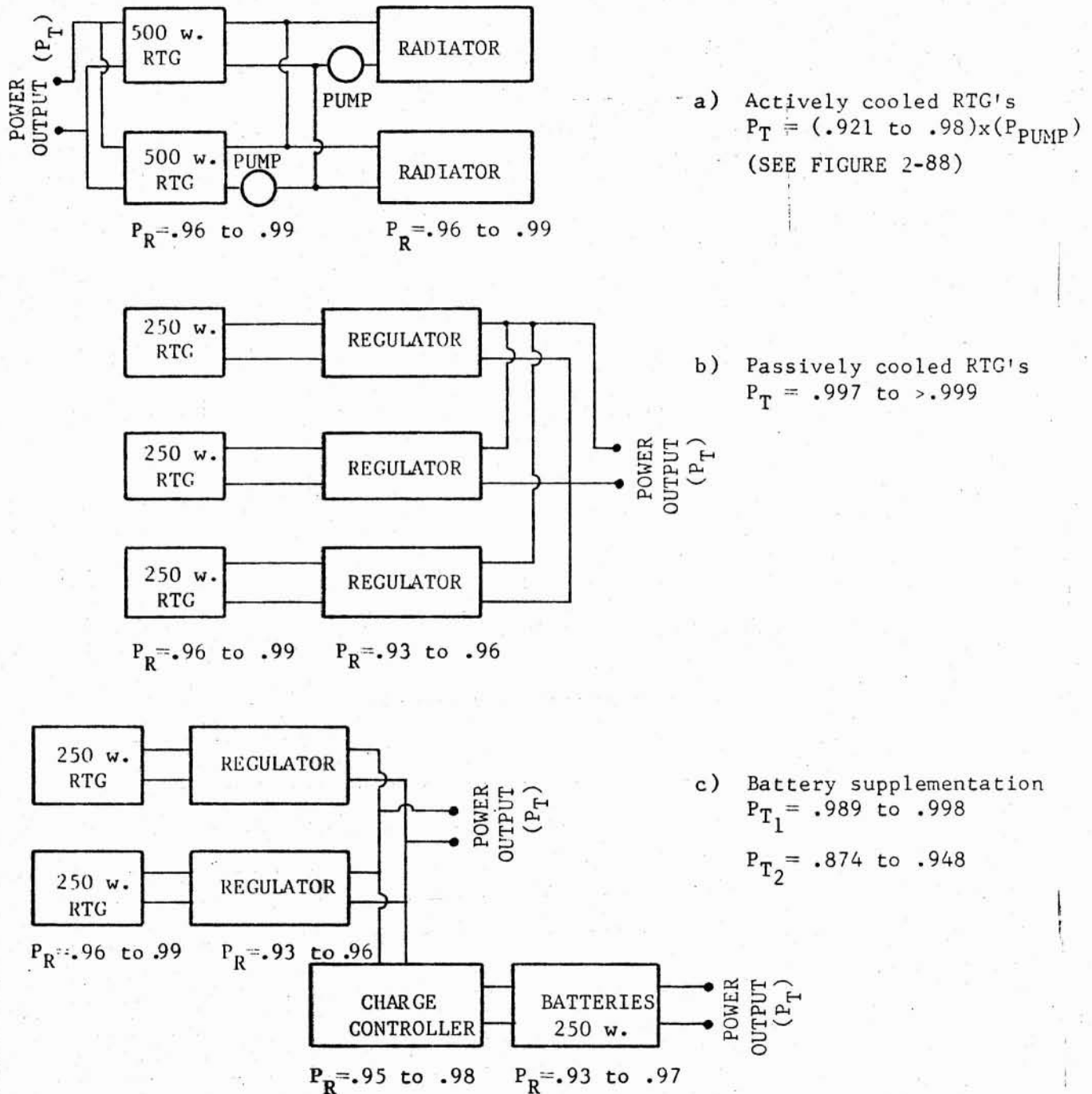


Figure 2-90. RELIABILITY OF ALTERNATE POWER SUPPLY SYSTEMS USING Pu-238 FUEL

(SEE FIGURE 2-90 FOR POWER SYSTEM SCHEMATICS)

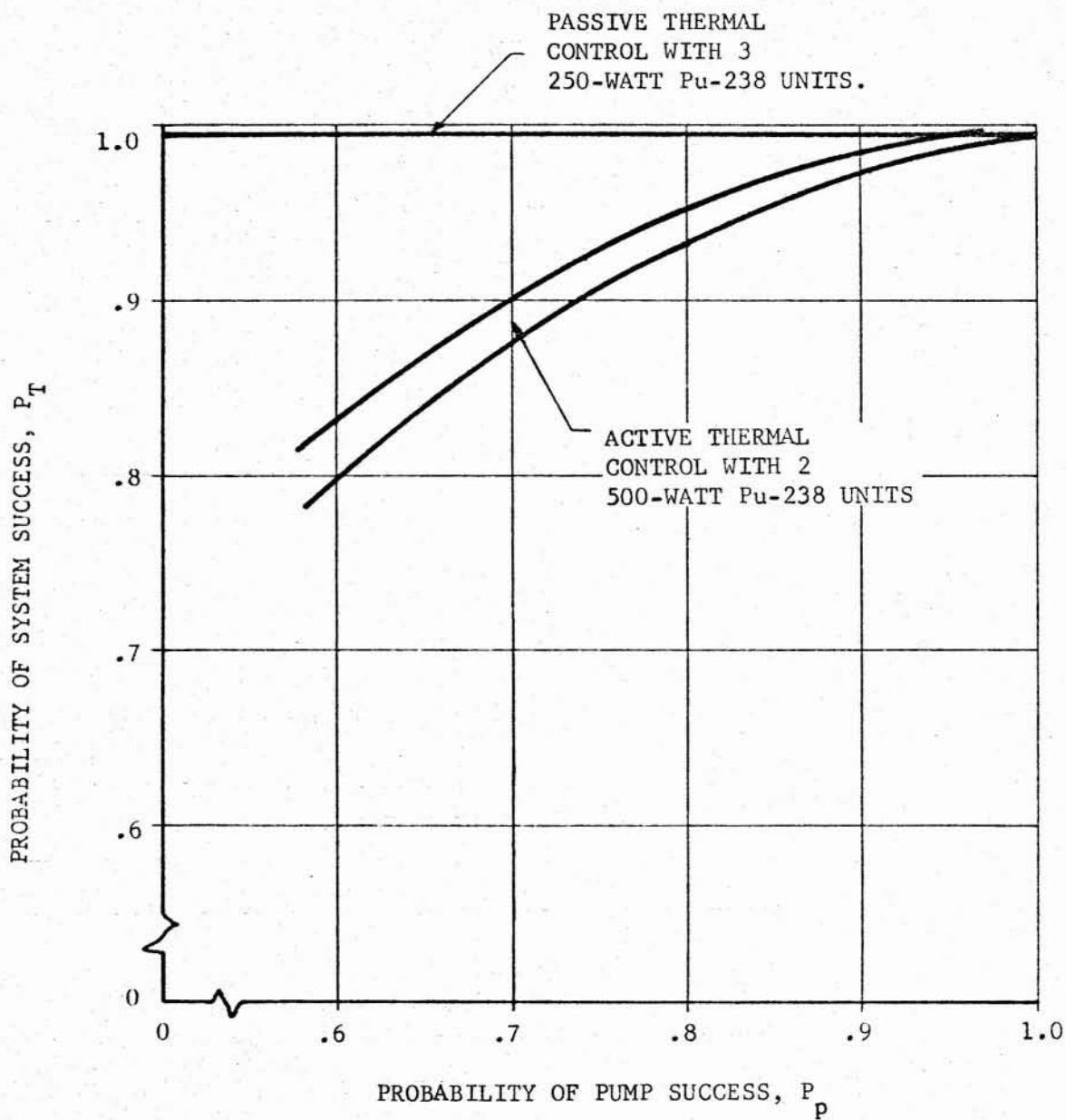


Figure 2-91. POWER SYSTEM SUCCESS PROBABILITY VS PROBABILITY OF PUMP SUCCESS

Table 2-13. RELIABILITY AND MASS FOR ALTERNATE POWER SYSTEMS COMPARISON

CONCEPT	Prob. of Success		System Masses				TOTAL
	Min.	Max.	RTG	PUMP	BATTERIES	OTHER	
Active thermal control	.987*	.995*	312 kg	8 kg	---	(radiator) 380 kg	700 kg
Passive thermal control	.997	.999	228 kg	---	---	(regulators) 8 kg	236 kg
RTG with batteries	.874	.948	152 kg	---	2.5 kg/hr	(regulator and controller) 10 kg	162 kg +2.5 kg/hr

* Reliability of pump ~.95

2.2.5.3 Utilization of Waste Heat From Power Subsystem. Based on the candidate RTG units and the power requirements discussed above, it can be shown that considerable heat is available for thermal conditioning of the Jupiter orbiter/solar probe. Considering the passively cooled 250-watt unit using the Pu-238 fuel, a heat source of at least 9×10^5 joules/hour is available. This energy is radiated from the cooling fins continuously at an equilibrium temperature of about 350°K. Assuming these units are mounted externally to the spacecraft, control louvers on the spacecraft skin could be designed to absorb radiative heat from these fins and transfer this energy to a circulating fluid for conditioning of the subsystems, components, and propellants. The actively cooled 500-watt RTG system already has a circulating fluid system and thus could be more easily adapted to the thermal control function. The NaK temperature at the radiator outlet is about 385°K. External louvers on a portion of the power system radiator could regulate this temperature as a function of the spacecraft system thermal control requirements to insure a constant cooling rate for the RTG unit.

In addition to the excess heat generated by the RTG, the preceding section of this report indicated that excess electrical power was available over that required to operate the spacecraft. This power can be diverted to thermostatically controlled electrical heaters located at critical points in the spacecraft. This represents a more desirable system since it does away with the circulating fluids, the heaters can be designed integral with the subsystems or components for optimum heating efficiency, and a high reliability can be expected. For the Jupiter orbiter spacecraft, using three 250-watt units, approximately 400 watts of electrical power is available during heliocentric coast beyond the range of the omnidirectional communications system. For the emergency condition of one RTG unit failure, 140 watts of electrical power is still available for thermal control during the heliocentric portions of the mission.

In Jupiter orbit, more power is needed to operate all the experiments and less would be available for thermal control. However, during this phase of the mission, there is no longer any need for propellant conditioning and the continuous operation of all onboard systems will reduce the thermal control requirements.

For the solar probe, using two 250-watt passively cooled units and about 60 watts of batteries, approximately 46 watts of electrical power is available for thermal control during the heliocentric phases. This system requires that the batteries be continuously recharged between communication functions.

The thermal control of the Jupiter orbiter and close-solar-probe spacecraft was discussed in detail in subsection 2.2.4 of this report. It can be stated here that sufficient electrical power is available for the required heating.

2.2.5.4 RTG Ground Handling and Installation. Because radioisotope materials continuously emit heat and radiation, some thought must be given to ground handling and launch vehicle RTG installation. The spacecraft for this mission must undergo preflight checkout and assembly with unfueled RTG units. After the preflight checkouts are complete and the systems are properly assembled,

September 1966

the RTG units are brought up to operating temperature with electrical heaters. This is necessary to prevent thermal shock to the thermoelectric elements when inserting the fuel blocks. In addition, performance verification checks can then be made. The RTG power generation and the associated power conversion and regulating equipment operation can be verified.

Upon completion of this phase, the fuel blocks are brought to the launch pad and the fueling process begun. Due to the heat generation and radiation, special handling of the fuel blocks is necessary. Tools and handling fixtures are required and would be a necessary part of the ground support equipment designed for these spacecraft. Conventional remote manipulators adapted for use on the launch service tower could be utilized. This equipment is used to remove the electrically heated dummy fuel blocks and to immediately insert the encapsulated Pu-238 slugs. After fueling, a large quantity of waste heat must be dissipated from the RTG units before launch. This is especially necessary in the event of a substantial delay in the vehicle launch. The vehicle structure and spacecraft systems must be prevented from exceeding their temperature limits. This entails a detailed heat transfer analysis considering the characteristics of the booster, spacecraft, and aerodynamic shroud. Only a brief analysis was undertaken in this study, and further detailed computations are required. Using convective heat transfer only, the data in Figure 2-92 was developed for 5 passively cooled, 250-watt RTG units. It can be seen that at the operating temperature of 350°K, the radioisotope units can probably be kept cool with air circulation.

Handling of the Pu-238 fuel blocks raises concern with the radiation hazard for the ground crew. Fortunately, this isotope is an α -particle emitter and can easily be shielded. However, even direct exposure to the source for short periods is not a dangerous condition. A worker three-feet away could remain for two minutes without exceeding the safe weekly tolerance of normal industrial practices. At ten feet, a worker could remain almost an hour. This means that in an emergency, workers could safely leave by simply walking away from the fuel source.

2.2.5.5 Advanced Power and Propulsion System Concept. The installation of a radioisotope energy source on the Jupiter/orbiter probe leads to consideration of an advanced system in which this unit is utilized for power generation, thermal control, and propulsion. It is possible to conceive of the systems diagramed in Figure 2-93, wherein a single radioisotopic core provides energy for all of the functions noted. A radioisotopic core is simple in concept but has the unique characteristic of radiating energy continuously. Thus, a means to expel waste heat during low power loads must be provided.

The direct heating method of thrust development offers the best compromise of performance and reliability for the Jupiter mission. These designs are similar to solid-core nuclear reactor systems but are simpler because there are no nucleonic control problems associated with reactor criticality. The core can be any geometric arrangement consistent with proper structural integrity and heat transfer optimization. In designs for high temperature operation, the isotope fuel can be imbedded and clad with a refractory material such as tungsten. The operating temperatures of such systems is limited by the cladding, but can be as high as 2480°K if relatively short thrust periods are used. The thrust of direct heating, solid-core isotopic engines depends on many parameters.

- FIVE 250-WATT UNITS
- HEAT OUTPUT = 9×10^5 JOULES/HOUR EACH UNIT
- SURFACE AREA = $.17 \text{ m}^2$ EACH UNIT

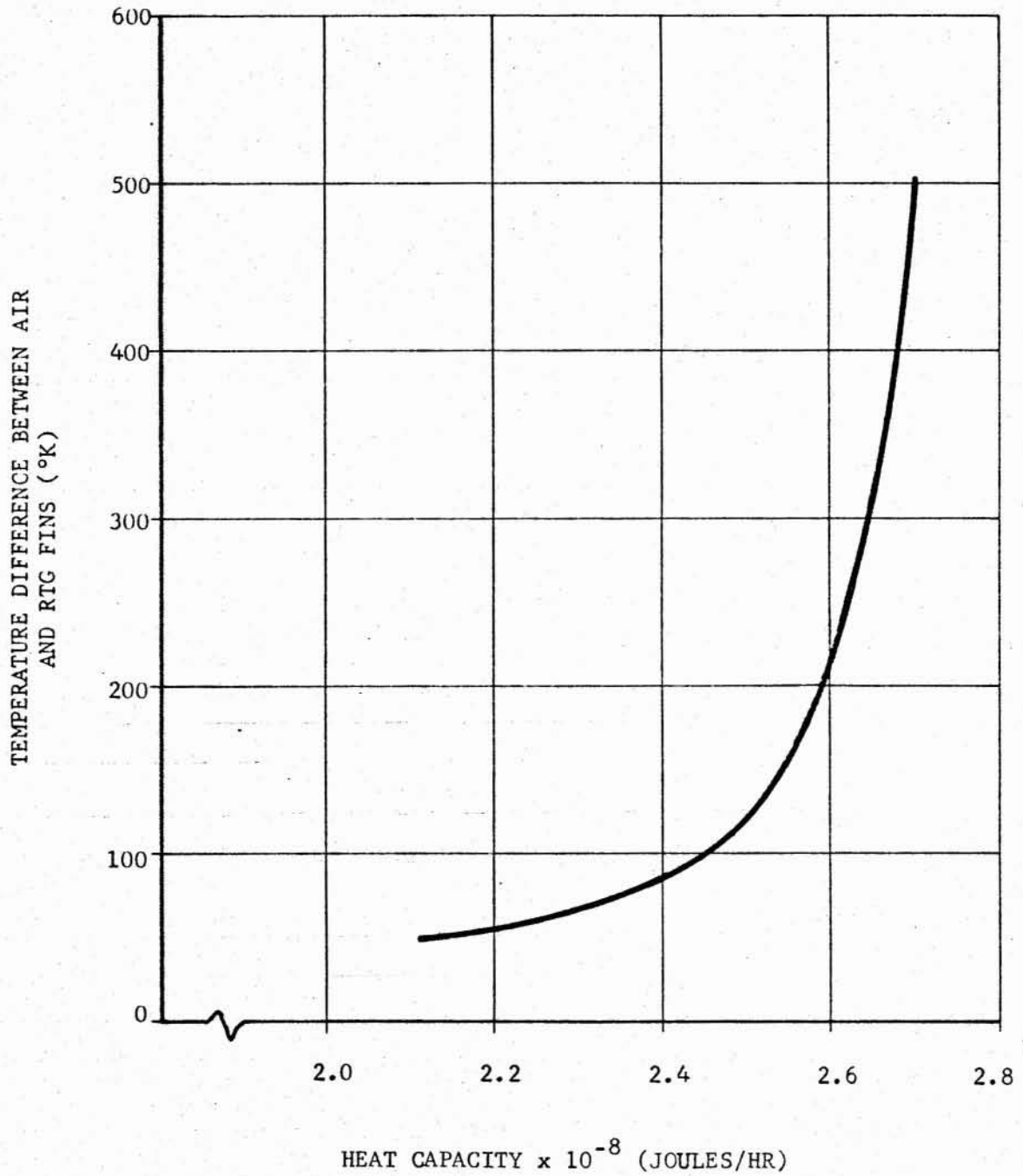
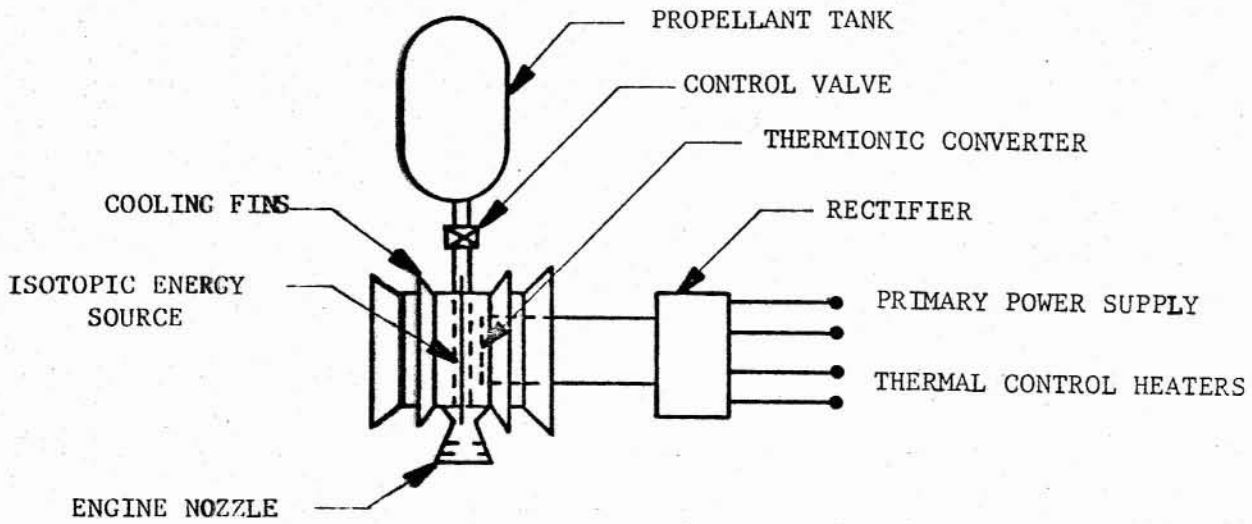
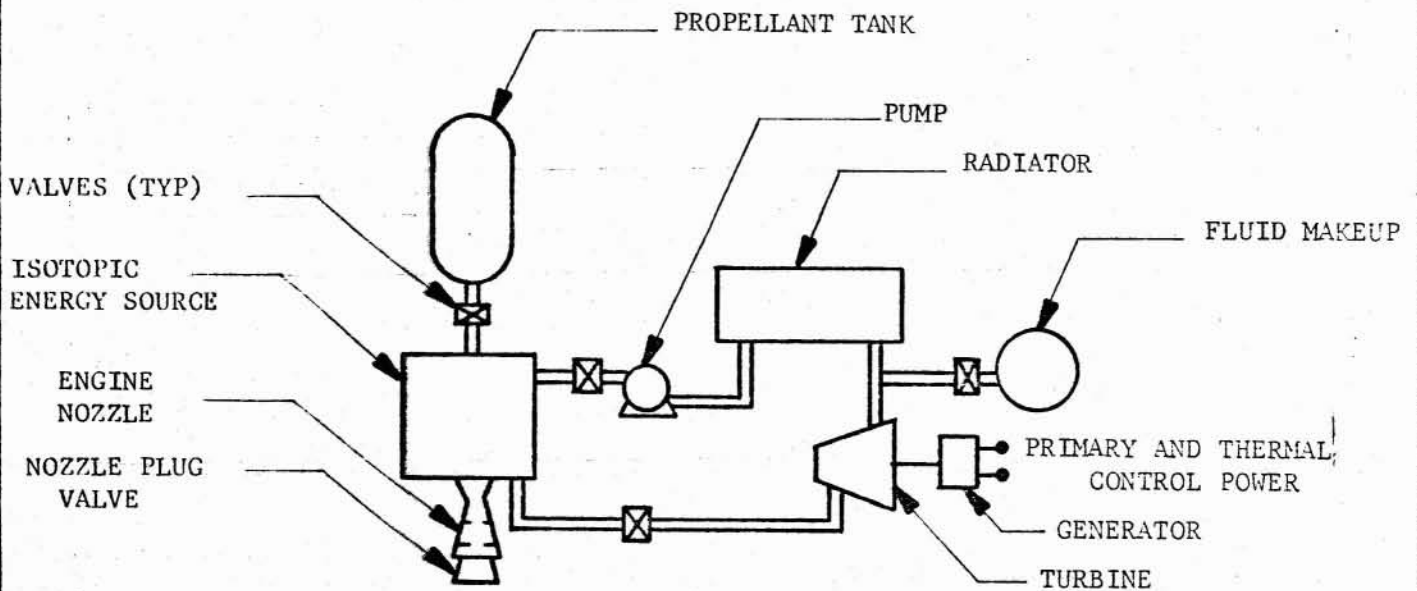


Figure 2-92. RTG FIN TEMPERATURE VS FIN HEAT CAPACITY



a. THERMIONIC POWER CYCLE



b. FLUID POWER CYCLE

Figure 2- 93. COMBINED ISOTOPIC POWER AND PROPULSION UNITS FOR THERMIONIC AND FLUID POWER CYCLES

It is beyond the scope of this report to analyze such systems in detail, but as an approximation to determine the order of magnitude of typical system performance, the following can be presented.

Using hydrogen as the propellant at an outlet temperature of about 2420°K, a specific impulse of 800 seconds can be achieved at chamber pressures of 1 atmosphere. Fueled with Po-210 with a power density of approximately 134 kw/kg, thrusts of the order of magnitude of 100 to 150 Newtons are possible with an engine mass of about 100 kg. Better performance can be obtained with isotopes of higher power density such as Nb-95 but the half-lives of such elements are generally too short for the mission under consideration. At the same operating temperature mentioned above, a hydrogen-propelled radioisotope engine fueled with Nb-95 would have a specific impulse of about 1200 seconds for the same engine mass.

Isotope availability is the major obstacle in utilizing radioisotopic engines for propulsion. For the examples discussed above, many kilograms of the isotope are required. Unless specific efforts to produce these quantities are made, these requirements may not be met in the next decade. Table 2-14 below indicates the expected availability of suitable isotopes by 1970.

Table 2-14. ISOTOPE AVAILABILITY

ISOTOPE	DECAY PRODUCTS	PRODUCTION SOURCE	HALF LIFE (DAYS)	POWER DENSITY (KW/KG)	EXPECTED AVAILABILITY KW (THERMAL)
Cm-242	Alpha Particles Neutrons	Reactor Product	156	98	10
Po-210	Alpha Particles	Reactor Product	138	134	1000
Ce-144	Beta and Gamma Rays	Fission Product	285	~4	1330
Nb-95	Gamma Rays	Fission Product	35	189	500-1000
Y-91	Beta Rays	Fission Product	59	19	500-1000

This data indicates that Po-210 represents the best fuel from the viewpoint of half life, power density, and availability.

Radioisotope power decays with time and the performance of engines of this type must consider this feature. Thus, if an engine is initially fueled with P_0 kw of isotope power, after time t , the power will be:

$$P = P_0 e^{-\frac{t}{L}}$$

where L = isotope half life.

Engine thrust related to the power density, will also be decreased. The spacecraft thrust-to-mass ratio at time t can be calculated from the following:

$$(T/W)_t = \frac{T_{0e} - .693 t/L}{W_0 - W_t}$$

where T_0 = thrust at fueling
 L = isotope half-life
 W = vehicle initial mass
 W_t = vehicle mass at time t .

In addition to the degradation of thrust throughout the life of the spacecraft, a slight thrust decay will be experienced during thrusting. Figure 2-94 shows this effect for Po-210 systems. It can be seen that the thrust-to-mass ratio increases rapidly after a few days as the propellant is utilized.

It is of interest now to study a typical Jupiter mission and develop some data for this concept. It is assumed that a total velocity correction of 150 m/sec will be required for midcourse correction and that spacecraft gross weight is 7350 kg. Using the system described by Figure 2-94, the hydrogen required amount is 67 kg and the engine burn time is a little more than 3 hours. This is reasonable for midcourse corrections.

For braking into a Jupiter capture orbit, it can be assumed that a spacecraft gross mass of 3600 kg will be available and a ΔV of 2.3 km/sec required for the maneuver. For this maneuver the hydrogen required is somewhat more than 910 kg and the engine burn time is almost 2 days. This must be carefully analyzed from a system optimization viewpoint to determine the precise trajectory, navigation, and guidance techniques required for this long-duration thrusting in the vicinity of Jupiter. As discussed in subsection 2.2.6.1 of this report, storage of this quantity of hydrogen for the 500 to 600 days of the heliocentric portion of this mission poses many problems in system design.

Also, the isotope engines discussed above require an isotopic core with nominally 300 to 400 kw depending on the efficiency. For a 600-day mission to Jupiter, this means that a Po-210 unit with a half life of 138 days must be fueled to about 6 to 8 megawatts at launch. This will require about 53 kg of Po-210 and appears unreasonable at this time.

For midcourse corrections, a lower thrust and corresponding longer burn times may be considered reducing the fuel quantity required. However, it is concluded that for the next decade, an isotopic propulsion system does not offer significant advantages for this mission.

2.2.6 Propulsion and Attitude Control Subsystems

Propulsion subsystems are necessary on the Jupiter orbiter/solar probe for attitude control during heliocentric coast, midcourse correction maneuvers, and capture-orbit braking. The requirements for these subsystems depend on the specific trajectory and vehicle mass. Typical subsystems were developed in this study based on the selected mission profile and spacecraft design. The following subsections discuss the requirements and subsystem considerations for the various propulsion maneuvers expected for this mission.

2.2.6.1 Planetary Orbit Capture. The braking maneuver into an orbit around Jupiter represents the largest propulsion requirement. The velocity increment required for capture ranges from 1500 to 3000 m/sec depending on the transfer type, launch date, and the capture-orbit parameters. If the spacecraft is designed for a fixed ΔV capability, then candidate propulsion systems for this maneuver include solids, monopropellants, and bipropellants including cryogenics.

September 1966

The major factor that distinguishes orbital capture from other maneuvers is the extremely long time that the propulsion subsystem is exposed to the space environment before activation. The transit time may range up to 600 days. For liquid propellants, at least some and possibly all components in the propulsion system will be exposed to their working fluids at pressures close to the operating value for the complete mission duration. This represents a sizeable extension in the required lifetime for all of these components. Additionally, any pressurization system for the liquids must maintain its pressure level during the long heliocentric coast. However, the greatest problem with liquid systems is thermal control. Freezing of the space-storable systems using hydrazine, UDMH, N_2O_4 , etc. must be prevented and the cryogenic systems exhibit large boil-off losses.

Based on the maximization of the velocity increment available, high specific impulse propellants are, in general, desirable. Fluorine, hydrogen, oxygen, and oxygen difluoride are suitable. Whether or not these propellants are employed for long-duration missions is a function of the amount of propellant available after the space storage. The major source of propellant loss is attributable to boil-off caused by heat leakage into the propellant tank. The sources of heat input are solar radiation, planetary albedo, infrared radiation, and heat generation within the spacecraft system.

Figure 2-95 shows the results of a detailed study for selection of propellants. Spacecraft gross mass is plotted as a function of storage time for several propellant combinations employing tanks with optimum superinsulation thickness for each mission duration. It is evident that for long missions of the order of two-years duration the cryogenic propellants cannot be considered. The storables exhibit little boil-off but the permissible temperature range of the storables is considerably narrower than that of the cryogenic propellants and will require precise thermal control. Electric heaters using excess electrical power from RTG power supply units will be necessary. As noted in subsection 2.2.5 of this report, considerable energy is available for this function. However, to minimize this power drain, the propellant tanks would be insulated. Modern superinsulations combine low thermal conductivity with low specific mass and hence provide maximum propulsion system performance.

Figure 2-96 shows the plot of insulation mass versus heat flux developed in this study. Each line is plotted for constant density insulation, the only variable being the thickness of insulation. The lines are plotted at $540^\circ R$, $600^\circ R$, and $800^\circ R$ showing the effect of increased temperature of the warm boundary. The insulation studied herein has an apparent thermal conductivity of 2.4×10^{-5} BTU per hour-foot- $^\circ R$. Applying this data to actual propellant tanks, curves of continuous power heating necessary to maintain bipropellant storables at room temperature were developed. These are presented in Figure 2-97 for various masses of propellants. In this analysis, it was assumed that the propellant was divided into four spheres, two for oxidizer and two for fuel. Other assumptions are shown on the curve. It can be seen that with superinsulation only minimal propellant heating is required.

Solid propellants offer considerable storage advantage over the liquid propellants, since there is no boil-off, pressurization, or slosh problem.

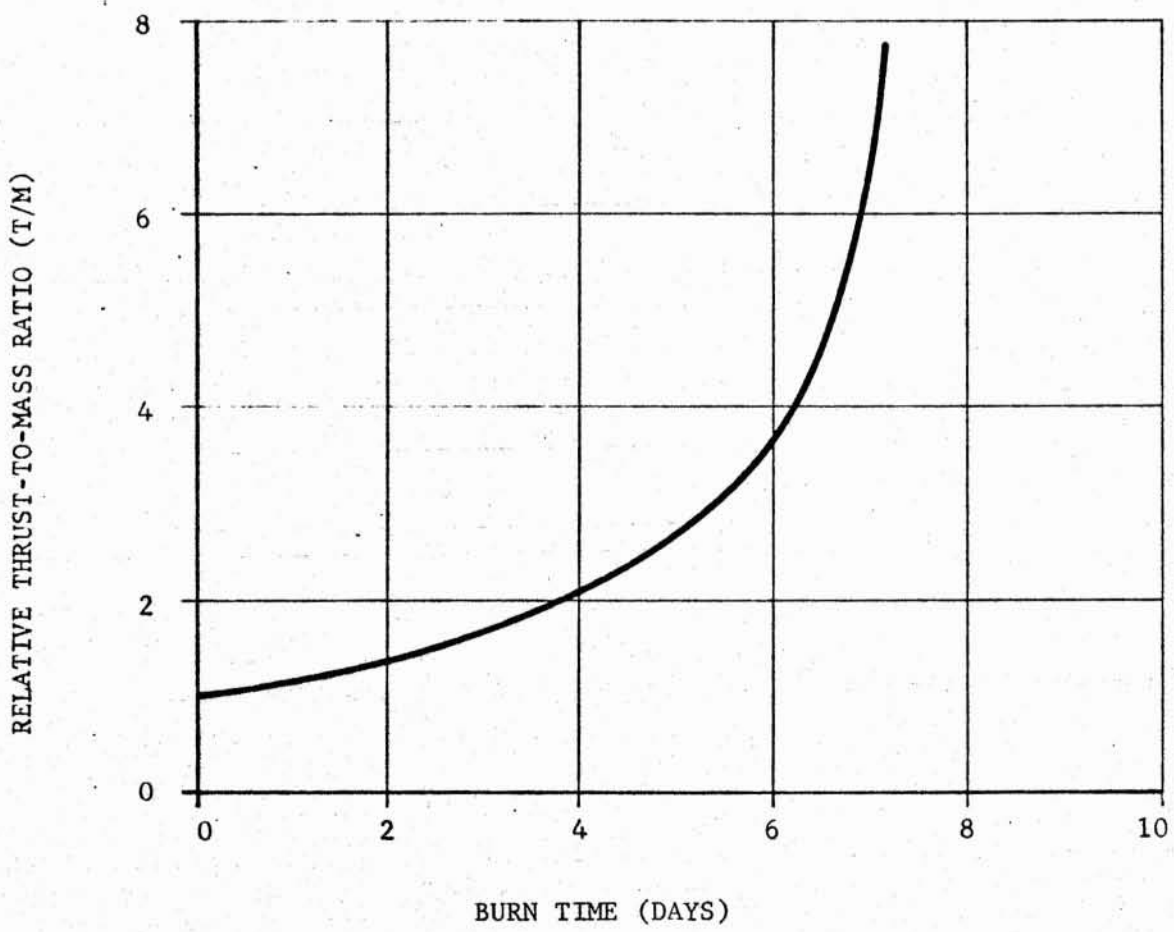
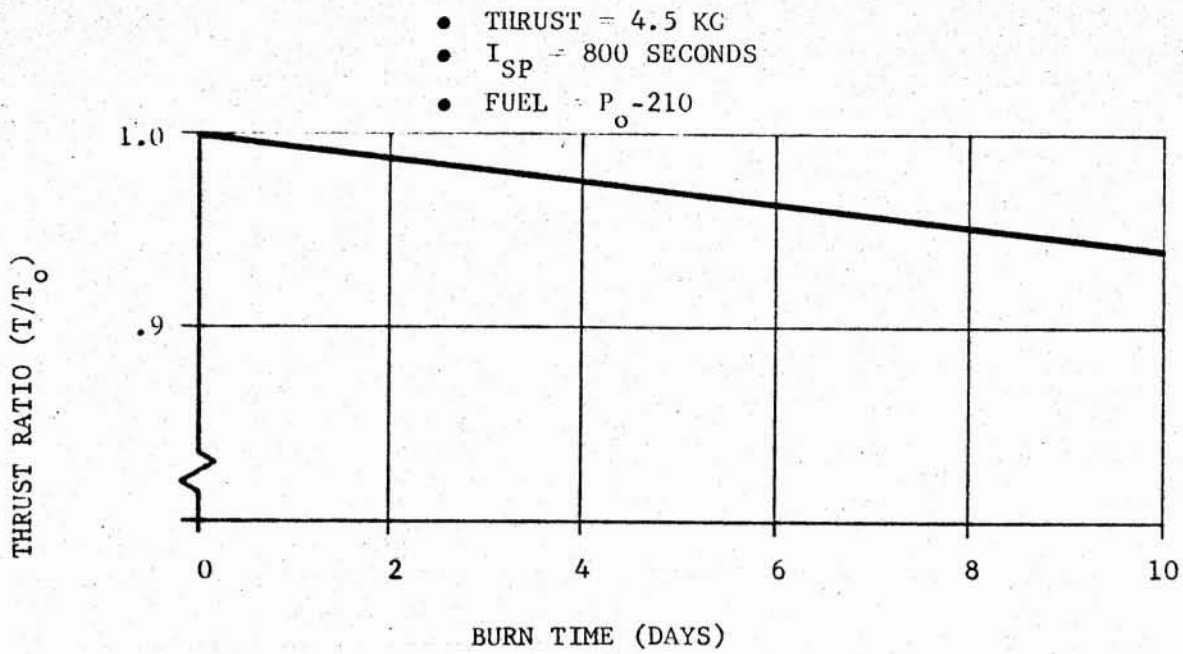


Figure 2-94. PERFORMANCE OF ISOTOPIC PROPULSION SYSTEMS WITH BURN TIME

SUBSYSTEMS
PROPELLANT STORAGE

- WITH SUPERINSULATION $\sim 9 \times 10^{-6}$ WATTS/METER - °K
- BRAKING $\Delta V \sim 2$ KM/SEC
- FIXED WEIGHT ~ 4400 POUNDS

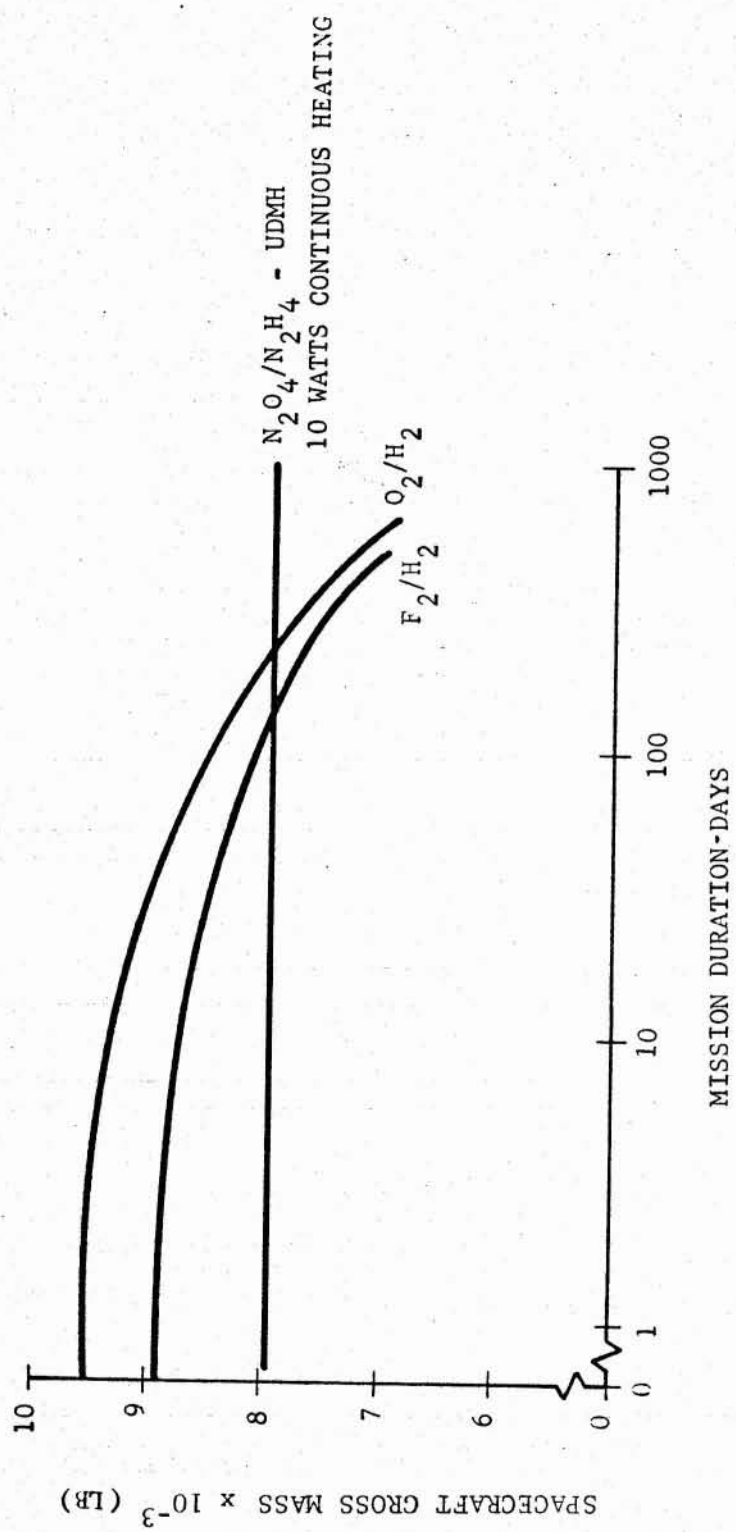


Figure 2-95. PROPELLANT PERFORMANCE VS MISSION STORAGE TIME

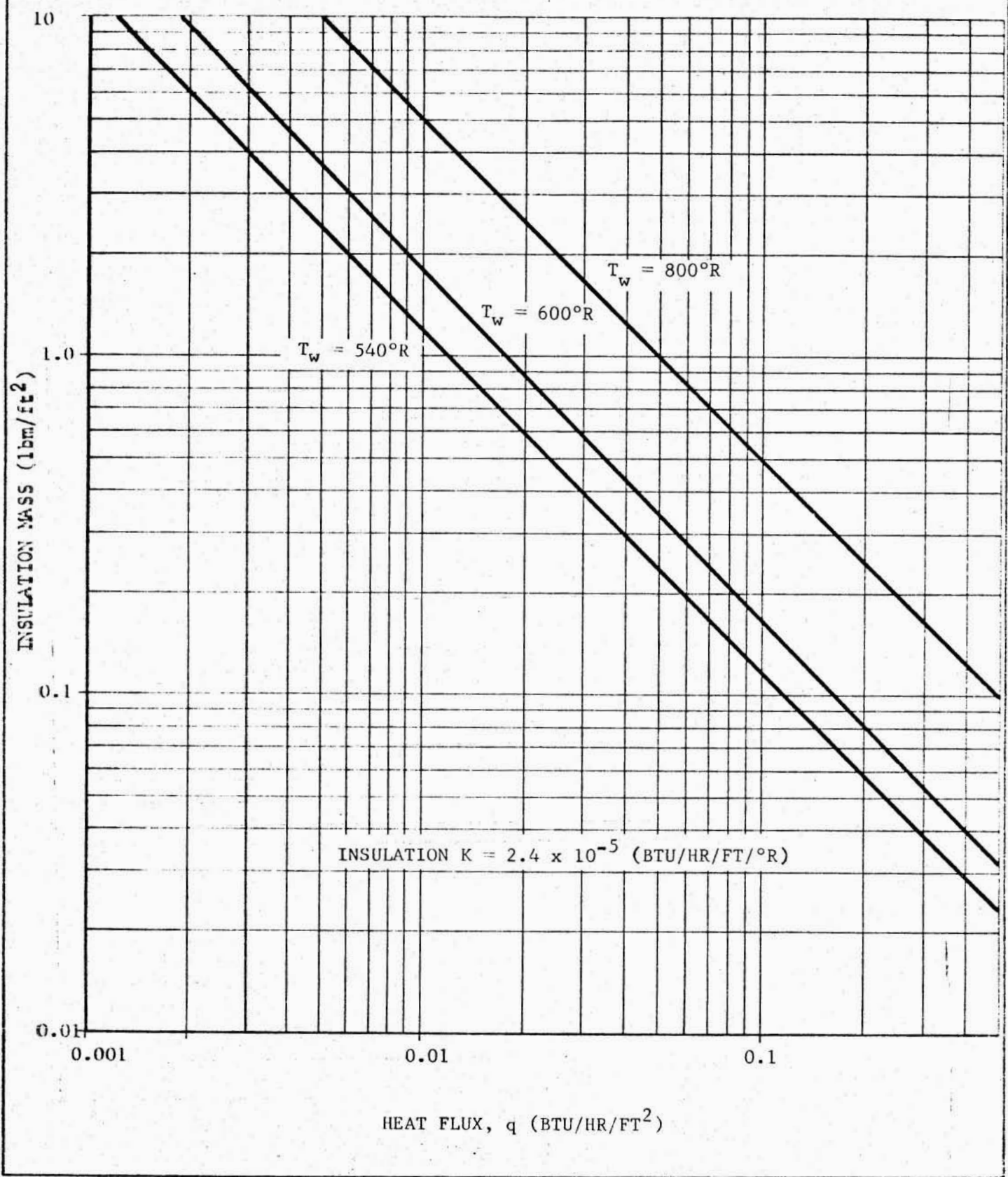


Figure 2- 96. VARIATION OF SPECIFIC INSULATION MASS WITH HEAT FLUX FOR VARYING INSULATION SURFACE TEMPERATURES

- CONDUCTIVITY = 2.4×10^{-5} BTU/HR-FT-°R
- PROPELLANT TEMPERATURE $\sim 440^\circ\text{K}$

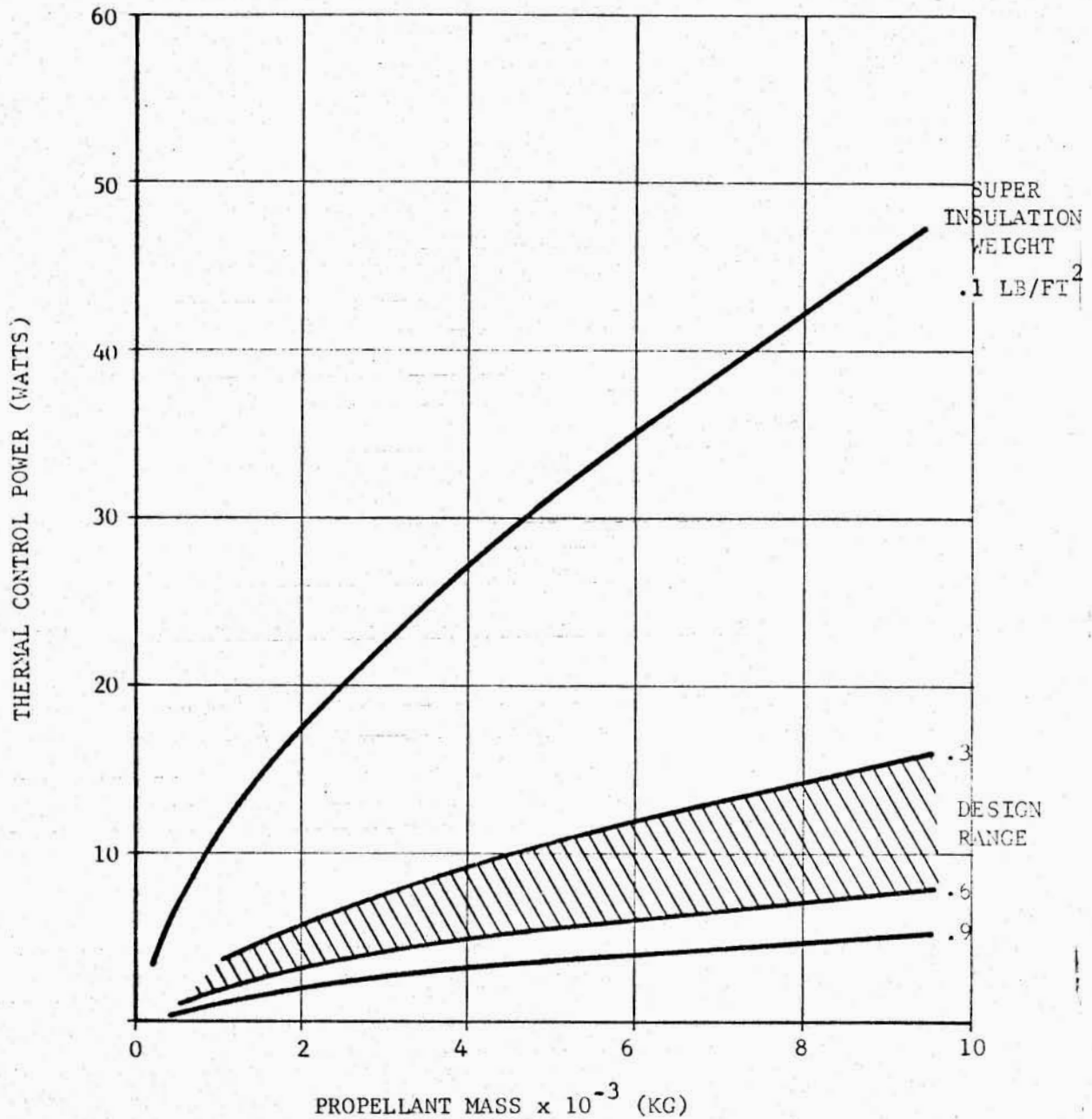


Figure 2-97. HEATING REQUIRED TO MAINTAIN STORABLE LIQUID PROPELLANTS AT ROOM TEMPERATURE

The practical temperature range for storing solids is 220°K to 340°K and with electrical heaters and insulating blankets this should be easily maintained. One problem related to solids is their high thrust and vibration level. The burning rates available from proven solid propellants limit the maximum burn-time to less than 200 seconds. To deliver the required total impulse for Jupiter capture, the thrust-to-mass ratio will be high at burnout. This is a major disadvantage in that disturbing forces will be high and a large attitude control force and total impulse will be required. Also, structural criteria for antenna mounts, instrument booms, etc. must account for these high forces. In addition, a solid propellant burns rougher than a liquid and the induced vehicle vibration will be higher.

Based on the factors discussed above and the apparent ease with which storables can be thermally controlled, the Jupiter capture maneuver propellant should be storable liquids. The selection of the actual propellant combinations will depend on a detail comparison of candidate systems. A performance comparison of monopropellant and storable bipropellant systems was conducted considering a number of propellants. Hydrazine and hydrogen peroxide are the most common monopropellants in use. The specific impulse of hydrazine (235 sec) when compared with hydrogen peroxide (160 sec) makes it the more attractive of the two. In the past, hydrazine systems have required the use of N_2O_4 slugs to restart the system, but new catalysts under development are now precluding the necessity for these slugs. In the next decade, it is believed that catalysts with lifetimes capable of satisfying the Jupiter orbiter mission requirements will be available. Thus, the hydrazine monopropellant system can be selected as representative of this class for comparison with bipropellants.

Bipropellant systems are relatively complex and require an accurately regulated pressurization system to maintain proper fuel/oxidizer mixture ratios. This complexity is offset by a higher specific impulse resulting in better system performance. This class of propulsion systems is compared with the monopropellant in Figure 2-98 for various propellant masses. Two types of monopropellant pressurization schemes are shown.

It can be seen that little difference in system mass occurs between the different systems. This implies that selection of the braking-maneuver propulsion subsystem may be made based on other criteria such as complexity, performance, and existing component availability. Since the LEM ascent stage bipropellant propulsion subsystem represents a suitable thrust level and is designed for space operation and storage, it was selected for the Jupiter orbiter mission. Figure 2-99 presents a block diagram of this system.

2.2.6.2 Attitude Control Subsystem. To accomplish guidance maneuvers, perform scientific experiments, and permit communications with Earth, attitude control of the Jupiter orbiter/solar spacecraft is required. Several different aspects of the mission exist wherein the attitude control requirements may be different. These can be summarized as follows:

- During midcourse or braking propulsion maneuvers, the attitude control system must orient the spacecraft and direct the thrust vector in the direction of a computed velocity increment. Required accuracy for attitude control is high and an onboard computer must recognize thrust misalignment and take necessary steps

• JUPITER CAPTURE ORBIT BRAKING MANEUVER

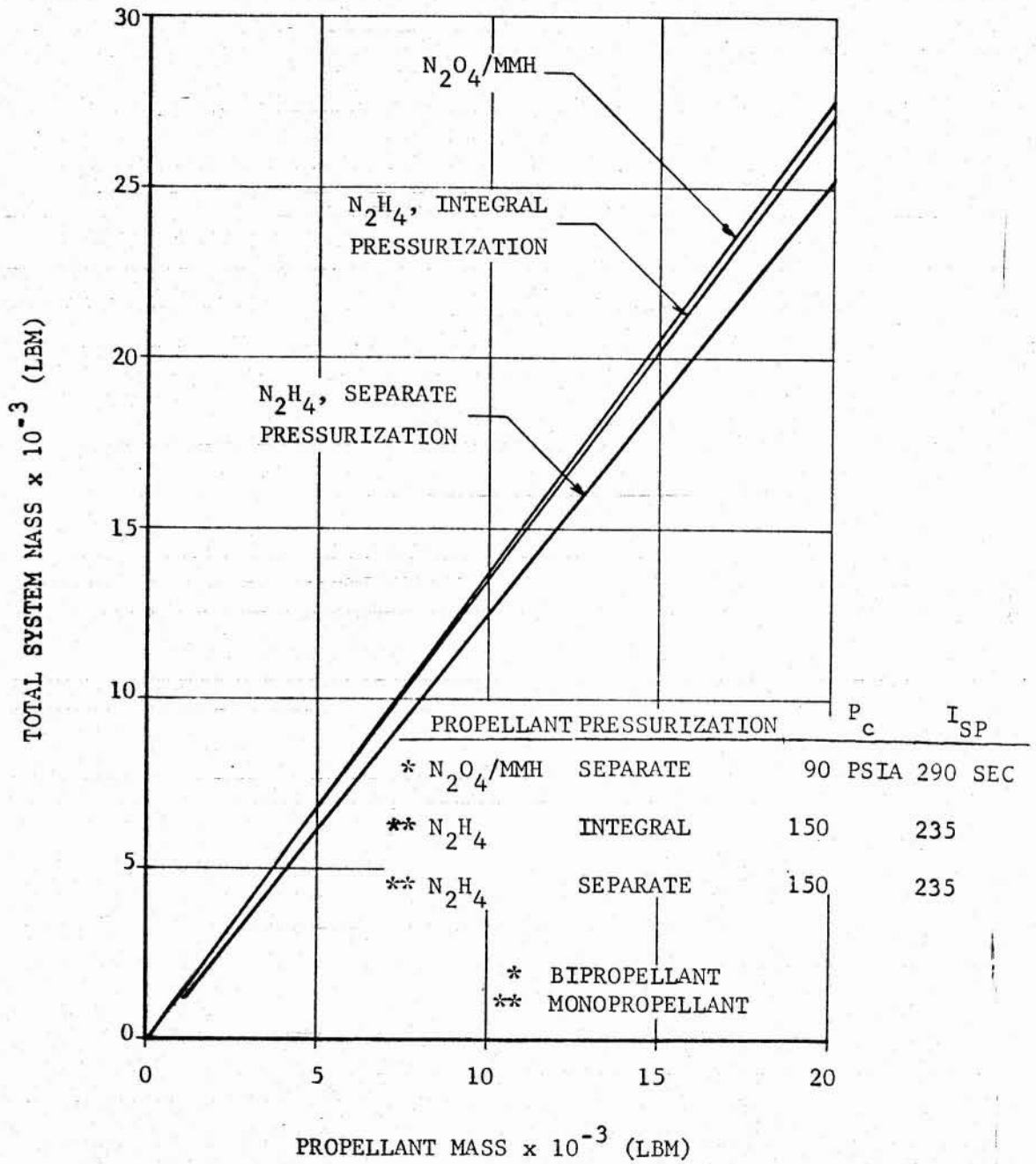


Figure 2-98. TOTAL SYSTEM MASS COMPARISONS FOR MONOPELLANT AND BIROPELLANT SYSTEMS

• BASED ON LEM ASCENT-STAGE ENGINE

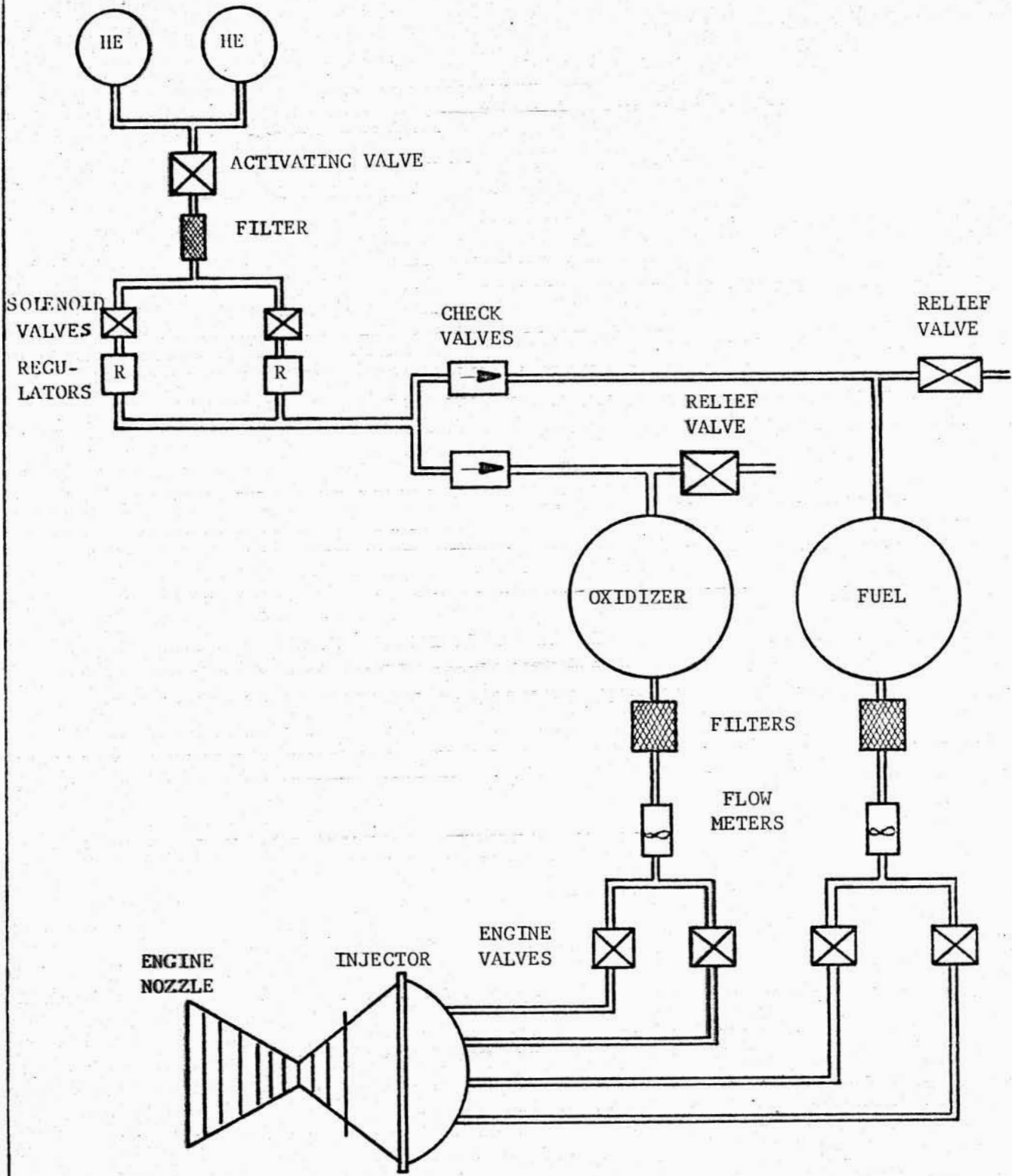


Figure 2-99. JUPITER CAPTURE PROPULSION ENGINE SYSTEM

for corrective attitude realignment.

- During communications with Earth, the antennas must be pointed at Earth with high accuracy depending on the radiated beam width. If the antenna is gimballed, gimbal motors will perform that function. However, the entire vehicle must be stabilized to counteract gimbaling torques and prevent loss of Earth-lock.
- For much of the scientific instrumentation, a specific direction or orientation is necessary to achieve valid experimental data. In general, stabilization requirements for this function are not severe. For some modes of operation, the vehicle must be oriented to permit both experimentation and communication with Earth.
- At Earth ejection, high tumble rates may be imparted to the spacecraft upon separation from the launch vehicle. The spacecraft must be able to stabilize itself, initiate Sun and Canopus search procedures, and establish a heliocentric coast mode orientation. Torques required for these functions may be relatively high.
- In the event of a break in Sun or Canopus lock during the heliocentric coast, the attitude control subsystem must be capable of automatically initiating search modes and reacquiring the heliocentric coast orientation. If the disruption was due to impact with a small asteroid mass, tumble rates may be relatively high and large restoring moments required to stabilize the spacecraft.

A review of the above functions indicates that two attitude control thrust levels may be necessary. A low-thrust system will produce the highly accurate stabilization required during coast and communications periods. For control during thrusting and for gross orientation after booster separation or in the event of asteroidal impact, a higher thrust is desirable. Depending on the results of further analysis, the higher thrust system may be integral with the midcourse correction propulsion system. A common propellant and feed system could be designed with both attitude-control nozzles and a midcourse correction motor.

To analyze and select the attitude-control systems, the above mentioned modes must be studied to determine the total impulse and torque requirements. A major factor in selection of the attitude-control subsystems is the lifetime requirement. Many years of operation are necessary for both the Jupiter orbiter/solar probe. It would be extremely desirable to use passive control wherever possible and to accomplish the various control functions in the least complex manner. Solar vanes were therefore initially considered in this study for coast stabilization but cannot be used in deep interplanetary space due to the lack of sufficient solar radiation. The following subsection discusses these considerations and present the analysis of the selected attitude-control subsystems.

The total impulse of the low-thrust attitude-control subsystem depends primarily on the spacecraft size and mass, extent of maneuvering, pointing accuracy requirements, and disturbing torques. A precise analysis requires the definition of a specific spacecraft and its multi-axial moments of inertia. Parametric data was developed in this study covering the range of values anti-

anticipated for the final Jupiter orbiter/solar probe configurations. These are presented in Figure 2-100 with the approximate range of values anticipated for the conceptual designs developed in subsection 2.3 of this report. For this analysis, it was assumed that the spacecraft moments of inertia are the same around all axes.

These curves show that for a nominal maneuver rate, say $.1^\circ/\text{sec}$, the Jupiter orbiter attitude-control subsystem should have about 50 newton-meters torque and be sized for at least 10^3 newton-meter-seconds/month. The equivalent solar probe parameters are about 20 newton-meters torque and about 500 newton-meter-seconds/month. These represent the stabilization requirements for the low-thrust attitude-control subsystem.

At this point in the development of conceptual designs, the exact moments of inertia, thruster lever arms, and thrust levels are not known. The above requirements are therefore not exact. However, these control characteristics are reasonably close to the proper values and will be used in this study as the spacecraft requirements.

Superimposed on the above requirements is the presence of disturbing forces peculiar to the space environment. Solar pressure, micrometeoroid impacts, gravitational gradients, and antenna gimbaling all produce minute but significant disturbing torques. At close-solar distances, an offset between the center of pressure of solar radiation and the center of mass of the vehicle will also produce a disturbing torque. The low-thrust attitude-control system must be capable of overcoming these torques at angular rates great enough to prevent loss of Sun and Canopus lock.

To estimate the magnitude of these effects, consider a body about 2.5 m in size, .50 reflectivity, and a deviation of .25 m between the centers of pressure and mass. This is not an exact replica of the spacecraft configurations developed, but will provide an appreciation for the forces which are of interest. The following table then summarizes the results of the disturbing torque analysis.

Table 2-15. MAGNITUDE OF DISTURBING FORCES

DISTURBANCE	APPROXIMATE TORQUE (newton-meters)	RESTORING MOMENTUM (newton-meter-sec)
Solar Radiation:		
.1 AU	3.3×10^{-5}	90.0
2.7 AU	2.85×10^{-6}	7.5
5.2 AU	4.3×10^{-7}	.63
Meteoroid Impact:		
1×10^{-5} gms/sec	2.7×10^{-4}	~ 430
7.5×10^{-7} gms/sec	7.5×10^{-6}	21.0
Antenna Gimbaling:	1.4×10^{-2}	~ 2800.0
Gravitational Gradients:	(Negligible)	(Negligible)

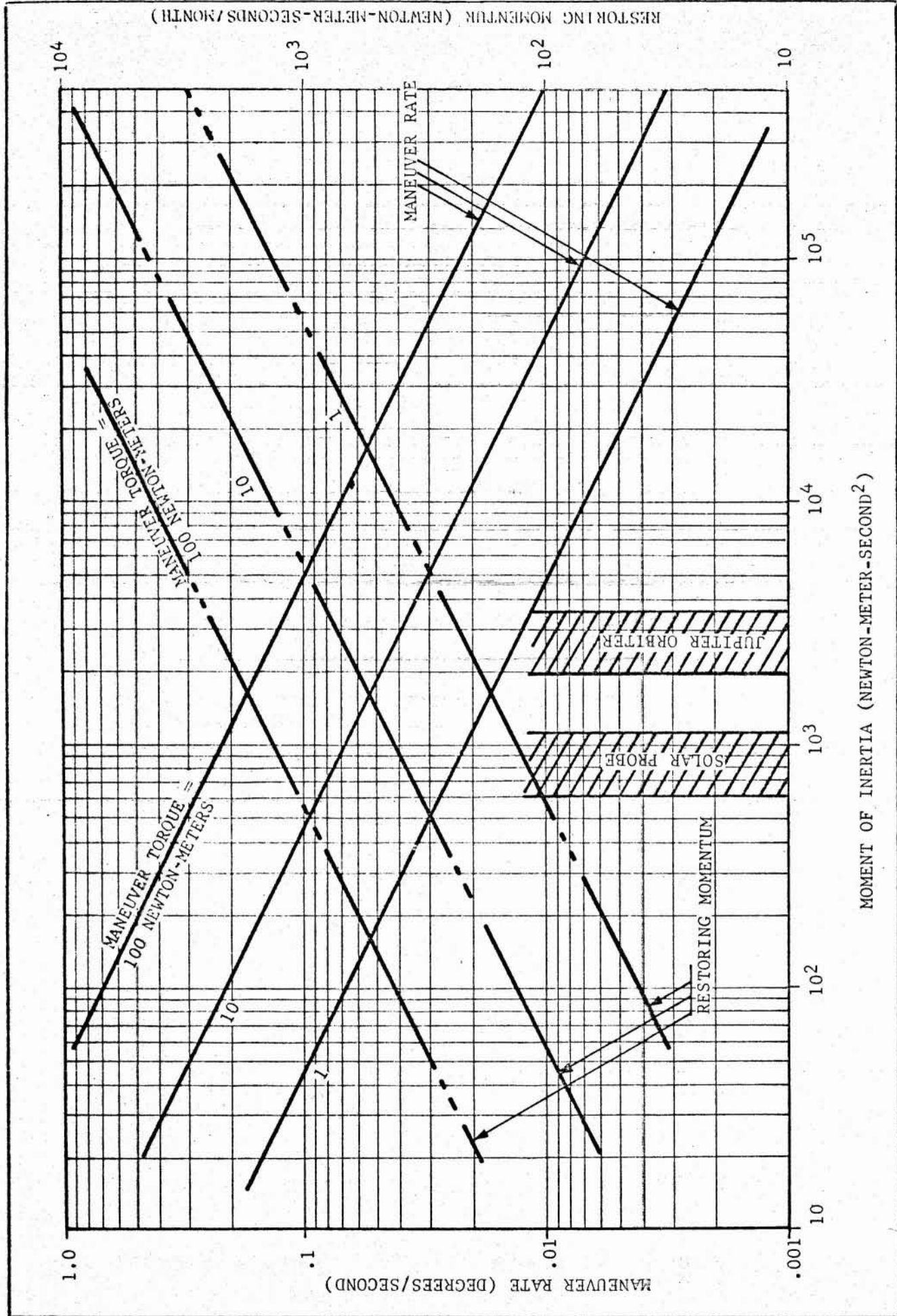


Figure 2-100. STABILIZATION CHARACTERISTICS FOR JUPITER/SOLAR PROBES

It can be seen that of the disturbing parameters, antenna gimbaling is the most severe. Also, if larger meteoroid fluxes are encountered, this impulse requirement is very significant.

To determine the total impulse requirement of a high-thrust attitude-control subsystem the disturbing torques must be known. At this time it is impossible to estimate the tumble rates at booster separation or in the event of an asteroid-mass impact. However, these should be of the same order of magnitude or less than the thrust misalignment torque at planetary braking. It will therefore be assumed that this latter maneuver represents the design condition for the high-thrust attitude-control system for the Jupiter orbiter. The solar probe does not have propulsion and does not require such stabilization.

The planetary-capture thrust and misalignment torque will be dependent on the spacecraft mass, moment of inertia, and propulsive system used. As a maximum case, the LEM ascent-stage motor can be considered. With a misalignment of 2° , disturbing torques can be as high as about 200 newton-meters for the configuration developed in subsection 2.3 for the Jupiter orbit. Figure 2-101 presents the trades of thrust and moment arm for the attitude-control subsystem to react this misalignment. It can be seen that relatively high thrusts are necessary, even at large moment arms.

To summarize the anticipated total impulse requirements for the Jupiter orbiter/solar probe, Table 2-16 shows nominal values with lever arms of about 2 m. These were selected for a typical trajectory and configuration and would change with different spacecraft and missions. For the purposes of this study, they will be considered the design conditions.

At close distances to the Sun, the radiation pressure is very intense. This leads to consideration of utilizing this pressure to help stabilize the solar probe towards the Sun. This concept was used in the Mariner IV program and should offer significant advantages for a close solar probe. Thermal control of the surfaces may be a problem. However, as discussed in subsection 2.2.4.2, conical surfaces of the proper l/d configuration and material can be directly exposed to the Sun at close solar distances without exceeding the temperature limits of the structure. An analysis was therefore conducted to determine the effectiveness of solar vanes for attitude control.

The sources of torque in a radiation attitude-control system arise from a momentum transfer from individual photons and particles. The reflectivity of the surface is therefore important. Also, torques arising from the spacecraft itself must be accounted for. If large differences in the amount of radiated energy from various parts of the satellite occur due to differences in temperature, color, or surface characteristics, it is possible that large disturbing torques will be present. Thus, this concept requires careful design of the entire spacecraft.

The pressures arising from the solar radiation come from two sources: electromagnetic radiation pressure and solar wind pressure. The electromagnetic radiation pressure is a function of the distance from the Sun and reflectivity of the body. Figure 2-102 shows this pressure over the range of parameters of interest. The solar wind pressure is variable and, due to the rotation of the Sun, not exactly radial. Little data is currently available, but based on the

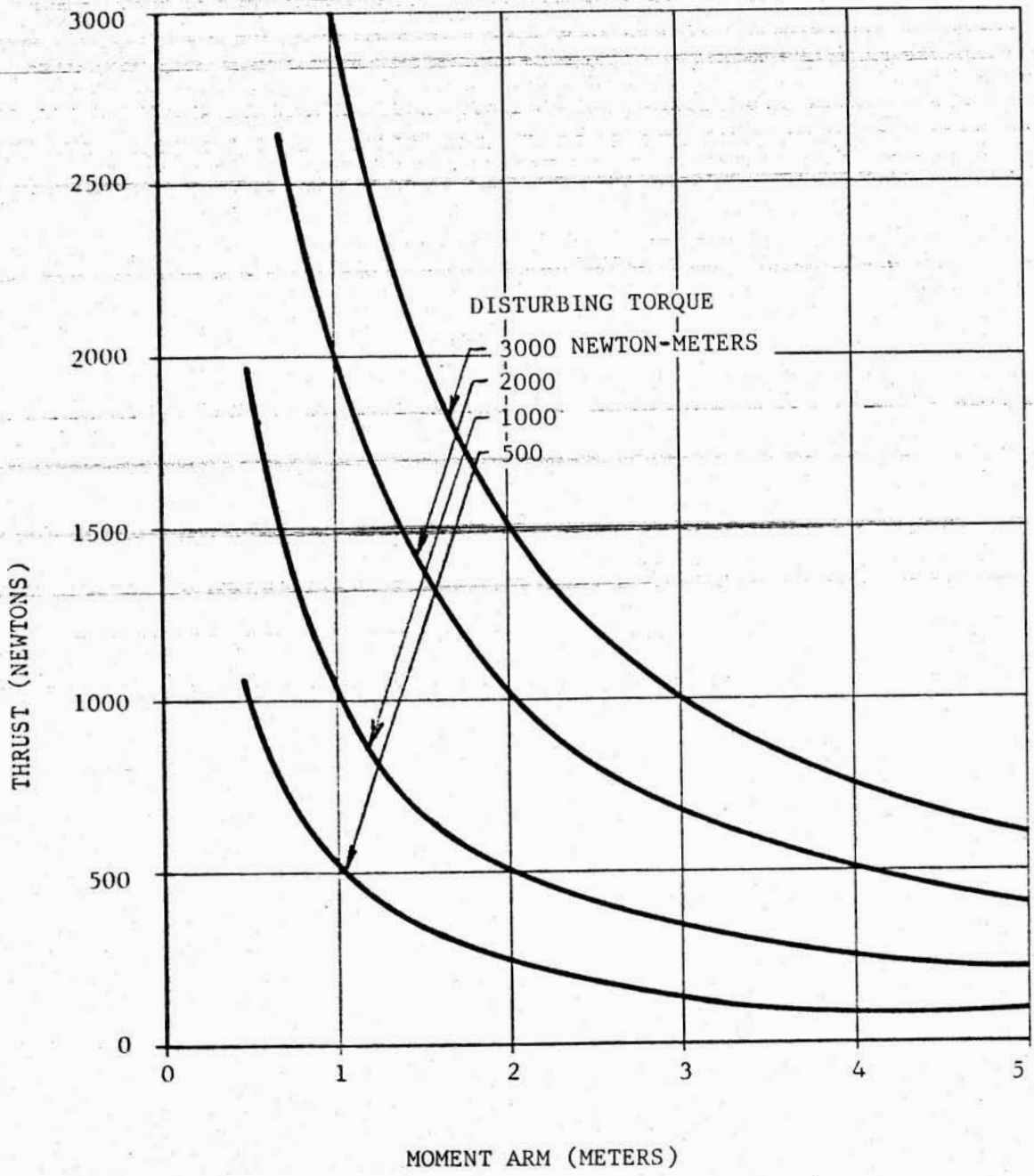


Figure 2-101. ATTITUDE CONTROL THRUST REQUIREMENTS VS THRUSTER MOMENT ARM

Table 2-16.

ATTITUDE CONTROL REQUIREMENTS-JUPITER ORBITER/SOLAR PROBE

LOW-THRUST SYSTEM:

Controlling Function	Torque (newton-meters)		Momentum (newton-meter-secs/mo)		Total Impulse (newton-seconds)	
	Jupiter	Solar	Jupiter	Solar	Jupiter	Solar
Coast stabilization	50	20	3×10^9	500	3.0×10^4	5.0×10^3
Antenna gimballing reaction	1.4×10^{-2}	1.4×10^{-2}	10	10	0.01×10^4	0.1×10^3
Other disturbances	$\sim 3 \times 10^{-4}$	$\sim 3 \times 10^{-4}$	$\sim .5$	$\sim .5$	(small)	(small)
Contingency	—	—	—	—	0.5×10^4	$.5 \times 10^3$
TOTALS					3.51×10^4	5.6×10^3

HIGH-THRUST SYSTEM:

Controlling Function	Torque (newton-meters)	Momentum (newton-meter-secs/event)		Total Impulse (newton-seconds)	
		Jupiter	Solar		
Thrust misalignment	200	5×10^4	—	5×10^4	
Booster separation torque	—	—	—	1×10^4	
Others and Contingency	—	—	—	1×10^4	
TOTAL					7×10^4

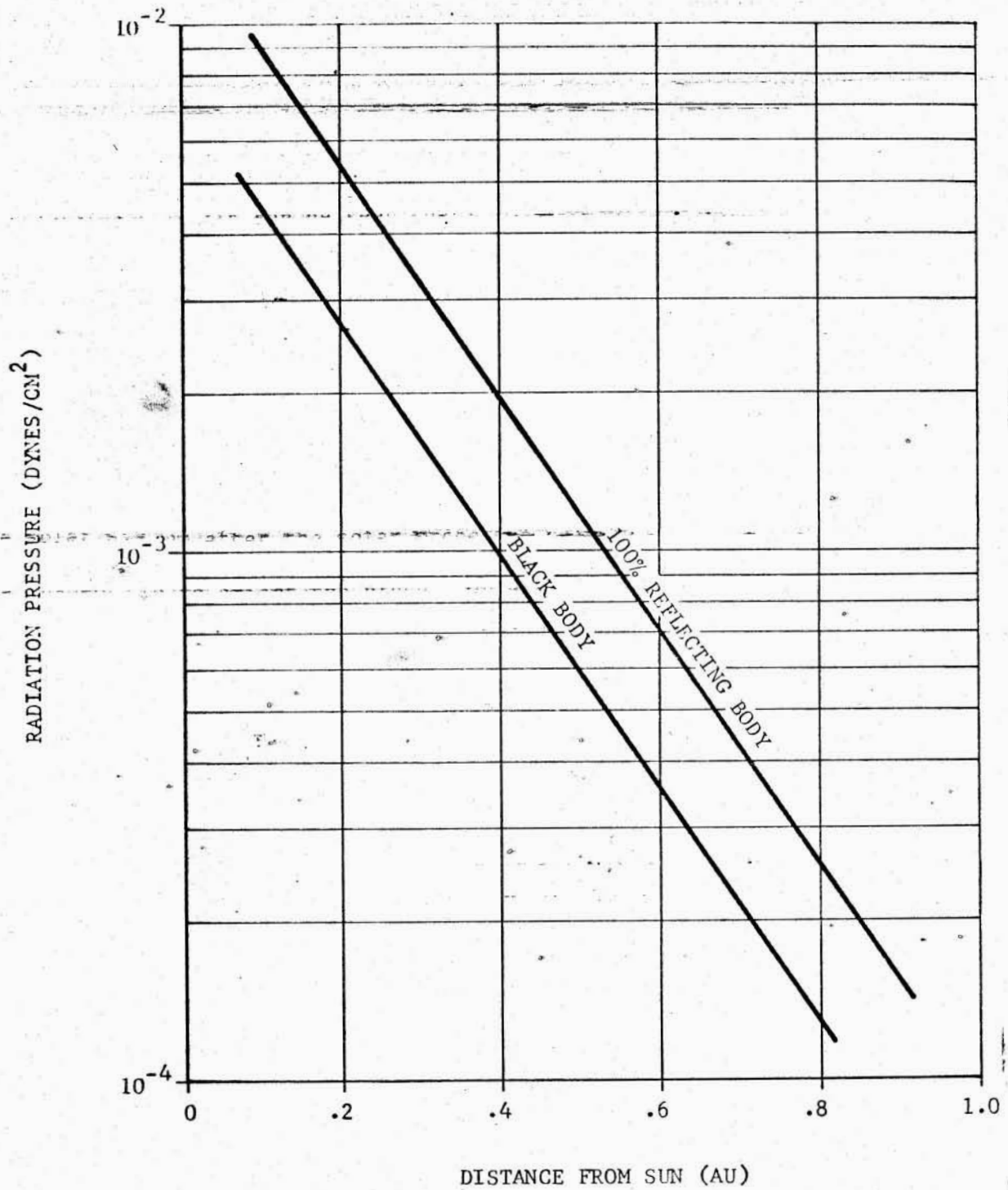


Figure 2-102. SOLAR RADIATION PRESSURE VS DISTANCE FROM SUN

Mariner spacecraft experiments, gross estimates can be made at this time. This is shown in Figure 2-103. It should be noted that this pressure is strongly dependent on solar surface activity and can vary considerably within the values shown herein. However, the pressure contribution of the solar wind is very small compared to the electromagnetic radiation pressure and only the latter effect need be analyzed for the passive attitude-control subsystem.

To convert this data to attitude control restoring torques, the concepts summarized in Figure 2-104 were developed. It can be seen that for reasonable configurations the solar pressure control subsystem produces quite small forces. To obtain reasonable torques, long moment arms must be considered for the control subsystem surfaces. This poses problems with thermal control of the booms or other structure supporting the surfaces from the spacecraft. By using large conical surfaces, it is believed that torques of the order of magnitude of 3×10^{-3} newton-meters can be achieved for a reasonable configuration. A review of Table 2-16 shows that this is the same order of magnitude as the antenna gimbaling and other disturbing torques. It can be concluded that the use of solar vanes will significantly contribute to the spacecraft stabilization at close-solar distances.

In the deep regions of the solar system after the solar probe has been separated from the Jupiter orbiter spacecraft, the solar radiation pressure attitude-control subsystem will be inadequate to orient the probe. An active subsystem using reaction gas nozzles will be required. It can be shown this subsystem is certainly useful at close-solar distances, also. The solar probe primary shadow shield must be continuously oriented toward the Sun during the close-solar approach. The perihelion velocity of the spacecraft is very high, as is the yaw rate to maintain orientation. For a typical mission, the close-solar probe travels from easterly to westerly elongation in about 7 days. This corresponds to a continuous yaw rate of 3×10^{-4} degrees/second. For the moments of inertia expected for the configuration in subsection 2.3, maneuver torques of about 10^{-4} newton-meters are required. This can be achieved by solar radiation pressure with the configurations under study. The reaction gas system can be used during the close-solar approach to maintain the gross Sun alignment of the spacecraft with the solar vanes acting as a redundant attitude-control subsystem.

The most common attitude-control subsystem used on spacecraft today is the reaction-gas subsystem. Much work and analysis has been undertaken on these systems so that their performance and limitations are well documented. Table 2-17 summarizes the primary characteristics of the three common concepts and Figure 2-105 presents the general mass trade-off relationships. The latter figure also indicates the order of magnitude of the total impulse anticipated for the Jupiter orbiter/solar probe. It can be seen that for the Jupiter orbiter a cold gas system is many times heavier than either the monopropellant or bipropellant systems. Also the bipropellant system does not offer a significant performance improvement at low total impulses over the monopropellant system considering the decrease in the reliability which the bipropellant system would impose on the spacecraft.

The midcourse maneuver generally consists of a number of separate corrections with a total impulse requirement of about 1.4×10^6 newton-seconds. Thus, a dual subsystem for midcourse correction and attitude control would have

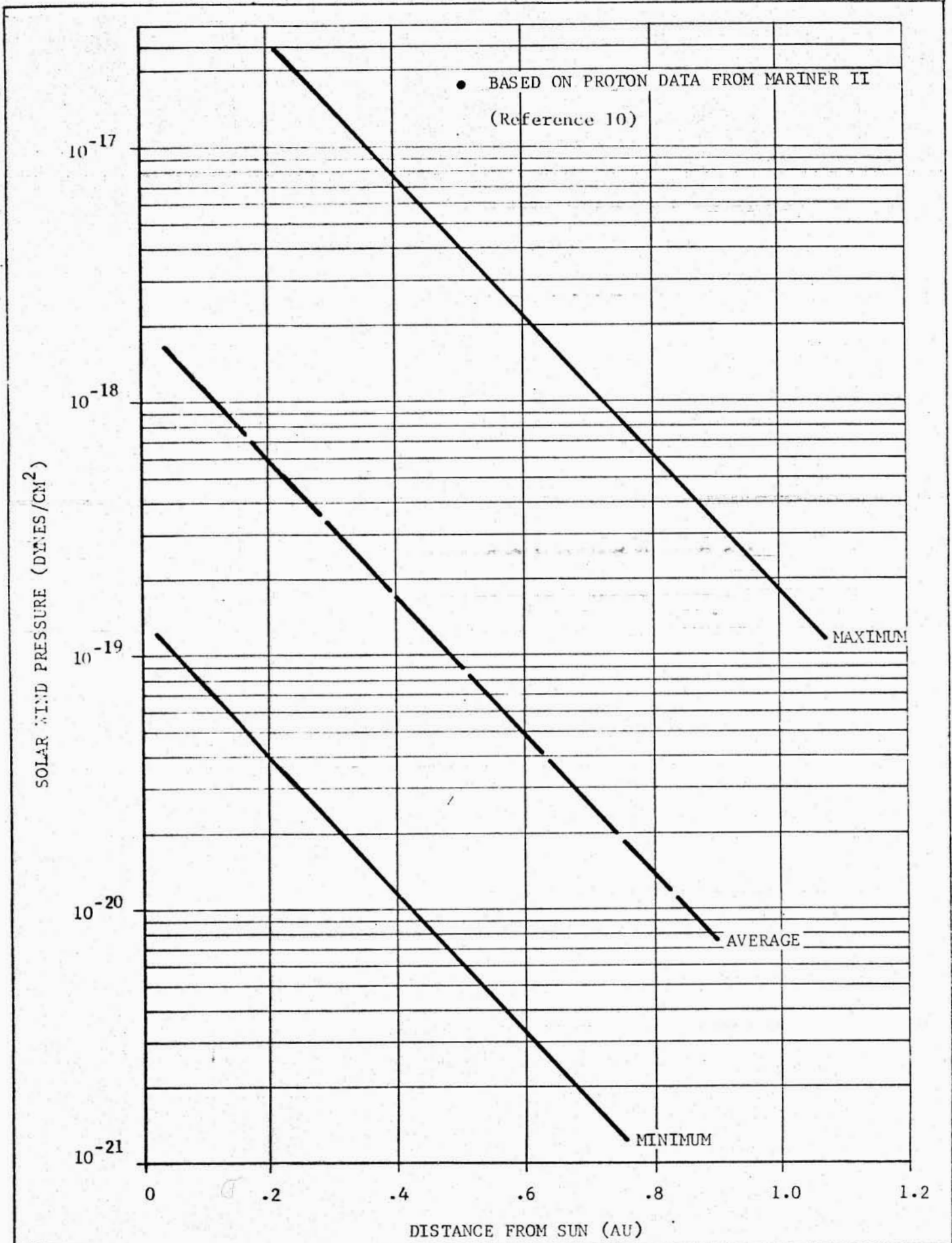


Figure 2-103. SOLAR WIND PRESSURE VS DISTANCE FROM SUN

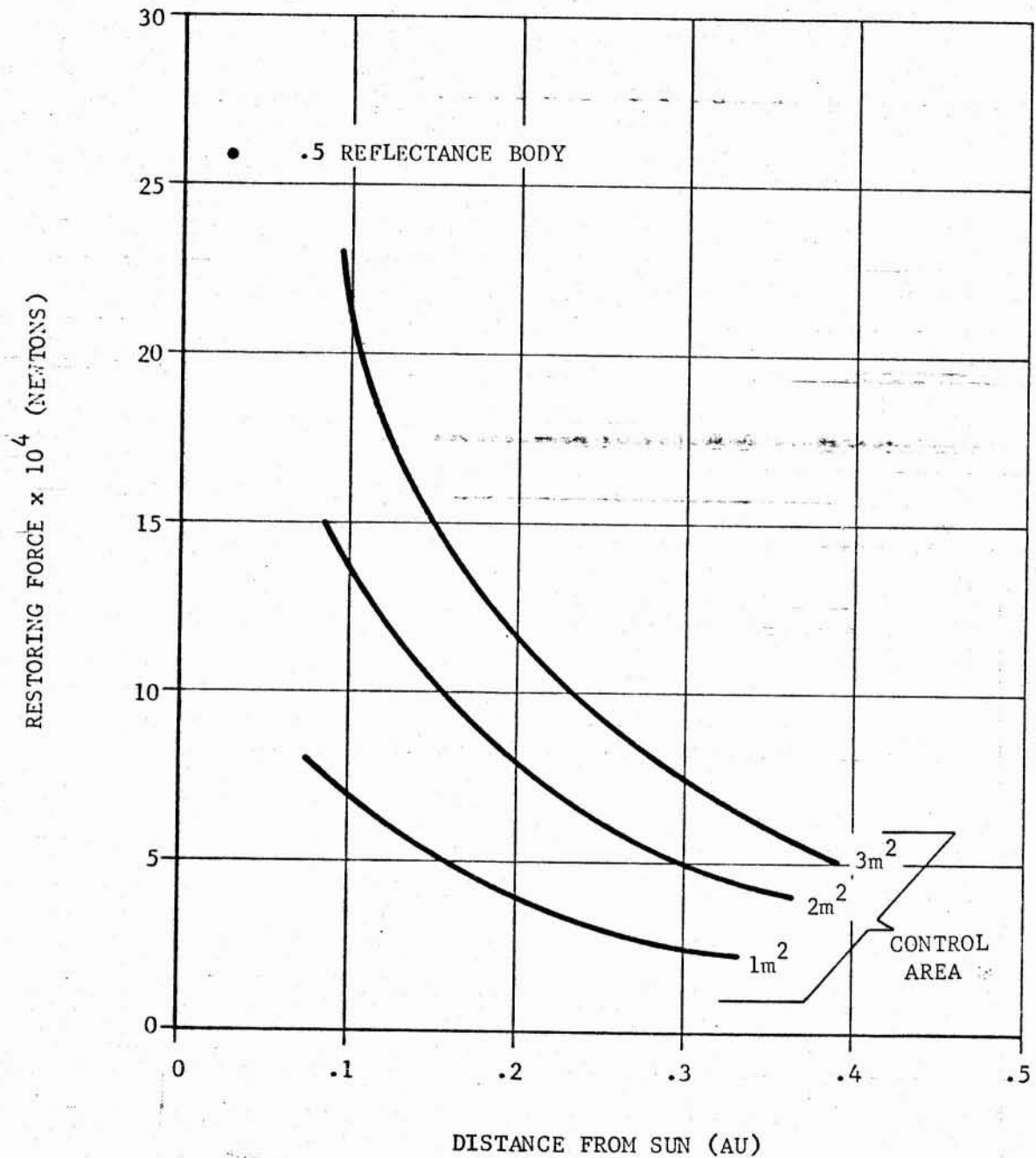


Figure 2-104. SOLAR RADIATION CONTROL FORCES VS DISTANCE FROM SUN

Table 2-17.
REACTION GAS SYSTEMS FOR ATTITUDE CONTROL

Control System	Engine Performance (Pulse-Mode)	Storage Requirements	System Performance	Reliability
<ul style="list-style-type: none"> • Stored Gas (unheated N_2) 	<ul style="list-style-type: none"> • $I_{sp} = 65$ sec • Response $\sim .010$ sec to 90% chamber pressure. 	<ul style="list-style-type: none"> • Large number of leak-tight valves. • No temperature problem although should be kept high. 	<ul style="list-style-type: none"> • For total impulse < 900 Newton-seconds lightest weight system. • Longest lifetime. 	<ul style="list-style-type: none"> • Simplest and most reliable
<ul style="list-style-type: none"> • Mono-propellant ($.75 N_2H_4 - .25 N_2H_5NO_3$) 	<ul style="list-style-type: none"> • $I_{sp} = 180$ sec • Response $\sim .035$ sec to 90% chamber pressure (warm bed) 	<ul style="list-style-type: none"> • Fuel freezes at $255^\circ K$ and must be insulated. • Large number of leak-tight valves and regulators. 	<ul style="list-style-type: none"> • Generally lightest weight system for total impulse > 900 Newton sec but < 3000 Newton sec. • Lifetime longer than bi-propellant. 	<ul style="list-style-type: none"> • More reliable than bi-propellant but less than stored gas.
<ul style="list-style-type: none"> • Bi-propellant ($N_2O_4 / .5 N_2H_4 - .5 UDMH$) Radiative cooling. 	<ul style="list-style-type: none"> • $I_{sp} = 200$ sec • Response $\sim .045$ sec to 90% chamber pressure. 	<ul style="list-style-type: none"> • Propellant freezes at $261^\circ K$ so must be insulated. • Large number of leak-tight valves and regulators. 	<ul style="list-style-type: none"> • Optimum for total impulse > 3000 Newton seconds. • Shortest life. 	<ul style="list-style-type: none"> • Least reliable

2-167

TR-292/3-6-075

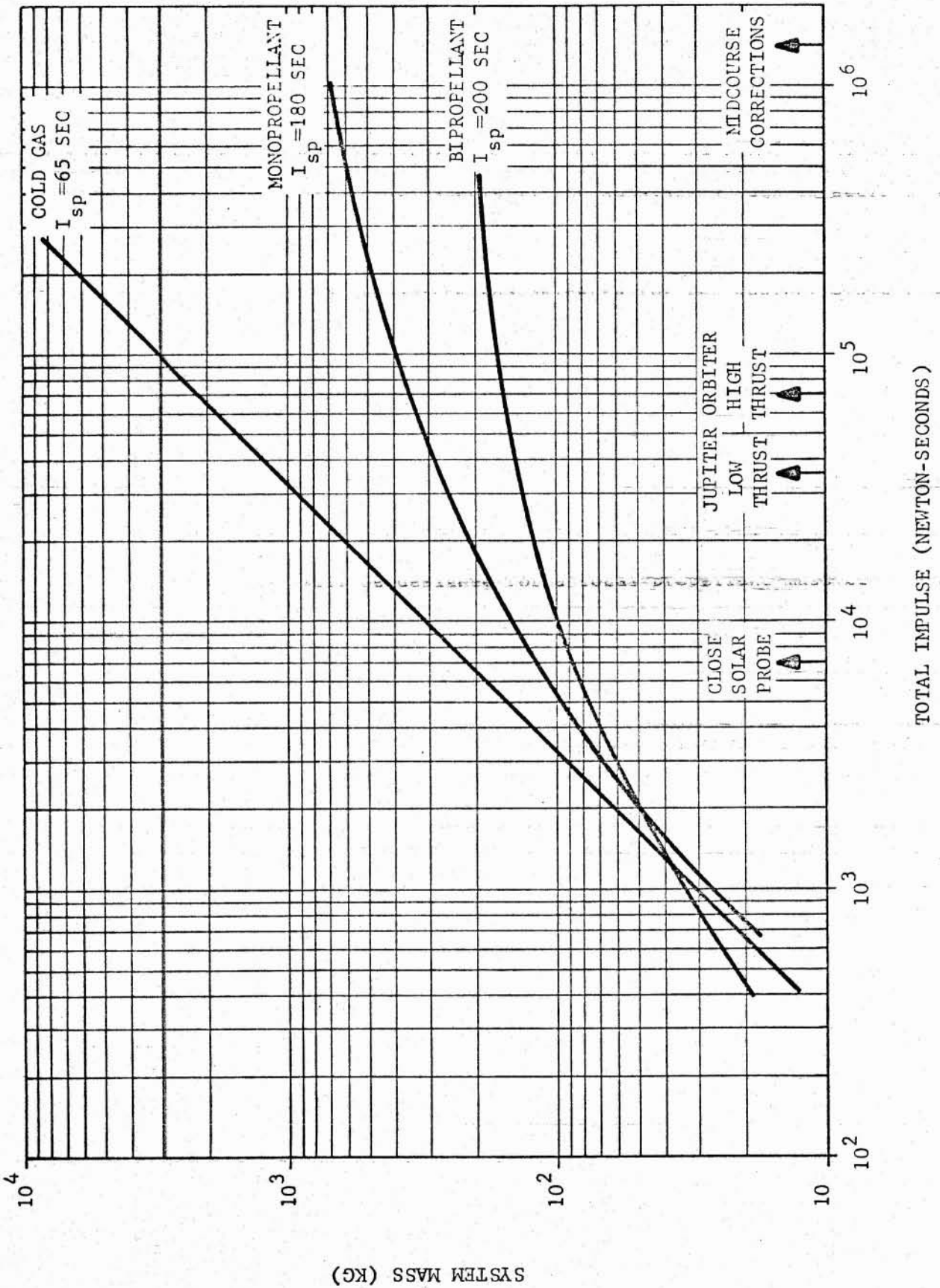


Figure 2-105. MASS VARIATION OF REACTION GAS ATTITUDE-CONTROL SYSTEMS VS TOTAL IMPULSE

to provide up to 1.5×10^6 newton-seconds total impulse. Table 2-18 summarizes the subsystem mass for different operational modes which can be considered. It can be seen that some mass saving could be realized by using a complete bipropellant system at these total impulses. However, the reliability of bipropellant equipment is relatively low, especially for subsystems such as attitude control which are actuated very often for short burn times. Based on previous experience, the weight penalties of using the monopropellants for attitude control should be accepted to maintain the subsystem reliability required. The monopropellant attitude-control subsystem was selected for the Jupiter orbiter. Both the high-thrust and low-thrust systems can use common propellant storage tanks.

It should be noted that subsystem mass is strongly influenced by the thrust misalignment torques at planetary capture braking. The preceding analysis used a total impulse of 7×10^4 newton-seconds for this function. This is rather high and represents a worst case condition. To optimize the spacecraft design, great care should be taken to permit symmetrical loading of the spacecraft and accurate alignment of the thrust vector at spacecraft assembly. Common practice for other propulsion systems in the space program specifies actual thrust misalignments less than one degree. The Jupiter orbiter spacecraft monopropellant attitude-control subsystem will be designed for a total propellant mass of about 80 kg which assumes that thrust misalignment of the planetary capture propulsion subsystem will be held to about .75 degrees.

The midcourse correction subsystem on the Jupiter orbiter could logically be a bipropellant subsystem using the propellants stored in the Jupiter capture propulsion subsystem tanks. This concept requires that the main tanks be kept pressurized throughout the mission. The disadvantage of maintaining this pressure is that the propellant lines and subsystem components will be subjected to working pressures for extended periods of time. This will have an effect on subsystem reliability. However, it may be argued that the simplicity achieved in integrating these propellant functions rather than provide a separate propulsion subsystem will offset this.

For the solar probe, the distinction between subsystems is less clear and to keep the tank volumes small, the monopropellant subsystem was selected. About 15 kg of propellant are required for the total impulse and thrust level discussed in the preceding subsection.

To summarize the selected systems, Table 2-18 presents the propellants, mass, and control parameters for the Jupiter orbiter/solar probe.

2.2.7 Guidance and Navigation

The guidance concept considered is the multiple-impulse radio command midcourse guidance system used in the Ranger and Mariner missions. The basic requirement is that the spacecraft have all the necessary onboard logic and control to complete its entire mission except for the numerical values of navigational quantities necessary for midcourse and terminal maneuvers. The navigation necessary to define the midcourse and terminal maneuvers will be based on a two-way Earth communications system with angle-tracking, doppler, and ranging information being analyzed to determine the proper maneuver commands. This guidance concept requires full attitude stabilization and is de-

Table 2-18. REACTION GAS SYSTEM MASS

Jupiter Orbiter Spacecraft

CONTROL PROPULSION			SYSTEM MASS		
Low thrust	High thrust	Course Correction	Monopropellant	Bipropellant	Total
Monopropellant	Monopropellant	Monopropellant	700 kg	—	700 kg
Monopropellant	Monopropellant	Bipropellant	550	170 kg*	720
Monopropellant	Bipropellant	Bipropellant	275	170 *	445
Bipropellant	Bipropellant	Bipropellant	—	190 *	190

ATTITUDE CONTROL SUMMARY FOR JUPITER ORBITER/SOLAR PROBE

FUNCTION	PROPELLANT		TOTAL IMPULSE		THRUST LEVEL			SYSTEM MASS	
	Jupiter	Solar	Jupiter	Solar	Jupiter Low	Jupiter High	Solar	Jupiter	Solar
Stabilization (Low thrust)	Mono.	Mono.	3.5×10^4 (n. sec)	5.6×10^3 (n. sec)	25 newtons	—	15 new.	} 120 kg	15 kg
Stabilization (High thrust)	Mono.	—	7×10^4	—	—	100 newtons	—		—
Course Correction	Bipro.	—	1.4×10^6	—	—	1000 newtons	—	170 kg	—

* Assuming bipropellant storage in planetary capture propulsion system tanks.

pendent on reliable communications over much greater transmission distances than have been previously attempted.

Attitude stabilization will require slaving two spacecraft axes to suitably selected celestial bodies so that inertial directions are continuously known with respect to the vehicle. Previous experience indicates that the Sun and the star Canopus are ideally suited for references. The Sun is ideal primarily because of mathematical convenience and also because well-designed sensors are available. Highly reliable units will be available in the next decade with accuracies better than 0.1 degree.

The star Canopus lies about 15° off the south celestial pole. It is a bright star and sensors are also available. In the next decade multiple-star trackers may be available to supplement a Canopus sensor and increase system accuracies. These devices accept light from many stars and track a portion of the star field. They have the potential advantage of nearly eliminating the problem of false identification.

For the early phases of the mission, prior to establishment of the heliocentric coast attitude, a secondary reference system is needed onboard the spacecraft. An inertial unit containing three gyroscopes must be included to permit the spacecraft to perform search modes to acquire the Sun and Canopus. This system is also necessary if the primary heliocentric coast reference frame is lost during the mission. The vehicle can initiate procedures for solar and Canopus search modes or orient an antenna to Earth using the secondary reference frame.

Floated rate-integrated gyros mounted to the body of the spacecraft will probably be utilized. In the next decade, other inertial components such as vibrating reed and fluid rotor gyroscopes may be available. They will provide greater reliability for the same accuracies.

There does not appear to be any particularly difficult problems associated with guidance and navigation for the Jupiter orbiter/solar probe mission other than subsystem reliability for the long durations.

2.2.8 Reliability Analysis

If there is more than one identical spacecraft available for launch in a space program, the probability of total program success can be defined as the probability that at least one of the spacecraft properly completes its mission. It can be shown that the mathematical relationship governing this probability is as follows:

$$P_T = 1 - (1 - p)^n ,$$

where P_T = probability of total program success
 p = probability of success of one spacecraft
 n = number of spacecraft in program .

This equation assumes that the probability of success of all the individual spacecraft in the program is identical. Figure 2-106 graphically depicts this relationship. The following discussion is presented to estimate the number of spacecraft required for a combination Jupiter/solar probe for a given program

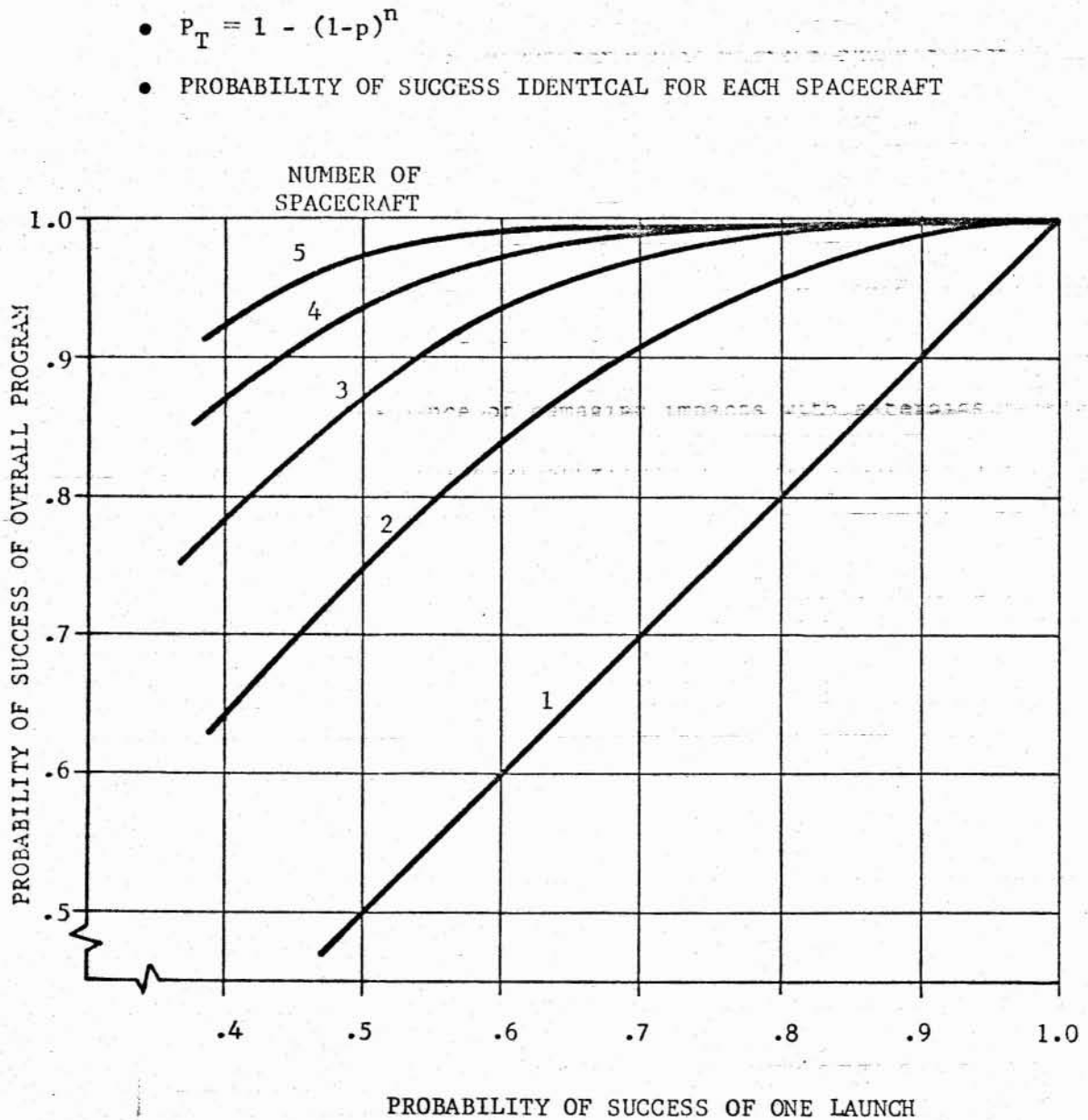


Figure 2-106. PROBABILITY OF PROGRAM SUCCESS AS A FUNCTION OF MULTIPLE SPACECRAFT LAUNCHES

success goal.

The probability of success of any one spacecraft is as follows:

$$p = (p_1)(p_2)(p_3)\dots(p_n),$$

where $p_1, p_2, p_3, \dots, p_n$ are the success probabilities of various functions of the spacecraft. For the purposes of this analysis, it can be stated that the functions of interest in a deep-space probe are those defined and discussed below.

p_1 = probability of successful Earth launch and injection. This is a function of the reliability of the launch vehicle, ground tracking and command systems, and ejection propulsion system.

p_2 = probability of electronic system success. That is, lack of random failures of electronic components. Such failures are naturally inherent in any spacecraft and can be minimized only by careful system design, proper testing, and improvement in the mean-time-to-failure of the components themselves.

p_3 = probability of avoidance of damaging impacts with asteroids. This is an independent function. Proper selection of launch dates and interplanetary trajectories can maximize successful avoidance.

p_4 = probability of success of all spacecraft subsystems such as proper thermal control, power generation, structural integrity, etc. This implies the successful completion of all maneuvers such as Sun and Canopus acquisition, midcourse corrections, braking maneuvers, etc. These are dependent on many onboard spacecraft subsystems acting in proper conjunction with one another.

p_5 = probability of proper design and installation of the scientific experiments so that the data returned is valid and interpretable. For missions to unknown regions of the solar system and distant planets this can become an important aspect of program success.

p_6 = probability of successful operation of the ground systems associated with tracking, command and control, data retrieval, etc.

From this list, it can be seen that the accurate prediction of the probability of program success is very complex. In this analysis only the problems associated with the spacecraft will be considered and it will be assumed that successful ground-system operations are achieved. Also, no attempt will be made to evaluate the probability that onboard experiments are valid. These assumptions are equivalent to stating that $p_5 = p_6 = 1$. The initial equation defining the probability of any one spacecraft's success then reduces to:

$$p = (p_1)(p_2)(p_3)(p_4).$$

The following subsections discuss these parameters in detail and present a range of values for $p_1, p_2, p_3,$ and p_4 to be expected for the Jupiter orbiter/solar probe. Anticipating those results and summarizing the probability of total program success, Tables 2-19 and 2-20 present the parametric data developed in

this study for the spacecraft on a 600- and a 1200-day mission. This is believed to represent the range of mission durations typical for Jupiter/solar probes. Based on the assumptions shown with the data, Tables 2-19 and 2-20 present the total individual spacecraft success versus launch year. These values can then be used in conjunction with Figure 2-106 to indicate the number of spacecraft required to achieve any given total-program-success goal.

For the Jupiter orbiter/solar probe mission with both spacecraft launched together, complete mission success can be defined as both probes from one launch successfully completing their experiments. Likewise, partial mission success can be defined as only one of the probes of any one launch completing its experiments. For the latter case, total program success can then be achieved only by another launch of both spacecraft (because of the integrated design) even though one probe has already been successful. Thus, for the purposes of this study to determine the number of spacecraft desired in the program, this latter case can be considered as a failure since another launch is necessary.

If it is assumed that the Jupiter probe has a mission life of 600 days and the solar probe a mission life of 1200 days, the total probability of success for any one launch is the product of the individual spacecraft successes shown in Tables 2-19 and 2-20. Finally, Table 2-21 summarizes the number of spacecraft required in the program for various program-success goals. Because we are considering SATURN V launches, it can be concluded that it will be expensive to achieve very high program-success probabilities with a conservative extrapolation of subsystem failure rates. Up to 4 SATURN V launches may be required early in the next decade.

2.2.8.1 Probability of Successful Launch (p_1). The history of American launch vehicles is summarized in Figure 2-107. This curve is a comparison of some of the more commonly used boosters developed in this country for unmanned satellites or space probes. The data shows the history of the cumulative probability of successful launch on an annual basis throughout any booster's program. That is, at the end of any given year, the curve indicates the proportion of successful launches completed to that date.

It can be seen that, except for Juno II, all programs exhibited a steady improvement early in their history and then a general tendency to level off. For this to occur, the probability of success for each individual launch must continuously increase throughout any program. This effect is shown in Figure 2-108 for the same launch vehicles. On this curve, the probability of success for each specific launch is shown throughout the space of the U. S. booster development program. A range of values due to the spread of data in Figure 2-107 occurs for the early portions of the space program.

This data shows that a reasonably high launch reliability is currently possible. Extrapolating into the next decade, values greater than .97 for any one launch appear possible.

Because this data is a composite of many launch vehicles, it may not be exact for a specific booster type. For example, the Thor-Delta booster has demonstrated an individual performance history better than average and the SATURN and Titan families have experienced perfect performance. However, for the purposes of this study, the extrapolation shown on Figure 2-108 was used.

Table 2-19.

PROBABILITY OF JUPITER ORBITER SUCCESS FOR 600-DAY MISSION

Parameter	Year	1968	1970	1972	1974	1976	Assumptions
p_1 = probability of successful launch.		.971	.976	.980	.983	.985	Extrapolation of past booster history.
p_2 = probability of electronics success.		.915	.940	.952	.956	.957	Two complete and equal electronics systems. Two component failures end one system's usefulness. Conservative failure rate extrapolation.
p_3 = probability of avoidance of asteroid-induced failure.		.99	.99	.99	.99	.99	Postulated asteroid flux. Average asteroid velocity = 30 km/sec. Time in asteroid belt = 16% mission duration. Structural skin density = 336 kg/m ² .
p_4 = probability of systems success.		.955	.965	.975	.977	.980	Extrapolation of past system history.
$p = (p_1)(p_2)(p_3)(p_4)$.840	.876	.899	.966	.969	Combined Probabilities.

Table 2-20.

PROBABILITY OF CLOSE SOLAR PROBE SUCCESS FOR 1200-DAY MISSION

Parameter	Year	1968	1970	1972	1974	1976	Assumptions/Remarks
p_1 = probability of successful launch.		.971	.976	.980	.983	.985	Extrapolation of past booster history.
p_2 = probability of electronics success.		.85	.89	.91	.92	.924	Two complete and equal electronic systems. Two component failures end one system's usefulness. Conservative failure rate extrapolation.
p_3 = probability of avoidance of asteroid-induced failure.		.98	.98	.98	.98	.98	Postulated asteroid flux. Average asteroid velocity = 30 km/sec. Time in asteroid belt = 16% mission duration. Structural skin density = 336 kg/m ² .
p_4 = probability of systems success.		.955	.965	.975	.977	.980	Extrapolation of past system history.
$p = (p_1)(p_2)(p_3)(p_4)$.771	.820	.853	.865	.873	Combined Probabilities.

Table 2-21.

NUMBER OF SPACECRAFT REQUIRED TO ACHIEVE DESIRED SUCCESS PROBABILITY FOR JUPITER ORBITER/SOLAR PROBE

Year	Probability of success of Jupiter probe	Probability of success of solar probe	Probability of success per launch	Mission success goal	Number of spacecraft in program	Mission success goal	Number of spacecraft in program	Mission success goal	Number of spacecraft in program
1968	.840	.771	.648	.8	2	.9	3	.99	5
1970	.876	.820	.718	↓	2	↓	2	↓	4
1972	.899	.853	.768	↓	2	↓	2	↓	4
1974	.966	.865	.836	↓	1	↓	2	↓	3
1976	.969	.873	.846	↓	1	↓	2	↓	3

2-177

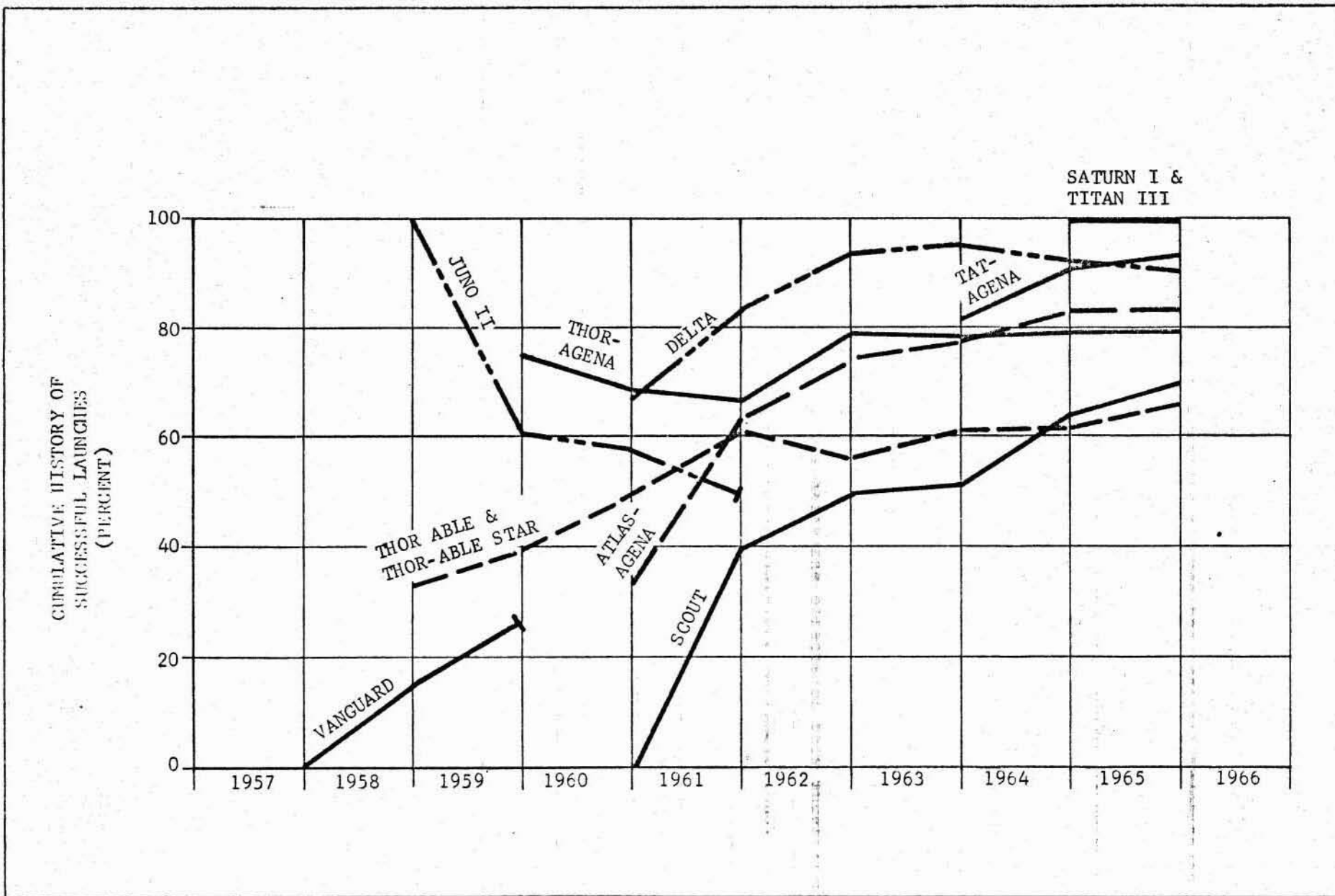


Figure 2-107. BOOSTER SUCCESS HISTORY VS LAUNCH DATES (UNMANNED SPACECRAFT)

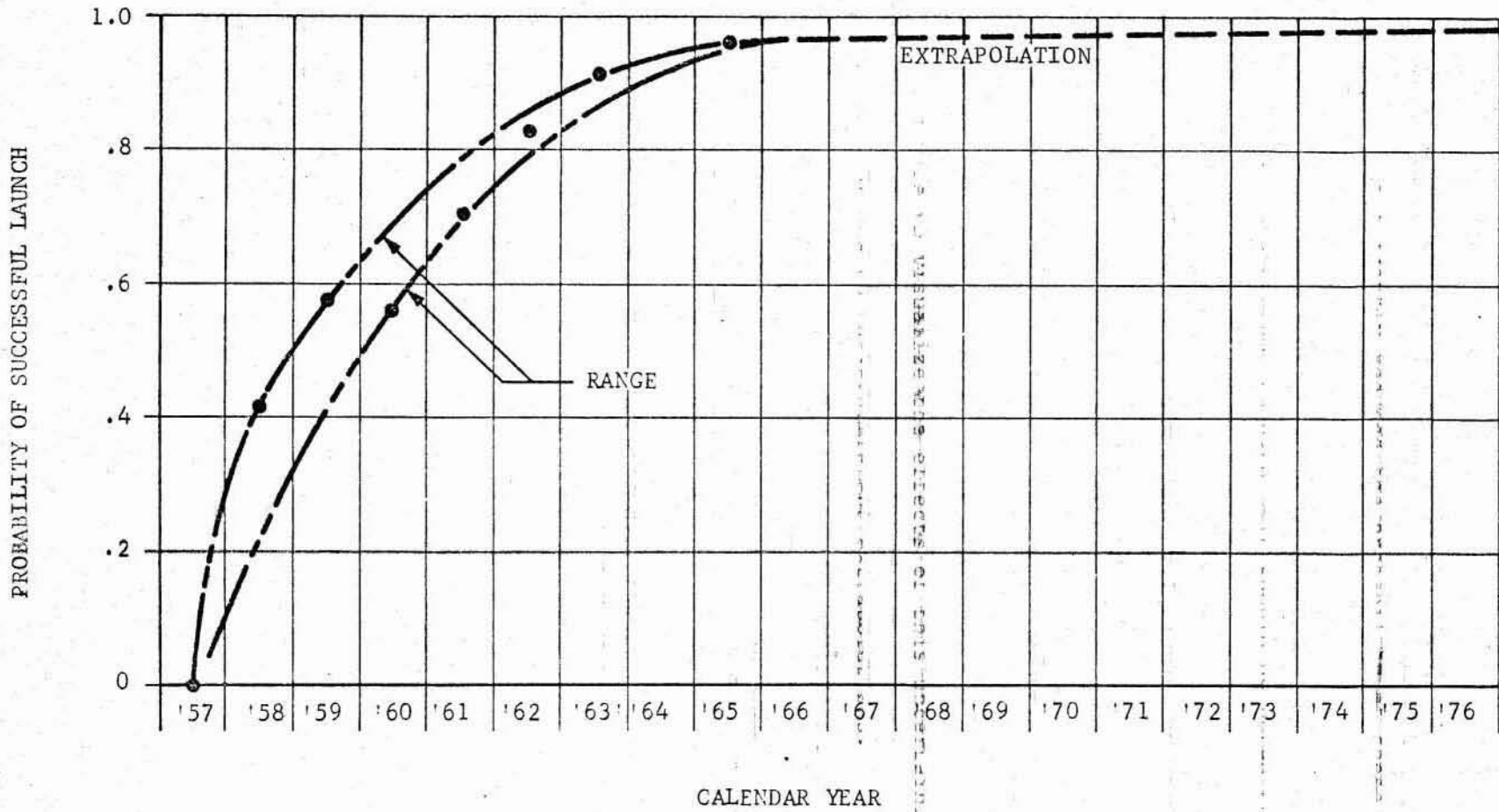


Figure 2-108. LAUNCH SUCCESS EXPECTATION (UNMANNED SPACECRAFT)

2.2.8.2 Probability of Success of Electric Components (p_2). Due to the normal problems associated with manufacturing, testing, and operating, all components in electronic systems are subject to random failures. Improvement in fabrication techniques in recent years have greatly reduced the probability of these failures and further advances are expected. Figure 2-109 shows the evolution in electronic component failure rates since the beginning of the space age. This data was compiled from research completed by the Bell Telephone Laboratories on the electronic failures of American space systems to date. It should be noted that this data and the following analysis does not include such system failures as poor solder joints, short circuits, broken wires, etc. The results must therefore be qualified somewhat to account for these modes of electronics failure.

In this analysis, a weighted average was developed and extrapolated into the next decade. This weighted average, shown on Figure 2-109, is based on what is considered the typical proportions of electronic components in space systems. Any specific satellite will deviate from this breakdown but probably not enough to significantly alter the broad results of this study.

Both a conservative and optimistic extrapolation of the expected component failure ratio was made to visualize the effects of this uncertainty. It will be shown that a significant difference in the predicted probability of program success will occur due to these different extrapolations.

The failure rates of electronic components can be converted to mean-time-to-failure (MTF) through the use of Figure 2-110. In this relationship the number of components onboard the spacecraft are important and, the figure shows typical values for small satellites, large deep space probes, and Apollo-type manned systems.

It should be noted that these curves assume that one component failure results in termination of the system life. This may be true if the component is in a critical circuit, but in the past some spacecraft have experienced one or two component failures and still remained in operation. Although their use may be compromised, such occurrences cannot be categorized as program failures. We will discuss later the effects which accepting multiple component failures have on the probability of system success.

The system MTF can now be converted to probability of success through the well known exponential reliability law noted on Figure 2-111. Finally, all this data can be combined to show the probability of electronic system success as depicted in Figure 2-112. In this figure, the effects of variances in extrapolating the component failure rate data as discussed above are apparent. If component failure rates are improved according to the optimistic extrapolation, very high electronic system reliability can be expected in the next decade. However, for the conservative extrapolation, means to further improve the system reliability should be considered.

The technique most often used for increasing the probability of electronics success in space systems is redundancy. In this analysis, two techniques were studied as follows:

- Provide one or more equal onboard electronic systems which all operate continuously. The failure of one system does not interfere

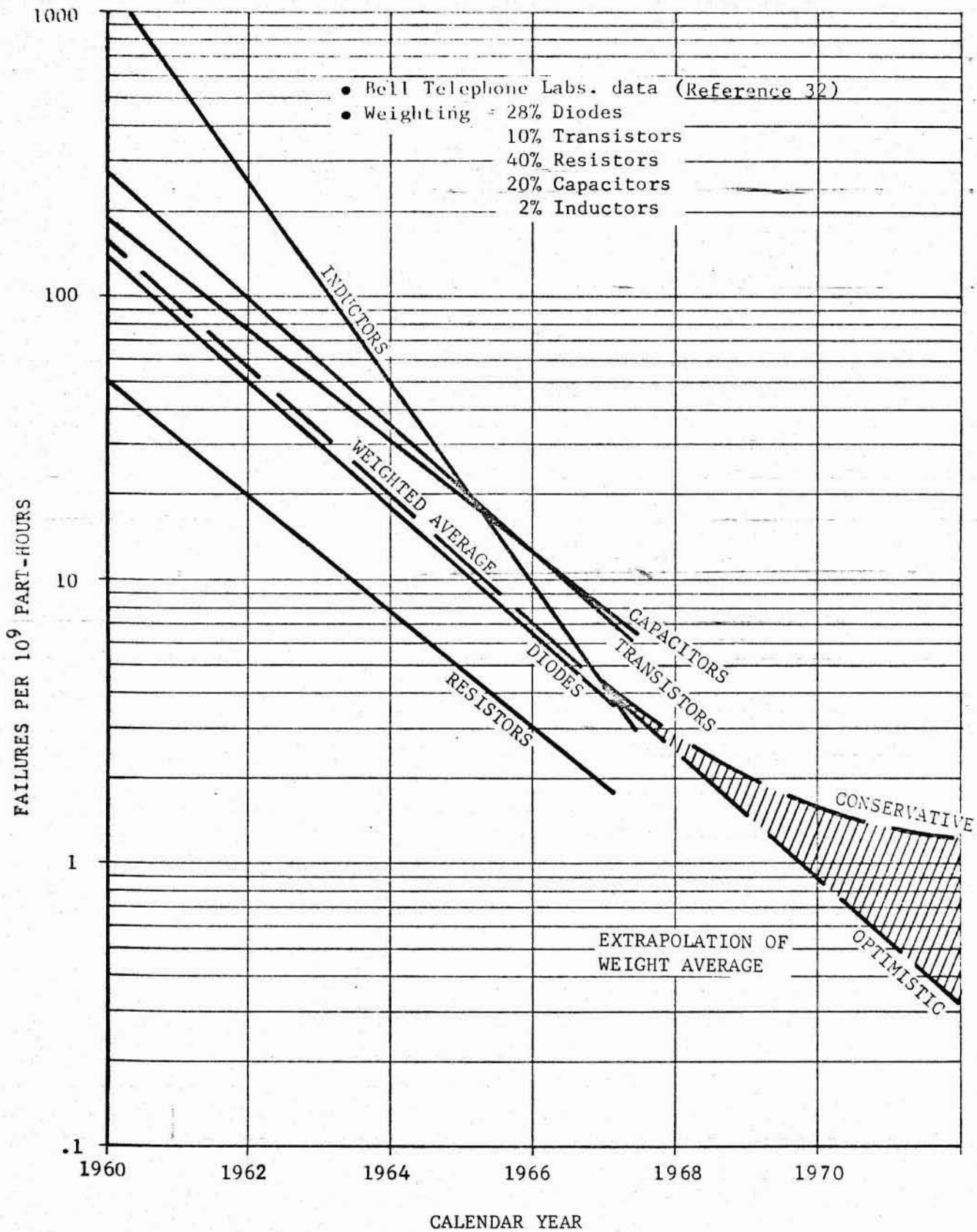


Figure 2-109. COMPONENT LIFETIME IMPROVEMENT

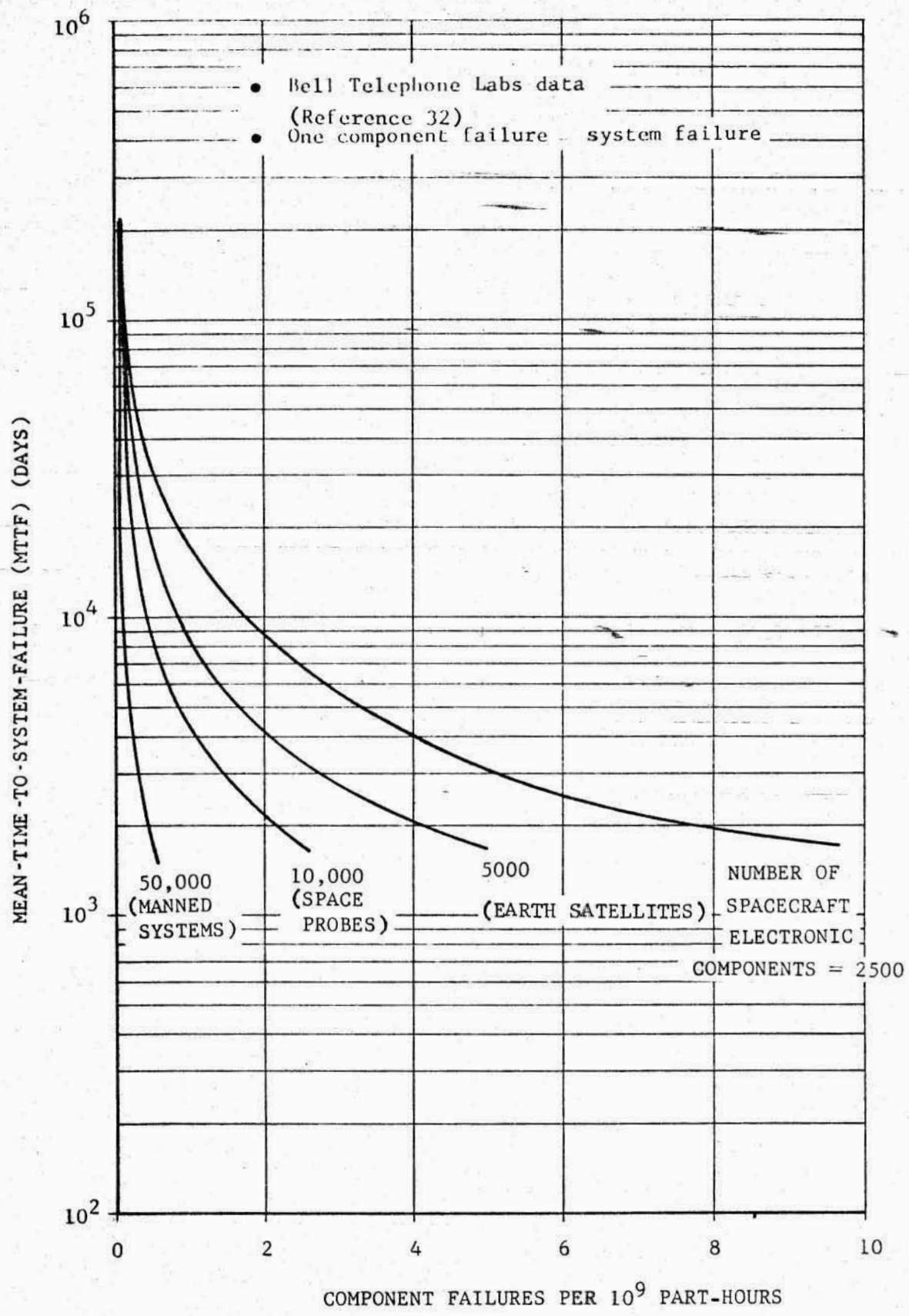


Figure 2-110. MEAN-TIME-TO-FAILURE VS COMPONENT FAILURE RATES

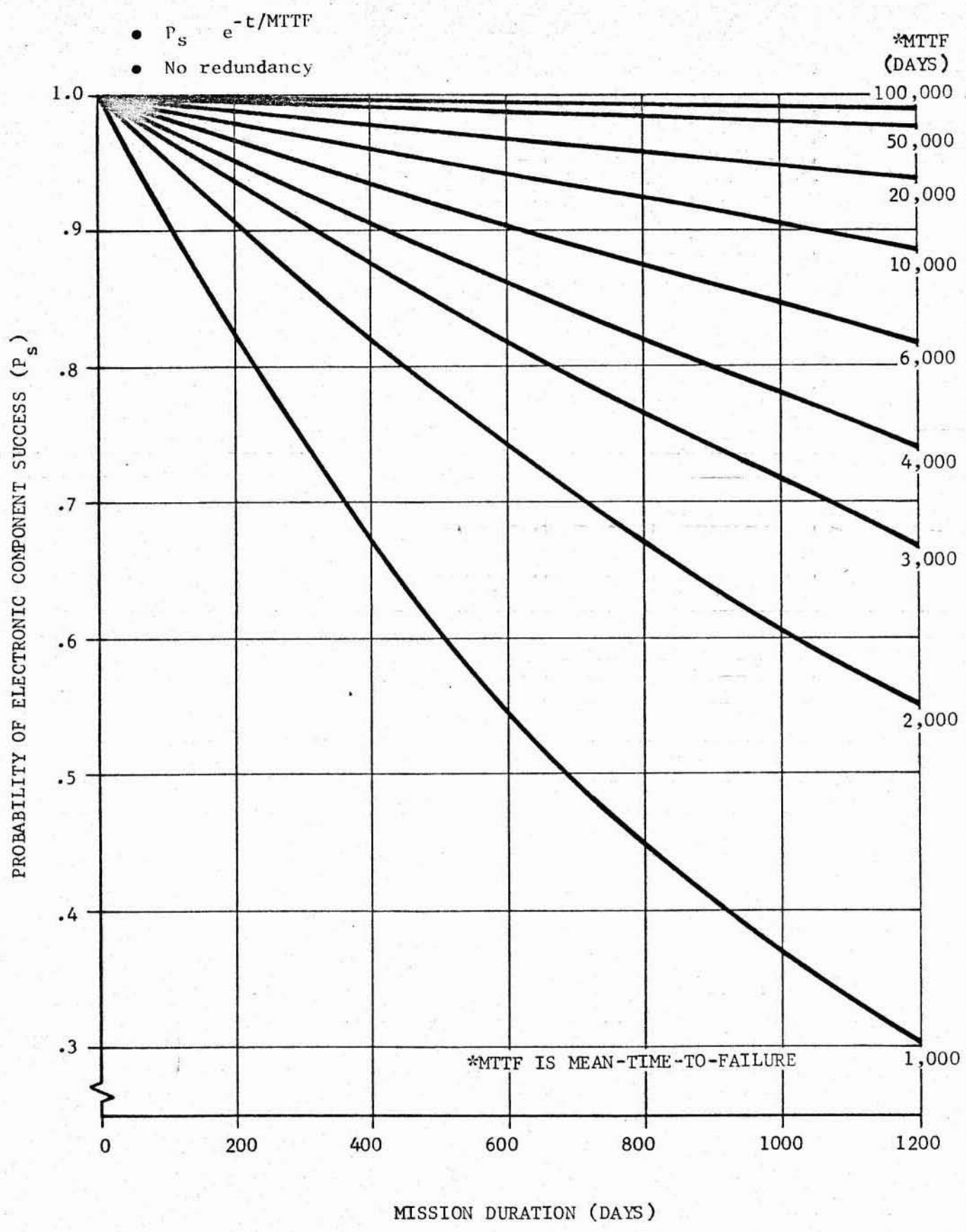


Figure 2-111. PROBABILITY OF ELECTRONIC COMPONENT SUCCESS VS MISSION DURATION

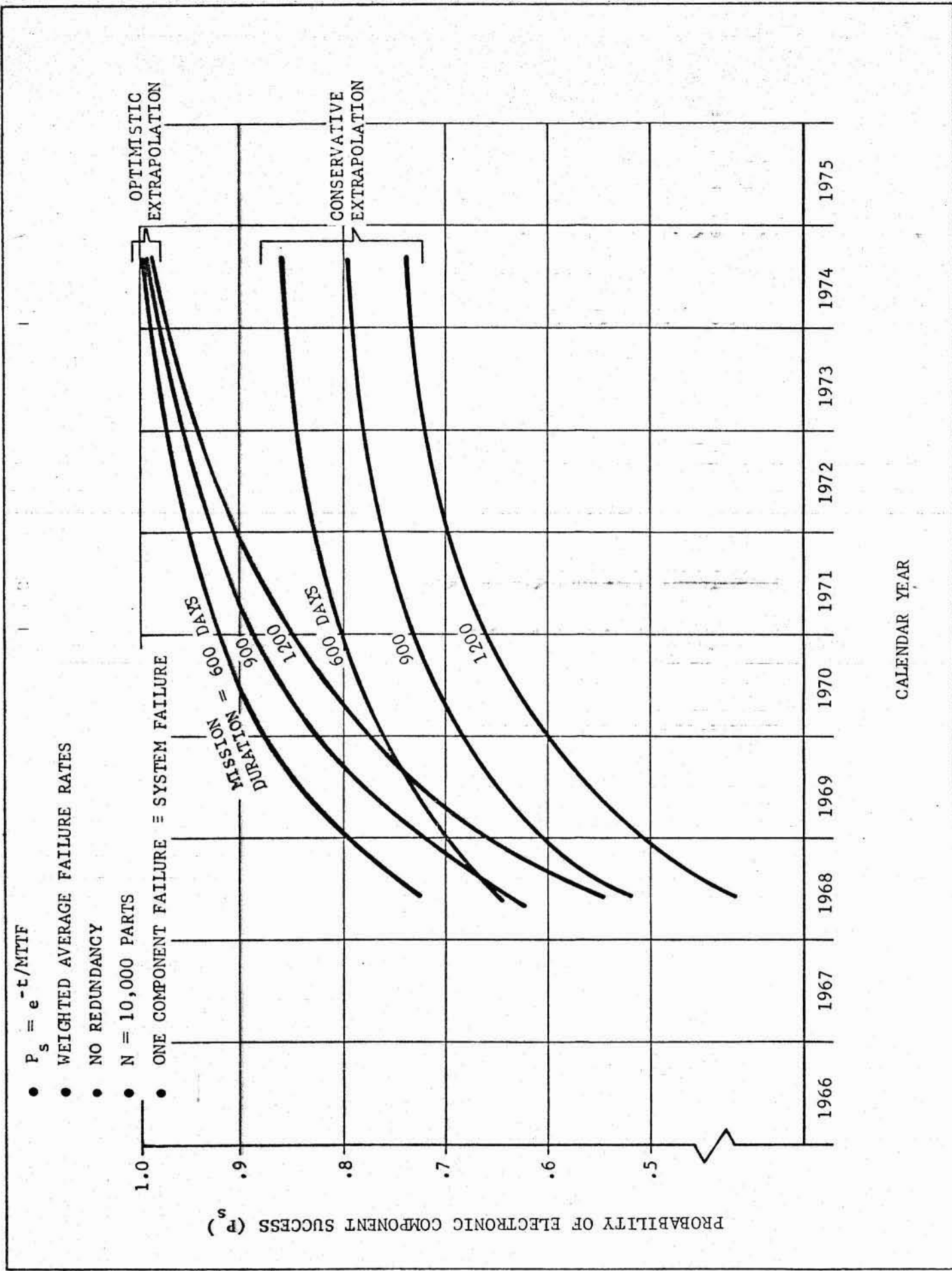


Figure 2-112. EXPECTED ELECTRONIC COMPONENT SUCCESS OF DEEP-SPACE PROBES VS TIME

September 1966

with the operations of the other systems. System lifetime requirement is identical for all systems and equal to the mission lifetime.

- Provide one or more equal onboard electronic systems which are operated sequentially. At some predetermined point in the mission or at the time of one system failure, a new electronic system, which has not been used up to that time, is activated. System lifetime is, on the average, only the $1/n$ proportion of the mission lifetime where n is the number of equal onboard systems.

Figure 2-113 indicates the improvements to be expected in the first case. These curves were drawn for a specific failure rate of 2 failures per 10^9 part-hours as an example. For other failure rates the same effects would be noted but the position of the curves would be displaced on the grid. From this data it can be seen that, as an example, to achieve a .9 probability of success for a 1200-day mission (approximately 3.3 years), five equal redundant electronic systems are required onboard the spacecraft. It can also be seen that to increase the probability of success to .99 an absurd redundancy of about 58 equal systems is necessary. A review of Figure 2-106 will show that it appears to be more reasonable to provide more than one spacecraft in a program to achieve high program-success probabilities if the failure rate depicted in Figure 2-113 has to be accepted.

For the second mode of redundancy, i.e., sequentially switching electronic systems, the lifetime for which any one component is expected to operate is considerably reduced but the problems concerned with storage, checkout, and inflight switching are introduced. It is not known at this time what probability of success can be expected for such functions. However, the parametric data summarized in Table 2-22 indicates that for the first half of the next decade, switching reliability must be of the order of .985 to more than 1.0 for this operational mode to show an advantage in overall mission probability of success. This approach appears useless for further consideration.

In all of the preceding analyses, it has been assumed that one electronic component failure constitutes a system failure. As discussed earlier, this may occur if the component is in a critical circuit. However, space systems have survived single failures many times in the past. Figure 2-114 shows the probability of electronics success for various multiple component failures. Considerable improvement can be noted if the spacecraft can accept more than one failure. This effect, combined with redundancy, raises the probability of success to satisfactory values in most cases.

To summarize this analysis of electronic component failures, let us postulate a typical mission, and develop the probability of success of the electronics systems for a single spacecraft. Consider a 1200-day mission as an extreme example, launched in 1974. From Figure 2-114, a total electronics system success of .735 can be expected for the conservative extrapolation of component failure data. If we are lucky and the spacecraft survives one component failure, Figure 2-114 shows that this value is increased to .85. Finally, by providing completely redundant electronics, a further increase to .92 is achieved.

By a similar process, the data presented in Tables 2-19 and 2-20 was

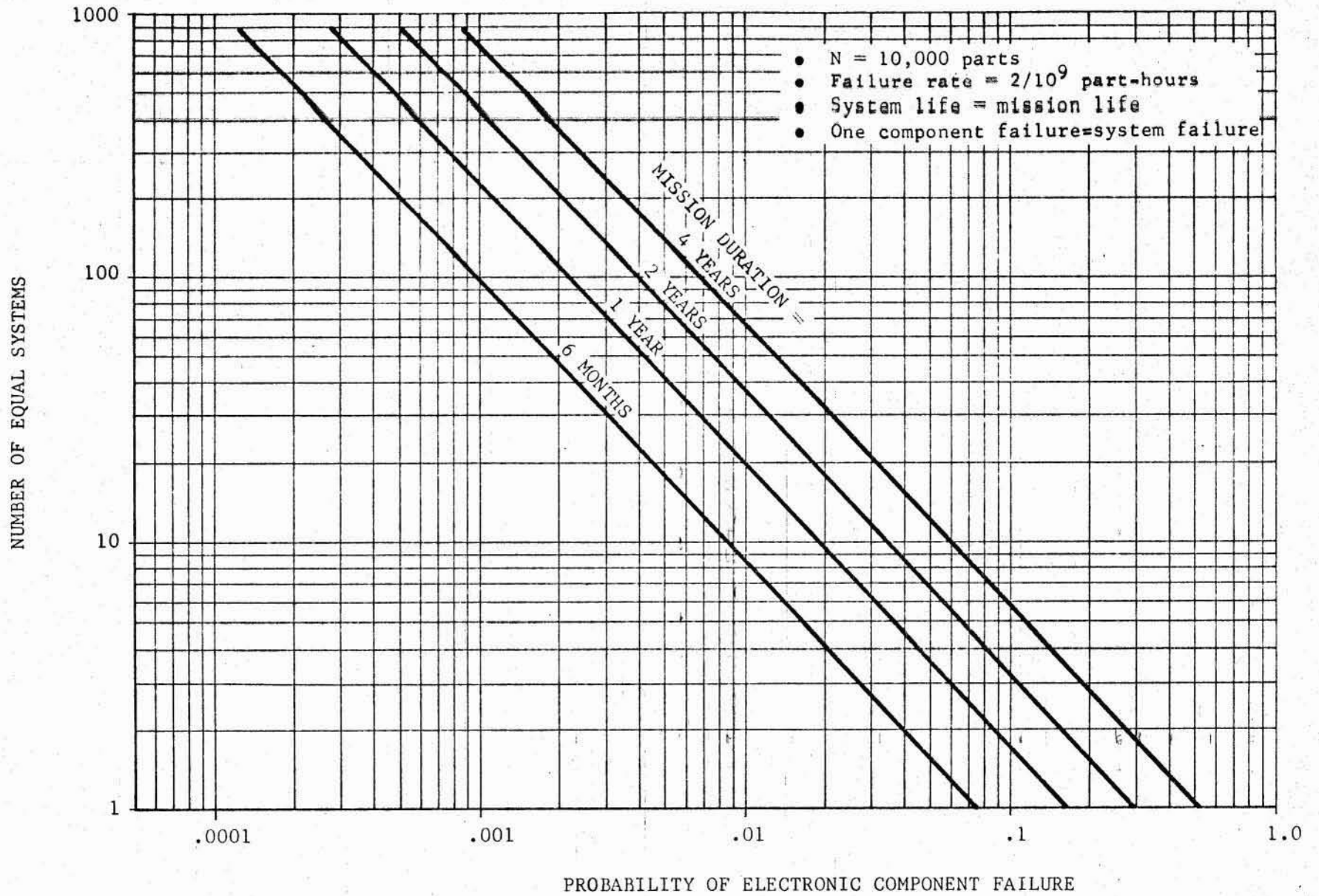
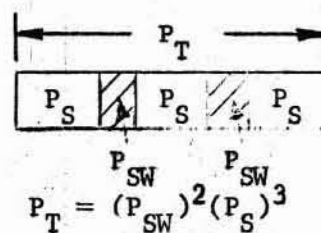
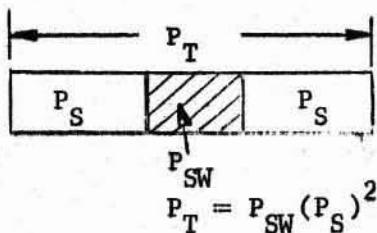


Figure 2-113. EFFECT OF REDUNDANCY UPON ELECTRONIC COMPONENT FAILURE

Table 2-22. SEQUENCING DUPLICATE SYSTEMS TO ACHIEVE DESIRED MISSION SUCCESS



Year	T (days)	t (days)	P _S	P _T	P _{SW} Reqmt.
1968	600	300	.817	.658	.985
	1200	600	.658	.436	.995
1970	600	300	.900	.813	.995
	1200	600	.813	.660	1.000
1972	600	300	.918	.843	1.000
	1200	600	.843	.710	1.000
1974	600	300	.925	.858	>1.000
	1200	600	.858	.736	>1.000

Year	T (days)	t (days)	P _S	P _T	P _{SW} Reqmt.
1968	600	200	.871	.658	1.00
	1200	400	.757	.436	1.00
1970	600	200	.931	.813	>1.0
	1200	400	.870	.660	>1.0
1972	600	200	.943	.843	>1.0
	1200	400	.891	.710	>1.0
1974	600	200	.949	.858	>1.0
	1200	400	.901	.736	>1.0

Definitions:

P_T = Total probability of success to duplicate single system operation with no redundancy and one component failure terminating system life.

P_S = System probability of success of lifetime t.

P_{SW} = Switching probability of success required to achieve at least P_T.

T = Total mission duration.

t = System average lifetime requirement.

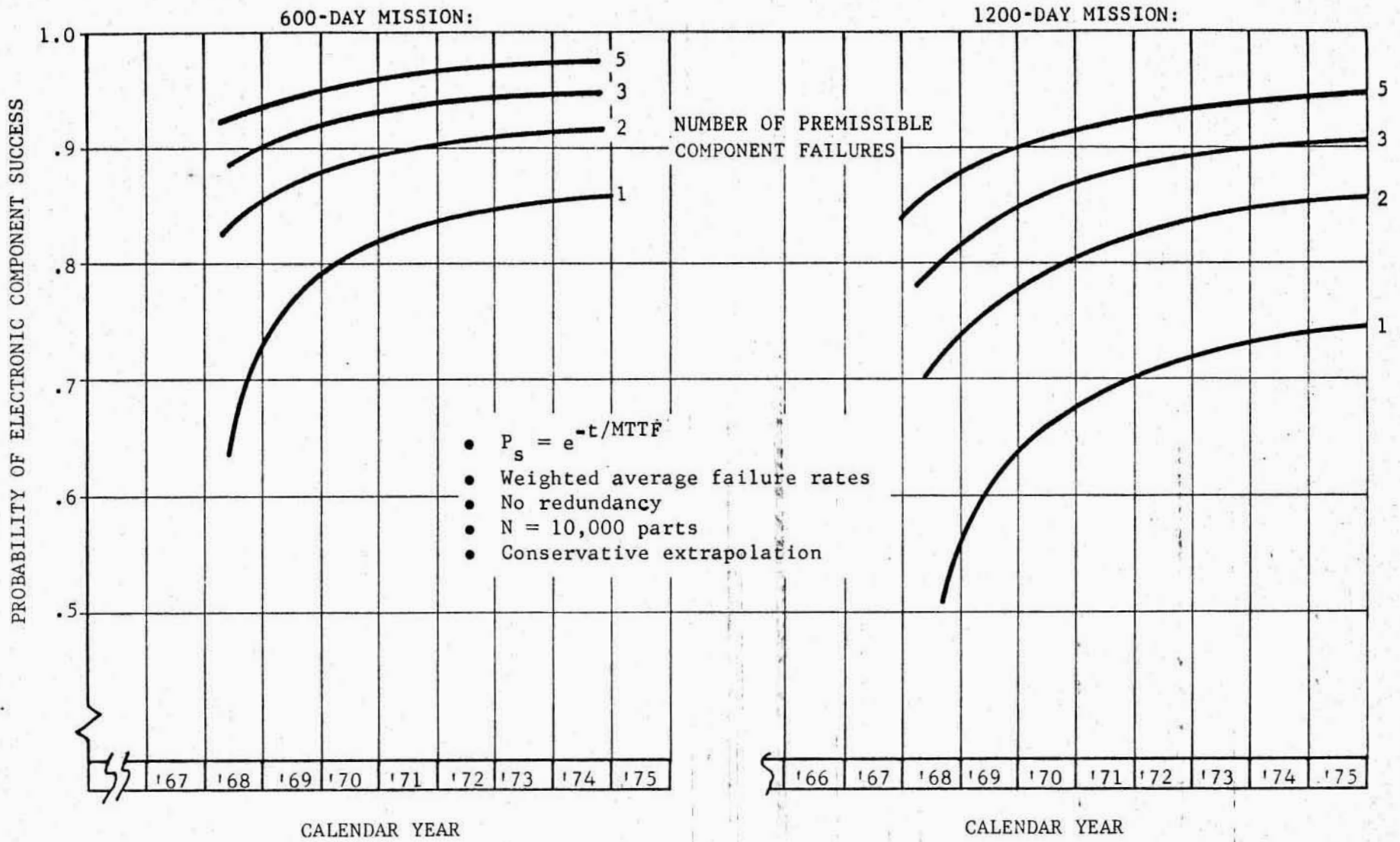


Figure 2-114. EFFECT OF MULTIPLE COMPONENT FAILURE ACCEPTANCE UPON MISSION SUCCESS FOR 600- AND 1200-DAY MISSIONS

prepared to indicate the estimated electronics reliability for spacecraft through the early part of the next decade. As noted earlier, such failures as poor solder joints, short circuits, broken wires, etc. are not accounted for herein and the data must be considered a little optimistic because of the possibility of these failure modes occurring.

2.2.8.3 Probability of Asteroid Avoidance (p₃). All of interplanetary space is apparently filled with particulate matter ranging from microscopic dust to large asteroids. The asteroid belt, lying between Mars and Jupiter contains the greatest mass concentration. Accurate data on the size and flux of this matter is not available, but fragmentary results from astronomical observations and the few interplanetary probes launched to date give preliminary indications of two classes of particles of apparently different origin. The most common are asteroidal particles, with a density of 3 to 8 gm/cc, concentrated in the asteroid belt and diminishing in flux both towards the Sun and outward to deep space. The others are cometary particles, with a density of less than 1 gm/cc. These are more common close to the sun and decrease in flux with increasing distance from the Sun. Concentrations of these particles have been detected in what is believed to be cometary orbits.

Figure 2-115 shows the postulated flux versus particle mass and distance from the Sun for both the cometary and asteroidal particles. These meteoroid models were developed under NASA contract NAS9-3499 (reference 21) for studies of manned Mars and Venus flyby using Apollo hardware and systems.

Spacecraft failures can occur by either a direct impact with a large asteroid or a long-term erosion due to continuous bombardment by micrometeorites. For the latter case, empirical design laws for structures have been developed and used successfully. Erosion of thermal-control surfaces, solar cells, antennas, etc. is of concern but is difficult to predict and can usually be accounted for in the spacecraft design. For the purposes of this analysis, it will be assumed that deterioration of the spacecraft due to general erosion can be accepted and will not lead to a mission failure.

It is then of interest to determine the probability of impact with a large asteroid which will destroy the spacecraft or cause a mission failure by puncture of a system. The minimum size asteroid which is of concern is dependent on the relative velocity. This relationship is shown in Figure 2-116 for a range of particle densities. For this analysis, it is assumed that particles having enough energy to penetrate a .1- to .5-cm thickness of aluminum are of concern.

By combining this data with Figure 2-115 and assuming a spacecraft cross-section of 2 m², the probability of an asteroid collision for a 600-day mission can be estimated assuming one passage through the asteroid belt. This is shown in Figure 2-117 for cometary and asteroidal meteoroids and a range of particle penetration energies. Superimposed on this data are lines of meteoroid heliocentric velocity. It can be seen that for an average particle velocity of 30 km/sec, which is postulated for interplanetary space, very significant numbers of meteoroid impacts will occur. In fact, the probability of avoiding particles of the size believed to be of concern is zero for the asteroidal meteors.

It is important now to evaluate the above analysis in terms of space-

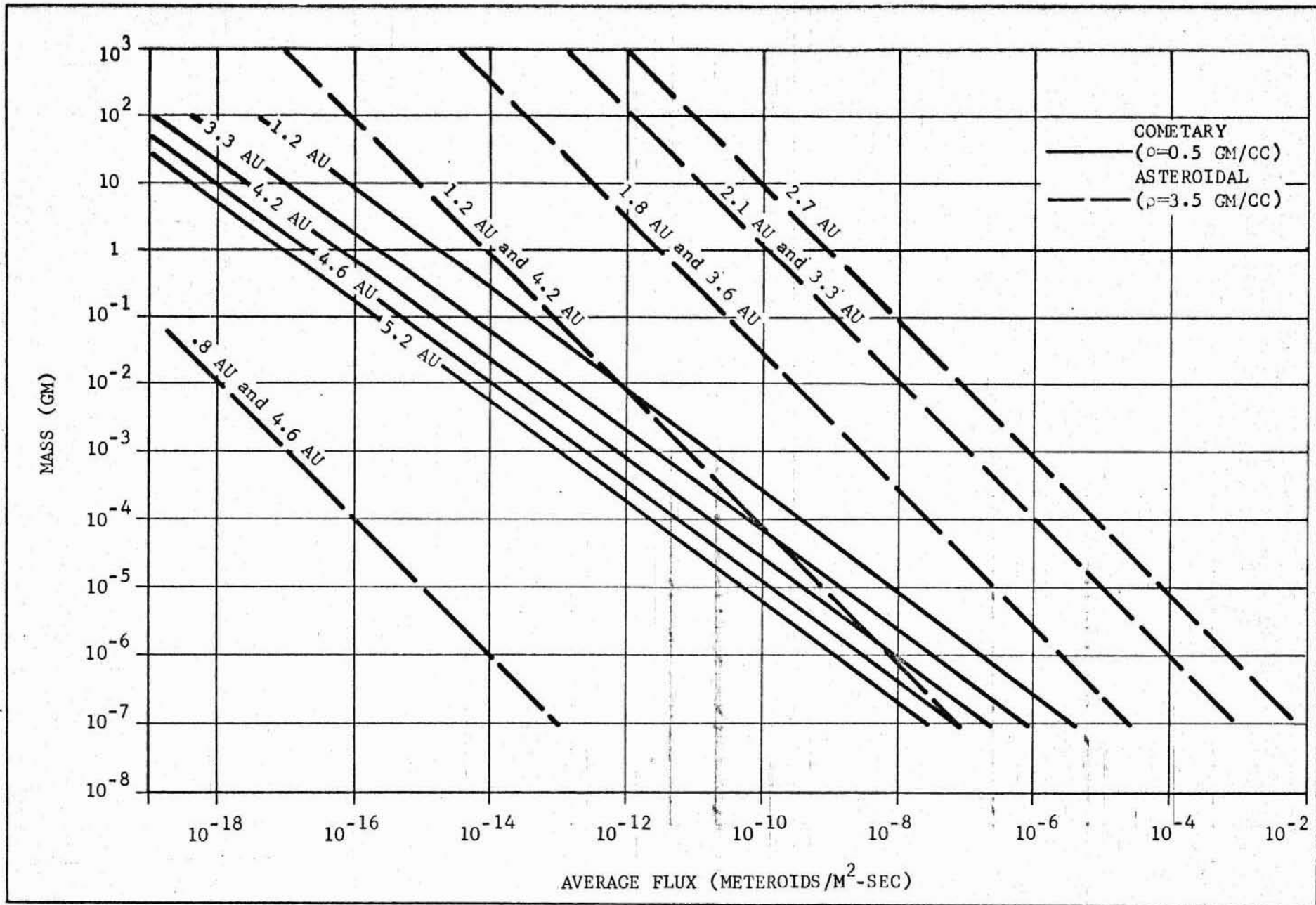


Figure 2-115. COMETARY AND ASTEROIDAL METEOROID MASS DISTRIBUTION VS SOLAR DISTANCE

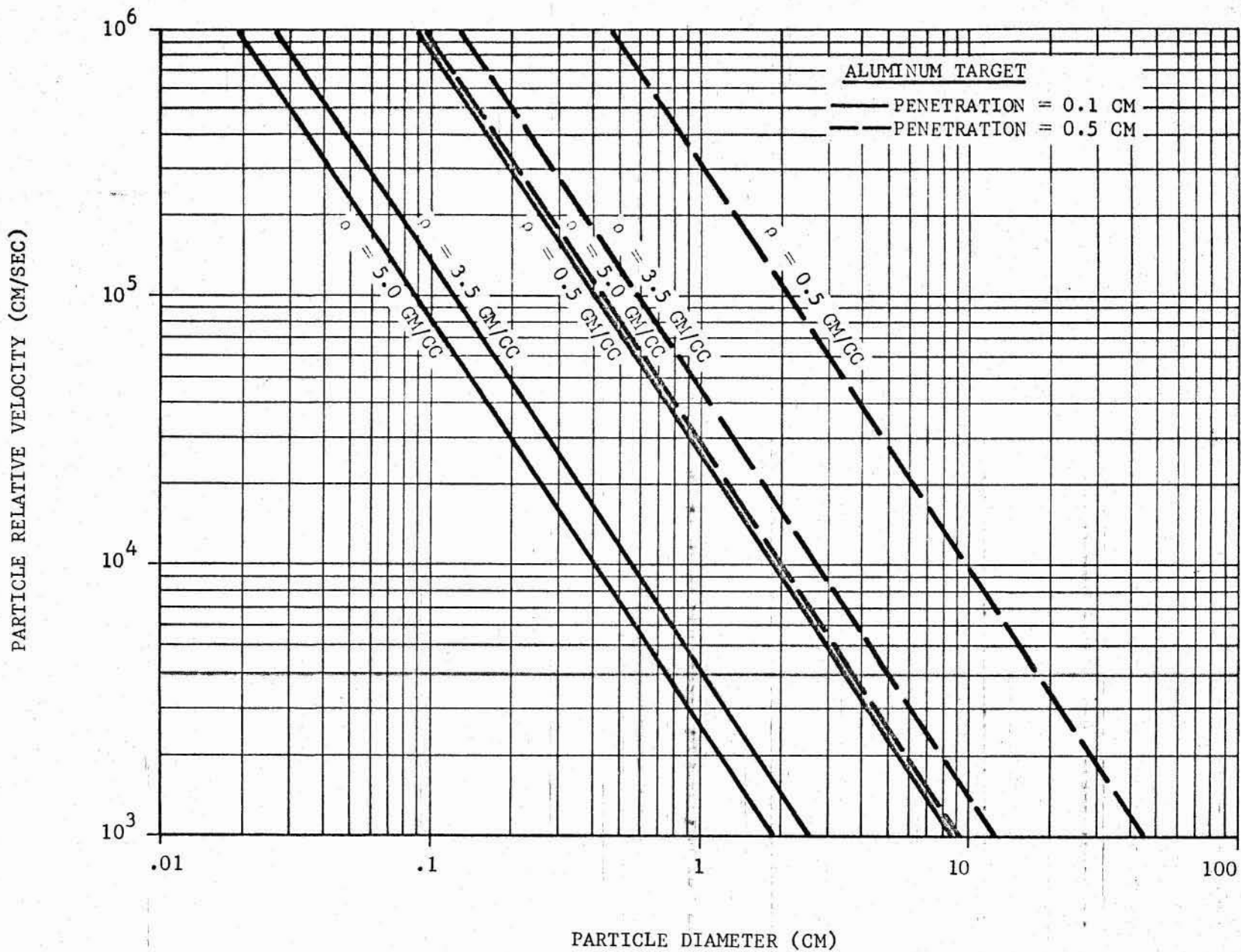


Figure 2-116. MINIMUM PARTICLE RELATIVE VELOCITY, DIAMETER, AND DENSITY TO CAUSE PUNCTURE LEADING TO SPACECRAFT FAILURE

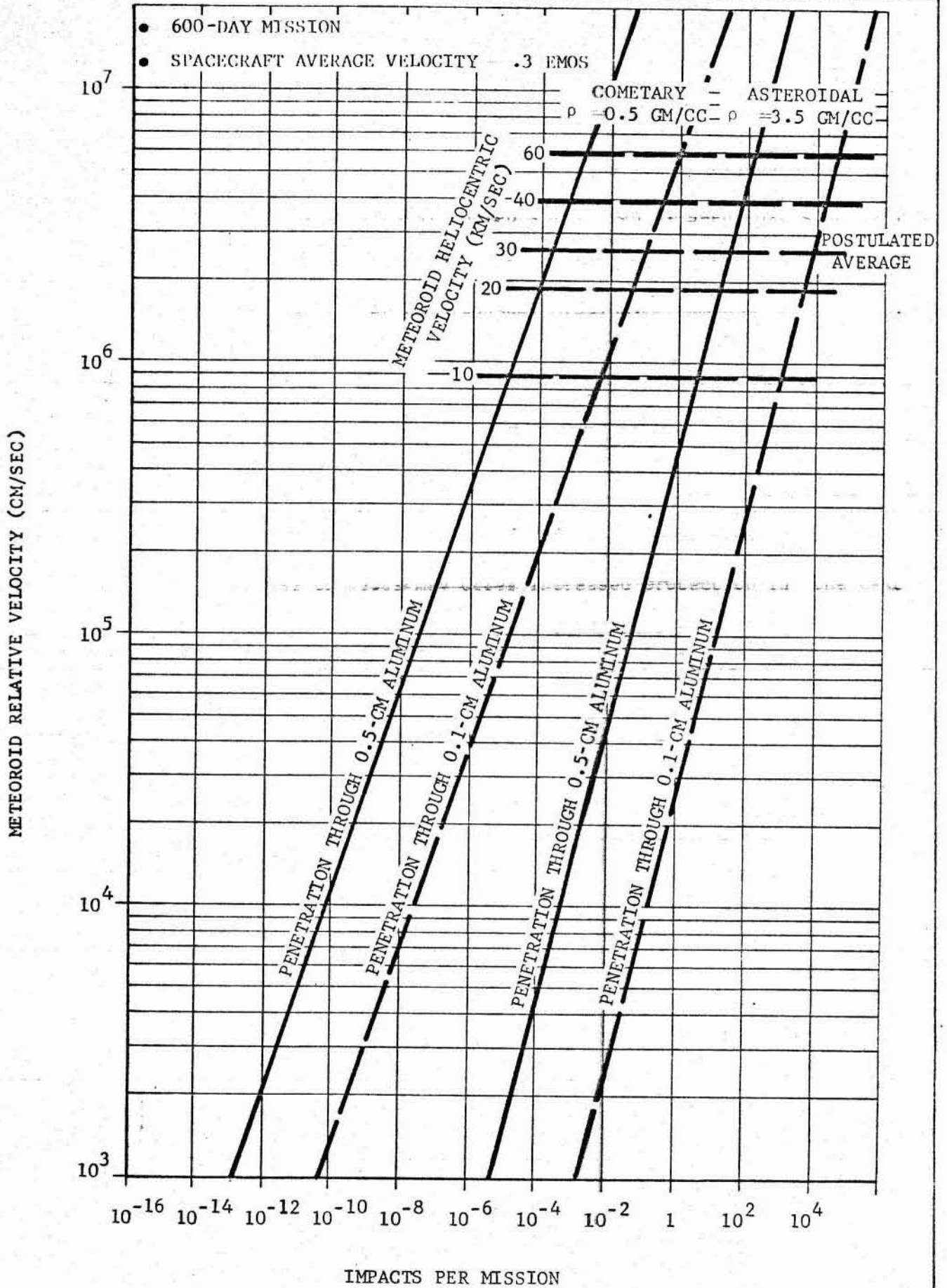


Figure 2-117. COMETARY AND ASTEROIDAL METEOROID RELATIVE VELOCITIES VS NUMBER OF IMPACTS AND PENETRATIONS IN ALUMINUM PLATES

craft failures. Much work has been completed on meteoroid shielding designs for interplanetary spacecraft under various NASA and USAF contracts. For this analysis again, the work completed under NAS9-3499 which is associated with the meteoroid models of Figure 2-115 will be used. Thus, Figure 2-118 is presented from reference 21 for various structural concepts. It can be seen that sophisticated and heavy structures are required to achieve satisfactory probabilities of success. For use in Table 2-19 and 2-20, the design point indicated on Figure 2-118 was used and it was assumed that the probability of puncture was identical for the inbound portion of the 1200-day mission.

Knowledge of the asteroid concentration in space is limited at this time and the above analysis must be considered approximate. The asteroid belt particle flux is particularly unknown. As further data becomes available, the above analysis could be refined to better estimate the probability of collision. Also, much work is underway to develop self-sealing structures for interplanetary vehicles. As such concepts are further developed, the probabilities of failure due to meteoroid impacts will decrease and alter the above analysis accordingly. Figure 2-119 summarizes the work completed under Contract NASR-102 (reference 26) which shows that, for the missions under consideration herein, self-sealing structures may permit essentially no failures. This work must be considered preliminary at this time, but these concepts may offer increased protection in the next decade over that shown in the preceding analysis.

2.2.8.4 Probability of Subsystem Success (p_s). The analysis of the success to be expected from subsystems other than electronics is again based on an extrapolation of past satellite data in this report. The degree of detail comparable to the data compiled for electronic component failures is not available, but a review of American satellites launched through December 1965 is presented in Figure 2-120. This curve shows the cumulative propulsion and mechanical failures which have occurred for satellites in orbit.

Some difficulties in developing this data should be mentioned to obtain the proper study perspective. First, it is often difficult to distinguish what satellite failures are not electronic since electrical systems are so integrated with the other systems. For example, a failure to deploy a boom or antenna was considered a mechanical failure in this analysis although it is realized that a failure in an electronic system, component, or connection may have been the reason the deployment did not occur. Likewise, a propulsion system failure may in fact be traced to an electronic failure in the same or other subsystems. Nevertheless, to be conservative, the data in Figure 2-120 is considered to be indicative of the subsystem failures to be expected.

The second difficulty experienced in developing this data is the inclusion of lifetime considerations. A review of the satellite failures shows that subsystem failures of this type usually occur early in a satellite's history. Once these subsystems have been actuated, they are not usually expected to operate again. For example, the deployment of booms is not a repetitive procedure. Also, once propulsion maneuvers are undertaken to achieve certain desired orbits, the propulsion system is never reactivated. Thus, the different requirements of the Jupiter orbiter/solar probe, wherein mechanical and propulsion systems are to be actuated after more than a year's storage in space is not really duplicated by the data shown in Figure 2-120. In lieu of better data these probability histories were used in this analysis.

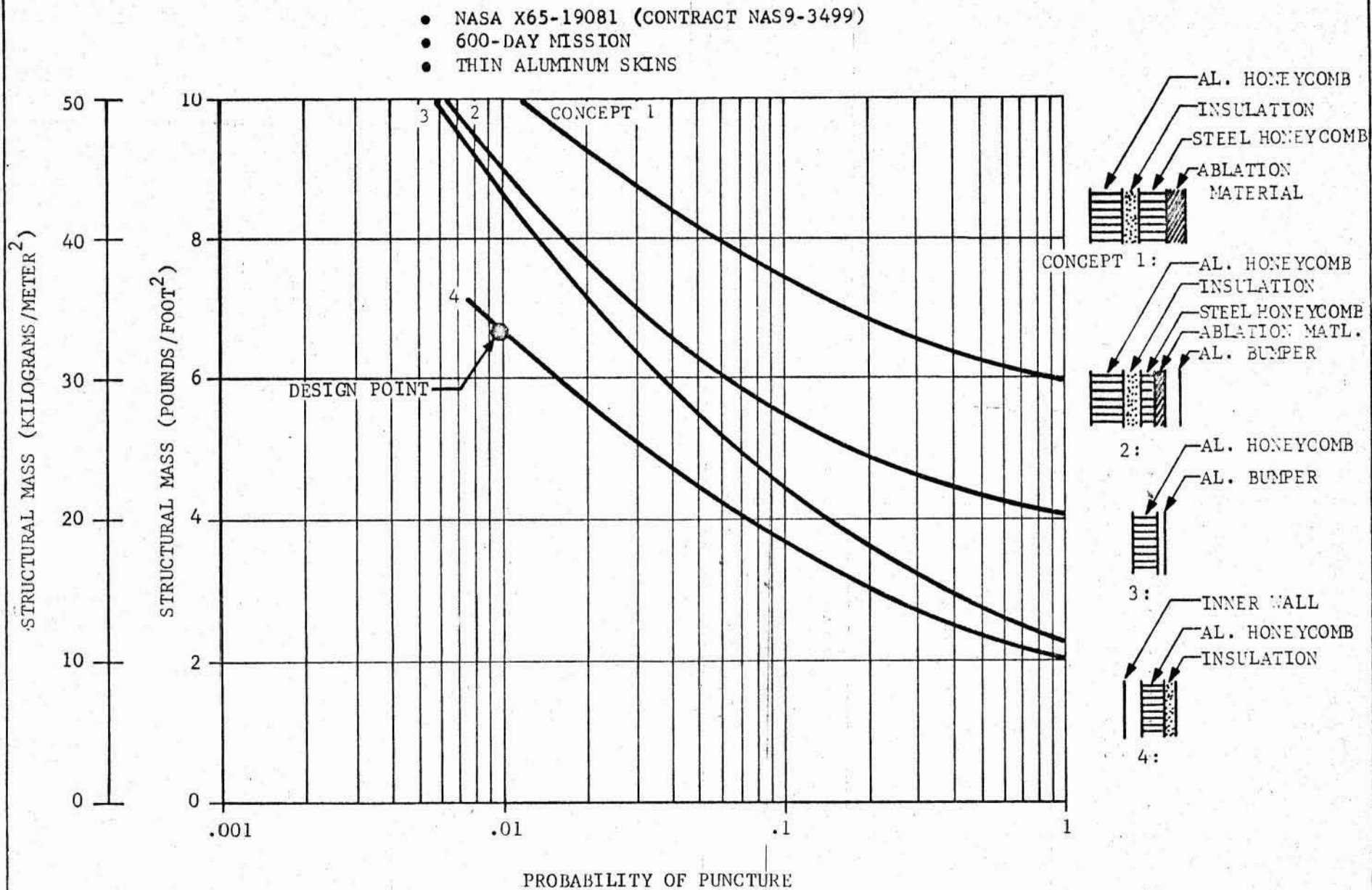


Figure 2-118. STRUCTURAL MASS VS PROBABILITY OF METEOROID PUNCTURE FOR VARIOUS STRUCTURAL CONCEPTS

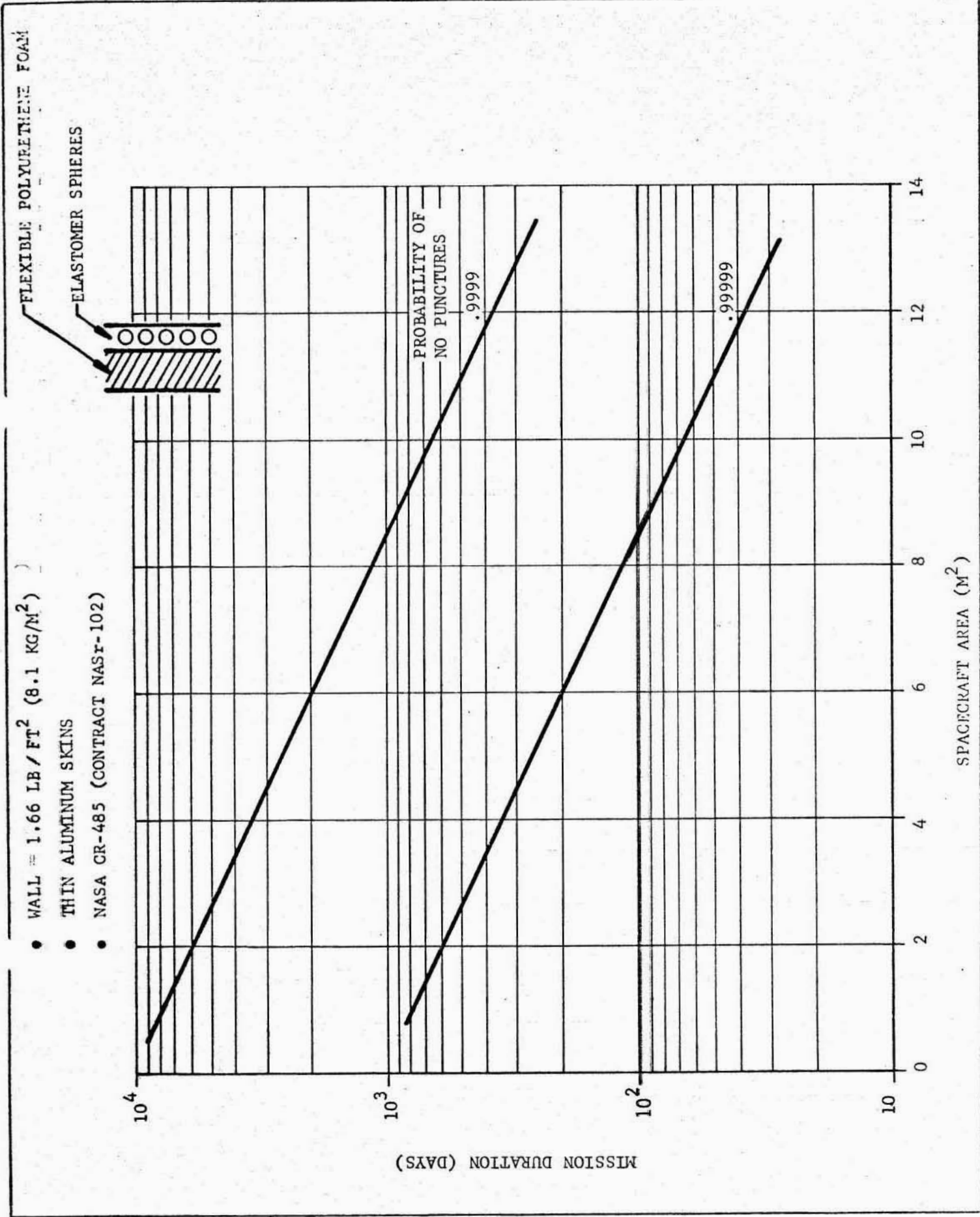


Figure 2-119. MISSION DURATION VS SPACECRAFT AREA AND PROBABILITY OF NO PUNCTURES FOR A SELF-SEALING STRUCTURE CONCEPT

- UNMANNED SATELLITES
- BASED ON TRW SPACE LOG AND GODDARD SATELLITE SITUATION REPORTS (Ref. 22 and 25)

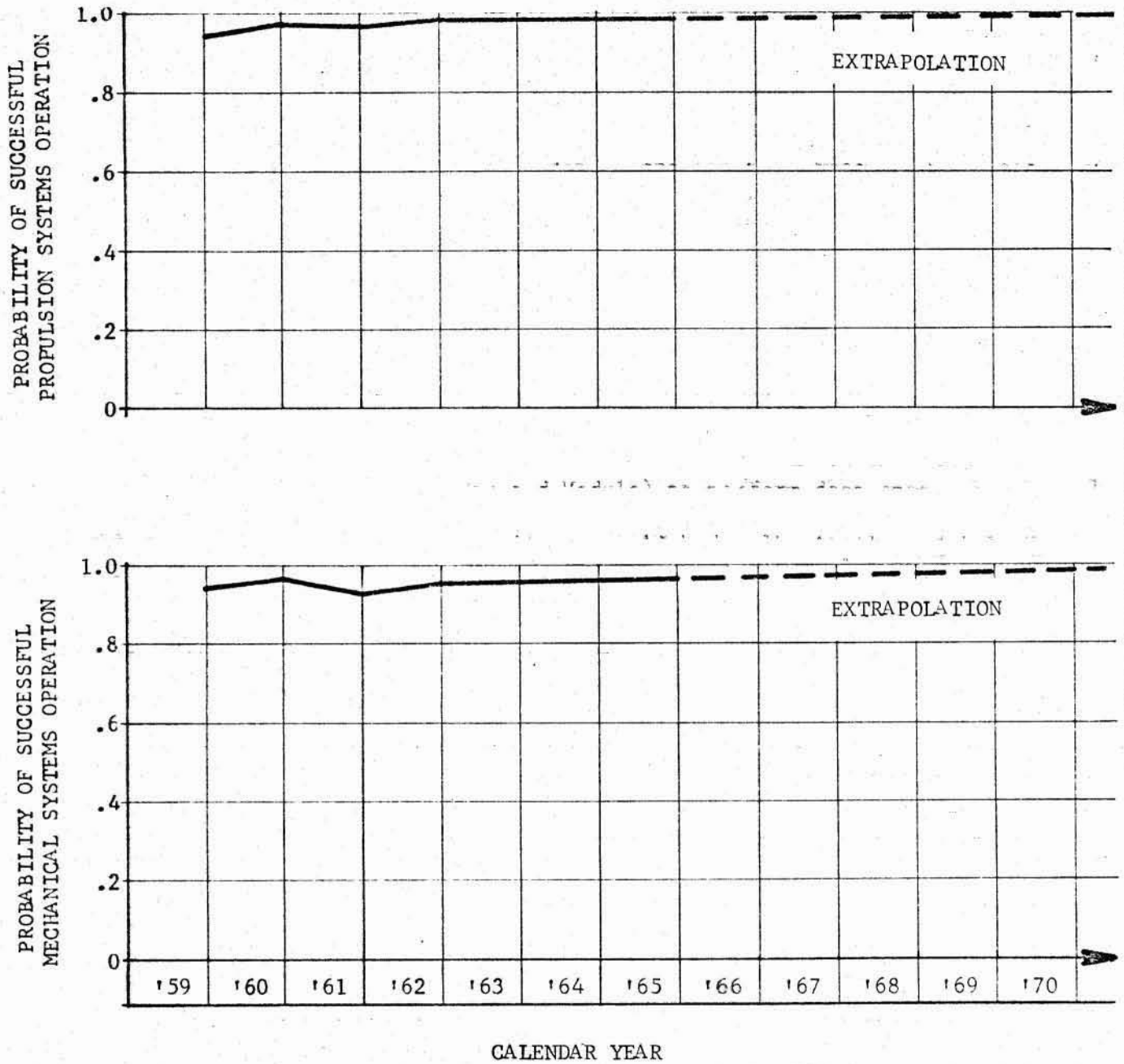


Figure 2-120. SUBSYSTEM PROBABLE SUCCESS HISTORY

September 1966

The subsystem success probability in the next decade is shown in Table 2-23. In this table, a constant .995 factor was added to account for other subsystems and contingencies in order to be conservative.

Table 2-23. SUBSYSTEM SUCCESS PROBABILITIES

Year Subsystem	1968	1970	1972	1974	1976
Mechanical	.970	.980	.990	.993	.995
Propulsion	.990	.990	.990	.990	.990
Other	.995	.995	.995	.995	.995
Total	.955	.965	.975	.977	.980

2.3 SPACECRAFT CONCEPTUAL DESIGNS

One of the primary purposes of the study was to investigate the feasibility of using Apollo spacecraft modules (i.e., the Lunar Excursion Module, Apollo Service Module, or Apollo Command Module) to perform deep space unmanned interplanetary missions. As noted in the report of work previously completed (reference 1), this is not easily accomplished. The Apollo modules represent unique designs for undertaking a manned lunar landing mission. Mass, volume, subsystem performance, structural criteria, configuration, and many other parameters are incompatible with unmanned exploration of the solar system. In this study, therefore, emphasis was placed on the use of existing subsystems and hardware developed in the Apollo program rather than the major modules themselves. As will be noted below, existing propulsion subsystems were adapted to these missions. This is economically advantageous as these subsystems usually represent the greatest development effort in a space program.

The data of the preceding subsections presented preliminary indications of many features of the Jupiter orbiter/solar probe. In particular, the thermal control analysis of the close solar probe dictated the general arrangement of that spacecraft to a great extent. Other analyses of advanced missions to be presented in Section III of this report also exerted an influence on the sizing of the spacecraft.

The spacecraft configurations are constrained by the interface requirements and aerodynamic shroud of the Saturn V launch vehicle. Throughout all this study effort, the standard MSFC nose cone for the Saturn V booster was retained. Also, room was allotted for the S-IVB instrument unit (IU) cable rack located around the periphery of the IU above the staging plane. Based on these constraints, the launch configuration depicted in Figure 2-121 was developed for the Jupiter orbiter/solar probe configuration.

The solar probe is configured for approaches up to 0.1 AU from the sun. A passive shadow shield nose cone is used with a superinsulation-protected secondary shield. To assist the monopropellant attitude-control subsystem, solar vanes are installed which provide significant stabilizing torques. The close solar probe has no propulsion and after Jupiter swingby is incapable of

PART No.		REVISIONS			
ZONE	SYM	DESCRIPTION	DATE	APPROVAL	

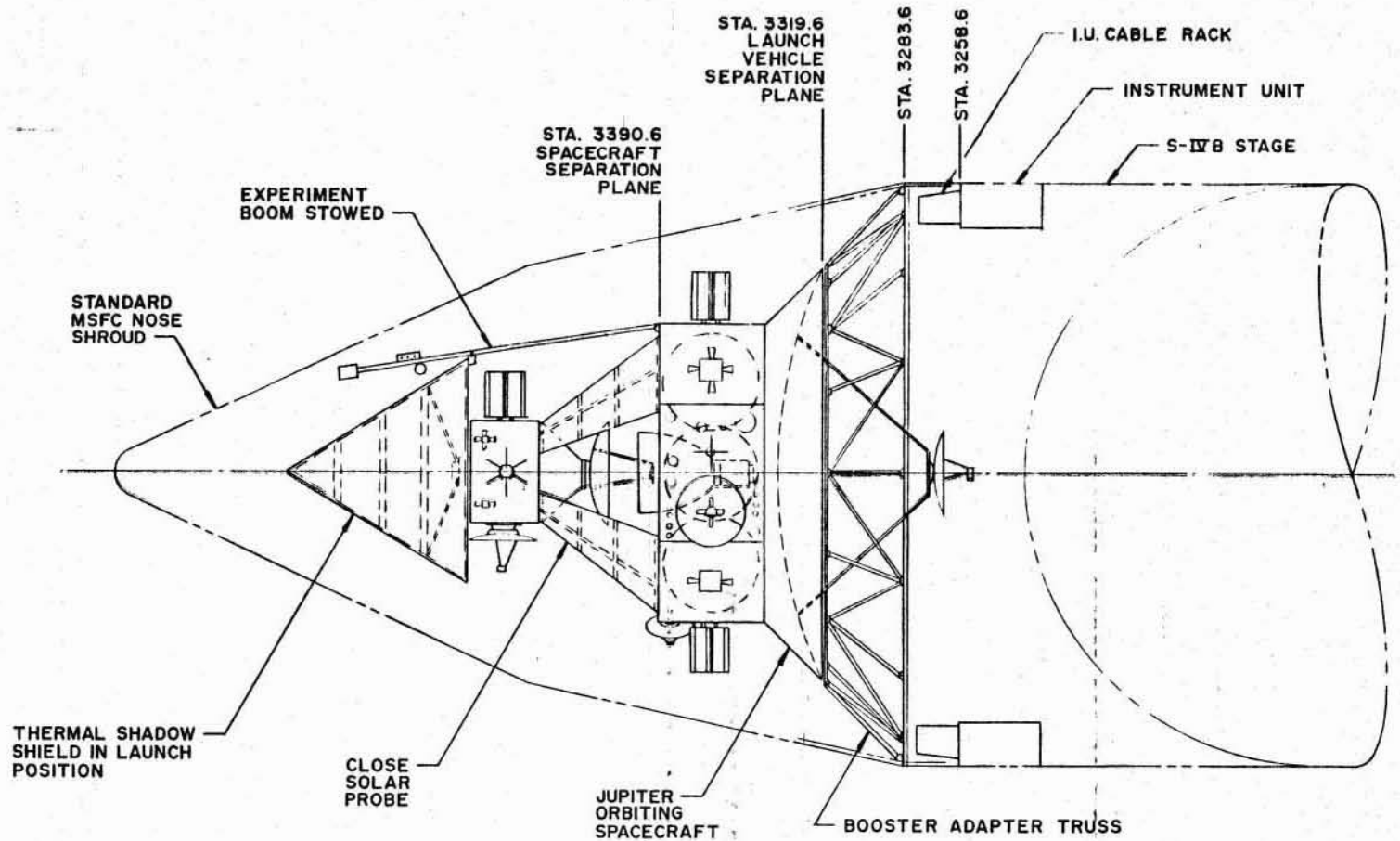


Figure 2-121

DWG
SIZE
C

UNLESS OTHERWISE SPECIFIED			ORIGINAL DATE OF DRAWING		LAUNCH CONFIGURATION JUPITER ORBITER WITH CLOSE SOLAR PROBE	NORTHROP CORPORATION NORTHROP SPACE LABORATORIES HUNTSVILLE, ALABAMA
DIMENSIONS ARE IN INCHES			DRAFTERMAN	CHECKER		
TOLERANCES ON FRACTIONS DECIMALS ANGLES			CHECKER	STRESS		
MATERIAL			ENGINEER	ENGINEER		
HEAT TREATMENT			PROJ ENGINEER		SCALE	UNIT WEIGHT
NEXT ASSY	USED ON		APPROVED			
APPLICATION			FINAL PROTECTIVE FINISH		R E V	

2-198

making course corrections. The following paragraphs summarize the subsystem features of the probe designs.

2.3.1 Propulsion

Planetary Capture. The LEM ascent primary propulsion system, which utilizes Earth-storable propellants, is used for the planetary capture maneuver. The system is modified to match the Jupiter orbiter performance requirements of this mission and is not activated until target planet encounter is achieved.

Attitude Control. The Jupiter orbiter attitude control system (ACS) is composed of two separate systems: a low-thrust system, to provide control during heliocentric and capture orbit coast; and a high-thrust system to provide control of the vehicle after Earth injection, to orient the vehicle for the midcourse correction, and to control the vehicle during braking into Jovian capture orbit. The ACS consists of twelve 25-N thrusters and twelve 100-N thrusters. Fuel is a monopropellant consisting of 25% $N_2H_5NO_3$ and 75% N_2H_4 .

The solar probe ACS uses the same monopropellant. Thrusters are 15 N and 12 thrusters are used.

State-of-the-art gyros can be used on both spacecraft to measure angular rates and position changes about all three axes of the spacecraft. The gyros would have the capability to operate in the integrating mode to provide the necessary angular position information to establish and hold an arbitrary orientation independent of the celestial reference.

Midcourse Correction. To provide the midcourse corrections a vernier system utilizing the main propellants was selected. The system uses one 445-N vernier engine.

2.3.2 Power Supply

An isotopic power system is installed which uses passively cooled Pu-238 units. It is anticipated that three units will be required for the Jupiter orbiter and two for the solar probe. Batteries are used on both spacecraft for peak loads. Because these isotopic units are α -particle emitters, shielding is not critical.

2.3.3 Communications

A 4.5-m high-gain antenna is mounted on the Jupiter orbiter to provide deep-space communications to the Earth's DSIF system. The antenna is not gimballed and pointing is achieved by attitude maneuvering. The input power level of the system is estimated at 200 watts. Bit-rate capability will be approximately 90 bits/sec minimum under high background noise conditions.

The solar probe uses a smaller high-gain antenna which is gimballed. In addition, the system input power is also 200 watts.

Both spacecraft have omnidirectional antennas for transmitting to Earth at close distances and to receive command and control orders.

2.3.4 Thermal Control

In the far regimes of the solar system, thermal control for both spacecraft is achieved by superinsulation and electric heaters in critical areas. Excess power is available from the RTG units to maintain proper temperatures in the electronic and propulsion subsystems.

Close to the Sun, the solar probe is kept relatively cool by a passive shadow shield. Proper attitude control keeps the spacecraft equipment compartment in the shadow zone of the primary nose-cone shield. A secondary flat plate with superinsulation maintains reasonable spacecraft temperatures.

2.3.5 Guidance and Control

Sun Sensor. The sun sensors to be used on both probes consist of photoconductive cells connected in a bridge circuit positioned around a plane perpendicular to the spacecraft axes to be controlled. The system would be mounted to control the yaw and pitch axes so that there is a complete 4π steradian field of view for the Sun sensors. For the solar probe, these sensors will be kept in the shadow cone and the bridge circuit designed to prevent the solar energy from impinging on them.

Canopus Sensor. The Canopus sensor will be used to control the spacecraft about the roll axis. A position error signal is derived and controlled by an automatic-gain-control loop. The indication of the apparent brightness of any object being tracked is the input to the Canopus acquisition logic.

Central Computer and Sequencer. The overall spacecraft control timing, and sequencing for all operations is provided by a central computer and sequencer. The design concept successfully used for the Mariner IV central computer and sequencer can be applied to deep-space missions. Three counters would be required. These are, (1) a launch counter for early events such as activating the attitude-control system, starting the Canopus acquisition, etc., (2) a maneuver counter for midcourse corrections, and (3) a terminal counter to control the planetary capture maneuver and solar encounter.

2.3.6 Inboard Profiles

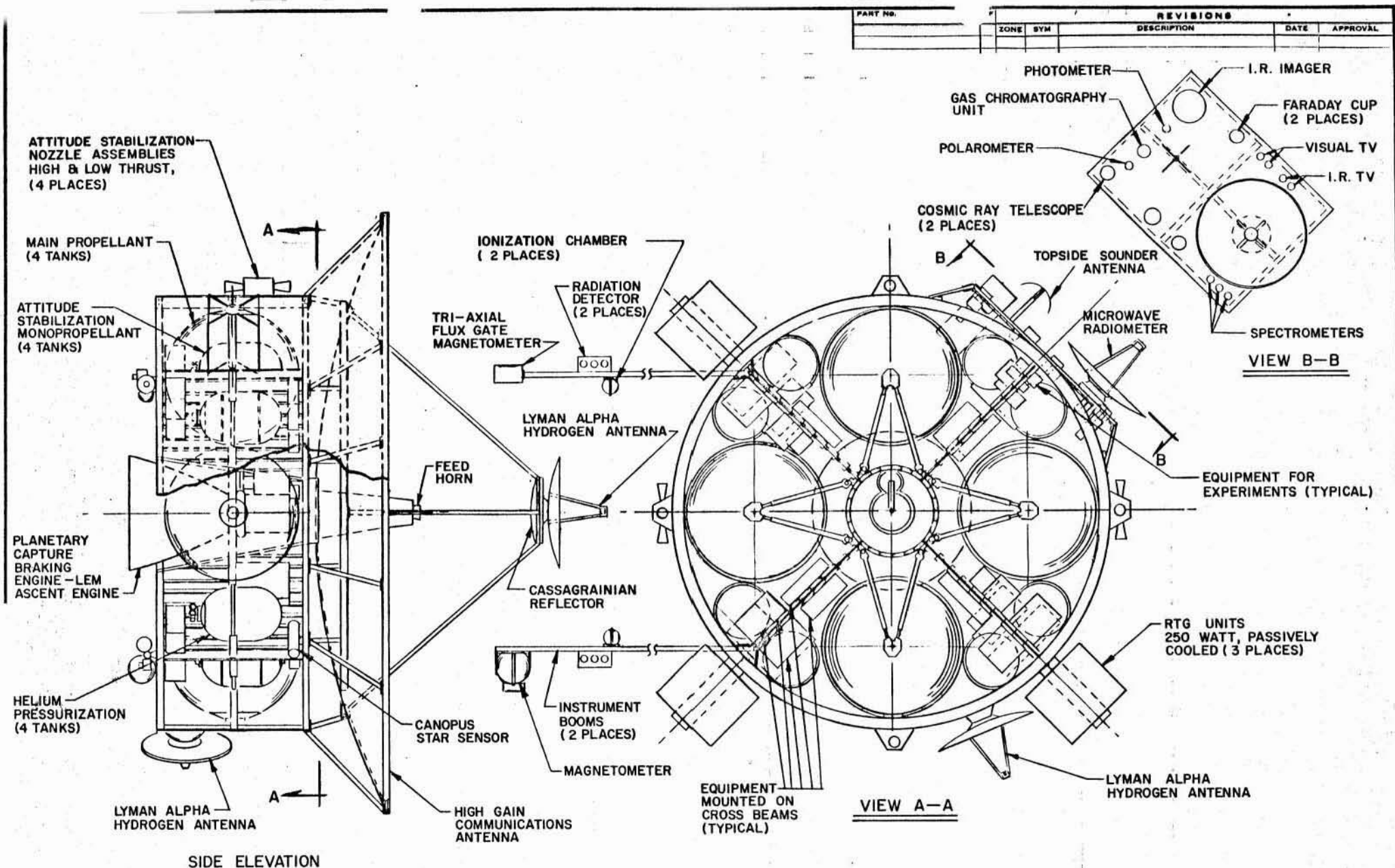
A detailed mass breakdown is shown in Table 2-24 for both spacecraft. The nominal trajectory parameters for the Jupiter orbiter are a 600-day lifetime and a capture orbit of $n = 40$ and $r_p = 1.1$ Jupiter radii. The solar probe has a design lifetime of about 1200 days to close solar approach of 0.1 AU. Figures 2-122 and 2-123 present inboard profiles of these spacecraft.

These drawings indicate the general size and arrangement of the spacecraft systems and equipment. The Jupiter orbiter spacecraft is characterized by its large DSIF antenna designed integral with the spacecraft. This antenna is rigidized by a trusswork and is capable of supporting both the Jupiter orbiter and solar probe during launch.

The body of the spacecraft is a cylinder with cross-beam primary structure. A conical compartment in the center houses the LEM ascent engine which is used for Jupiter capture braking. Propellants are loaded in the four spherical

Table 2-24. MASS SUMMARY

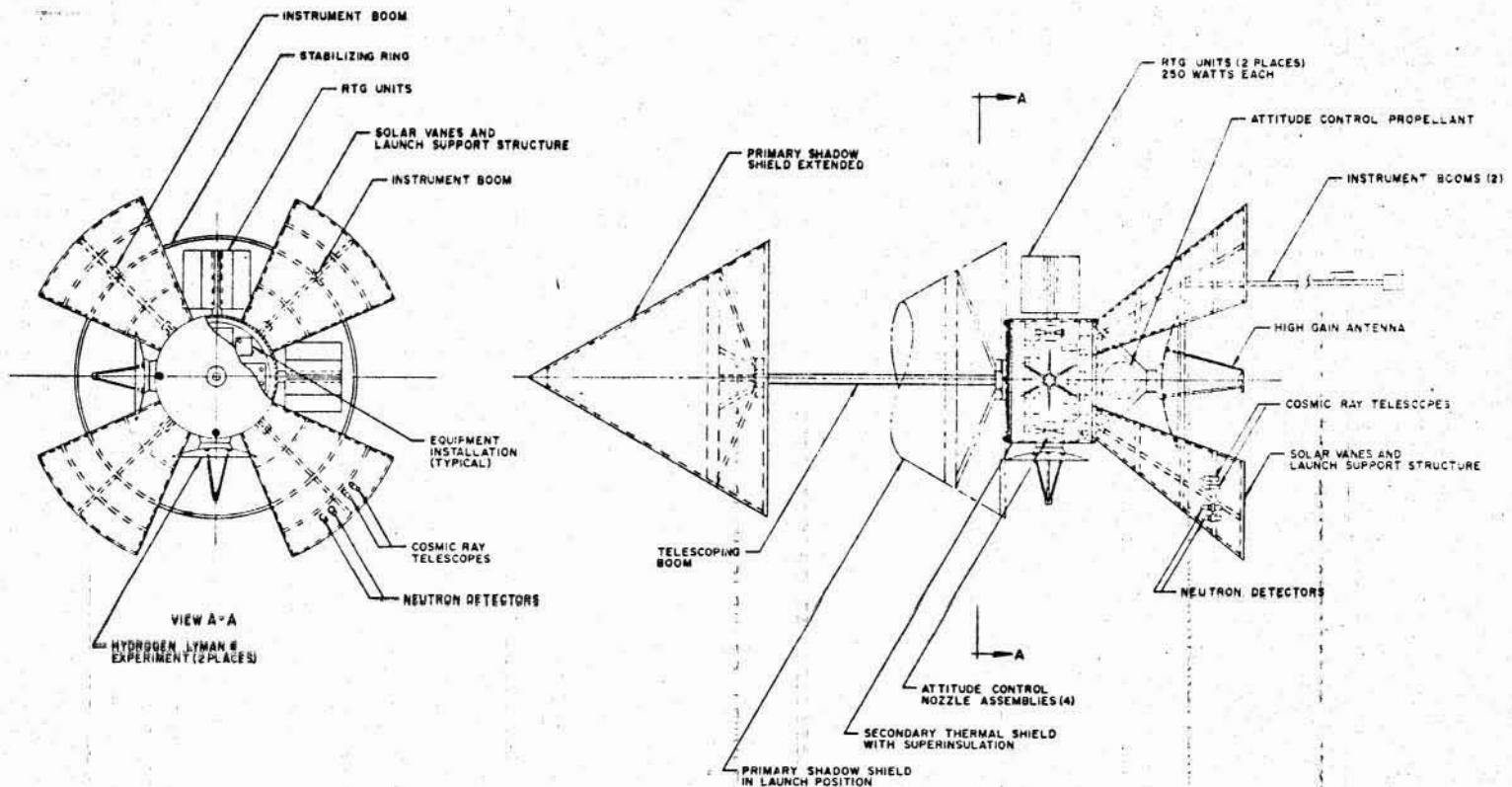
ITEM	JUPITER ORBITER		CLOSE-SOLAR PROBE	
	lbm	kg	lbm	kg
Structure	1770	805	450	204
Stability and Control	185	84	40	18
Attitude Control	(60)	(27)	(40)	(18)
Vernier System	(125)	(57)	—	—
Navigation & Guidance	255	114	350	159
Thermal Control	100	45	30	14
Power Supply	635	257	380	172
RTG Units	(500)	(228)	(335)	(152)
Distribution	(135)	(29)	(45)	(20)
Communications	115	52	55	25
Antenna, Support	(80)	(36)	(35)	(16)
Electronics	(35)	(16)	(20)	(9)
Propulsion Inerts	915	415	—	—
Operational Instruments	150	68	75	34
Dry Mass	4125	1840	1380	646
Unusable Fluids	275	125	—	—
Helium	(75)	(34)	—	—
Residuals	(200)	(91)	—	—
Fixed Mass	4400	2000	1380	646
Usable Fluids	5910	2680	440	200
Monopropellant	(660)	(300)	—	—
Bipropellant	(5250)	(2380)	—	—
Cold Gas	—	—	(440)	(200)
Gross Mass	10,310	4,680	1,820	846



UNLESS OTHERWISE SPECIFIED			ORIGINAL DATE OF DRAWING 8-25-66		INBOARD PROFILE, JUPITER ORBITING SPACECRAFT		NORTHROP CORPORATION NORTHROP SPACE LABORATORIES HUNTSVILLE, ALABAMA	
DIMENSIONS ARE IN INCHES			DESIGNED BY	CHECKED				
TOLERANCES ON FRACTIONS DECIMALS ANGLES			DRY TRAM					
			Vansmore					
MATERIAL			CHECKED					
HEAT TREATMENT			ENGINEER					
NEXT ASSY USED ON			PROJ ENGINEER					
APPLICATION			APPROVED					
FINAL PROTECTIVE FINISH								

606-6

REV	DATE	BY	CHKD	APPROVED
1				
2				



UNLESS OTHERWISE SPECIFIED		DIMENSIONAL UNITS OF DRAWING		APPROVED
SYMBOL	DESCRIPTION	UNIT	SCALE	
FRONT VIEW	FRONT VIEW	INCHES	AS SHOWN	NORTHROP CORPORATION NORTHROP SPACE LABORATORIES <small>MEMPHIS, ALABAMA</small> 4-11
REAR VIEW	REAR VIEW	INCHES	AS SHOWN	
LEFT SIDE VIEW	LEFT SIDE VIEW	INCHES	AS SHOWN	
RIGHT SIDE VIEW	RIGHT SIDE VIEW	INCHES	AS SHOWN	
TOP VIEW	TOP VIEW	INCHES	AS SHOWN	
BOTTOM VIEW	BOTTOM VIEW	INCHES	AS SHOWN	
ISOMETRIC VIEW	ISOMETRIC VIEW	INCHES	AS SHOWN	
SECTION A-A	SECTION A-A	INCHES	AS SHOWN	
SECTION D-D	SECTION D-D	INCHES	AS SHOWN	
OTHER VIEWS	OTHER VIEWS	INCHES	AS SHOWN	
HEAT TREAT	HEAT TREAT	INCHES	AS SHOWN	
APPLICATION	APPLICATION	INCHES	AS SHOWN	

Figure 2-123. INBOARD PROFILE CLOSE SOLAR PROBE

tanks between the main crossbeam structure. These tanks are supported at their center diameter by the conical thrust structure in the center of the spacecraft and by the circumferential structure forming the exterior of the Jupiter orbiter. A circumferential ring is designed for this purpose which transmits the propellant tank loads to the main crossbeam structure. The propellant tanks are stabilized by a truss network at the base of the cylindrical portion of the spacecraft.

The tanks for the helium pressurant and monopropellant attitude control subsystem are mounted symmetrically around the orbiter on the crossbeam structure. Also, the electronic components associated with the various systems are mounted on this same structure. This design permits easy access to all the subsystems through the nonstructural top face of the spacecraft.

An exterior panel is located at one quadrant of the primary crossbeam structure to support the experiments which are used to view the target planet. This panel provides a flat surface which can be oriented toward Jupiter when the spacecraft is in capture orbit and collecting data. Electronics associated with these instruments can be installed on the rear of the panel and on the crossbeam structure close by. Again, access can be had through the top of the spacecraft.

Experiments which must be operated at distances remote from the onboard systems are shown installed on booms. These instruments are magnetometers, ionization chambers, and radiation detectors. The booms are deployed after Earth injection and are fixed throughout the remainder of the mission.

The configuration of the solar probe is dictated very strongly by the design of the passive thermal shadow shield discussed previously in this report. The primary shield is stowed during launch and erected after Earth injection. The spacecraft itself is a cylindrical body with a conical bottom. The top of the cylinder is the secondary shadow shield and supports a layer of superinsulation. The equipment associated with the subsystems and experiments for the probe are installed on floor structure in the cylindrical portion of the spacecraft. The conical bottom serves to contain the attitude control monopropellant spherical tank and also act as the support structure for the high-gain communications antenna.

The high-gain antenna can gimbal through $\pm 30^\circ$ for communications with Earth. This means that during the close-solar approach when the probe must be oriented radially toward the Sun, high-gain communications can be accomplished only if Earth is within the 30° cone of the spacecraft's base. However, all experimental data can be stored and transmitted at a later time when communications geometry is more favorable.

Four structural panels are installed around the base of the spacecraft which serve a number of functions:

- They form the primary support structure for the solar probe during launch and throughout the heliocentric coast until separation of the spacecraft at Jupiter.

- During the close-solar approach they act as solar vanes and add a significant stabilizing torque to the vehicle.
- They support solar experiments which view the Sun during the flyby maneuver.
- They support and provide a shadow area for experiments which are mounted on booms and trailed far behind the spacecraft in the undisturbed interplanetary environment.

Because of the high solar intensity, the primary thermal shield and four solar vanes will be constructed of titanium. Other structural concepts are conventional for deep-space spacecraft.

SECTION III

ADVANCED MISSIONS

In the context of this study the term "advanced missions" is applied to those mission concepts involving Jupiter capture or gravity assist wherein the scientific objectives of the missions are related to the specific body(s) of interest and do not include the objectives of the Jupiter orbiter/solar probe mission. More specifically, the advanced missions considered here are exploration of the Jovian moons, Saturn and Uranus capture missions via Jupiter gravity-assist, and inspection of regions of the asteroid belt. To accomplish these missions a family of spacecraft is defined which uses the Jupiter orbiter as a basic module. The advanced mission configurations, and the data on which they are based, must be considered preliminary at this time as many important aspects of their development must be further studied in detail. One such aspect is the effect of a finite launch period requirement.

Notwithstanding the cursory analysis of some aspects of the missions under consideration several significant conclusions can be reached. They include:

1. Meaningful inspection of the Jovian moons during a Jupiter capture mission will require close passes to the moons. The present technique of the mission analyst in dealing with such trajectories, that of the patched conic approach, is inadequate for the Jovian satellite system.
2. Communication with acceptable data transmission bit rates is feasible for S-band systems of the Jupiter orbiter spacecraft design anywhere in the solar system up to and including the orbit of Uranus.
3. Inspection of some regions of the asteroid belt is an acceptable secondary mission via a Jupiter swingby mode, but due to the inclination and diameters of most of the asteroids an inspection enroute to Jupiter will not be possible.
4. A family of spacecraft utilizing the Jupiter orbiter as a basic module can be designed to provide an extensive solar system exploration program, but due to the long lifetimes required, extrapolation of present subsystem reliability indicates that a reasonable mission success goal would require a major national program in terms of Saturn V launches.

3.1 JOVIAN MOON EXPLORATION

During the Jupiter mission a natural scientific objective would be inspection of the Jovian satellite system. Of particular interest, due to their size and proximity to Jupiter, would be the four inner or Galilean moons. The following three subsections are addressed to the problems of exploration of these Jovian moons. For background, the first subsection gives a brief description of the orbital characteristics of the satellite system. The second subsection relates these characteristics to communication distance between the various moons and the spacecraft during a mission, and points out the infeasibility of using radar detection to orient the spacecraft to a desirable position for television

September 1966

pictures by onboard command. Concluding, then, that very close passes (less than one Jupiter radii) are required for effective inspection of the moons, the third subsection investigates the problem of flight mechanics in the vicinity of one of the moons and indicates the inadequacy of present techniques (other than fully integrated machine trajectories) in dealing with this problem.

3.1.1 Description of the Jovian Satellite System

Jupiter has 12 known satellites ranging in size from 20- to 30-km diameter to about 4000-km diameter, or approximately the size of Mercury. The larger satellites are grouped closely about Jupiter and revolve in nearly circular orbits inclined at a maximum of less than 0.5° to Jupiter's equator (ref. 34). This inner group of four satellites is known as the Galilean satellites after their discoverer. Actually there is a fifth satellite (JV) interior to this group revolving at about 2 Jupiter radii, which due to its small size (40- to 80-km diameter) was not discovered until the advent of more sophisticated optical equipment (circa 1900). Although the inclination of JV is small (0.5°) it experiences a precession rate of $916^\circ/\text{year}$ due to the marked oblateness ($1/15.3$) of Jupiter.

Laplace discovered the following interesting relationship among the first three (Io, Europa, Ganymede) Galilean satellites. If L_i is the longitude of satellite i ($i = 1, 2, 3$) from some arbitrary initial point, then

$$L_1 - 3L_2 + 2L_3 = 180^\circ,$$

and implicitly from above

$$\frac{1}{T_1} - \frac{3}{T_2} + \frac{2}{T_3} = 0,$$

where T_i is the period of the i^{th} satellite.

The Galilean satellites, JV, JVI, JVII, and JX revolve about Jupiter in a counter-clockwise motion or directly, while JVIII, JIX, JXI, and JXII exhibit clockwise or retrograde orbits. All of the satellites are subject to mutual perturbation. In addition, the outer satellites experience considerable solar perturbation. JVIII and JIX have been observed to vary their eccentricity by as much as 100 percent during a single revolution and variations in the semi-major axis of 10 percent have been recorded (ref. 35). During the outer part of their orbits the solar force can even reach a stage of predominance over Jupiter's gravitational attraction and during conjunction it is possible that a satellite may be lost to the Sun. Indeed, such a possibility has led to the theory that some of Jupiter's satellites, particularly the smaller ones, may be captured asteroids.

There is some evidence from photometric observations to suggest the satellites always turn the same side to Jupiter (ref. 36). Table 3-1 summarizes some of the physical and orbital parameters of the Jovian satellite system. The values are taken from references 34, 37, and 38.

Table 3-1. SELECTED PHYSICAL AND ORBITAL PARAMETERS OF THE JOVIAN SATELLITE SYSTEM

SATELLITE		SEMI-MAJOR AXIS OF ORBIT IN JOVIAN RADII	ECCENTRICITY	INCLINATION TO JUPITER'S EQUATOR (MIN)	ROTATIONAL SENSE	DIAMETER (km)
THE GALILEAN SATELLITES	I IO	5.9	0.0	0	DIRECT	3730
	II EUROPA	9.4	.0003	30	DIRECT	3150
	III GANYMEDE	15.0	.0015	10	DIRECT	5150
	IV CALLISTO	26.4	.0075	15	DIRECT	5180
	V	2.5	.0038	30	DIRECT	50-150
	VI	161	.155	-	DIRECT	100-150
	VII	165	.155	-	DIRECT	25-75
	VIII	330	.25 - .5	-	RETROGRADE	25-75
	IX	332	.1 - .4	-	RETROGRADE	22?
	X	165	.08	-	DIRECT	20-30
	XI	315	.21	-	RETROGRADE	20-30
	XII	-	-	-	RETROGRADE	-

3.1.2 Jupiter Orbiter - Moons Communication Distance

The variation in communication distance between the Galilean moon Io (JI) and the orbiter spacecraft as a function of time after the capture braking maneuver is shown in Figure 3-1. The launch date, trip time, and orbital parameters chosen for the figure are those of a typical mission for the Jupiter orbiter/solar probe. Data for other Galilean moons would be similar with different curve minimums and maximums. Figure 3-1 traces the variations over only 16 days but the pattern, which has been studied up to 60 days, is invariant. In fact, the minimums vary less than 3 to 4 Jupiter radii over the 60-day period. Variation over a complete set of orbital parameters, namely, perijove distance, apsidal ratio, inclination, right ascension of the ascending node, and argument of perijove, produces two types of variation in Figure 3-1; (1) in the time scale, and (2) fluctuation of the maximum/minimum values. The most significant variations would, of course, occur for a rotation of the line of apsides in space in combination with a variation in inclination. The same pattern, however, is still maintained. The significance of Figure 3-1 is that to attain a closest approach distance to one of the Galilean moons less than, say, one Jupiter radii would require a precise timing of arrival at perijove. Collision trajectories with the moons can be postulated for a certain set of orbital elements chosen for a specified arrival time, but slight variations in the selected elements or arrival time would cause a quick recession from a minimum point or distance of closest approach. This is evident from the slope of the curve. The timing must be even more precise when the restriction in minimum inclination is imposed. This restriction limits the inclination of the orbit to a minimum equal to the declination of the incoming hyperbolic-excess velocity vector assuming a planar braking profile. Since a trace of minimum points will itself be absolutely minimum if the moon's and orbiter's planes are coincidental, this means the minimum trace is not, in general, attainable. The insert of Figure 3-1 lists the maximum and minimum points over a 60-day interval for the parameters listed at the top of the figure. In view of the restriction in inclination, however, they are generally valid as the minimum trace of the absolute minimums.

The infeasibility of using radar detection of the moons to actuate onboard commands to orientate the spacecraft for television pictures of the object moon is illustrated in Figure 3-2. A one kilowatt, x-band antenna is assumed and range to target is plotted against target diameters for one- and three-meter antenna diameters. The shaded area of the figure represents the Galilean moon diameter range. At one Jupiter radii distance it can be seen that an antenna in excess of three-meters diameter would be required. Two possible alternatives to the radar detection system would be establishment of spacecraft orientation based on calculated ephemeris of an object moon and search via onboard television. The first method would require availability or calculation of precise ephemeris of the object moon as well as precise ephemeris of the orbiting spacecraft. While any of the Galilean moons would present a relatively large disk with respect to the spacecraft at the distances of close approach, this minimum is quickly passed so that slight errors in timing will find the disk considerably reduced.

The second possibility of breaking Jupiter lock and instituting a real time television search mode monitored on Earth appears infeasible because of the relatively low bit rate of the spacecraft communication system.

- LAUNCH DATE 27 JUNE 1975 (244-2590 J.D.)
- 500-DAY TRIP TIME
- PERIJOVE RADIUS=1.1 JUPITER RADII
- APSIDAL RATIO=40
- INCLINATION OF SPACECRAFT PLANE TO JUPITER'S ORBITAL PLANE=175°
- ORBIT OF SPACECRAFT IS RETROGRADE
- INITIAL LONGITUDE OF $I_0=0^\circ$

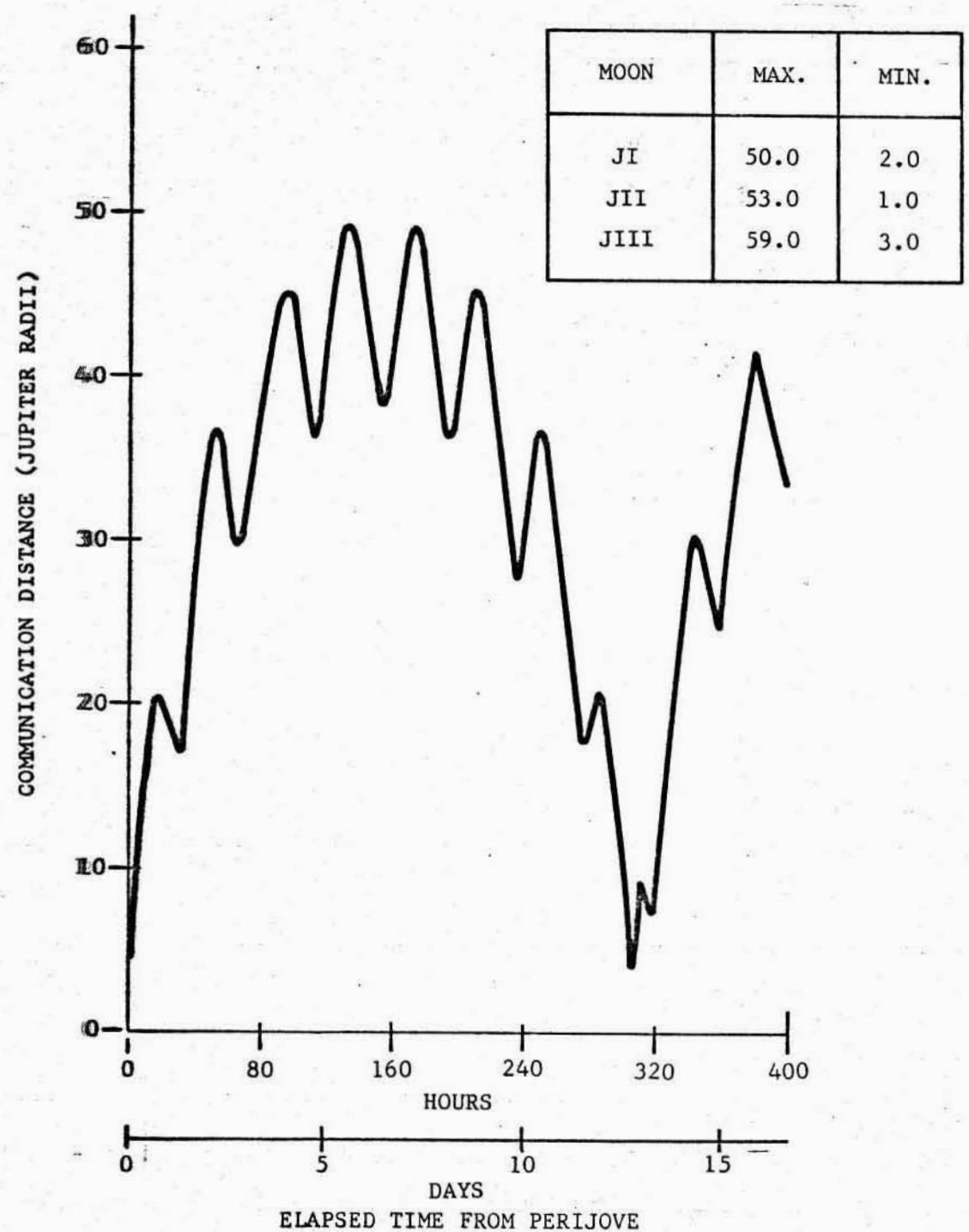


Figure 3-1. COMMUNICATION DISTANCE BETWEEN THE JOVIAN SATELLITE I_0 AND THE ORBITING SPACECRAFT VS ELAPSED TIME AFTER PERIJOVE ESTABLISHMENT

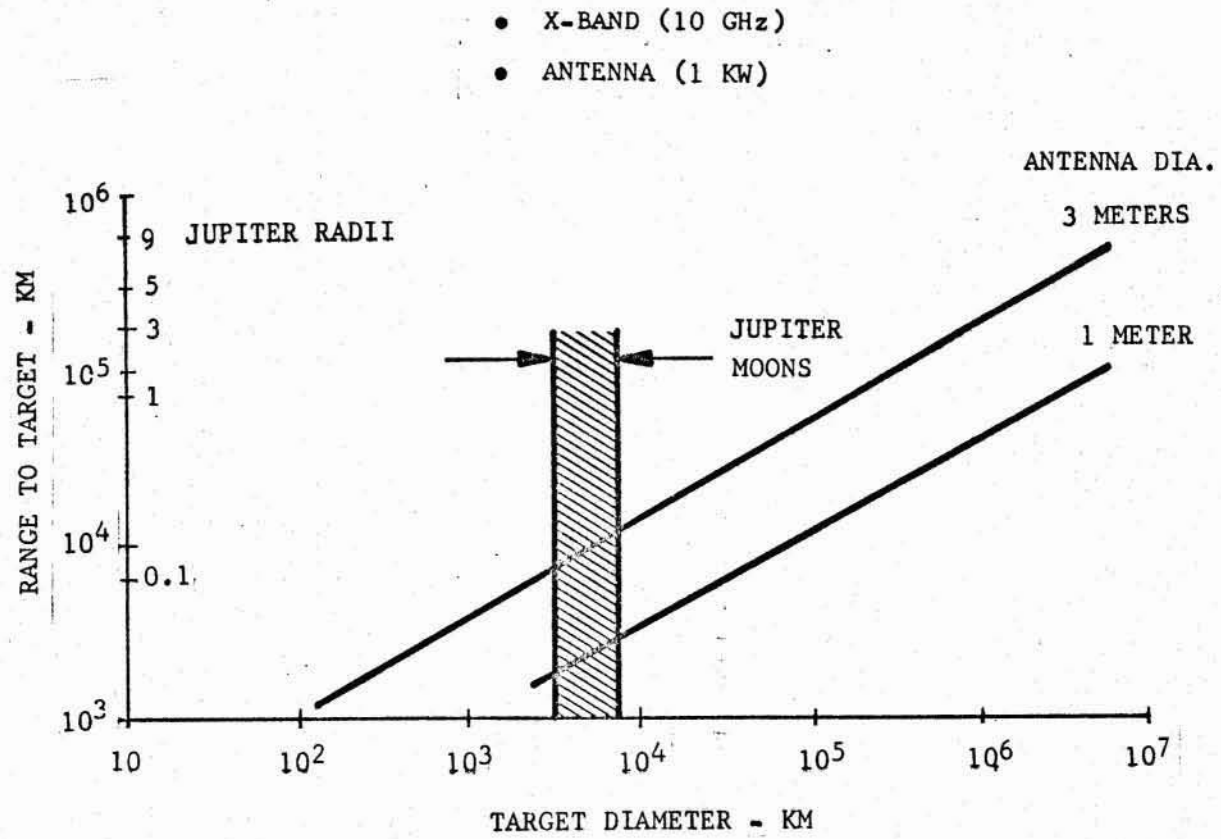


Figure 3-2. RADAR DETECTION (JUPITER MOONS)

In reference again to Figure 3-2, it can be seen that radar detection of a moon and consequent spacecraft reorientation would require pass distances on the order of 7000 km. At such distances the gravitational field of the moon probably will dominate or at least introduce considerable perturbations on the spacecraft trajectory. The flight mechanics of the spacecraft in close proximity to the moons should be investigated.

3.1.3 Sphere-of-Influence Concept for the Jovian Moon

Laplace's classic expression for the "sphere-of-influence" radius of a body in the presence of a gravitational field of another significantly larger body requires that the smaller body be "significantly removed" from the larger. Hence, the closer the body falls to the more heavily shaded region of Figure 3-3 on the force-distance curve the better the approximation holds.

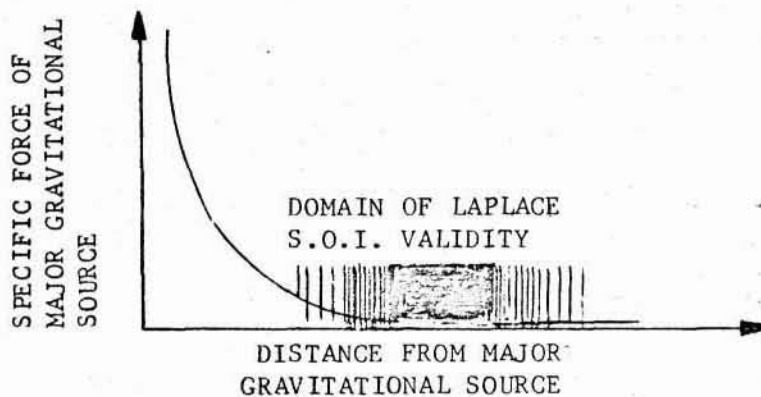


Figure 3-3. LAPLACE SPHERE OF INFLUENCE DOMAIN OF VALIDITY

In the case of Jupiters' Galilean moons, application of the Laplace formula would be questionable for two reasons:

1. Close proximity of the satellites to Jupiter
2. Powerful gravitational field of Jupiter.

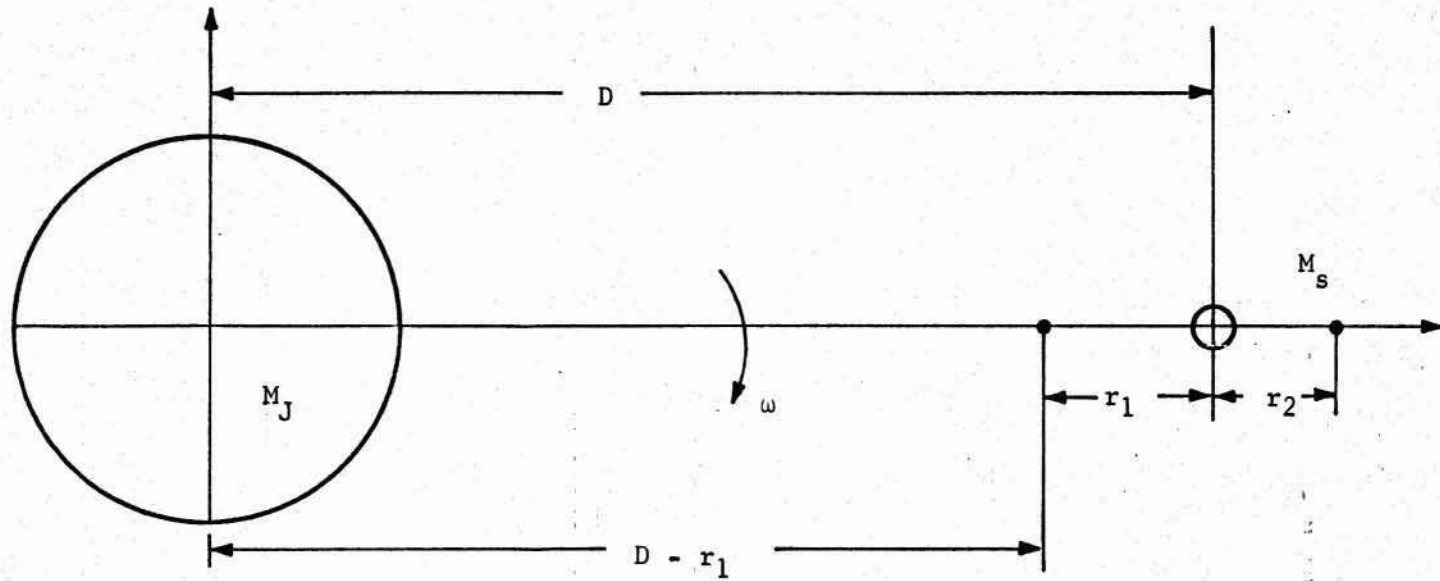
Another approach to a sphere-of-influence concept is then needed.

Let r_1 and r_2 represent the distance of the inferior and superior conjunction libration points relative to a given moon and let ω be the angular velocity of the Jupiter-satellite system as depicted in Figure 3-4. Then equating inertial and gravitational terms

$$(D - r_1) \omega^2 = \frac{M_J}{(D - r_1)^2} - \frac{M_S}{r_1^2},$$

where

- M_J = Jupiter mass
- M_S = Satellite mass
- D = Separation of masses



M_J = mass of Jupiter

M_s = mass of Satellite

Figure 3-4. LIBRATION POINT GEOMETRY

where the units have been chosen such that the universal gravitational constant is unity. Rearrangement of the above equations shows quickly that the form has taken that of Lagrange's famous quintics

$$\omega^2 (D - r_1)^3 \dot{r}_1^2 = M_J \dot{r}_1^2 - M_S (D - r_1)^2$$

or

$$\zeta^5 - \zeta^4 - \zeta^3 - \rho \zeta^2 + \rho = 0,$$

where $\zeta = \frac{r_1}{D}$ and $\rho = \frac{M_S}{M_J}$.

Neglecting terms of the fourth and fifth order and solving the resulting cubic yields

$$\zeta = \rho - \frac{1}{3} \rho \quad \text{or} \quad r_1 = D \left(\frac{M_S}{M_J} \right)^{\frac{1}{3}} - \frac{1}{3} \left(\frac{M_S}{M_J} \right).$$

Using the same approximations for $\zeta = \frac{r_2}{D}$ will produce an identical equation in r_2/D . This is due to the relatively small magnitudes of ζ and ρ .

As a very rough approximation to the out-of-plane characteristics of the "sphere", consider Figure 3-5 where a vehicle has come into close proximity with a satellite but is out of its orbital plane with respect to Jupiter. The encounter occurs at a distance D' from Jupiter and y from the satellite. It may be said, a priori, that y is small and, therefore, $D' \approx D$. Assuming for simplicity that the velocity of the vehicle at encounter is V_A and V_A is some percentage, P , of the satellite velocity, then by equating inertial and gravitational force terms and simplifying, the expression for y is

$$y = \frac{D}{P^2} \left(\frac{M_S}{M} \right).$$

Introducing the proper values of mass and distance into the equation for y indicates that y is extremely small (less than 200 km for Callisto). Hence, the "sphere-of-influence" would assume the shape of a very flat disk. Capture with such a target area would, of course, present forbidding problems.

For the sake of comparison with the Laplace concept, Table 3-2 presents the results of applying the derived solution to the Galilean satellites for a nominal encounter velocity of 75 percent of circular velocity. The last column of Table 3-2 presents the derived value of r_1 in terms of satellite radii. Consider now the relationship between energy, distance, and velocity

$$\frac{1}{a} = \frac{2}{r} - v^2,$$

where a = semi major axis (body radii)
 r = distance from attracting body (body radii)
 v = velocity at r (circular satellite units).

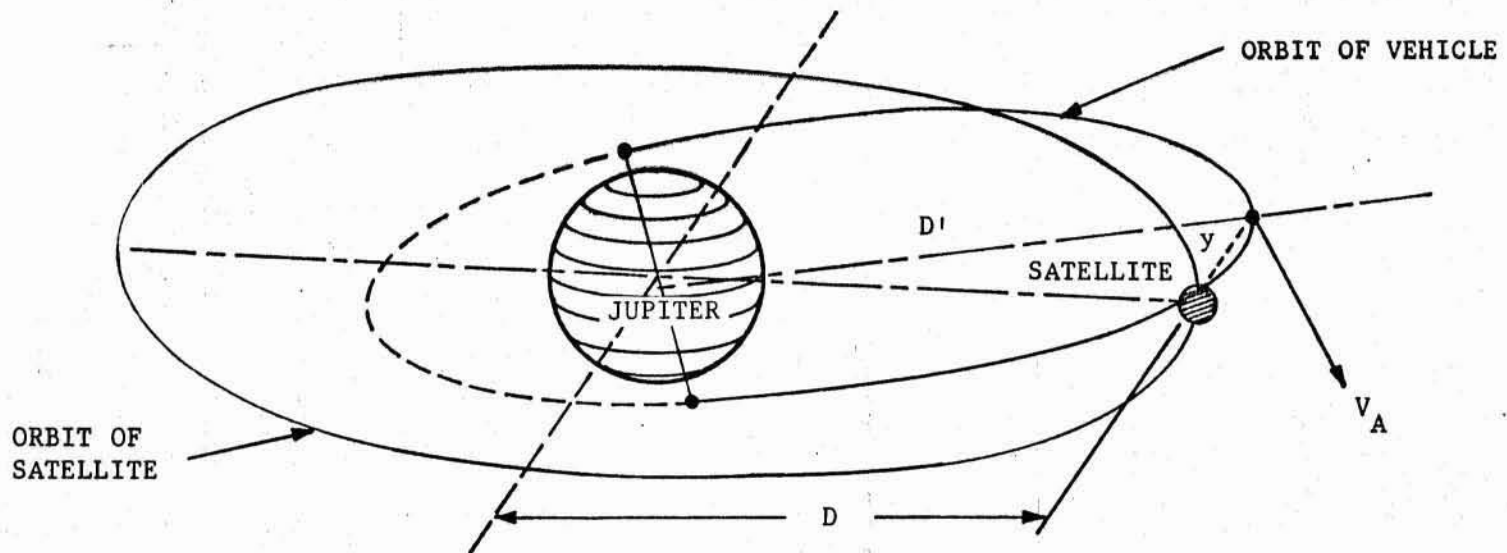


Figure 3-5. GEOMETRY OF THE OUT-OF-PLANE ENCOUNTER

Table 3-2. COMPARISON OF SPHERE OF INFLUENCE CONCEPTS

Satellite	r_1 (km)		y^*	r_1 (satellite radii)
	Laplacian	Quintic (Cubic)		
IO	6500	13,900	30	3.7
EUROPA	8700	19,200	30	6.1
GANYMEDE	22,600	45,000	180	8.8
CALLISTO	32,800	68,400	190	13.2

* Arrival Velocity = .75 percent Satellite Velocity

September 1966

Evaluating the expression at the sphere of influence gives

$$\frac{1}{a} = \frac{2}{r_{\text{SOI}}} - v_{\text{SOI}}^2$$

In the usual case r_{SOI} (radius of the sphere of influence) is very large in terms of body radii (in fact $r_{\text{SOI}} \rightarrow \infty$ in the theoretical limit) so that the term $2/r_{\text{SOI}}$ may be neglected. If the velocity at arrival at SOI is zero, relative, of course, to the attracting body, then $a = \infty$ and the orbit is a parabola. Recalling the values of $r_1 = r_{\text{SOI}}$ (in plane) from Table 3-2 it may be seen that the term $2/r_{\text{SOI}}$ is not negligible and further attempts at analytical expressions based on the sphere-of-influence concept produce amusing but invalid results.

In conclusion, it may be said that the Laplacian sphere-of-influence concept will not hold for the inner Jovian satellite system. Derivation of Lagrange's classical quintics and solution of the resulting cubic after neglecting fourth- and fifth-order terms is also unsatisfactory. Iterative solution of the quintics yields solutions almost identical to the cubic. Machine-integrated trajectories could, of course, be utilized, but this is cumbersome at best for the preliminary mission analyst, particularly where a wide range of parametric data is desired. It is suggested that further study is required to develop a sphere-of-influence concept for bodies in close proximity to a powerful gravitational field. One possible approach might be the development of a "transition zone" between the domain of validity of two-body mechanics in the major and minor gravitational fields. Reference 39 outlines such an approach for the Earth-Moon system. Its application to the Galilean satellite system of Jupiter is unproven. Validity by comparison with fully integrated trajectories is untested for either case.

3.2 OUTER SOLAR SYSTEM EXPLORATION VIA THE JUPITER SWINGBY MODE

Other advanced mission possibilities for Saturn V launches include Saturn and Uranus missions and asteroid belt exploration. The following two subsections briefly discuss their potential.

Reference 1 compares Saturn V performance capability for direct and Jupiter-flyby Saturn and Uranus missions and concludes that for comparable trip times the gravity-assist mode would limit these missions to flybys due to the high energy at planet arrival. Admissibility of higher trip times, however, permits consideration of the swingby mode for capture missions with attendant higher payload capability. The first subsection treats the Saturn and Uranus capture mission potential and indicates the feasibility of utilizing the basic Jupiter spacecraft for their achievement.

The asteroid belt represents one of the oddities in the solar system and is thus of great interest. Actually, three belts have been distinguished which have the following characteristics:

1. 2.0 to 2.6 AU - relatively low concentration of material
2. 2.6 to 3.2 AU - major belt containing the greatest mass of material
3. 3.2 to 4.0 AU - contains the greatest amount of small particles but small total mass.

These asteroid belts are of basic scientific interest, but may also represent a hazard to the spacecraft probing deeper regions of the solar system. The investigation of the distribution and composition of material is important in any program of exploration of the solar system. The second subsection explores the potential of inspecting regions of the asteroid belt enroute to Jupiter, concludes that this is infeasible, and suggests alternatives for achievement of this objective, one of which utilizes the basic Jupiter spacecraft.

3.2.1 Saturn and Uranus Missions

Saturn V performance capability for Saturn and Uranus capture missions via a Jupiter gravity assist mode is reflected in Figure 3-6. The capture orbit apsidal ratio is 40 and periapsis values range from 1.05 to 5 planet radii. In the case of Saturn the minimum capture orbit perispsis would be about 3 planet radii if flight through Saturn's rings is disallowed. The performance curves are based on single spacecraft stage braking to establish capture orbit. Trip times for Saturn are seen to range from 1500 to 2000 days and for Uranus from 3000 to 4000 days. Trip time can be reduced by permitting higher planet arrival energy and reducing gross mass in capture orbit. As trip time is reduced, however, the energy requirements become large enough to require two-stage spacecraft braking. Further reductions in trip time result in planet arrival energies which would limit outer planet missions to flybys.

Figure 3-7 presents a sketch of a possible two-stage spacecraft for outer planet capture missions via a Jupiter swingby. It includes the basic Jupiter spacecraft of the Jupiter orbiter/solar probe mission and a modified Titan transtage as an upper stage. Figure 3-8 reflects the capability of the two-stage concept for Saturn and Uranus capture missions. It indicates that the 4400-lb Jupiter spacecraft could be placed in Saturn or Uranus orbit with reduced trip times of 1300 and 2900 days, respectively.

Communication with an earth-based receiving station from Saturn and Uranus is marginally feasible with the Jupiter spacecraft communication system. Figure 3-9 shows the data bit rate as a function of spacecraft antenna diameter for a 64-meter diameter, earth-based receiving antenna (Goldstone Tracking Station). The 5-meter antenna design size is indicated on the curves and it can be seen that at this point the order of magnitude of data rate is 10 bits per second. For the sake of comparison the bit rate in Jupiter orbit is about 1000 bits per second. At the bit rate realizable for Saturn and Uranus missions it would take about 8 hours to transmit a normal 250,000 bit television picture of low resolution. This is felt to be the lower limit of practicality.

3.2.2 Asteroid Belt Mission

During the Earth-Jupiter phase of a Jupiter mission it would be desirable to investigate some of the major asteroids during a "close pass". The separation distance of the spacecraft and the asteroids Ceres and Vesta was determined during the 1970-1980 decade launch opportunities. It was found that the 1975 opportunity provided the nearest pass distances for both Ceres and Vesta. Figure 3-10 illustrates the variation in asteroid-spacecraft distance during the 1975 opportunity for various trip times. The launch date is taken in the middle of the launch period. It may be seen from the figure that Vesta affords the closest passes to the asteroids during 1975; this is also true throughout the decade.

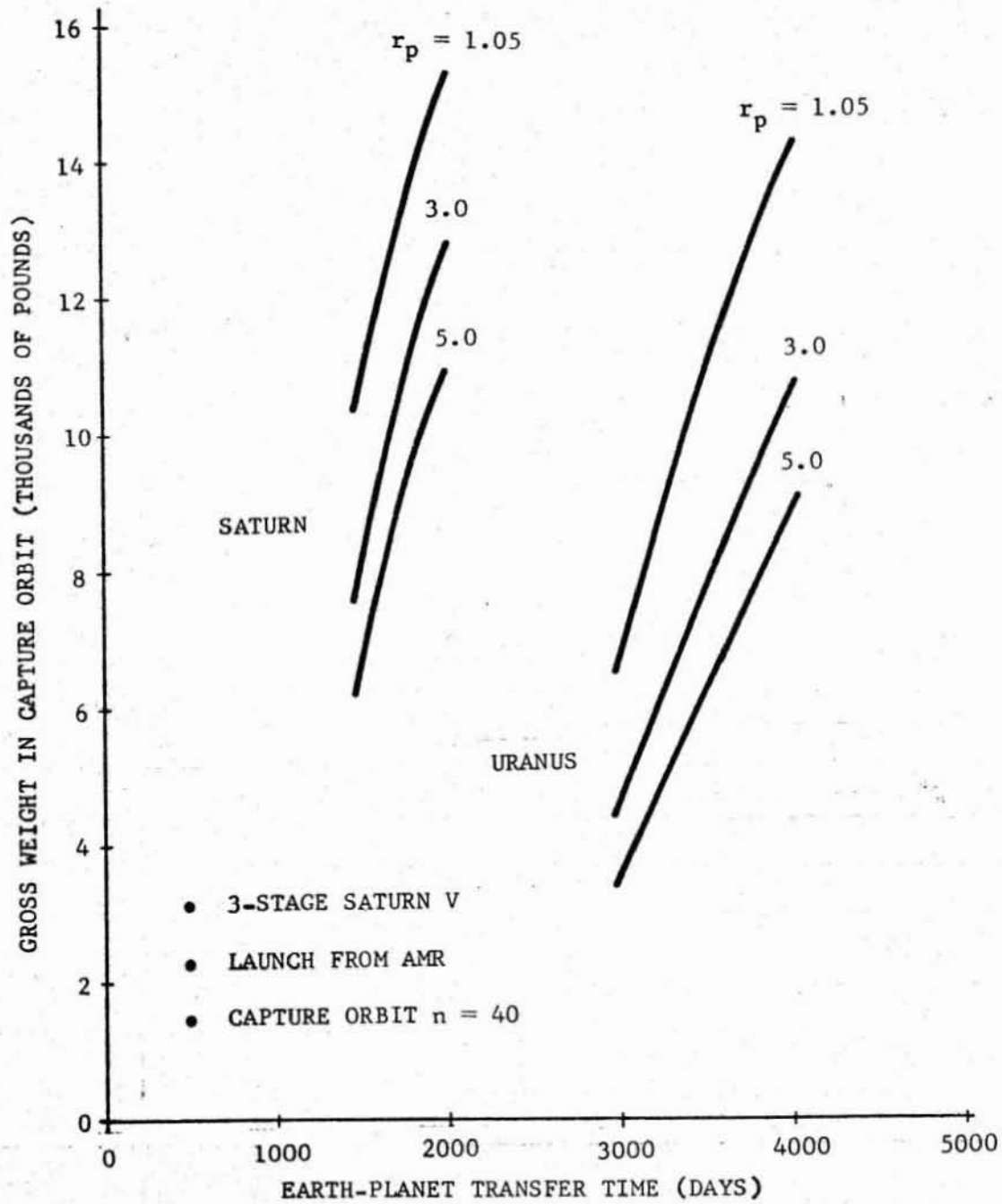


Figure 3-6. SATURN V PERFORMANCE CAPABILITY FOR SATURN AND URANUS CAPTURE MISSIONS (JUPITER SWINGBY MODE)

MASS SUMMARY:

ORBITER	10,550	lbs
ADAPTERS	700	
TRANSTAGE	14,100	
	<hr/>	
	25,350	lbs

3-15

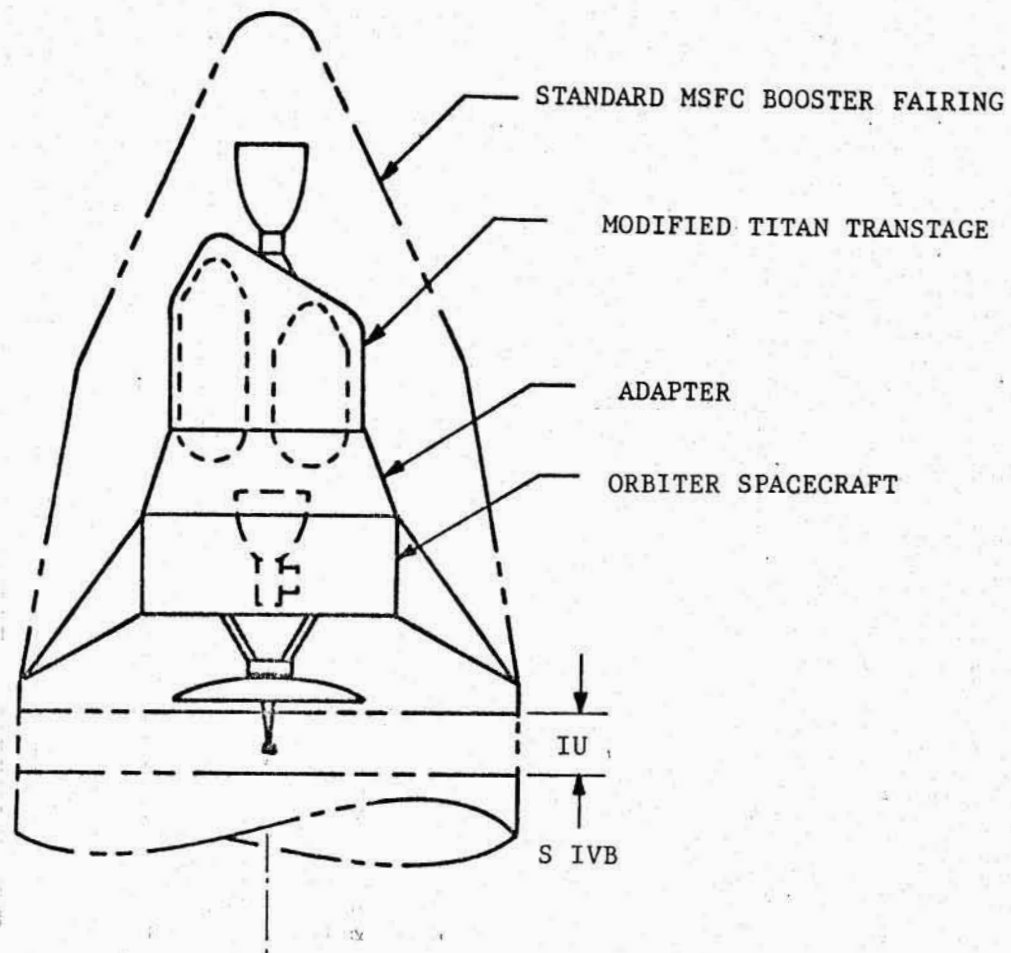


Figure 3-7. ADVANCED CAPTURE DESIGN (SATURN OR URANUS)

- TWO-STAGE BRAKING
- $I_{sp}=310$ SECONDS
- 2nd STAGE 10,750 POUNDS

3-16

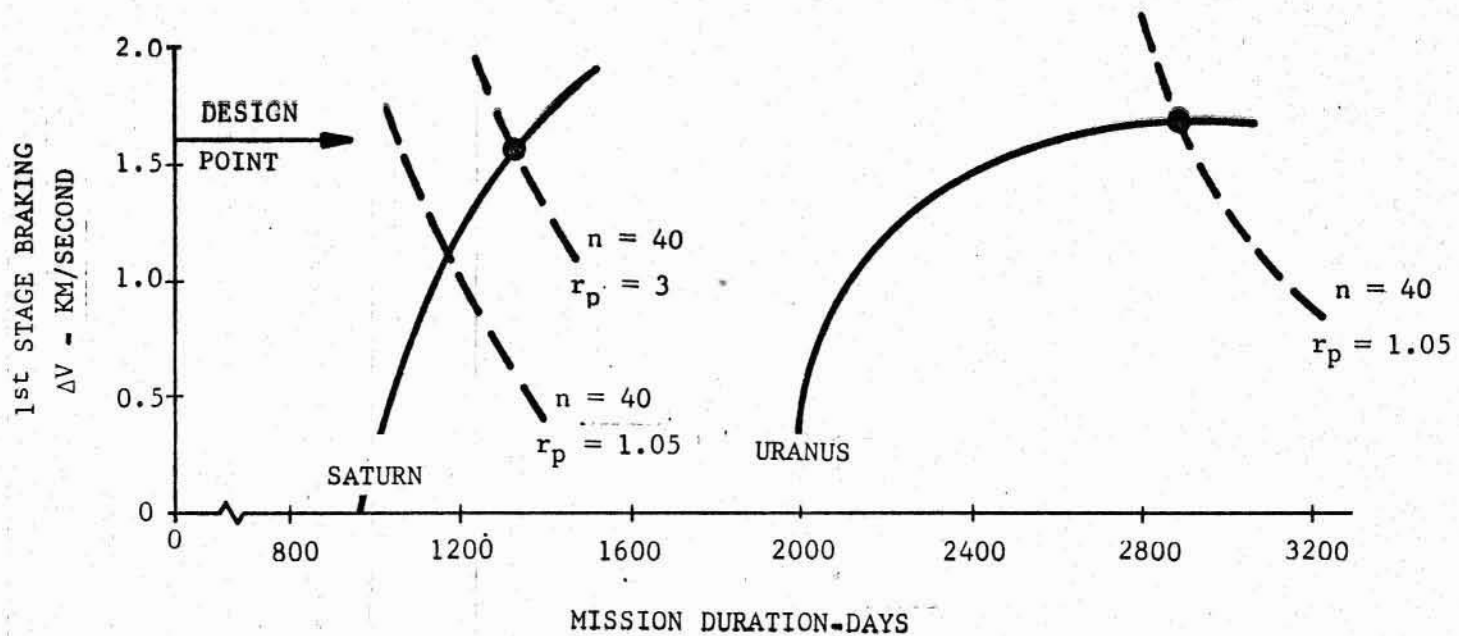
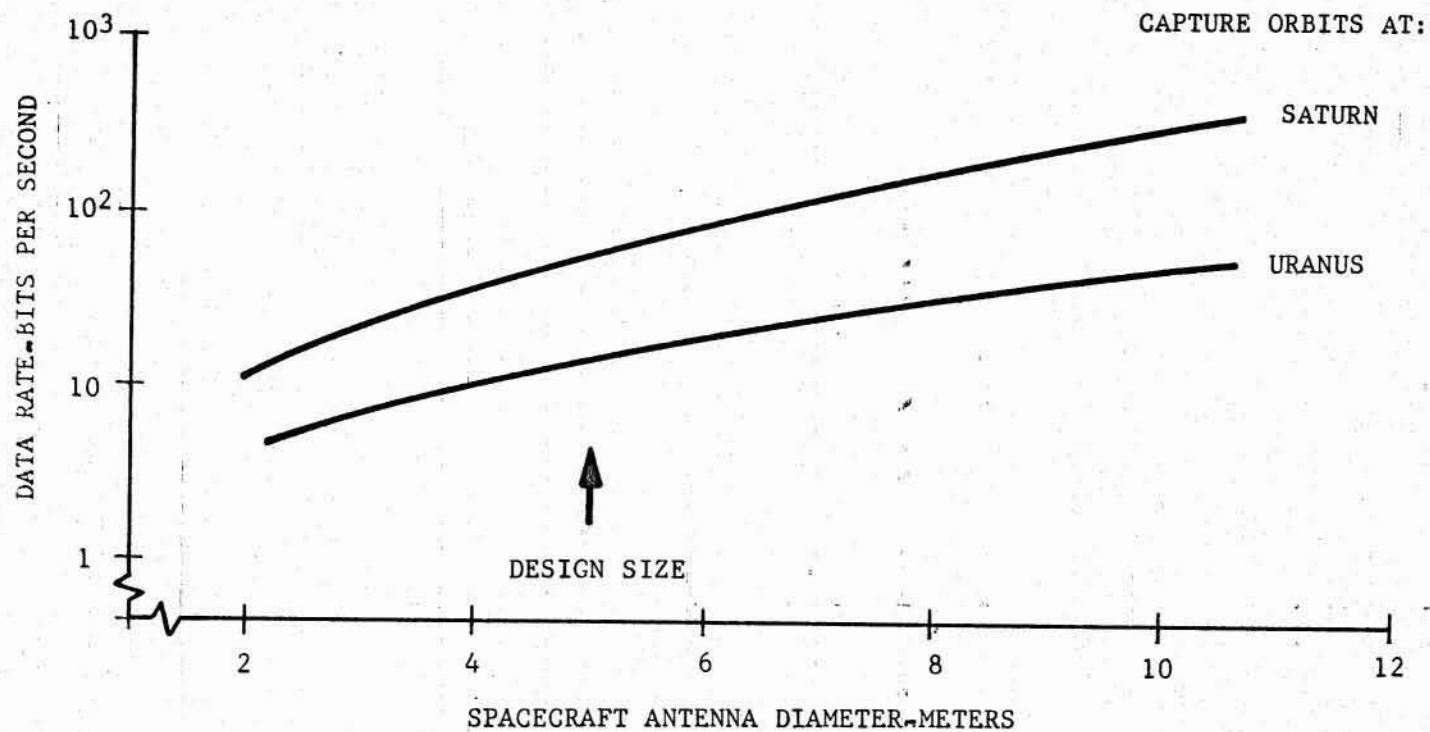


Figure 3-8. SATURN & URANUS CAPTURE

- DSIF COMMUNICATIONS WITH 64 M. ANTENNA
- INTERNAL SYSTEM LOSSES ~ 35 DB.
- 200 WATTS INPUT POWER



3-17

Figure 3-9. DEEP SPACE COMMUNICATIONS

3-18

- 1975 JUPITER MISSION
- LAUNCH DATE 27 JUNE

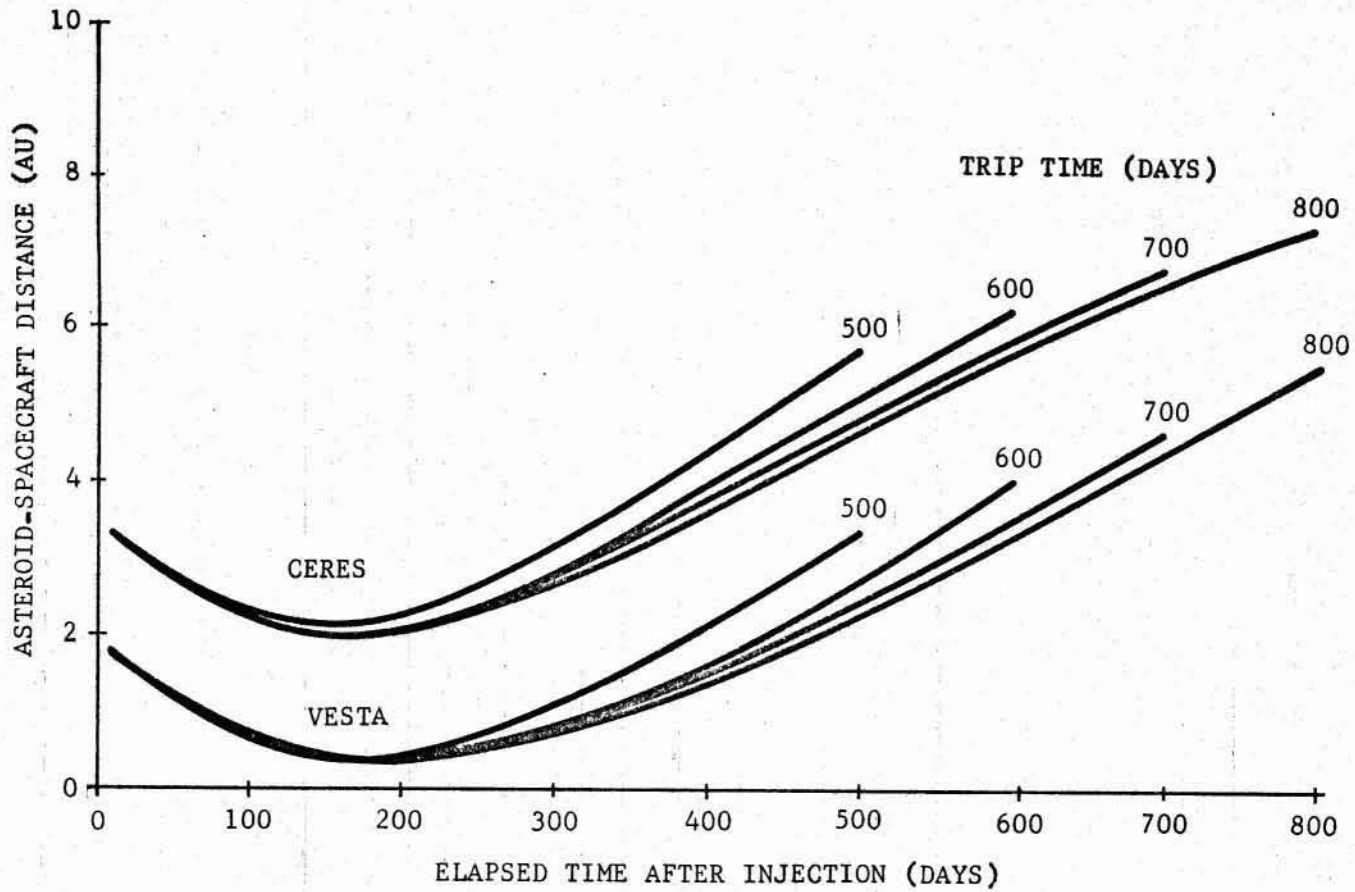


Figure 3-10. ASTEROID-SPACECRAFT COMMUNICATION DISTANCE

The distance of closest approach, occurring about 180 days after injection, is about one-third of an astronomical unit. By varying the launch date across the launch period (Figure 3-11) the distance of closest approach may be reduced to about one-fourth of an astronomical unit. Figure 3-11 is presented for 500-day Earth-Jupiter transfers which provide the least distance of closest approach throughout the trip time range.

At one-fourth astronomical unit the disk of Vesta is approximately 0.001 degree so that mere detection would be a problem. Hence, it may be concluded that inspection of the asteroids Ceres and Vesta is impossible during Jupiter missions in the 1970-1980 decade. In fact, due to the relatively high inclination of the major asteroids (10° - 25°) and their small diameters, inspection enroute to Jupiter under most any circumstances will be impossible. The possible exception here would be a fortuitous meeting in the vicinity of the asteroids' orbital nodes.

Analysis of certain opportunities for a Jupiter mission and potential post-encounter orbits in the swingby mode indicates that some heliocentric orbits will result with perihelion and inclination arguments which would place a portion of the post-encounter orbit in the asteroid belt. If a spacecraft or probe on such a trajectory had propulsion capability sufficient to establish a circular or quasi-circular orbit at perihelion, then an "inspection station" could be established in the asteroid belt for the lifetime of the spacecraft/probe. Figure 3-12 demonstrates such capability for the Jupiter spacecraft.

Obviously such a mission would not be primary since a direct mode would exhibit considerably less trip time. Also, it could be accomplished with a smaller launch vehicle than the Saturn V. However, by mounting two Jupiter orbiter spacecraft atop the Saturn V a dual Jupiter orbiter/asteroid belt mission might be accomplished utilizing the same basic spacecraft module. Such an arrangement is schematically represented in Figure 3-13. An approximate 4-foot conical extension section would be required above the Instrument Unit to accommodate the dual spacecraft mount. An alternative here would be the design of a small probe such as the solar probe with attached retro package to accomplish the secondary asteroid belt mission.

3.3 SPACECRAFT FAMILY

The primary subsystem problem for advanced missions is communications. Power or antenna sizes must be increased to obtain acceptable data transmission bit rates. Parametric trade-offs for communication distances out to 20 AU were developed. It was concluded that with proper design and available power, S-band system communications can be utilized virtually anywhere in the solar system inside of Neptune's orbit.

Extensions of the thermal control, guidance and navigation, propellant storage, and power supply concepts developed for the Jupiter orbiter are appropriate for the missions considered. The various concepts for utilization of the basic Jupiter spacecraft are schematically summarized in Figure 3-14. They include:

1. The basic Jupiter mission
2. Dual spacecraft for secondary flyby mission to the asteroid belt
3. The Jupiter orbiter/close solar probe mission

- 1975 JUPITER MISSION
- 500-DAY TRIP TIME

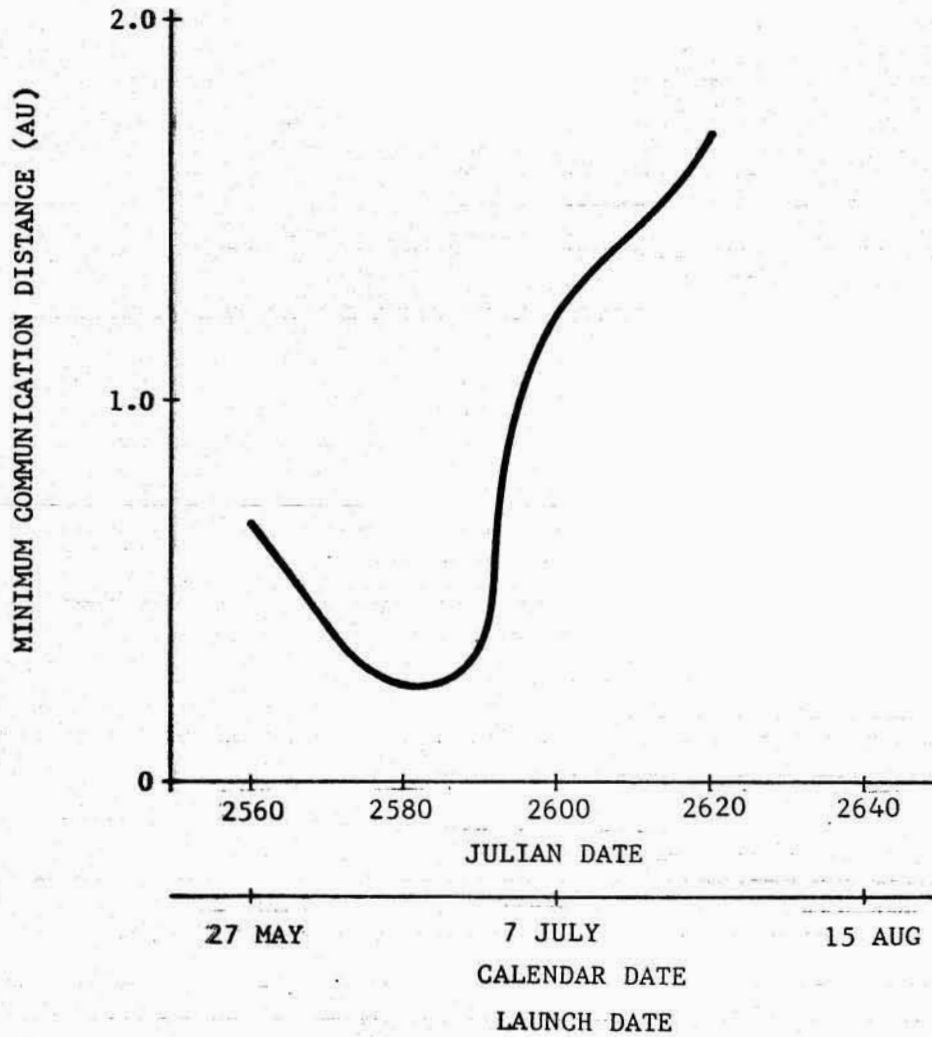


Figure 3-11. VESTA DISTANCE OF CLOSEST APPROACH

- BASIC JUPITER ORBITER SPACECRAFT
- APHELION ~ 5.2 AU
- BRAKING $\Delta V \sim 2$ km/sec

3-21

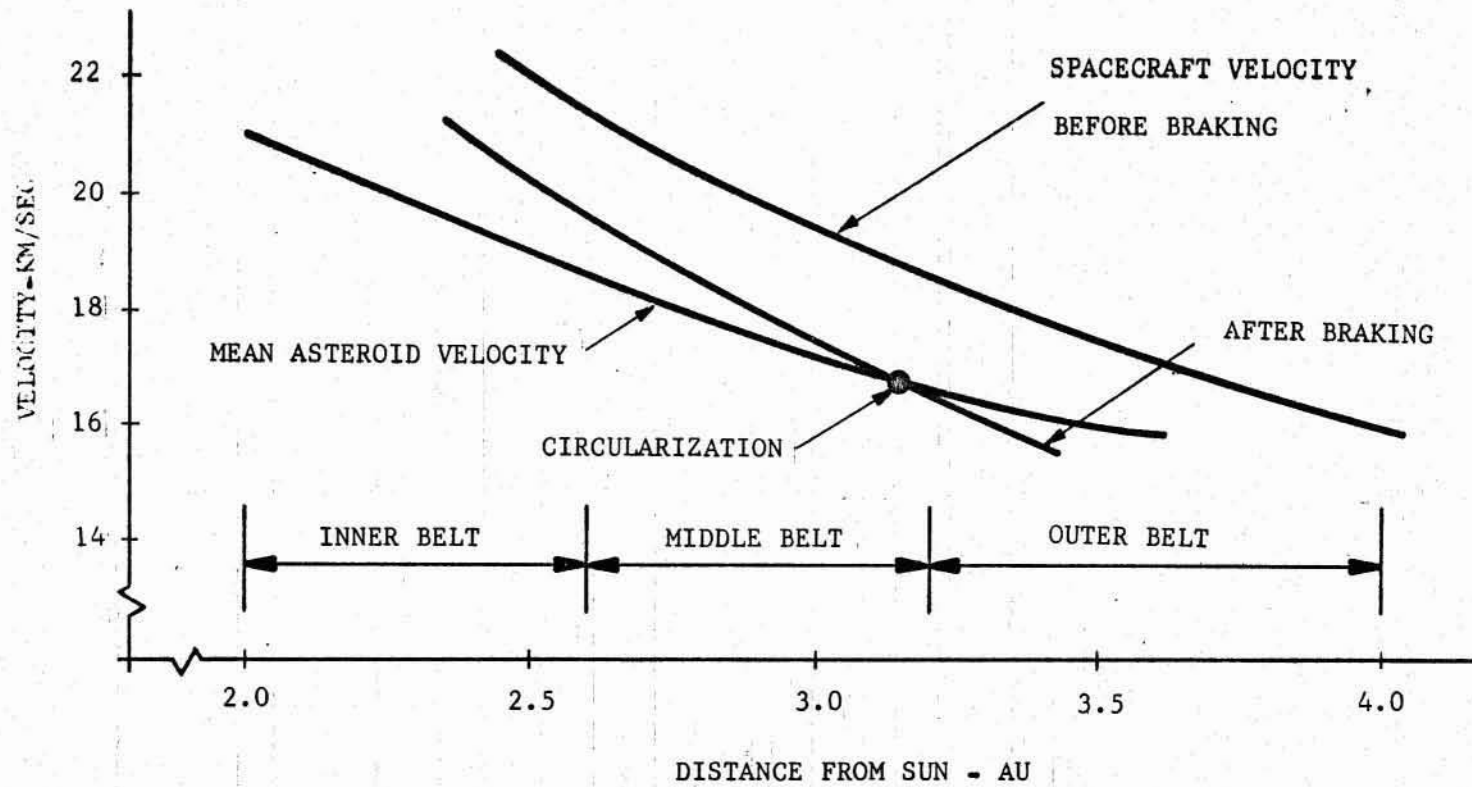
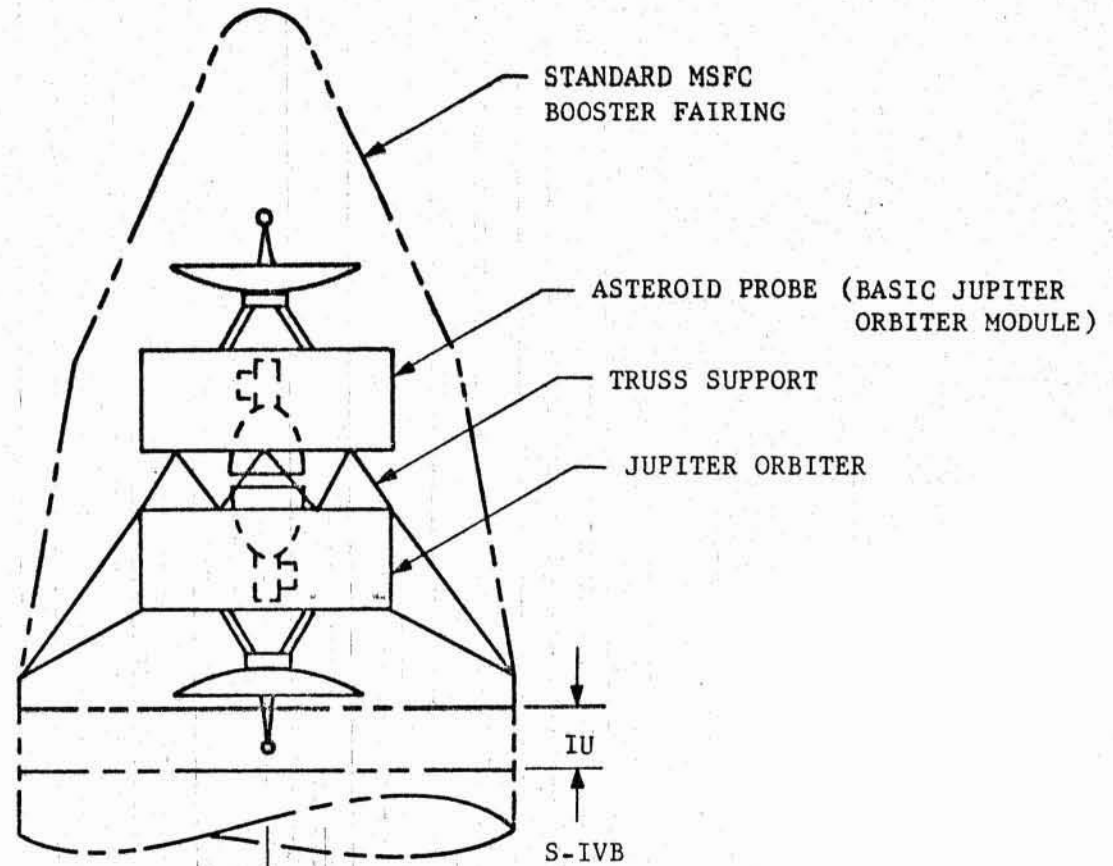


Figure 3-12. ASTEROID BELT CIRCULARIZATION

MASS SUMMARY:

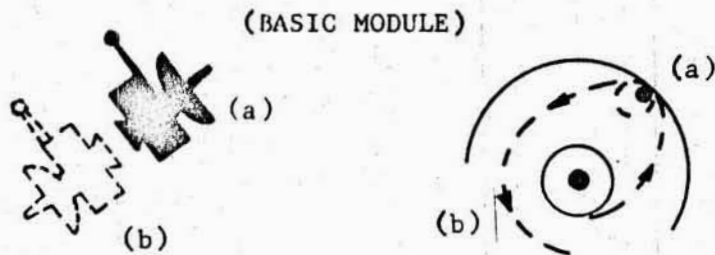
JUPITER ORBITER	10,550 LB
ASTEROID PROBE	10,550
ADAPTER & TRUSS	<u>~3,900</u>
	-25,000 LB



3-22

Figure 3-13. JUPITER ORBITER/ASTEROID PROBE

JUPITER CAPTURE AND
ASTEROID BELT PROBE



JUPITER ORBITER WITH
CLOSE-SOLAR PROBE



JUPITER ORBITER WITH
ATMOSPHERIC ENTRY PROBE



SATURN & URANUS ORBITER
(JUPITER SWINGBY MODE)

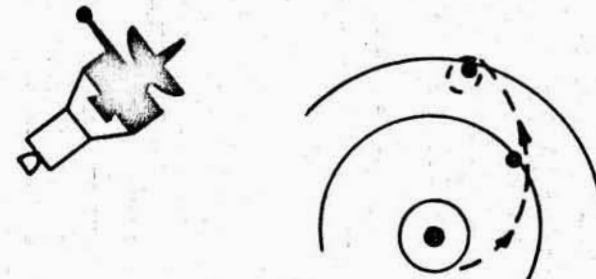


Figure 3-14. CONCEPTUAL FAMILY DESIGNS

September 1966

4. The Jupiter orbiter/atmospheric entry probe mission
5. Saturn and Uranus capture missions via Jupiter flyby.

The greatest concern in the family of concepts is the long lifetimes required for the spacecraft. It is not possible at this time to state the probability of success for these mission durations nor to predict whether they are even possible.

To gain an order of magnitude appreciation for expected spacecraft reliabilities, a brief analysis was conducted extrapolating current satellite success data into the next decade. The results of this analysis are shown in Figure 3-15. The spread of individual spacecraft success data is shown to account for the uncertainties inherent in the reliability analysis. This extrapolation is necessarily only a preliminary estimate at this time. As noted in subsection 2.2.8 of this report, the spacecraft success data can be converted to program success by including the number of spacecraft in a program. Figure 3-15 also shows this conversion. It can be seen that generally more than one spacecraft must be funded and launched for long duration missions in the next decade.

If it is assumed that an extensive program of exploration of the solar system is desired, a tabulation of missions and performance requirements can be made as shown in Table 3-3. Based on these conservative extrapolations of system success data, it was concluded that for an extensive exploration program of selected points of interest in the solar system a relatively high number of spacecraft must be launched in an overall program. This is summarized in Table 3-4 for an individual mission success goal of .95. It can be seen that for the postulated program of missions and the extrapolation of minimum and maximum individual spacecraft success, about 13 to 17 Saturn V launches would be required in the next decade. This represents a major national program.

3-25

• 1976 TIME FRAME

• $P_T = 1 - (1-p)^n$

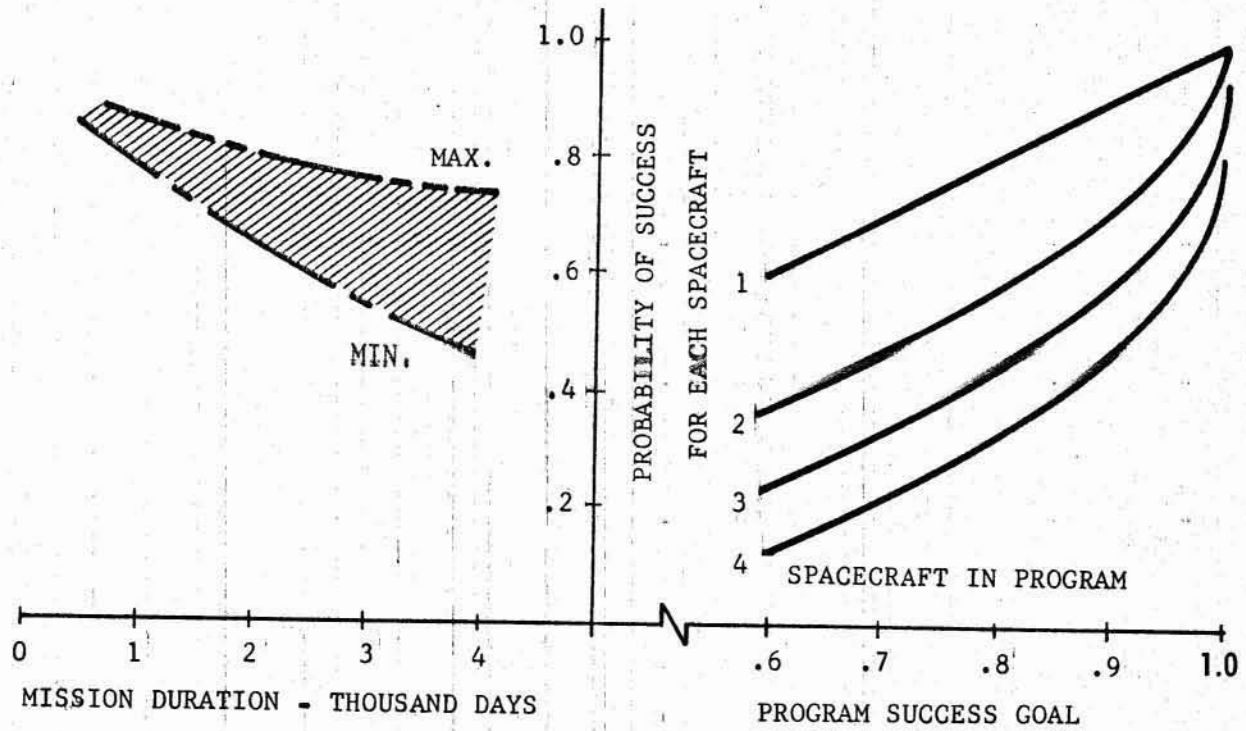


Figure 3-15. ADVANCED MISSION SUCCESS

Table 3-3. EXTENSIVE EXPLORATION PROGRAM

MISSION	PAYLOAD MASS		SATURN V INJECTED MASS	LIFETIME	
	ORBITED	FLYBY OR ENTRY		ORBITER	FLYBY
JUPITER ORBITER WITH CLOSE SOLAR PROBE	4400 LBS	1400 LBS	~12,000 LBS	600 DAYS	1200 DAYS
JUPITER ORBITER WITH ATMOSPHERIC ENTRY PROBE	4400	600	~12,000	600	600
SATURN ORBITER	4400	--	~25,350	1400	--
URANUS ORBITER	4400	--	~25,350	2800	--
JUPITER ORBITER WITH ASTEROID BELT PROBE	4400	4400*	~25,000	600	2000

* MISSION COULD BE FLOWN WITH SMALLER MORE OPTIMALLY DESIGNED PROBE

Table 3-4. NUMBER OF SPACECRAFT

- 1976 TIME FRAME
- MISSION SUCCESS GOAL ~.95

MISSION	MISSION TRIP TIME	INDIVIDUAL LAUNCH SUCCESS		NUMBER OF SPACECRAFT REQUIRED	
		MAX.	MIN.	MIN.	MAX.
JUPITER ORBITER/CLOSE SOLAR PROBE	600 AND 1200 DAYS	.74	.64	3	4
JUPITER ORBITER/ATMOSPHERIC ENTRY	600	.88	.85	2	2
SATURN ORBITER	1400	.82	.71	2	3
URANUS ORBITER	2850	.76	.55	3	4
JUPITER ORBITER/ASTEROID BELT PROBE	600 AND 1200	.70	.54	3	4
TOTAL FOR EXTENSIVE EXPLORATORY PROGRAM				13	17

SECTION IV

REFERENCES

1. Odom, P. R., Brown, B. G., Hill, A. S., et al., "Application of Saturn/Apollo Hardware to Unmanned Scientific Exploration of the Solar System," TR-292/3-6-003, Northrop Space Laboratories, April 1966.
2. _____, "Space Flight Handbook," Volume 3, Planetary Flight Handbook, Part 5, NASA SP-35, 1966.
3. Hill, A. S. and Lucas, W. C., "Survey of Experiments for a Jupiter Orbiter/Close-Solar Probe," Northrop Report TM-293-6-049, MSFC Contract NAS8-20082, Appendix F-1, Schedule Order 17, Task Directive 5, July 1966.
4. Jicha, J. J., Jr., "Saturn Radioisotope Power Supply Study," Martin Reports MND-3251-1 through -3, MSFC Contract NAS8-20092, July 1965.
5. Lundholm, J. G., Jr., et al., "A Close-Approach Solar Probe Design Feasibility and Mission Study," Journal of Spacecraft and Rockets, Vol. 2, No. 4, July-August 1965.
6. Romero, J. B., "Potentialities of Radioisotope Propulsion for Space Probes," Journal of Spacecraft and Rockets, Vol. 3, No. 4, April 1966.
7. deMoraes, C. A., and Gage, D. D., "Mission Objectives and Design Considerations for a Scientific Solar Probe," AIAA Manned Spacecraft Meeting, Los Angeles, California, March 1965.
8. Gubin, S., et al., "Lasers vs. Microwaves in Space Communications," Journal of Spacecraft and Rockets, Vol. 3, No. 6, June 1966.
9. Dabul, A., "Information Transfer Systems in Space Communications," NASA TN D-3405, May 1966.
10. (Various authors), "Mariner 4 Flight Results," Astronautics and Aeronautics, Vol. 3, No. 10, October 1965.
11. Uslenghi, P. L. E., "Studies of Antennas for Space Vehicles," NASA CR-159, March 1965.
12. (Various authors), "Proceedings of the Apollo Unified S-Band Technical Conference," NASA SP-87, July 1965.
13. Fang, P. H., "Thermal Annealing of Radiation Damage in Solar Cells," Goddard Space Flight Center, Report X-713-65-469, NASA N66-17236, November 1965.
14. Gaumer, R. E., and McKellar, L. A., "Thermal Radiative Control Surfaces for Spacecraft," Contracts AF 04(647)-563, -564, and -558, Lockheed Report LMSD-704014, NASA AD-264, 127, March 1961.
15. van Vliet, R. M., Passive Temperature Control in the Space Environment, the Macmillian Co., 1965.

16. (Authors unknown), "Thermophysics Design Handbook," Lockheed Report LMSC 8-55-63-3, NASA N63-20841, July 1963.
17. Baker, R. H., et al., "Study of a Small Solar Probe", NASA Grant NASr-249, MIT Report PR-5255-5, NASA N65-32722, July 1965.
18. (Various authors), "Asteroid Belt and Jupiter Flyby Mission Study," Contract JPL-950871, Lockheed Report M-49-65-1, February 1965.
19. Magistrale, V. J., "Engineering Problems in Capsule Sterilization," Astronautics and Aeronautics, Vol. 4, No. 2, February 1966.
20. Phillips, C. R., and Hoffman, R. K., "Sterilization of Interplanetary Vehicles," Science, Vol. 132, No. 3433, October 1960.
21. Jenes, A. L., and McRae, W. V., Jr., "Manned Mars and/or Venus Flyby Vehicle Systems Study," NASA X 65-19081, Contract NAS9-3499, 18 June 1965.
22. Space Operations Control Center, Goddard Space Flight Center, "Satellite Situation Report," Vol. 5, No. 20, NASA N66-14256, 21 October 1965.
23. Dubin, M., "Meteoroid Effects on Space Exploration," NASA TND-1839, 1963.
24. Johnson, F. S., Satellite Environment Handbook, Stanford Univ. Press, 1965.
25. Branigan, T. L., Editor, TRW Space Log, Vol. 5, No. 4, Winter 1965-66.
26. D'Anna, P. J., and Heitz, R. M., "Evaluation of Self-Sealing Structures for Space Vehicle Application," NASA CR-485, Contract NASR-102, May 1966.
27. (Authors unknown), "Mariner-Venus 1962 Final Project Report," NASA SP-59, 1965.
28. Smith, R. E., "Space Environment Criteria Guidelines for Use in Space Vehicle Development," NASA TM X-53142, September 1964.
29. (Various authors), AIAA Unmanned Spacecraft Meeting, Los Angeles, AIAA Publication CP-12, March 1965.
30. Skuridin, G. A., et al., "Transaction of the All-Union Conference on Space Physics," NASA TT F-389, May 1966.
31. Haviland, R. P., Handbook of Satellites and Space Vehicles, D. Van Nostrand Co., 1965.
32. Peck, D. S., and Shennum, R. H., "Long Life Electronics," Space/Aeronautics, Vol. 45, No. 3, March 1966.
33. Neswald, R. G., "The Meteoroid Hazard," Space/Aeronautics, Vol. 45, No. 5, May 1966.

34. Ehricke, K. A., Space Flight, Vol. 1, "Environment and Celestial Mechanics," Norstrand Co., 1960.
35. Blanco, V. M. and McCurkey, S. W., Basic Physics of the Solar System, Addison-Wesley, 1961.
36. Stebbins, J., "The Light Variations of the Satellites of Jupiter and Their Application to Measurement of the Solar Constant," Pub. Astron. Soc. Pacific, 38, 1926.
37. Sampson, R. A., "Theory of the Four Great Satellites of Jupiter," Memoirs Roy, Astron. France, 69, 1921.
38. de Sitter, W., "Jupiter's Galilean Satellites," 1931 George Darwin Lecture.
39. Forster, K., "Linearization for Certain Earth-Moon Trajectories in the Restricted Problem of Three Bodies," TRW Report No. 9863-6005-RO-000.